ABSTRACT

HAMOUDA, TAMER MOSTAFA. Smart Textiles: Evaluation of Fiber Optic Sensors Embedded in 3D Orthogonal Woven Composites and their Impact on the Host Structure Integrity. (Under the direction of Dr. Abdel-Fattah Seyam and Dr. Kara Peters).

3D woven preforms are known for their advantages over the nonwoven and 2D woven preforms in that they provide higher resistance to crack propagation, eliminate delamination, faster in resin transfer, and higher fiber volume fraction. These types of structures are being implemented in different field and have the potential in numerous applications such as aerospace, civil engineering, transportation, and wind mills. With the increase in the awareness of safety, the need of Structure Health Monitoring system that can detect the damage and monitor structure behavior to predict the potential damage is increased. Due to the straight path of the constituents of the 3D orthogonal woven structures, they are excellent host for optic fiber sensors.

The main goal of this research is to evaluate different types of optic fibers and identify their potential use as sensors for predicting composite structure failure. This research is focused on relatively newly developed graded index, perfluorinated POF (GI-PF-POF) as potential embedded sensors. End to end loss and backscattering techniques using Optical Time Domain Reflectometer (OTDR) were used to investigate and characterize sensing properties of embedded optical sensors. In this dissertation, literatures are reviewed in chapter 2 research objectives are presented in Chapter 3.

Chapter 4 reports a study structured to evaluate the effect of the macrobending optical fibers on signal power integrity to identify its capability as integrated sensors into fiber reinforced composites. Newly developed Graded Index Perfluorinated POF (GI-PF-POF) and two types of SOFs were evaluated in 3-point macrobending test bed using laser light source. The relationships between the optic fibers signal loss and bending radius, bending deflection and wrap angle around the middle rod were established. The results showed that POF provides higher sensitivity and range of bending deflection compared to SOF. The work also unveiled the bending radius of optical fibers at which minimum or no signal loss occurred.

In Chapter 5, the effect of Vinylester and Epoxy resin systems on the signal loss of embedded perfluorinated, graded index POFs were measured. OTDR was used to monitor the signal attenuation and backscattering level of the POFs throughout the resin curing cycle. FTIR and optical analyses were also conducted to assess the results. Results showed that vinylester resin caused a significant increase in the backscattering level of POF sensors and therefore induced high fiber signal losses. On the other hand, the POF treated with Epoxy showed no change in backscattering level indicating no chemical or physical change had occurred to POF.

Chapter 6 presents systemic investigation to find out whether incorporating POF into 3D orthogonal woven composites affects their structure integrity and performance characteristics. Range of 3D orthogonal woven composites with different number of layers and different weft densities was fabricated with and without POF. Results revealed that the tensile and bending properties of 3D orthogonal woven composites were not affected by the presence of POF.

Chapters 7 report study designed to evaluate POF as an embedded sensors in 3D orthogonal woven composite structures. The evaluation included the sensor response during manufacturing process and under bending and repeated impact tests using OTDR. Results indicate minor effect of weave structures on POF signal loss and increase in signal loss as curing time increases. Under bending loads, signal loss increase as load increase until structure fails. POF recovered and loss decreased after unloading. Impact results indicate that different configuration of 3D orthogonal woven composite structure has different response on POF signal loss. Deformation of composite under impact tests transferred throughout the structures to POF. As signal loss at failure location increase as the distance that can be monitored decreases. While each of Chapters 4-7 includes a conclusion specific to the study covered in each chapter, Chapter 8 covers the overall conclusion based on the entire findings of the research. Abbreviation, Definition related to optic fiber, and OTDR specifications are included in appendix C, D, and F respectively.

Smart Textiles: Evaluation of Fiber Optic Sensors Embedded in 3 D Orthogonal Woven Composites and their Impact on the Host Structure Integrity

by
Tamer M. Hamouda

A thesis submitted to the Graduate Faculty of
North Carolina State University
in partial fulfillment of the
requirements for the Degree of
Doctor of Philosophy

Fiber and Polymer Science

Raleigh, North Carolina

2012

APPROVED BY:

_____	_____
Dr. Trevor Little	Dr. Philip Bradford
_____	_____
Dr. Abdel-Fattah M. Seyam Co-Chair of advisory committee	DR. Kara Peters Co-Chair of advisory committee

DEDICATION

Dedicated to my parents, grandmother, my wife, my children Alia and Allei-Eldeen, and to my country EGYPT.

BIOGRAPHY

Tamer Hamouda was born in Cairo Egypt. Tamer Hamouda graduated with a bachelor's degree in Spinning, Weaving, and Knitting from College of Applied Art, Helwan University, Cairo, Egypt. He received his Master of Science in Nonwoven Technology from College of Applied Art, Helwan University, Cairo, Egypt. Tamer had a Diploma in visibility study from College of economics and political science, Cairo University, Cairo, Egypt. He worked in the textile industries for 8 years before joining National Research center, Cairo, Egypt as an assistant researcher. Tamer has joined North Carolina State University in July 2007 as a visiting scholar under exchange mission between USA and Egypt until 2009. He started his PhD in Fiber and Polymer science in fall 2009.

ACKNOWLEDGMENTS

To whom who light up a glitter of light to my path, I am grateful

I am deeply indebted to my supervisor Prof. Dr. Abdel-Fattah M. Seyam for giving me the opportunity to pursue my Ph.D. at NCSU College of Textiles and for his invaluable guidance, suggestions, and encouragement throughout the course of this research. I would like also to express my sincere gratitude to Dr. Kara Peters for her invaluable discussion, support, and encouragement. The encouragement and support of Drs. Philip Bradford, Mansour Mohamed, Trevor Little, and David Dicky are highly appreciated.

I would like to extend my acknowledgment to my friends Ahmed Hassanin, Abdel-Rahman Abdel-Gwaad, Ali Kilic, Mehmet Ince and Dr. Hatem Tag-Eldin for their help. Also I would like to thanks Mr. Rob Cooper and Ms. Tywanna Johnson in TATM department for facilitating all type of paper works. I am so thankful to all of my friends at NCSU Issac Kumar and Ani Elayon, Jenifer West for their help and advice. I would like to extend my thanks to the Egyptian governments for the financial support in my first two years.

I would like to express my deep thanks to my brother Mohamed and his wife Heba, my sister Rania and her husband Mahmoud, My friends Sherif Abdel Messieh, Sherif Ismail, Atef Adeeb, and Mohamed Ali Maher for taking care of my parents during my staying in USA.

Last and not least, I am eternally grateful to my parents, my grandmother, my wife Sherin and my kids Alia, and Allei-Eldeen for their encouragement and spiritual support that gave me the patience and persistence to complete my thesis.

TABLE OF CONTENTS

LIST OF TABLES

LIST OF FIGURES

CHAPTER 1

1. INTRODUCTION

High maintenance, heavy weight and corrosion of steel have opened research areas to replace steel with fiber reinforced composite (FRC). Composite materials are known to be stronger, lighter than steel and resistant to corrosion. For example, composite pipe with 15 centimeters diameter weighs 1.8 kilograms per meter is much stronger, compared to cooper nickel pipe with the same diameter, which weighs 10.8 kg/ m. These advantages of composite material positioned the composite materials in competition with steel and alloy metals. Composite materials have established themselves in different markets like aerospace, automotive, windmill, military, bridges, and constructions. Boeing, the airplane manufacturer, moved from using the conventional alloy metal to use FRC to construct its 787-8 model (1), which is made from about 50% by weight fiber.

During their use, structures are subjected to stresses and they may unpredictably fail and cause loss in lives and money. Structures in areas of disasters (such as storms and earthquakes) may seem undamaged in the outside while the inside structure elements are failing. System that are able to predict such problems before damages take place are obviously desirable so measures can be taken to reinforce the structure and avoid failure. The development of these systems has been recently the subject of research. Systems that are based on transmission of electric signal through electric sensors are not small and not durable and cannot be embedded easily in a structure. In some cases the signal couldn't be discriminated from the noise because of the electromagnetic interference. For these reasons recent research dealt with fiber optic as an alternative to the electric sensor system in bridges, railway bridges, pipe lines, oil wells, and dams. One example of using fiber optic based system is the system developed to monitor the Wuhu Yangtze river bridge 2003 (2).

Fiber optic could be easily embedded in concrete, in the bridges wire, adhered in the middle section of carbon fiber (2) (3), or incorporated in a cable form that is attached to a pipe line, bridges or dams. Another application of fiber optic is a system known as "smart profile sensor" that monitor extreme temperatures as well as stresses using cable consists of four single mode or multimode fiber optic contained in a stainless steel loose tube (4). The

stainless steel provides the protection for the fiber optic. The system design combines strain and temperature sensors in a single package. This sensor consists of two bonded and two free single mode optical fibers embedded in a polyethylene thermoplastic profile. The bonded fibers are used for strain monitoring, while the free fibers are used for temperature measurements and to compensate temperature effects on the bonded fibers. For redundancy, additional two fibers are included for both strain and temperature monitoring. The profile itself provides good mechanical, chemical and temperature resistance. The size of the profile makes the sensor easy to transport and install by fusing, gluing or clamping.

As mentioned earlier, fiber optic sensors can be embedded into concrete, or adhered to structures elements for monitoring the strain, stress, crack formation and the extreme temperature. Adhering fiber optic to structures elements may not be advantageous as embedding since the stresses on the surfaces may not represent the internal stresses of the element to be monitored. Additionally, outside sensors may be subjected to whether conditions or rubbing stresses that cause damage to the system. Such systems require additional work for installation.

The overall objective of this research is to develop and evaluate a real time monitoring systems using embedded optical fiber sensors into composite structure and also evaluate a monitoring systems using end to end loss and back scattering technique with the aid of the photon counting in order to provide an accurate prediction method of structure failure and also localize the failure in short time to save time and money. These systems is for evaluating the use of fiber optic in combination of laser in detecting stresses of 3D woven composites and thus detect the failure before it occurs. The basis of such systems is to measure back scattering and power loss on the fiber optics due to different mode of stresses such as impact, and bending. The system could be used to evaluate different fiber optic types; such as glass or polymeric using laser-based and recently developed optical time domain reflectometer (OTDR). The target is to help in selecting fiber optic and detecting type (laser and OTDR) for specific structure elements with good enough sensitivity to detect power loss and back scattering for different strain types and levels. This is achieved by establishing strain-power

loss relationships at different span length of the structure member considered. The strain of the structure member to failure using standard test methods need to be known so that the system can be calibrated to flag problems before failure takes place.

CHAPTER 2

2. Literature review

2.1 Introduction

Civil engineering infrastructure such as bridges, dams, skyscrapers, airports, highways, railways, and tunnels are must for civilization. These infrastructures are heavy and take long time to be built and expensive to construct and maintain. On the other hand the infrastructure has a lifetime which depends on the location, surrounding atmosphere and also frequent maintenance needed to keep it safe for use. Because of its lightweight, easy to build, long life, less maintenance needed and high strength, composite materials are excellent candidates for replacing traditional material in infrastructure such as steel and concrete. For its lightweight and high strength, composites are used in numerous applications such as aircrafts, automobile, military, wind turbine blade, and they continue to find their way for many other applications that are mentioned in the literature review section.

Whether the infrastructure made of steel, concrete or composite it is vulnerable to failure under many conditions such as extreme load or natural disasters which can lead to loss in human life and money. Literature review (chapter 2) shows that many researches have been conducted in the area of developing systems that can provide a real time structure monitoring to avoid a sudden collapse to the structures.

It was indicated in the literature review chapter that the prior research in monitoring composite structure while subjected to strain of different modes did not take advantage of the recently developed GI-PF-POF, 3D orthogonal woven structure, and high resolution OTDR that measures backscattering and signal loss of optics fiber would allow measurement of power loss due to different modes of strain and deflection (tensile, bending, pressure, torsion) and temperature. The lack of research in this area is the inspiration behind undertaking the current research.

2.2 3D orthogonal woven Preform

Three-dimensional (3D) textile structures preforms are formed using different technologies such as nonwoven, stack of 2D woven, and 3D woven and hybrids of these. The 3D woven fabric preforms are known for their advantages over the nonwoven and 2D woven preforms in that they provide higher resistance to crack propagation, eliminate delamination, faster in resin transfer, and higher fiber volume fraction (5). The 3D woven fabric preforms are integrated structure with three yarn systems that are combined without interlacing (i.e. no crimp in yarns) (6) (7) (8). Fiber optic can be integrated in 3D woven preforms by embedding optics fiber in y-direction and/or x-direction (Figure 2.1) (9). This can be easily done during the formation of the preforms. Nonwovens or 2D woven preforms do not provide such advantage.

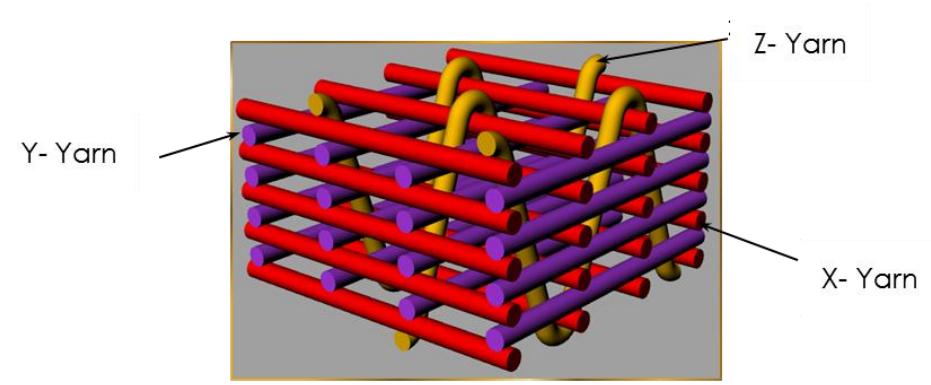

Figure 2.1 Schematic of integral 3D woven structure

2.3. Optical fiber

Optical fiber is made of glass or polymer and is used to transmit light along its length. Optical fibers are widely used in communication, which permits transmission over longer distances and at higher data rates "bandwidth" ~10-100 Gbps than other forms of communications. Fiber optic is used instead of metal wires because signals travel along them with less loss. Optical Fiber has many advantages such as lightweight, multiplex capability,

high sensitivity, and high broadband. Additionally, it is immune to electromagnetic interference. Numerous physical properties can be sensed with optical fibers like light intensity, temperature, pressure, rotation, strain, sound, magnetic field, electric field, radiation, liquid level, chemical analysis, and vibration (10).

The fiber consists of at least two optically dissimilar materials. One of these materials is low reflective index, which is called “cladding”, and the other material is placed in the center is called core which made of high reflective index material (Figure 2.2) (11).

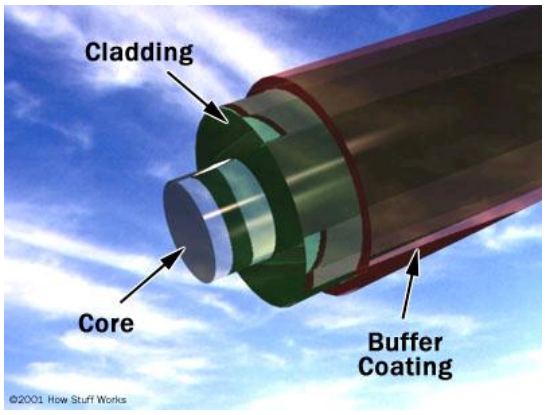

Figure 2.2 Fiber optic structure (11)

A light signal (waves) is transmitted through the core with low loss through the outer surface as a result of the presence of the clad (i.e. the light signal is trapped and allowed to transmit only along the core). Optics fiber sensors can be divided into three basic categories: phase-modulated sensors, intensity-modulated sensors, and wavelength modulated sensors (12).

2.4. Light rays

Light is an electromagnetic radiation of a wave length that whether it is visible or not. Light travels at a constant speed of approximately 300,000 km/second in vacuum. Light speed depends on the medium that the light travels through (13). Light sources are numerous,

sunlight is one of these sources, and sunlight emitted by the chromospheres of the sun around 6,000 Kelvin, 40% of the sunlight is visible. When light travels between different mediums it changes by either reflection or refraction depend on the medium whether it is a metallic or dielectric.

Light has many properties some of these properties such as interference, refraction and polarization can be explained with the wave model. But some other properties known as "photo effect" shows that the light made of very small particles called photons and doesn't behave like a continuous radiation (14). Each photon has energy expressed by Equation 1.

$$W = h * f \qquad [1]$$

Where W = the energy in Joule [J], h is Planck's constant = $6.626 * 10^{-34}$ Js and f is the frequency of the light in [Hz]. Frequency is calculated from c/λ, where c is the speed of light in vacuum ($2.99792458 * 10^{8}$ m/s) and λ is the wavelength of light in meter.

2.4.1. Reflection

Light ray can reflect not only on smooth metallic surface, but also on glass plates when the light incidents surface like a mirror with specific angle it will reflect with same angle. In this case the reflective angle will equal the incidence angle (Figure 2.3) (13). In general light ray reflect when the light travels from a medium with a refractive angle into a different medium with a different refractive angle, some of this light ray will refract where the incident light angle θ_1 equal the light reflected angle θ_2 as shown in Equation 6.

$$\theta_1 = \theta_2 \qquad [2]$$

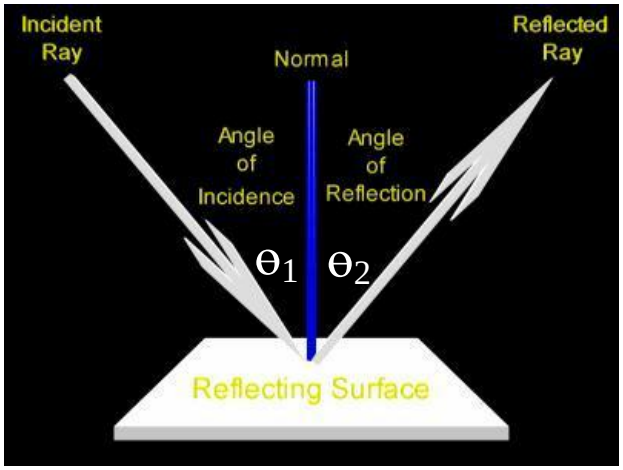

Figure 2.3 Incident angle angel and reflected angle
(Source: http://people.bu.edu/jwweider/Reflection.html)

2.4.2. Refraction

When light ray travels from medium to another the change of light direction will occur, this change in direction due to the change in light speed from one medium to another (Figure 2.4) (13) (14). When light travel from a thinner medium to denser medium at incident angle Θ it refracts at refraction angle α to the axis of incident, part of the light will reflect at angle Θ' to the axis of incident. Refraction is described by Equation 3.

$$\frac{Sin\ \Theta}{Sin\ \alpha} = \frac{n2}{n1} \qquad [3]$$

Where Θ is an incident angle, Θ' a reflection angle, and α is a refractive angle and n_1, n_2 are a refractive index of the thin and dense medium respectively.

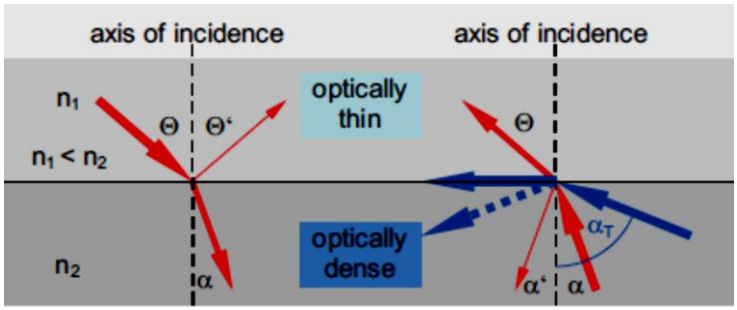

Figure 2.4 Refraction at a dielectric surface (14)

Critical Angle

When the light travels from a high dense medium to a low dense medium the refracted ray will refract away from the incident axis and the refracted angle Θ will increase. If the incident angle α kept increases the light ray will stop refract once α reaches a critical angle and then the light ray will reflect and this phenomenon called the total internal reflection (Figure 2.5). Critical angle θ_c is the smallest angle of the incident light that gives the total internal reflection; it can be calculated using Equation 4.

$$\theta_c = sin^{-1} n_2/n_1 \qquad [4]$$

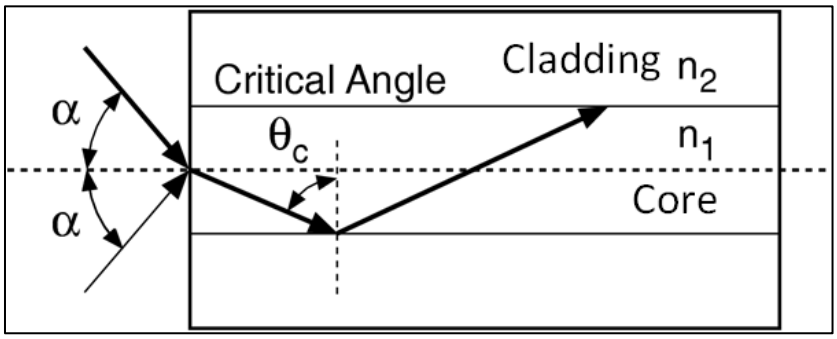

Figure 2.5 Critical angle θ_c (14)
Source: http://www.newport.com/images/webclickthru-EN/images/1381509.gif

Total Internal Reflection

Light transmit in the fiber optics with incident angle greater than the critical angle then the light ray will reflect in a series of total internal reflection between two medium core and cladding having two different reflective indices (Figure 2.6).

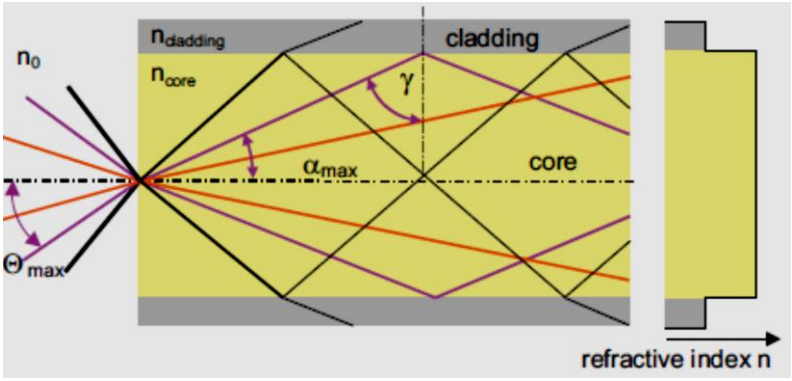

Figure 2.6 Light transmissions in optical fiber (14)

Refractive Index

When the light transmits from one medium to another the light velocity change, thus these change in the light velocity cause the light refraction. So the refraction index is a measure of how the light speed reduced inside this medium as shown in the Equation 5 (14).

$$n = c/v \qquad [5]$$

Where: n is a medium refractive index, c light velocity in vacuum and v phase velocity in the medium. Whereas the refracted light ray does not travel at same velocity as the incident light ray, Equation 6 shows the velocity of the refracted light ray (13)

$$v_2 = v_1 \cdot n_1/n_2 \qquad [6]$$

Where v_2 is the velocity of the refracted light ray, v_1 is the velocity of the incident light ray and n_1, n_2 are a refractive index of the two medium respectively.

Refractive Index Profiles

There are two refractive index profiles, namely step index and graded index profiles. In the step index, profile the refractive index for the core is constant along the cross section of the core diameter. The refractive index for the cladding is also constant. The profile of the refractive index of the core and cladding is shown in Figure 2.7 right. The light rays entered the optical fiber from one end are propagated along the fiber and exit from the other end (14). The light rays enter the fiber in many different angles to the fiber axis (Figure 2.7).

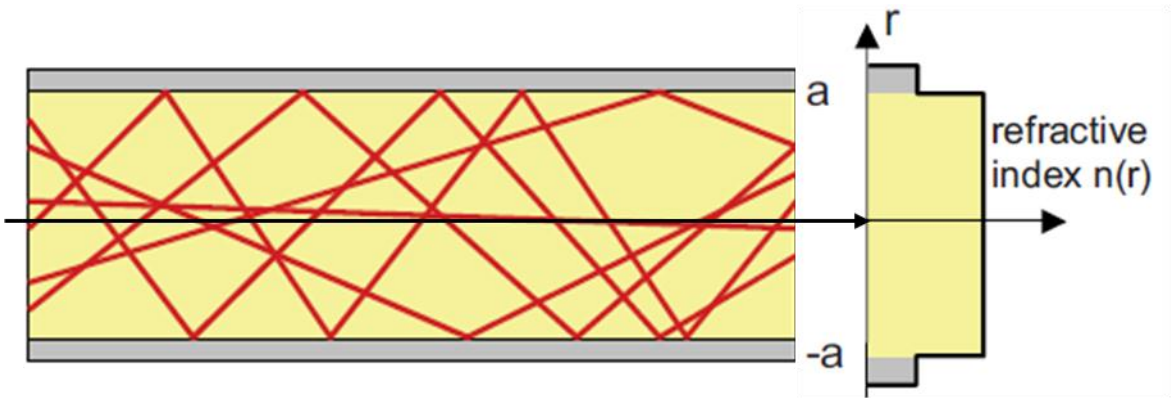

Figure 2.7 Light rays propagate into the step index (SI) fiber optics

Thus, not all the rays entered the optical fiber travel the same distance; the rays entered the fiber and being parallel to the fiber axis will travel the shortest distance while the rays that are at an angle to the axis travel longer distance. The rays with angles equal or smaller than the critical angle (see Figure 2.5) will be divided to reflected and refracted. This difference in distance cause a time delay between the light rays (15).

In graded index profile, the core made of radius-dependent refractive index and the cladding made of a constant refractive index (14). The refractive index in the center of the core is

higher than the refractive index of the core near to the cladding, so the light rays parallel to the fiber optics axis travel the shortest length with lower speed because the refractive index of the center of the core is high (see the profile of the refractive index of the core and cladding in Figure 2.8 right). On the other hand the smaller refractive index near to the cladding causes the rays to travel the longest distance at higher speed. Thus the light rays entered from one end will exit from the opposite end at the same time regardless of its position (Figure 2.8).

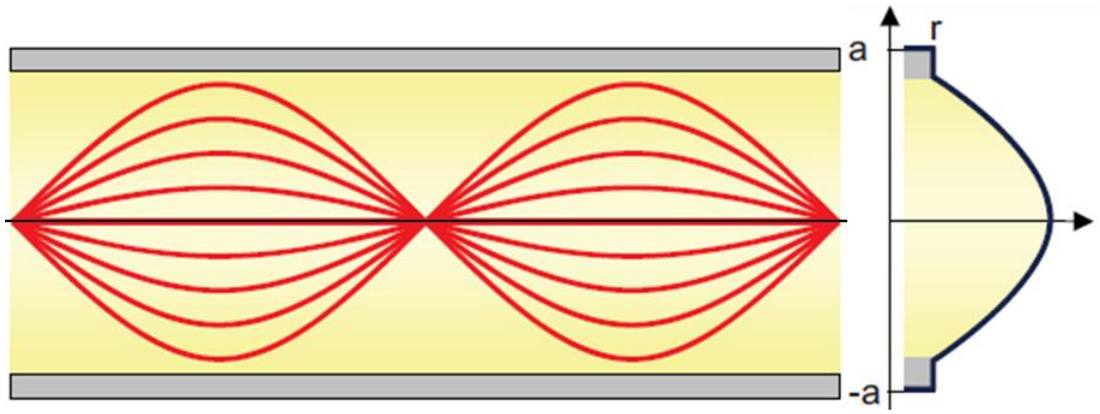

Figure 2.8 Graded index (GI) Fiber optics

Numerical Aperture

When light ray entering the optical fiber within a certain cone (Figure 2.9), which is known by the acceptance cone of the fiber, it will propagate through the core (16). Numerical aperture (*NA*) is the sin of the half angle of the full acceptance cone; *NA* is expressed in Equation 7.

$$NA = sin\ \theta_{max} \qquad [7]$$

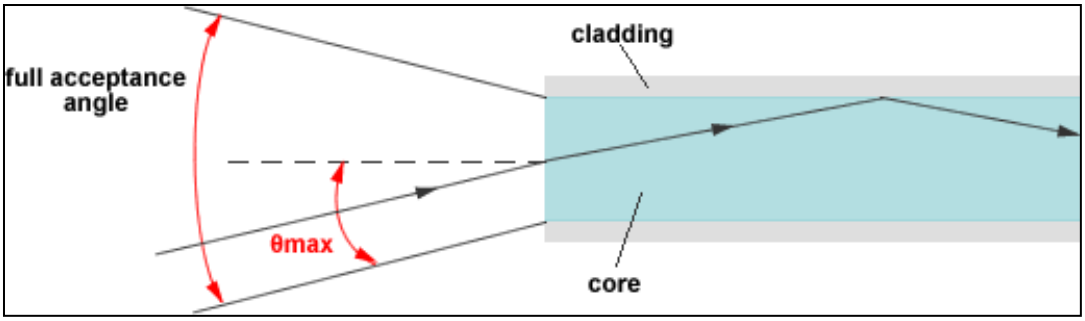

Figure 2.9 Acceptance cone (16)

2.5. Polymer Optical Fiber (POF)

Glass optical fiber (GOF) has been used in telecommunication for long time, glass fiber has a very high strength but at the same time it is very brittle and cannot handle bending, which makes it very hard to conform to small diameter. The brittleness of the GOF dictates the use of multi-layer of protective cable to protect the core (17). GOF core diameter ranges from 10 µm to 100 µm (15). Polymer optical fiber (POF) was developed in 1960's and was commercialized in 1970's (15). POF is flexible, easy to handle and economical compared to GOF. Additionally, POF is easier to splice and cleave compared to the GOF, which translates to low preparation cost when dealing with instrumentation using POF. Unlike the GOF, POF can be fabricated with large core diameter with less protected layers (17). POF core diameter ranges from 50 µm to 1,000 µm (15). Using a large diameter core simplify the light coupling through the fiber. However, POF are not suitable for long distance because of its high attenuation (18) (19).

Organic polymer polymethylmethacrylate (PMMA), polystyrene (PS) and polycarbonate (PC) are the most commonly used polymers as a core for the multimode fiber. These POF have a high attenuation of 1,000 dB/km, which limits it's used to a short distance communication. For instance, in case of PMMA core data can be transmitted at rate of 156 Mb/s over 100 m or 500 Mb/s over 50 m (18). One of the main reasons behind the high attenuation of the PMMA, PS and PC is the C-H bond vibration absorption, which can be

reduced by replacing hydrogen atoms with heavier atoms such as fluorine, chlorine and deuterium. These perfluorination and deuteration of polymers decrease the attenuation to <50 dB/km at the visible region of the spectrum.

Graded-index POF has been developed by professor Koike at Keio University, Tokyo, Japan in 1990. These fibers are made of amorphous flourinated polymers and commercially known as CYTOP®. The fibers have a low attenuation (≈30 dB/Km), which allows the transmission distance to be increased to 1 Km for a transmission speed of 1.2 Gb/s/km (15).

There are many applications based on POFs such as communications, images scanners, shape-defect detectors used in bottling plants, temperature, humidity, and liquid-level detectors. Conventional POFs established themselves in applications such as measuring distance; identify locations or positions (navigation systems), recognizing shapes, and detecting color, brightness, opacity, density, and turbidity (18).

2.5.1 POF Material

Extrusion process and drawing process are the two used method for producing the POF. Multimode step index (SI) fiber is considered the largest volume of fiber made in the recent years that is because it's easily mass-produced. On the other hand, the single mode fiber and gradient index fiber are more difficult to produce compared to multimode step index POF (17).

Core Material

In 1965, Du Pont introduced the first POF, with core made of PMMA, to the world (20). Thermoplastic such as PMMA, PS and PC are the best candidates for the POFs sensors (Figure 2.10). Amorphous polymers are the best polymer used as core of POF due to the uniform density of such polymers compared to the crystallized polymers which contain crystalline and amorphous regions (21). Table 2.1 shows the physical properties of PMMA, PS and PC. Thermoplastic polymers are high transparency and have a fiber forming ability, which makes it very suitable for producing the POF core or cladding. PMMA has an

attenuation of 1,000 dB/km at 650 nm wavelength. Most of the POFs have an attenuation <50 dB/km at wavelength 650 nm. Numerous research efforts have been conducted to address the reduction in the attenuation.

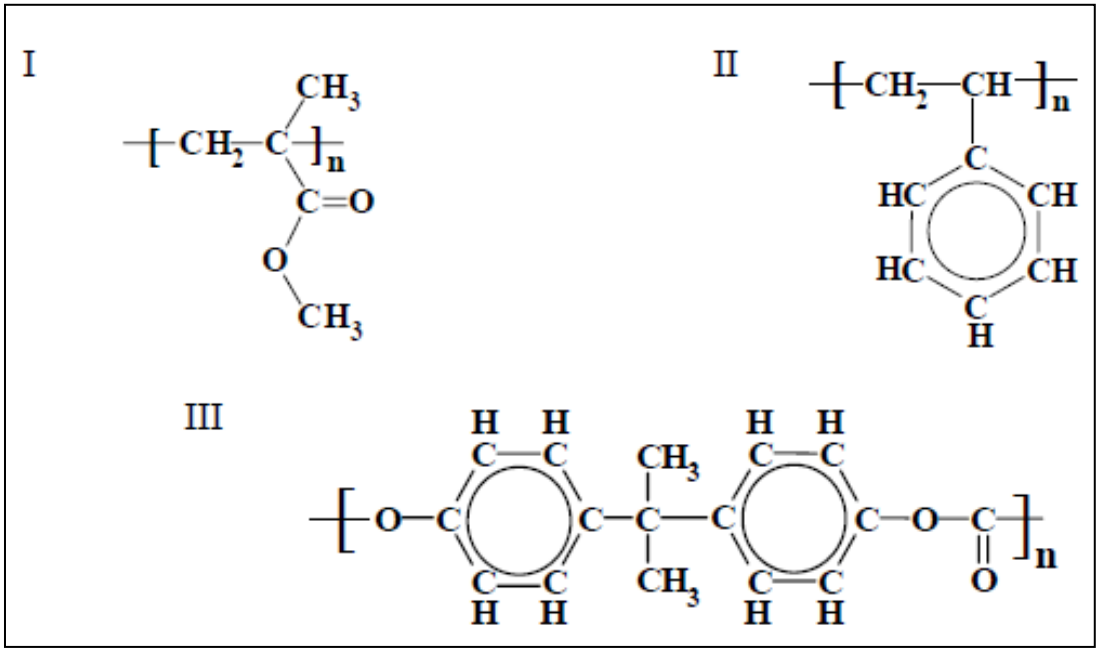

Figure 2.10 Molecular structure of (I) PMMA (II) PS (III) PC

Table 2.1 Physical properties of principal optical plastics **(21)**

Items	PC	PMMA	PS
Luminous Transmittance (%)	90	92	90
Refractive Index (n)	1.58	1.49	1.59
Abbe Value *(v)*	30	58	31
Glass Transition Temperature (F)	150	105	100

Poly Methyl Methacrylate (PMMA)

PMMA commercially is known by Plexiglass®. PMMA is made of the monomers methylmethacrylate (MMA) (Figure 2.11), and it is produced from ethylene, hydrocyanic acid and methyl alcohol. PMMA is characterized by resistant to water, petrol, diluted acid, mineral oil, turpentine oil. PMMA is a transparent material due to the amorphous structure of the polymerized material. All polymers from the methacrylate family are highly transparent, and have many advantages such as low cost, low processing temperatures, possibility of combining different materials, and easily modifying the original materials (22). Table 2.2 shows PMMA properties of the (14).

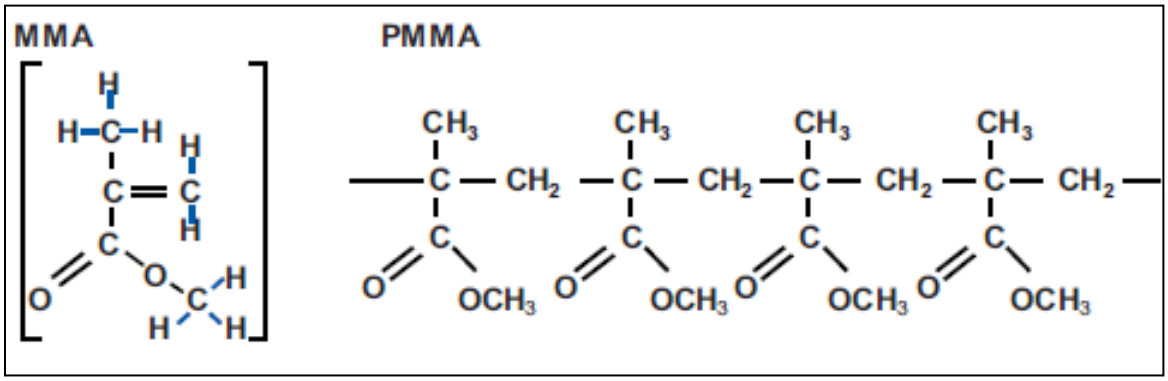

Figure 2.11 Molecular structure of PMMA

Monomers MMA consists of eight C-H bond, attenuation in PMMA POFs is caused by the vibration of C-H bonds or by its harmonic wave. Signal loss can be caused by the absorption or scattering of the light signal. Impurities such as voids, metal or water molecules on the fiber cause light absorption and scattering. This loss is function of the wavelength (23). Figure 2.12 show the transmission window of the attenuation at 530 nm, 570 nm and 650 nm. At wavelength 650 nm the attenuation is 125 dB/Km and at wave length 530 nm and 570 nm the attenuation is 90 dB/Km, which limit the length of the PMMA-POF to 100 m long (23).

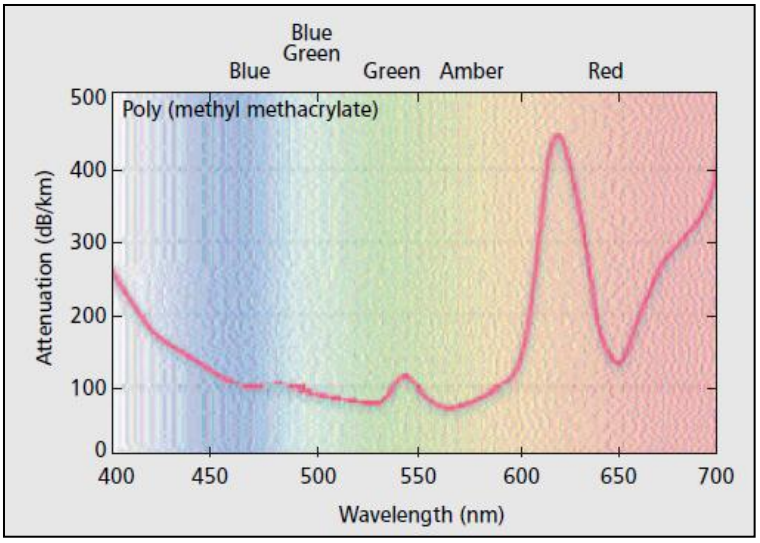

Figure 2.12 PMMA-POF attenuation as a function of wavelength

Table 2.2 Properties of the PMMA (14)

Properties	Value	Units	Test procedure
Refractive index	1.491	n_D^{20}	DIN 53491
Density	1.18	g/cm^2	DIN 53479
Tensile strength	80 (72)	MPa	DIN 53455
Charpy impact strength	15	kJ/m^2	ISO 179/1D
Flexural strength	115 (105)	MPa	DIN 53452
Modulus of elasticity	3300	MPa	DIN 53457
Glass transition temperature (T_g)	105	°C	[31]
Co-efficient of thermal expansion		K^{-1}	DIN 53752-A
-Linear	$7*10^{-5}$ (0-50 °C)		
-Volume	$2.72*10^{-4}$ ($< T_g$)		[31]
	$5.80*10^{-4}$ ($> T_g$)		
Shrinkage onset temperature	> 80	°C	[28]
Water absorption	30	mg	DIN 53495

Deuterated Polymer

Replacing the hydrogen atoms in C-H by heavy atoms like deuterium (heavy hydrogen) reduce the absorption loss of PMMA polymer significantly, which reduces the attenuation as it can be seen from Figure 2.13. Deuterium has twice the atomic mass compared to hydrogen, in nature 0.0156% of all hydrogen atoms are deuterium (≈1 atom every 6,400 atoms) (14) (15).

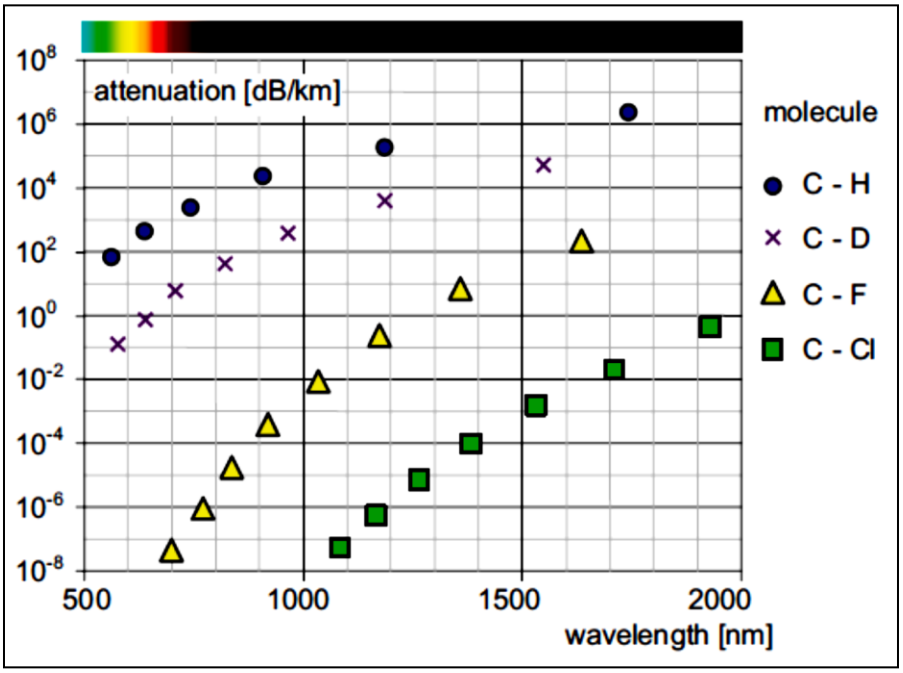

Figure 2.13 Absorption lines of C-X-bounds (14)

In 1977, DuPont developed the first step index (SI) POF with core made of deuterated PMMA (PMMA-d8) and its attenuation was 118 dB/km at 790 nm wavelength (24). In 1983, Nippon Telegraph and Telephone introduced the low loss SI-POF with 20 dB/km attenuation at 650nm wave length with core made of deuterated PMMA-d8 (24). The first deuterated PMMA-d8 Graded Index POF (GI-POF) was introduced by Keio University, Tokyo, Japan in 1992, the loss was 56dB/km at 688 nm wavelength and this fiber has the

highest band width of 2 GHz-km (24) (25). Figure 2.14 shows the attenuation loss of the PMMA and PMMA-d8.

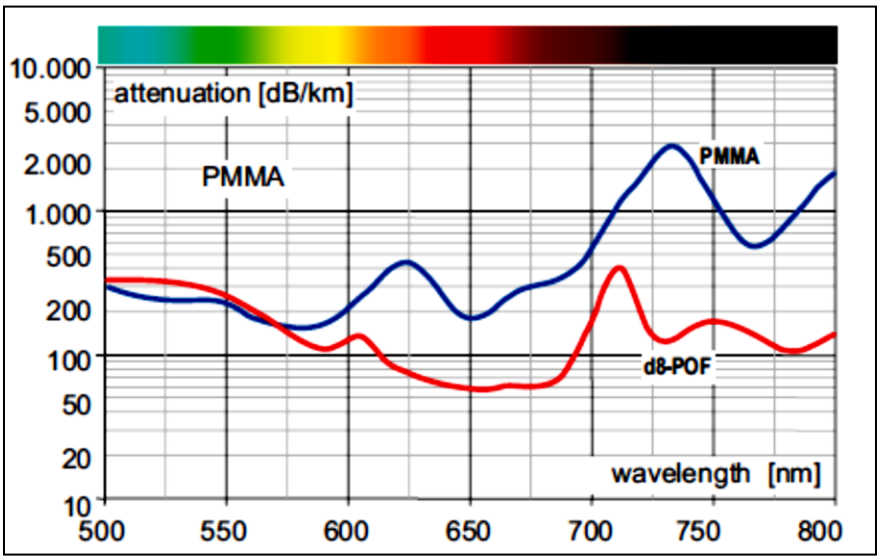

Figure 2.14 Attenuation of PMMA and deuterated PMMA (14)

GI-POF based on deuterated Polymer (PMMA-d8) has many advantages such as low attenuation and wide low absorption loss in wide spectrum near to the infrared (26). POF core and cladding made of PMMA-d8 has a low attenuation compared to POF core made of PMMA-d8 and cladding made of PMMA (Figure 2.15). Refractive index of PMMA is close to refractive index of PMMA-d8, so, PMMA-d8 can be used as a core material and PMMA can be used as a cladding material instead of using PMMA-d8 for core and cladding (27). Increase in the fiber diameter has a significant effect on the fiber handling; however, the small diameter has an effect on the cost reduction, thus, using the PMMA as a cladding will increase the ease of fiber handling and decrease the cost by keeping the core diameter small.

The disadvantage of the deuterated PMMA is the water vapor absorption. The deuterated PMMA absorb water vapor in the normal atmosphere, this water absorption lead to the hydrogen start slowly to replace the deuterium and increase the absorption loss which

increase the attenuation. This problem can be solved by coating the fiber using the water tight coating (14).

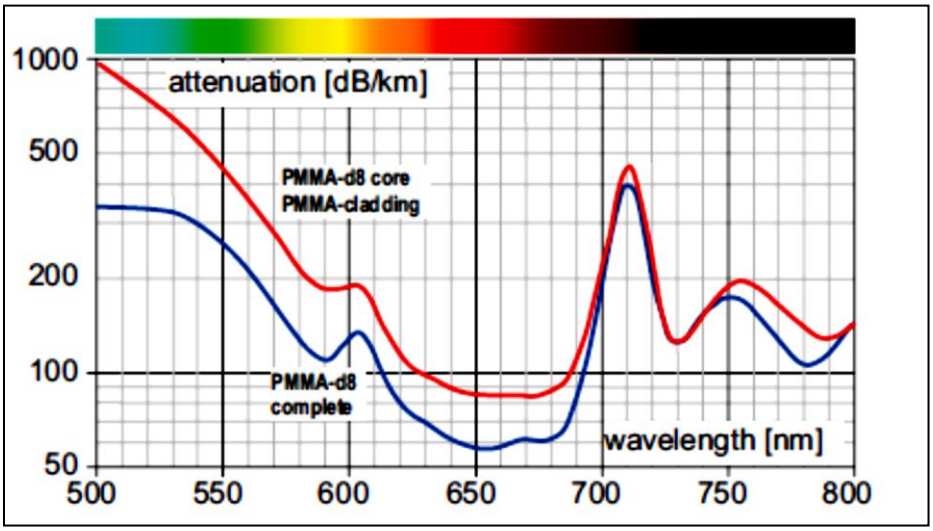

Figure 2.15 Effect of using PMMA and PMMA-d8 as cladding on the attenuation of POF made of PMMA-d8 core (14)

Fluorinated Polymers

Fluorine (F) is a chemical element that has an atomic number 9 and atomic mass higher than the hydrogen in C-H bond. Replacing the hydrogen in the MMA monomer (C-H) by fluorine to be (C-F) has a significant effect on lowering the attenuation of POF's compared to the deuterium and due to this replacement the absorption band is moved to the infra-red zone. Fluorinated polymer optical fiber (PF) has a lowest refractive index (n=1.340 at 650 nm, or n=1.336 at 1,300 nm) between all transparent polymer which is suitable for cladding. PF can't be used as SI fiber because there is no suitable material that can be used as cladding because the reflective index of the cladding material has to be lower than the reflective index of the core, which is not exist (28).

PF polymer optical fiber can be used as a graded index (GI) fiber with no cladding require, which require increase in the refractive index toward the fiber axis to achieve the GI-POF. Changing the refractive index across the fiber axis can be accomplished by doping and co-polymerization. In silica glass fiber the GI fiber can be achieved by changing the silica atoms with germanium (GE).

Doping is the process in which small molecules is added between the long chain of core material in order to increase the refractive index. Doping material has to stay within the core and not diffuse out. It has low absorption properties for the transmitted light at a desired wave length (28) (Figure 2.16).

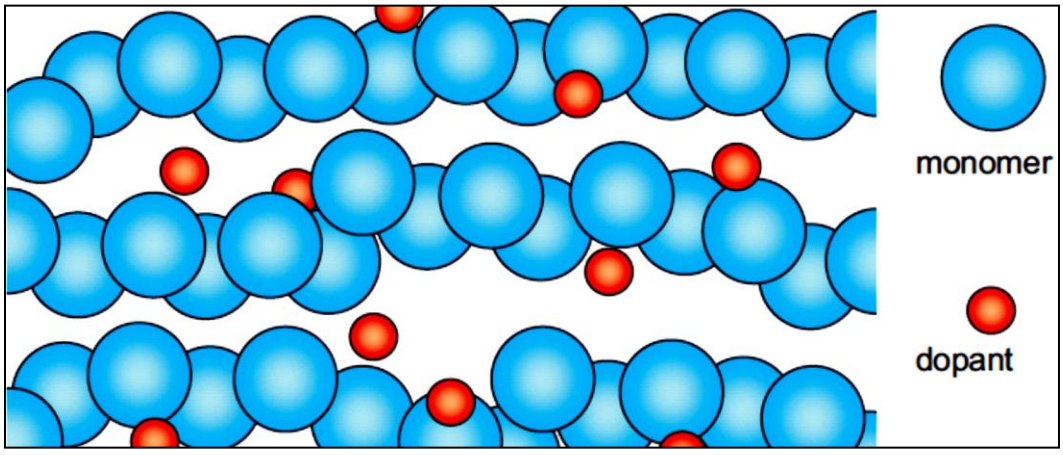

Figure 2.16 Refractive index variation by doping

Co-polymerization, Polymer's chain containing two different monomers, is a method that is used for producing GI-POF. PF-GI-POF refractive index depends on the ratio of the two monomers. Two monomers have to be transparent and the sequence has to be irregular otherwise the loss will increase due to the scattering. The forces between the two different monomers have to be higher than the forces between the molecules of the same monomers in order to decrease the vibration and attenuation (28) (Figure 2.17).

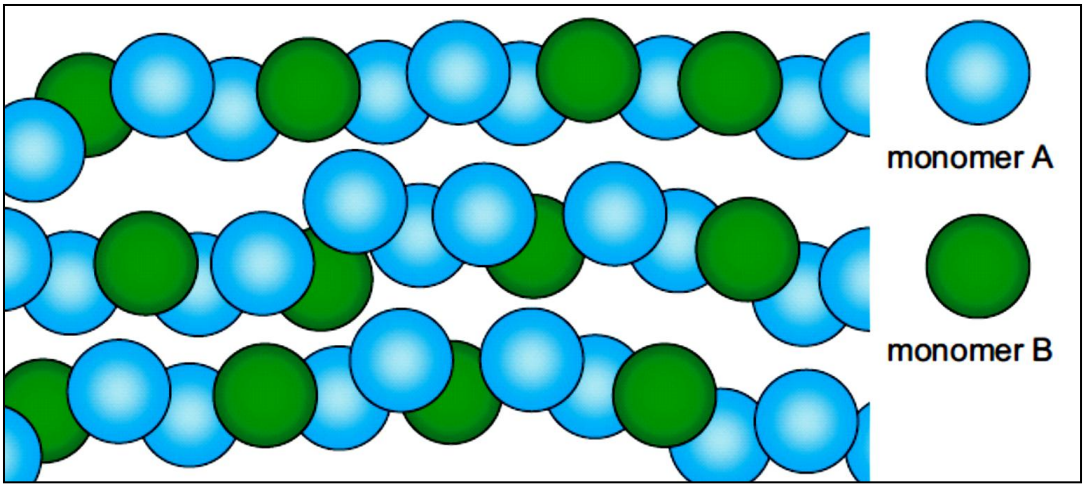

Figure 2.17 Refractive index variation by co-polymerization

2.5.2 POF Developments and Fabrication

Production of polymer optical fiber has many advantages over the glass optical fiber where the POF production can be done below 200 °C compared to glass optical fiber, which need over than 1,200 °C. There are four types of POF: SM-POF, multi core MC-SI-POF, multilayer (ML) step index ML-SI-POF, and graded index GI-POF (29). Figure 2.18 shows different types of POF (30). MC-POF composed of numbers of small core to decrease the bending loss. MC-POF has data transmission rate 500 Mb/s for 50 m. ML-SI-POF core is made of many layers and each layer has a different refractive index.

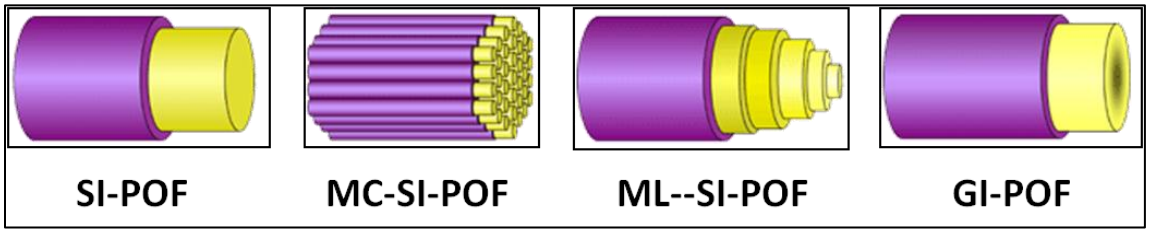

Figure 2.18 Different POF's profiles

Pure step index profile is the first profile of POF fibers, where the core has a higher reflective index than the cladding. Core is made of pure PMMA material with refractive index 1.49 and cladding made of Fluorinated polymer with refractive index 1.42 and 0.5 numerical aperture (NA). Du Pont has introduced the first POF in 1966 and was named "Crofon" with core material made of Polymethylmethacrylate (PMMA) and Fluorinated-polymer for cladding. In 1977, the first commercial SI-POF was produced by Mitsubishi Rayon under trade name "Eska". Asahi chemical and Toray also produced POF in 1980's.

Kaino et al. reported that lowest attenuation value at wavelengths 660, 780, and 850 nm was 20, 25, and 50 dB/km respectively. They produced POF's from polymethylmethacrylate as a core and Fluorinated alkyl methacrylate copolymer as cladding (31). Kaino et al. have developed a closed polymerization process and fiber drawing method for producing SI-POF. This developed system prevents any dust, contamination, air bubble that can affect the purity of the produced SI-POF. Eliminate such impurities and defects decreased the attenuation loss that led to the prevention of the light scattering.

Continuous Extrusion of Core and Cladding

Continuous extrusion is considered one of the most well-known methods for producing SI-POF. Mitsubishi Rayon has introduced this method for the first time in 1974; SI-POF was produced under name Eska. Purified monomers, initiator, and chain transfer agent are fed into a reactor. Gear pump is used to pump the resultant polymer from the extruder to devolatilizing extruder. Devolatilizing extruder develop a rapid reduction in pressure, which cause evaporation to the excess monomer and return the excess monomer to the reactor. Additional extruder is used to add the cladding layer, lower reflective index, to the produced core material. (Figure 2.19) (32).

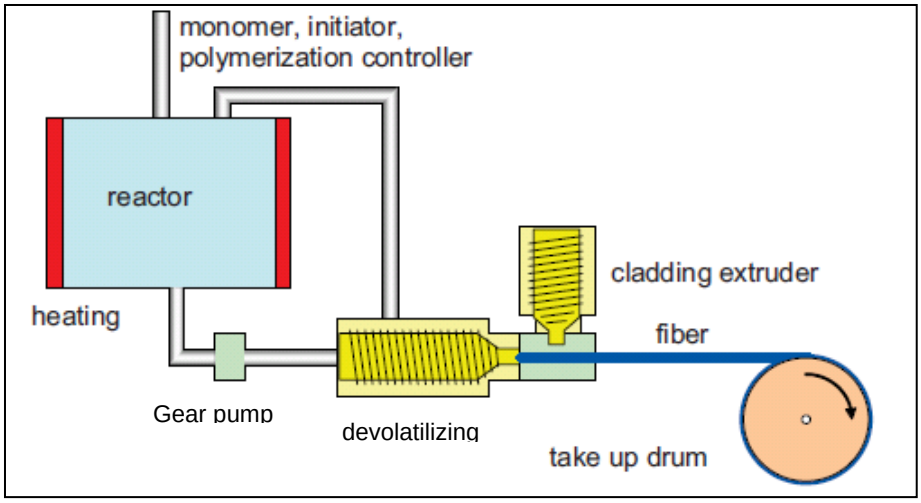

Figure 2.19 continuous extrusion

Continuous extrusion is a complex production method. Monomer purity, reaction temperature, amount of initiator, amount of chain transfer agent, and degree of polymerization has to be optimized to ensure a good POF quality. Polymer degradation is a disadvantage of this method and it occur due to the shear between the polymer and contacted metal during the pumping and extrusion, this shear cause increases the optical loss; reduce the produced fiber length and thermal degradation. Regular cleaning of the machine is required to reduce the fiber contamination from the preceded process.

Chromis fiber optics, previously Lucent (OFS), has developed the continuous extrusion for producing SI-POF and GI-POF (33). Two different extruders were used for producing the core and cladding material, doped polymer and un-doped polymer were used for core and cladding respectively. Melted core and cladding polymers are compounded in the co-extrusion head (Figure 2.20) to form core and cladding fiber with step index profile.

Graded index profile is produced by using a heated diffusion tube located below the co-extrusion to diffuse the low molecule dopant from the core into cladding. Wide variety of refractive index can be produced by means of controlling temperature, process time, and relative flow rate of core and cladding material. Additional layer is extruded for protection of

the POF. The extrusion of the protective layer is located below the heated diffusion tube. Resultant fiber is drawn to produce a desired fiber diameter (34) (35). Produced fiber has an attenuation of 25dB/Km at wave length 850 nm (Figure 2.21); band width of typical fiber at this wavelength is ≥400 MHz-km (36).

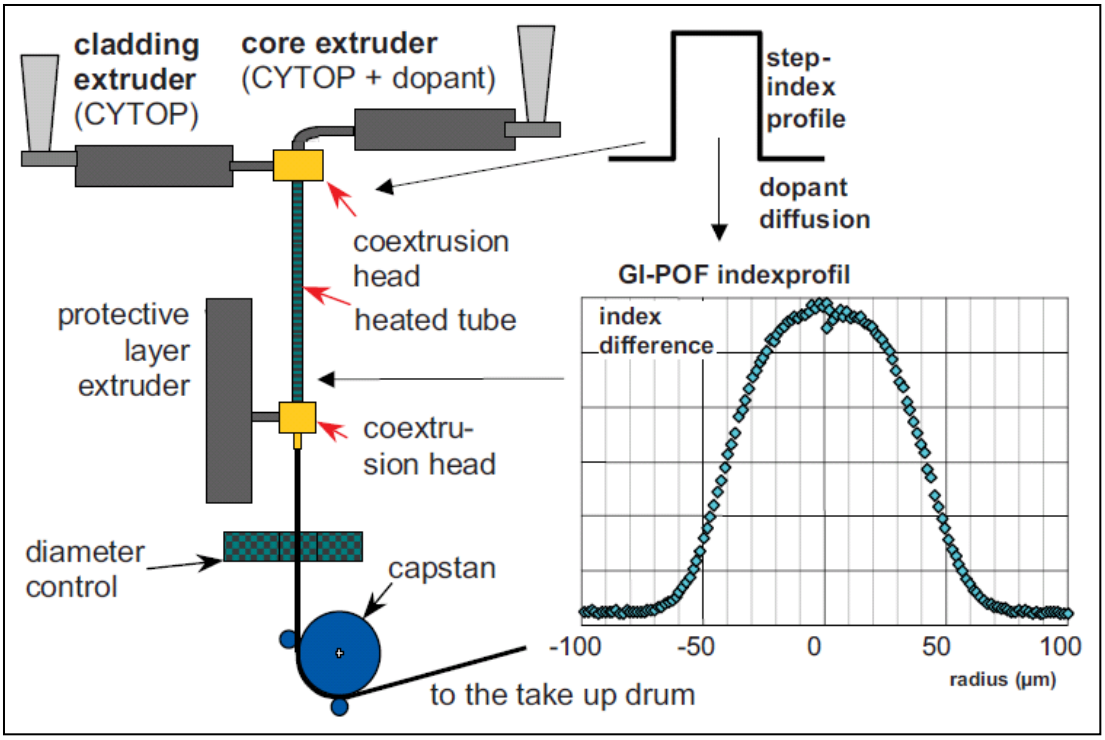

Figure 2.20 Chromis fiber optic continuous PF-GI-POF

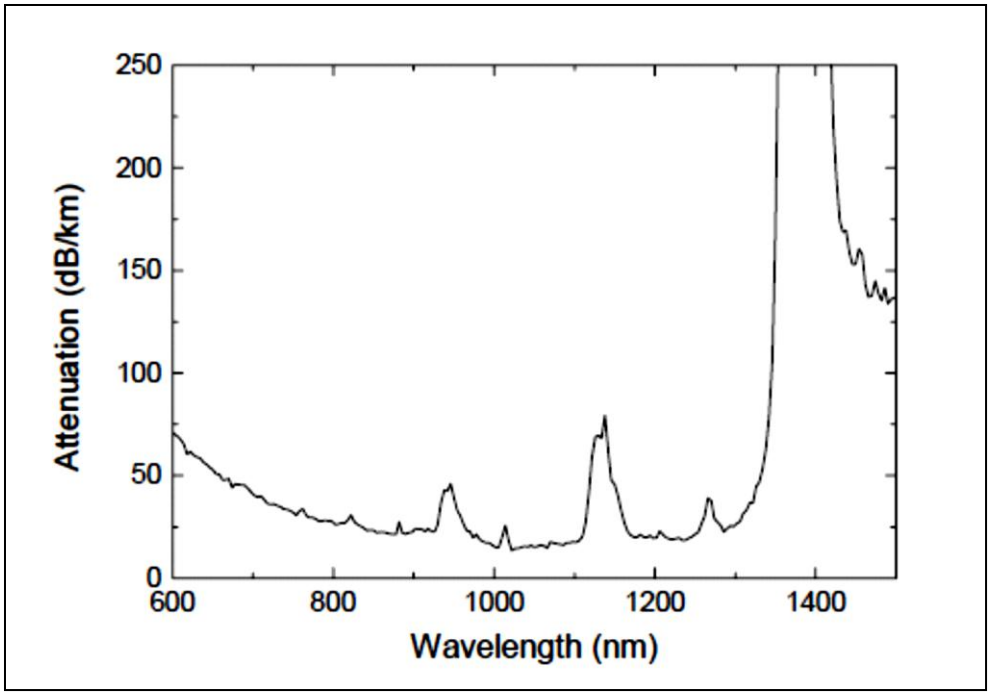

Figure 2.21 Chromis PF-GI-POF

2.6. Fiber Optics Loss Testing Method

There are many different methods for verifying optical fibers ability to carry light. These methods are used for testing optical fiber quality. These test methods, such as optical signal loss test and optical return loss (ORL) test, measure the loss of optical fiber using end to end loss technique. However, they can't determine the location of defects that cause such power loss. Today, there is test equipment known as optical time domain reflectometer (OTDR) that can measure fiber loss, determine the location of the defect, and may assist in defining the causes of this fiber loss (37).

2.6.1 Loss Test Set

For decades, measuring optical fiber transmission loss was the only avenue for measuring fiber optics signal loss. Loss test sets consist of light source such as laser device and power

meter (Figure 2.22). Laser device such as Helem Neon He-Ne (650nm) is used as a light source and located on one end of the fiber optics. Optical detector located on the other end of the optical fiber and connected to a power meter. Loss test set can only measure the transmitted loss through the optical fiber without determining the location of the problem or identifying the reasons (such as dirty connector, bad splice, bend or damage on the fiber, etc.) behind the signal loss. Loss test set can be used with glass or polymeric optical fibers. The main disadvantage of loss test set is that the test is maintained on both end of the fiber, which means the light source has to be connected to one end and the detector and the power meter have to be connected to the other end. As stated above this test method can't be used to determine the location of the problem so this test has to be repeated in different length in order to determine the location of the defect or the problem.

Figure 2.22 End to end loss test set

2.6.2 Optical Time Domain Reflectometer (OTDR)

OTDR is a used to test optical fiber, measure the transmission loss, determine the location of defects, and determine optical fiber length (38). Optical fiber manufacturer use OTDR to test optic fibers behavior for quality control purpose. OTDR is also used for testing optical fiber during the installation, maintenance and restoration of optic sensor based systems (37). Advanced OTDR can be used to determine the fiber signal loss, return signal loss at each connector, fusion splices and report whether this loss is within the tolerance range.

The principal of OTDR is sending a pulse of a light ray, with specific pulse width, into an optical fiber; light pulse will scatter along the optical fiber due to the impurities and the fiber imperfection. Part of the launched light is backscattered to the input direction, this reflected

pulses will be detected at the input with total time duration that taken the light to travel from the input to reflect back to the input again (39). OTDR can detect any change that may occur along the optical fiber through the attenuation. OTDR can be used to measure attenuation in distributed optical fiber sensors whether it's GOF or POF (40).

Pulse of light is launched into optical fiber end; the backscatter is detected and recorded as a function of time. The speed of the light, the time for light to launch and backscattered to the input, can be converted to a distance, thus the location of defect such as bending or fiber strain can be determined since each type of these defects affects the light backscattering in different ways. OTDR can be used to determine micro bending, temperature change, mechanical stress, and strain (41).

There are many types of OTDR; the simple and standard form of the OTDR can test optical fiber at only one wavelength. Single mode OTDR can only measure the optical fiber attenuation of single mode fiber at wavelength 1310, 1550 or 1625 nm whereas the multi-mode OTDR can measure the fiber attenuation at 850 and 1300 nm. Standard OTDR consists of laser and optical receiver. Laser is connected to the front panel connector where the tested optical fiber is connected to the OTDR through a coupler. Optical receiver (detector) is connected to the coupler with the laser (Figure 2.23).

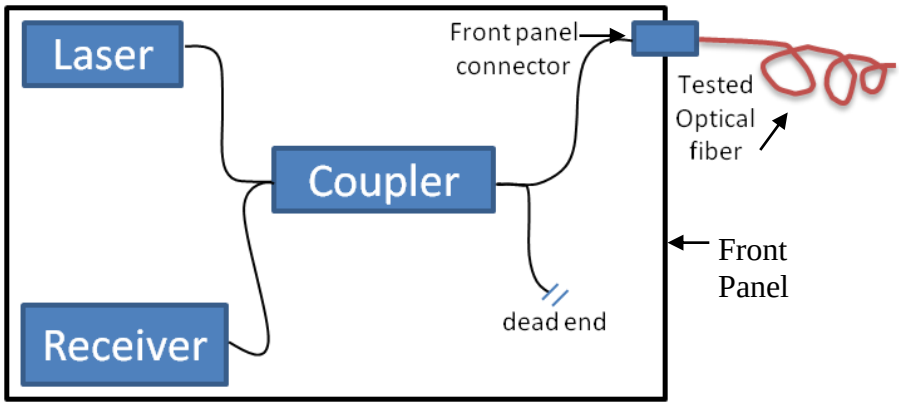

Figure 2.23 Standard OTDR principal components

Laser launce a short pulse of the light, this short pulse is directed to the coupler and then to the front panel to continue into the tested optical fiber. As the light travel through the optical fiber, some of this light will attenuate due to the splice, presence of connector or bend on the fiber. Some of the defects cause a Fresnel reflection (defined later) such as dirt connector, splice that causes the light to reflect back to the OTDR. Stains due to bending, tensile, torsion, and pressure and fiber impurities cause what is known by Rayleigh scatter (defined later). Some of light will back scatter toward the OTDR. Backscattered or back-reflected light arrive to the OTDR and reach the coupler which direct them to the receiver. Receiver is converting the optical power into an electric current and gives the loss, light reflection and the exact distance of the signal loss from the front panel connector (37).

Advanced OTDR can measure the fiber attenuation at two different wavelengths which require having two lasers, two optical detectors and wavelength-division multiplexer (WDM). Single optical detector can be used with single mode OTDR (Figure 2.24). Single mode OTDR has some difficulties over the multi-mode OTDR such as the backscattered power is less than the multimode OTDR and fabrication of the coupling device is very difficult (42).

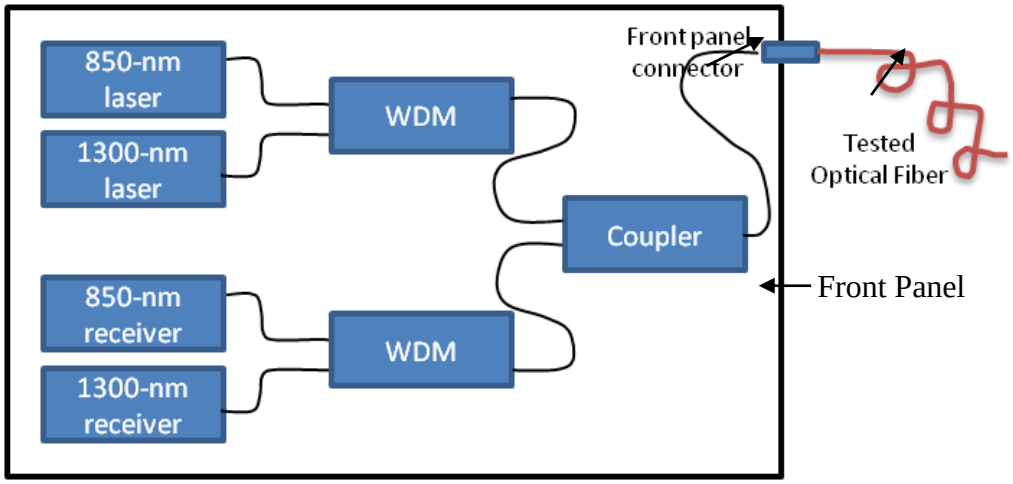

Figure 2.24 dual Multi-mode OTDR principal components

Photon counting detector module is considered the most advance detector implemented in the advanced OTDR. This type of photon-counting module is converting one photon at 1550 nm to one visible photon and detects this visible photon with a silicon photon-counting device (43).

OTDR Waveform

Figure 25 shows the typical OTDR signal trace or OTDR waveform. The output signal response is known as an optical fiber signature. The graph in Figure 2.25 shows the backscattered light level (attenuation) as a function of distance along the fiber length. Reflection and loss are shown in the graph as two different features along the fiber length (44). Reflection causes a sharp spike whereas the slope is caused by Rayleigh scattering and the drops in the straight line portions are caused by the loss. Reflection on OTDR signal can be caused by small bubbles in the fiber, Fresnel reflection caused by breaks, bad connector, strain and fiber under load. Drop on Rayleigh backscattering is due to the loss, which is caused by bending on the fiber or fusion defects. First and last spike shown in Figure 2.25 are caused by the front panel connector and fiber optic termination respectively, which always detected (45).

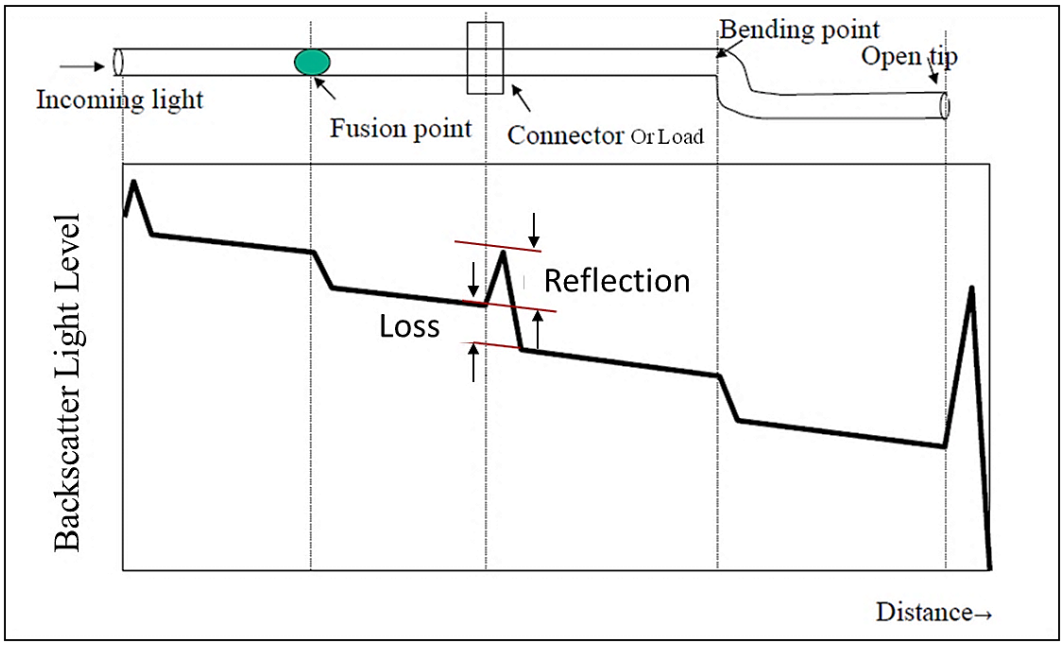

Figure 2.25 OTDR typical waveform, adopted (44)

2.7. OTDR Specification

There are many characteristics that affect the accuracy of the OTDR such as attenuation, dynamic range, Rayleigh scattering, attenuation dead zone, event dead zone and pulse width. These characteristics will be discussed to show how it can affect the quality and the accuracy of the OTDR.

2.7.1. Dynamic Range

Dynamic range is considered one of the very important specifications of the OTDR and reflects the measurement capability of the OTDR (45). Dynamic range is measured in decibels (dB). There are several definitions for the dynamic range but all have same bottom line. OTDR manufacturer are competing in increasing the dynamic range of their OTDR. Dynamic range can be defined as a maximum optical power P_{max} to a minimum optical power P_{min} as shown in Equation 8.

$$D=K * log\ (P_{max}/ P_{min}) \qquad [8]$$

P_{max} represents maximum observed backscattered power at the coupler or at the front panel connector and can be expressed by $P_{bs}(0)$.

P_{min} may represent the noise floor P_n or backscattered power from the far end of fiber and can be expressed by $P_{bs}\ (L)$, which is function of L (length of optic fiber).

K is a constant depends on the type of dynamic range. $K = 5$ for a one way loss and $K=10$ for two way loss (45). Equation 9 shows the dynamic range for K=5 (46).

$$D=5\ log\ (P_{bS}\ (0) / P_{bs}\ (L)) \qquad [9]$$

Where:

$$P_{bs}(0) = S\alpha_s \Delta z P_o T_s \qquad [10]$$

$$P_{bs}\ (L) = S\alpha_s \Delta z P_o T_s 10^{-2\alpha L/10dB} \qquad [11]$$

$$\Delta z = wc/ n_{gr} \qquad [12]$$

Where:

α_s – scattering coefficient, [1/km], as[1/km] = 0.23as[dB/km],

S – Backscattering factor,

P_o – optical power lunched in the fiber [W],

Δz – pulse length [m],

T_s – Coupler round trip losses,

w – Pulse width [s],

c – Speed of light, $2.99792458*10^8$ [m/s], and

n_{gr} – refractive index of optic fiber

Other dynamic range definition is the maximum length of fiber that the longest pulse can reach. The higher dynamic range is the longest distance that the light can travel inside the fiber in case there is no loss (Figure 2.26). In other words, connectors, splice, fiber bend and brakes cause loss on the signal, thus the distance that the pulse travel will be shorter than the distance the pulse travel with no loss at the same dynamic range. So, as OTDR dynamic

range increases the backscatter level increases and floor noise decreases. Most of the dynamic range specifications are given using the longest pulse width at a three-minute averaging time and signal-to-noise ratio (SNR) = 1 (47).

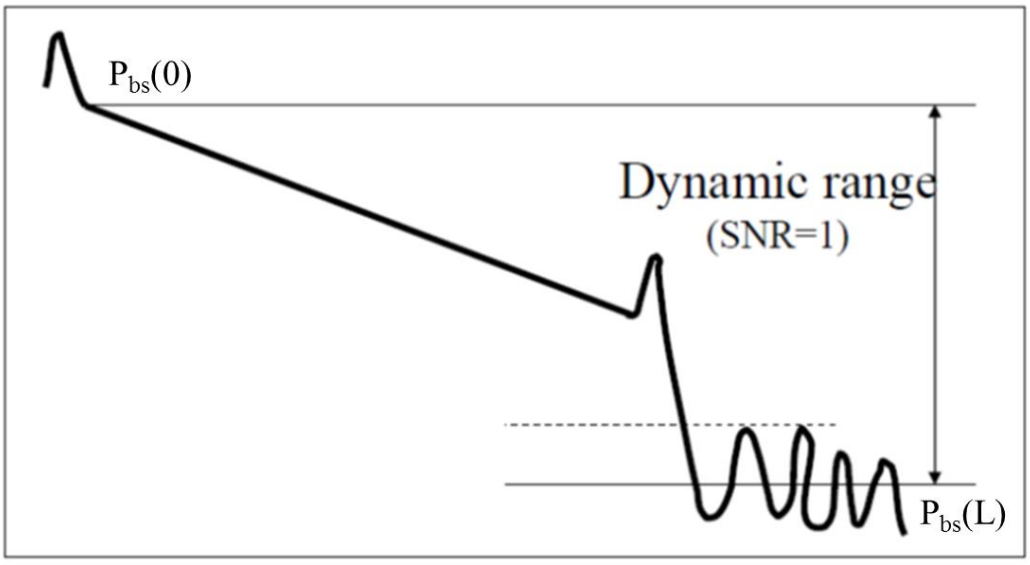

Figure 2.26 Dynamic Range (44)

2.7.2. Event Dead Zone

Event dead zone is defined as the minimum length of the fiber between two events that OTDR can detect separately. However, the individual loss of the two events cannot be measured if the two events occurred at length shorter than the attenuation dead zone. If two events occur below the event dead zone, the OTDR will not be able to distinguish them separately. In other words the two events will appear as one. Figure 2.27 shows an example of OTDR waveform with event dead zone of 1 m. Two reflections with 1 m apart can be detected but the individual loss can't be measured. Most common method of measuring the event dead zone is measuring the distance at -1.5 dB from each side of the reflective peak (Figure 2.28).

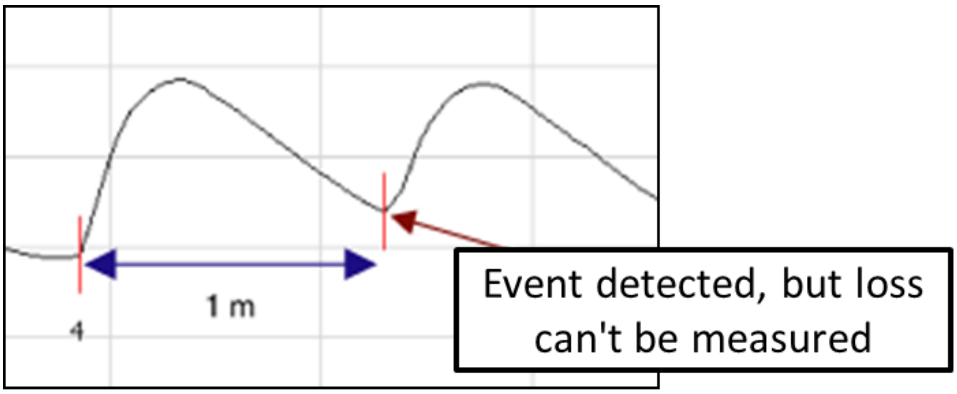

Figure 2.27 Event Dead Zone (47)

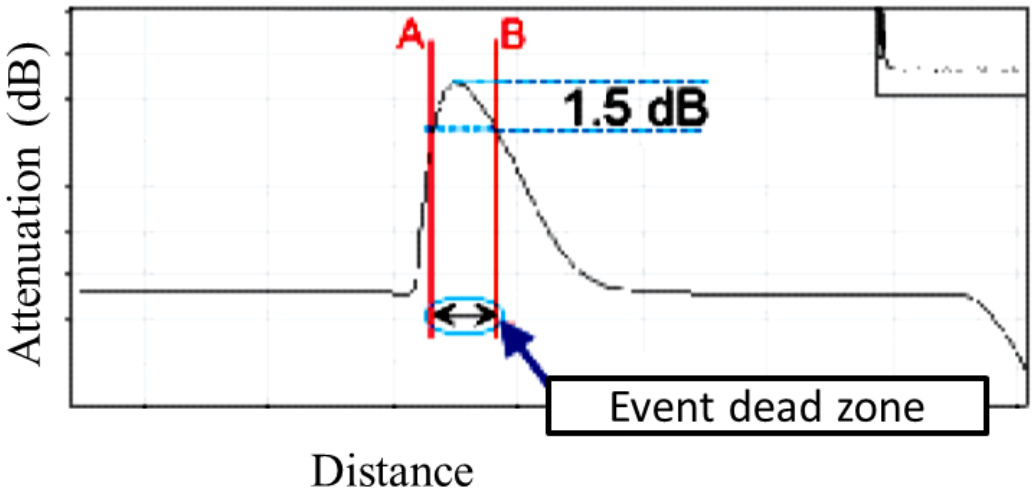

Figure 2.28 Event Dead Zone measuring techniques (47)

2.7.3. Attenuation Dead Zone

The attenuation dead zone is defined as the minimum distance from the beginning of the reflective event until the fiber backscattered return to 0.5 dB of its backscattered level. Attenuation dead zone can be described as the minimum distance after a Fresnel reflection until the OTDR can measure the event loss (Figure 2.29) (48).

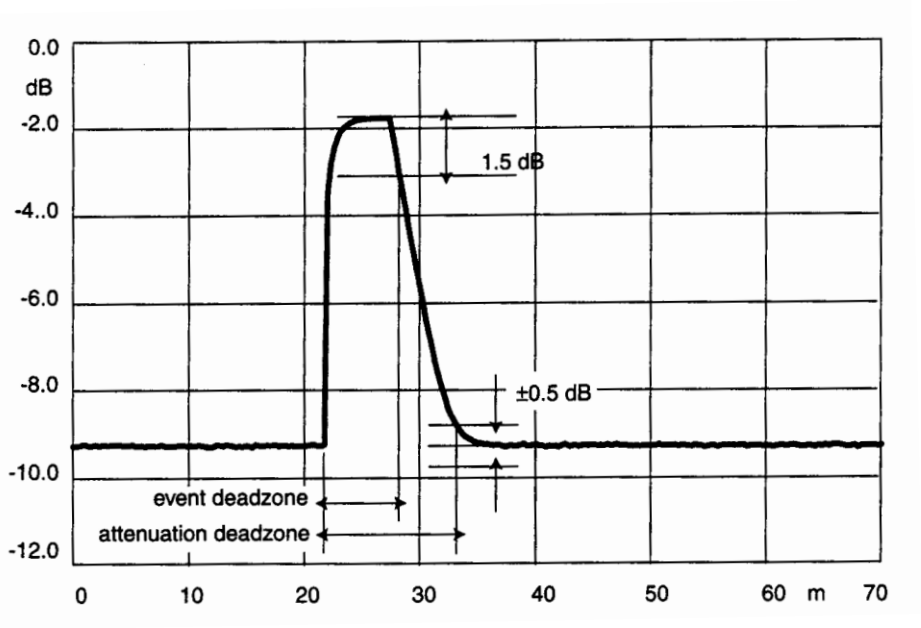

Figure 2.29 Attenuation dead zone (48)

2.7.4. Pulse Width

Pulse width is the amount of light that being launched into tested optical fiber, this pulse width controlled by the time of laser source being on. The time is converted to distance to give the length of the pulse. Each pulse carries energy that able to travel into the optical fiber and reflect back. If the pulse has a short width then the distance traveled is short. Long fiber needs longer pulse width to reach the fiber end and reflect back but the longer pulse width produce longer dead zone. This is a disadvantage of the OTDR for some applications when high resolution is required.

2.7.5. Rayleigh Backscattering

As shown in the typical OTDR waveform, the output signal consists of main slope which represent the signal attenuation according to Rayleigh backscattering and reflection spike according to Fresnel reflection. When light travels inside the optical fiber the fiber impurities cause signal attenuation and backscattering. The fiber impurities cause absorption and

reflection to the traveled light. When light hit fiber particles the light will scatter and redirected in different directions, which causes signal attenuation and backscattering (Figure 2.30). This phenomenon is called Rayleigh backscattering. Rayleigh backscattering is used to calculate the level of attenuation in the optical fiber as a function of distance, which is shown by a straight slope in an OTDR waveform signature (47).

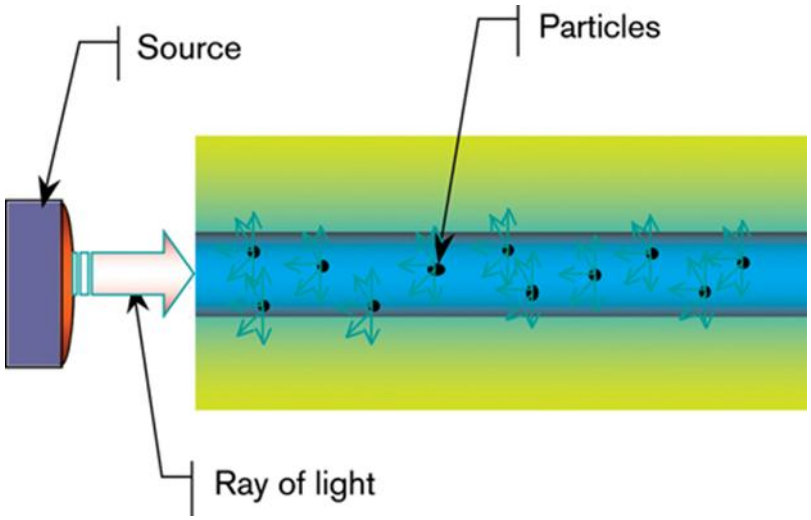

Figure 2.30 Rayleigh Backscattering (47)

2.7.6. Fresnel Reflection

As previously explained, OTDR waveform carries two types of backscattered light, Rayleigh backscattering and Fresnel reflection. Fresnel reflection is due to dirt connection, fusion or open fiber, these all can be considered as physical defects. Fresnel reflection occurs when suddenly change happened to fiber refractive index (change from fiber material to air) and causes the light to reflect back on the fiber. This Fresnel reflection appears as a spike on OTDR waveform (47).

2.8. Composite Material

As stated earlier, the overall objective of this research is to develop and evaluate a real time monitoring systems using embedded optical fiber sensors into composite structure. The literature review addressed the pros and cons of current evaluation systems of optic fiber and their signal analyses. This section of the literature review addresses the manufacturing processes of composite structures including the glass fiber, which will be used as the fiber to form the preforms to be used for this research. Understanding the preform structures of this research lead to the understanding of how the optic fibers will be embedded inside such preforms.

2.8.1. Glass Fiber

Glass fibers, which are commonly used in many applications of composites, are based on silica Sio_2 with additional of oxides of calcium, boron, sodium, iron and aluminum (49). Glass fibers are amorphous; heating glass fiber for long time at high temperature can cause reduction in strength due to some crystallization. The most popular types of fiber glass, Electrical glass (E-glass), (C-glass), (S-glass) and Reinforcement glass (R-glass). E-glass is distinct by corrosion and chemical resistance, well drawing, high strength, high stiffness, electrical, and weathering (high UV and visible light resistance) properties. C-glass characterized by high corrosion resistance, low strength and excellent chemical resistance. S-glass is high strength, high modulus, temperature resistance and more expensive than both E-glass and C-glass (49) (50). R-glass is used in reinforcing concrete because of its alkali resistance. S-glass fiber is 40 % higher tensile strength, 10 to 20 % higher compressive strength, and high abrasion resistance compared to E-glass (51).

Fiber glass has a high strength to the weight ratio compared to steel wire. Fiber glass is characterized by heat and fire resistant, chemical resistance and is not affected by bacteria or insects attack. High thermal conductivity coefficient of fiber glass increase moisture resistance and enhance thermal properties of fiber glass, which make it good for electrical insulation purpose. Because of its high strength and good electrical properties, fiber glass is

used for Radom application in aircraft industry. Printed Circuit boards are made of fiber glass due to its dimension stability and electrical properties (52).

Glass Fiber production

Glass raw materials are melting in reservoir or high temperature furnace. Melting temperature depends on the raw material composition, usually around 1260 °C (52). The molten glass fed into a platinum tank or bushing, this platinum bushing has a high numbers of holes (spinnerets) that permit the molten glass to pass through under the gravity to form the fibers (49). The fine filaments are drawn mechanically as the fibers come out from the spinnerets. Then the glass filaments (tow) are passed through water spray and revolving belt for lubricating or coating to provide protection. Produced fibers are wounded into packages and dried afterward.

Lubrication or coating process is very important for glass fiber manufacturing. Lubrication process provides protection to the fiber surface and bind glass filaments together. Lubricated or coated fibers can withstand the weaving process. Fiber glass can be coated with chemical treatments in order to provide good adherence properties to the resin during the composite formation process.

Fiber diameter is controlled by adjusting the viscosity of the melting raw materials. Material viscosity depends on the material composition, temperature, spinneret diameter, and winding speed. E-glass fibers diameter ranges from 8 to15 μm (50) (49).

Atomic structure of the fiber glass is responsible of fiber strength and modulus. Silica based fiber glass comprises a covalently bonded tetrahedral with silicon at the center and oxygen at the corners. These bonds break and form an ionic bond with oxygen by using low valiancy elements such as Ca, Na and K. Adding more valiancy elements decreases fiber stiffness and strength, which improve fiber formability.

Composite materials are rapidly spreading and replacing steel, aluminum, cooper and other engineering material. Composite materials are being used in many different applications such

as, aircraft, building, containers, armor vehicle and bridges. Composite material characterized with its light weight and good mechanical properties (52). Thus Composite material has many advantages over the metals materials (11).

Composite material consists of two or more material, these materials usually produced alone and bonded together afterward. Composite material properties are different from any of its components. There are many different types of composite such as Polymeric Matrices Composites (PMCs), Metal Matrix Composites (MMCs), and Ceramic Matrix Composites (CMCs). These types of composites are classified according to the matrix nature (49). PMCs usually reinforced with ceramic fibers, glass fiber or carbon fibers. These fibers are high strength and high stiffness fibers. MMCs present composite material with high temperature performance such as aluminum reinforced with ceramic particles or short fibers. MMCs is quiet limited in usage compare to PMCs. CMCs is less applicable due to difficulties in manufacturing, although the matrix has a high toughness compare to the MMCs and PMCs.
Fiber reinforced polymer composites withstand the dynamic load during the composite utilization, such as in bridges, aircraft and many other application. Thus the dynamic properties of the composite material are more important than the static properties (53).

Composite material properties rely on the properties of the constituents such as stiffness, strength and toughness; these properties define the final performance of the composite. Applications of composites have to be considered while designing the composite (49). Some composite structure achieved by aligning the fibers to the load direction (unidirectional), other types are achieved by having the fibers in multiple directions to provide the isotropic properties to the composite material in order to withstand the undefined load paths. Most aircrafts composite made as a quasi-isotropic whereas the fibers are aligned in x and y direction (52).

2.8.2. Composite Material Design

Composite material applications are very important in designing the composite material. Reinforcement fiber can change the microstructure of the matrix. However, reinforcement

fiber properties could also change in the matrix. Residual stresses from different thermal contraction during the manufacturing are potential (49). Using young modulus E plot with the density ρ is a useful method for comparing the combination properties available between the matrices and the reinforcement with the other conventional materials (54).

2.8.3. Composite Manufacturing Techniques

Manufacturing process is determined by matrix type, fibers type, and curing temperature. Also manufacturing process depends on the cost of the product, production volume and production rate. Desired Structure can carry some limitation over the production process, thus all the above variables have to be considered for designing the composite material. There are different composite manufacturing processes to solidify the preforms such as hand lay-up, prepreg lay-up, pultrusion, resin transfer molding RTM and compression molding.
Polymer composite manufacturing process undergoes several steps (55). Typical steps include:

1- Preparation of the desired fibers or textile material for the composite or formation of preform

2- Applying the resin in order to impregnate the preform

3- Curing the resin to attain the desired solidification of the matrix

4- Finishing the consolidation process and preparing the composite material for the end use

Vacuum Assist Resin Transfer Molding (VARTM)

In resin transfer molding, preform is placed on the mold and release agent is used to prevent the composite from sticking to the mold. The binder type depends on the fiber type and the resin used in the process (56). Used preform can be textile fabric, 3D preform, or nonwoven mat. After placing the preform in the mold, resin is injected to the mold through the resin inlet. After the fibers are impregnated with resin and the mold is full and the excess resin exit from the resin outlet, resin inlet and outlet are sealed letting the resin to cure (Figure 2.31).

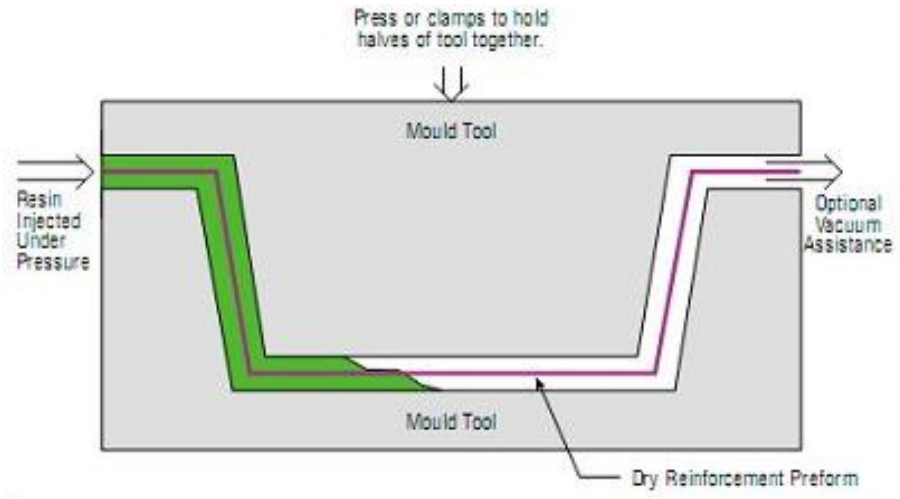

Figure 2.31 Resin Transfer Molding RTM (57)

Heat can be applied for resin curing if necessary. After curing the mold is opened and composite is removed from the mold. RTM is used for producing large fiber reinforced composite with complicated shapes. RTM products are used for complex aircraft, trains seat and automotive components.

Vacuum can be added to assist pulling the injected resin. This is known as Vacuum assisted resin transfer molding (VARTM). Resin is drawn to the mold through the resin inlet under vacuum pressure (Figure 2.32). Vacuum pressure is applied from the outlet. Since vacuum is used, half of the mold is replaced by vacuum bag, which known by an open mold. Resin flows and impregnate into the fiber reinforced under the vacuum pressure. When resin reaches the vacuum outlet the process stop for curing, curing occurs at room temperature under the vacuum pressure. Bleeder-Breath is used under the vacuum bag for uniform resin distributed. VARTM is cheaper process compare to RTM (Figure 2.32).

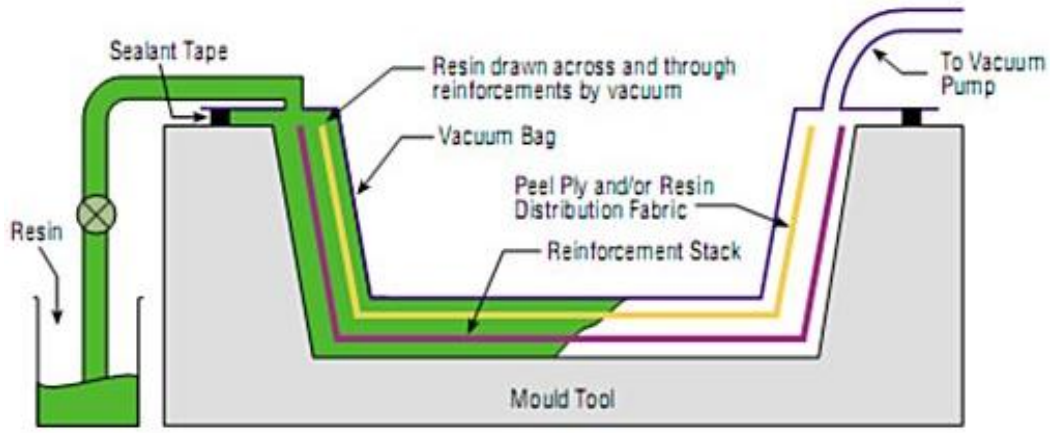

Figure 2.32 Vacuum Assisted Resin Transfer Molding (57)

2.9. Structural Health Monitoring Systems

Structural health monitoring is an intelligent system for real time monitoring for building and structures condition. This system increases the safety of the civil structure and reduces the cost of preparation and maintenance (58). Failure and collapse of the structures and buildings especially those over 50 years old attracted the attention and the concern about the structure integrity and durability (59). Predicting structure failure is very important. Most structures test for failure occurs when the sign of structure failure become noticeable. Sometimes these signs of structure failure are right before the damage. Thus, providing a real time monitoring and prediction system for failure is urging. These types of structure health monitoring systems can be used in airplanes or vehicles (60).

The need for structure health monitoring (SHM) system increases every day. For instance, in railway bridges with medium span, trains are the main load, dynamic response such as vibration; acceleration, strain, deformation and displacement are needed to be monitored to detect signs of failure before it occurs (61).

2.9.1. SHM Based on Electronic Sensors

Some of existed SHM systems relied on electronic sensors such as foil strain gage, piezoelectric transducer (PZT), piezoceramic, piezofilm (PVDF), and acoustic emission sensors AE. Many researchers have used these systems for SHM, some of these systems can be wire or wireless connected to the data acquisition systems (62) (63) (64) (65) (66). These sensors relay on electric signal transmission. Piezoelectric sensors are used to measure strain, pressure, force, and acceleration in sense of converting them to an electrical signal.

Strain gages have some advantages such as inexpensive, easy to handle due to its big size, sensitive to potential failure of civil structures. However, these electronic sensors carry some disadvantages. For instance, foil strain gages can be disturbed by any electromagnetic interference in its vicinity and characteristic by its low corrosion resistance. Also foil strain gages can't be multiplexed, therefore each strain gage has to connect to a separate data acquisition devices to be able to collect data about each spot (67). These types of SHM systems require several components such as sensor and actuator elements, processing and communication chips, and power supply, and these devices need to be integrate and protected (68).

Due to its large size and its need to be connected to many data analysis and data acquisition devices, these electronic sensors can't be embedded into civil structure. SHM electronic sensors have to be mounted on the surface of the civil structure; therefor these systems are vulnerable to adverse weather condition, which can add more cost. Mounting structure surface need to sanded and washed precisely to eliminate any contamination to provide a good adherence between the sensors and the epoxy. These cautions are time consuming and cost added (67). Conventional strain gage can only measure strain up to 3% of the steel structure under a cyclic load and no more than 1% of the concrete structure.

Therefore, optics fiber sensors provide a good solution for reliable SHM not only by eliminating all the disadvantage of the traditional sensors but adding much other advantage like ability of embed such sensors into the structure, multiplex and flexibility. Using optic

fiber sensor provides a real time monitoring along the structure not just a spot monitoring (2). Sensitivity to the temperature, strain, rotation electric and magnetic field can be converted to change in phase, frequency, amplitude, and wavelength in the optical properties of transmitted light (59).

2.9.2. Glass Optics Fiber Sensors for Structure Health Monitoring

Many researches have been done for health monitoring system for railways by attaching fiber optics sensors to building, railways or any other structures. One study, the researchers used Fabry-Perot optic sensors for real time strain monitoring in railway structure (2). This system was externally attached to the railway. Optical measuring system comprises transmitter, receiver, optical fiber, modulator element and signal processing units. Broadband white light source was used instead of the laser light for absolute, precise, linear measurements and for its insensitivity to the change of temperature. Strain gage was calibrated for Fabry-Perot strain gage sensors and the conventional resistive foil gage. The calibration results show well agreement between both. The researchers applied the Fabry-Perot SHM system to the Wuhu Yangtze River Bridge (WYRB), the whole span of the railway bridge is 10,616 meters. The SHM system was externally attached to the bridge structure. This avenue of attaching the SHM will limit the measurements to the external structure failure. Embedding the SHM system into the structure will avoid any adverse environmental condition. However, measuring the internal damage and internal strain provide an accurate measurement to the structure failure and good failure prediction. The researchers used an end to end loss technique to measure optical power loss, this method of measuring the power loss is expensive and require setup a light source on one end and a receiver on the other end of the optical fiber, which add more time and cost to the measuring and data acquisition process.

Some studies have used the intensity modulated sensors as embedded sensors into composite material for continuous structure health monitoring (69). The work aimed to prove that fiber optics sensors offer an alternative method for the robust piezoelectric transducer acoustic emission monitoring. Laminate composite made of Vicotex carbon-epoxy prepreg, sample prepared in unidirectional order where two plies lay-up in 0° and four plies in 90°. Two

multimode optical fibers were embedded into the middle layer in 90° direction, 60 mm distance between the two fibers are maintained. Fiber optics core and cladding diameter were 100 µm and 110 µm respectively. Exit point of the optical fibers were protected by using polymeric bore tube, whereas bore tube shrank around the fiber during the curing process and provide a protection to the fiber optics at this weak point. Tensile tests were performed on ten composite samples, tensile load applied continuously to the sample. 10 mW HeNe laser was used. Test results shows uniformity stress distribution at the beginning of the test, layer at 90° start cracking and delaminate. Layers at 0° sustain the stress with increasing the damage. Authors in this paper have collected the optical signal in a photodiode and used Modal Acoustic emission (MAE) in order to identify the damage through looking at the frequency generated from the occurred damage of the specimen. This method for detecting and analyzing the failure is complicated and not suitable for field monitoring. Many devices and wires have to be attached to the composite to collect data. Optical fibers were embedded into the 90° direction only. Proposed system can only monitor the failure without determining its location.

Due to their high sensitivity and low price, nondestructive method such as ultrasonic scanning, AE, and vibration have been used to assess damage of composite laminate. Online structure health monitoring using this system is very difficult. Fiber optics sensors made structure health monitoring possible and applicable, many researchers' used fiber optics acoustic emission sensors such as Fabry-Perot interferometric, Michelson and Machzehnder. The use of fiber optics AE was discussed in (70). Fiber optics AE sensors based on fused tapered and Coupler has been used as a sensor for detecting the damage in the composite by collecting the measurement of acoustic emission signals at different load for the composite laminate. Fiber optic sensor was attached to the surface of the glass fiber reinforced composite. Tensile test was conducted to the composite laminate. AE was generated by the tensile test of the composite. Authors claimed that AE can identify the damage in the composite whether it's cracking or fiber breakage. Health monitoring system has to be reliable and providing the predictability to the structure failure. In this work the fiber optics AE sensors were attached to the surface of the composite, thus, this system only monitor

cracks or damages on the structure surface. Also attaching the acoustic emission to the structure's surface is vulnerable to any damage and adverse weathering conditions. In addition the data won't be accurate because the AE sensors will be affected by the surrounding environment, thus, it will be difficult to distinguish the difference between the matrix crack and any other interference that can affect the monitored data.

Predicting the potential failures or crack propagation in composite flex beams has been studied by embedding fiber optics Bragg grating into composite material (71). Delamination of composites from stack of 2D preforms is the main failure in polymer matrix, this is due to the low inter laminar strength of composite materials due the lack of z-direction fibers. In (71) fiber optics sensors were embedded into the thickness of the composite to provide a useful method for measuring inter laminate stress. Fiber optic Bragg grating was embedded through the thickness of 19 plies of unidirectional graphite / epoxy prepreg using proprietary process. The small size of the sensors and insertion technique minimize any negative impact of the fiber optics on the composite structure. The test results show that the sensors were able to measure the Poisson's compressive strain and the crack propagation. The fiber optics sensors can be embedded through the thickness of the composite with no effect on the structure. Measuring the strain distribution through the thickness of the composite structure can be accomplished. Foster-Miller insertion technique of the fiber optics into the thickness of the composite plies is not described in the paper. This system requires a reference sensor that is not embedded into composite material. 2 m extra optic fiber require before the reference sensor, which make the sensor preparation hard and expensive. Light source, spectrometer and data acquisition system are required, which add more difficulties of installing the system into the field.

2.9.3. Mechanical Properties of Composite Material with Embedded Sensors

Embedded circuit board is major and important part of the system to enable sensor network, communication, data process and providing power to the electronic circuit. It was indicated that some potential defect due to the embedded circuit board such as, delamination as a result

of interlaminate stresses, increases of interlaminate stress near the sensors, stresses at the interface between the sensors and composite. Sensors can lose the sensitivity due to the delamination failure between the embedded sensors and the composite. For these reasons, several researchers studied the mechanical properties of composite materials with embedded GOF.

In one study, a preliminary work for developing a structural composite material with embedded fiber optics sensor network with capability of decision-making. The researchers studied the effect of embedding sensor network, two chip resistors and printed circuit board on the strength of the composite host material (72). Composite host material made of 0° unidirectional tape glass/epoxy prepreg laminate (S2/BT250E-1LV). Three samples were prepared, blank sample, sample with embedded two chip resistors, and sample with embedded printed circuit board. Chip resistors and printed circuit board are embedded into the middle layer. Quasi-static three point bending tests applied on the prepared sample to measure the short beam shear strength and observe the effect of embedding chip sensors and circuit board on composite structure properties. Chip resistors dimension were 2.03 mm x 1.27 mm and the circuit layer thickness was 0.18 mm. Vacuum infusion under 125 ton hot presser was conducted to prepare the prepreg samples. Short beam shear stress was calculated using Equation 13.

$$F^{SBS} = 0.75Pm/bh \qquad [13]$$

Where: F^{SBS} = short-beam shear strength, MPa

P_m = maximum load observed during test, N

b = measured specimen width, mm

h = measured specimen thickness, mm

Test results show that embedding printed circuit and chip resistors have a very small effect on the short beam shear stress measurement comparing to the blank sample. The authors depend only on images of tested sample to show the Interlaminar failure for the blank sample and embedded sample with circuit board and chip resistors. Tensile and impact test should

have conducted to the sample as well. No data show whether the chip sensors or the circuit board were destroyed. The authors showed images of an embedded chip sensor and one circuit board into the composite to illustrate the damage caused to the composite structure. Real system will definitely require more sensors to cover the whole area to be monitored. The effect of resin and the 125 ton pressure on the Chip sensors and circuit board was not referred to in the paper.

Mechanical properties of the composite material have been studied while optics fiber sensors were embedded into the composite material parallel to the reinforcement (73). Composite plates comprise 8 plies of five harnesses satin woven fabric pre-impregnated with epoxy resin (Fibredux 9l4C MS 5 42 prepreg, T300/Hexcel F263 carbon/epoxide with 54% by volume of Toray 300 carbon fiber) with total thickness is 1 mm, coated fiber optic with diameter ranging from 93 µm to 500 µm were embedded between the fourth and fifth plies. Tensile test was applied in longitudinal and transverse directions of the samples. Test results show that the embedded fiber optics with diameter 93 µm and 103 µm coated with polyamide and acrylate respectively has some effect on the composite strength. Due to the coating degradation at temperature 160°C (applied during infusion process), the shear strength decrease by 8% for the composite sample with fiber optics coated with acrylate. Reduction in longitudinal compression strength of composite by 25% when fiber optics was embedded perpendicular to the reinforced fiber into the composite material. In their research, the authors discarded samples containing voids. The effect of void is an interesting topic to study since in most cases the voids cannot be eliminated.

Embedding fiber optics sensors into composite material can cause resin pocket and geometric disturbance to the reinforced fiber around the fiber optics. Some of the prior works have evaluated the degradation of tension and compression strength in a composite laminate. Effect of embedding fiber optics sensors on the composite properties has been studied. In a study of this type, researchers evaluated the tension and compression degradation while fiber optics was embedded into composite structure at various angles such as 0^{o}, 30^{o}, 45^{o}, 60^{o} and 90^{o} with respect to the reinforced fiber direction. Laminate thickness was 8, 16, 20 plies

(74). Unidirectional carbon/epoxy prepreg tape (AS4/3501-6 by Hexcel) was used for preparing composite laminate. Polyimide coating optical fiber with core diameter of 9 µm and a cladding diameter 58 µm was used. Polyimide coating diameter was10 µm. Optic fiber was embedded into the middle layer of the laminate. End to end loss technique was used to measure the optic power loss during the processes and for micro-bending. Tensile test and compression test were applied on the specimens. Results showed insignificant change in the modulus, strength loss was 9.9 % and 4.7 % strength loss for 8 plies and 16 plies laminate respectively. Results show significant compression strength reduction ranged from 9.9 to 40 % and 1.2 to 14.9 % for the 8 ply and 16 ply respectively. Compression strength reduction decreases as optics fiber get parallel to the reinforced fiber. It has been noticed from the specimen images that embedded optical fiber caused a resin pockets and geometric disturbance of reinforcing fiber. This was considered as a failure initiation. The disturbance angle varied from 6.2° to 8.2° and the resin pockets size are between 7 and 10 times the area of the fiber optics. The authors didn't show any optical test results, although they have mentioned that light loss study was conducted but no results were shown. The integrity of the embedded optic fiber after the production process was not reported. Stripped optic fiber from the coated polyamide should have been used to compare the results with the un-stripped optic fiber. Images of embedded optic fiber at angle > 30° showed flattened cross-section as a result of manufacturing process. The flattened configuration of the optic fiber may cause optical signal loss which should have been considered.

Composite of E-glass woven fabrics were used to host Fiber optic Bragg grating sensors (75). Fiber optic strain system is used to identify the strain locations along the fiber optic through wavelength associated with each sensor. Composite material composed of 10 E-glass of 24 oz/yd^2. woven fabric piles was used in the research and fiber optic Bragg grating sensors were embedded between the 1^{st} and 2^{nd} plies and held by a small spots of adhesive before laying down the rest of the plies. Fiber optic parts were kept protruding out at the edges of the composite panel with length of 30 cm and connected to the distributed strain sensor system. Epoxy vinyl ester resin was infused using vacuum assisted system to prepare the

final composite panel. 4-point bending test was conducted at increment load starting from 50 lb to 500 lb. Foil strain gage (which was attached to the surface of the composite panel) output, fiber optic strain data and testing machine cross head displacement data were collected at each load increment. Results showed that the mechanical strain measurements (as measured by the foil strain gage) are somewhat comparable to optical strain measurements and with strain distribution along the sample length. However, there are some disagreements between the mechanical strain data and optical strain data. Authors attributed the discrepancy to the slippage of optical fiber sensors. Also the strain results detected by the optic sensors show small increase with increasing the load but not smooth as expected. The behavior was attributed to the woven fabric structure may cause local strain variation in form of stick slip mode.

Most of inaccurate measurement in this paper was due to the slippage of the fiber optics within the composite constituents. Fiber optic sensors have to be integrated to the textile composite, which means fiber optic sensor has to be woven into the woven structure to prevent any slippage. Glass fiber optic Bragg grating sensors are very brittle, which make them hard to handle and they may fail in trying to weaving them since in the weaving process yarns are experiencing bending, abrasion and impact forces. As a result of such brittleness, the authors reported that with exception of three samples all samples were unusable for sensor failure during manufacturing process. Fiber optics Bragg grating sensors are expensive, which make the distributed strain system very expensive since this system requires a high number of sensors to cover the entire composite panel.

Silva-Munoz *et al*. (76) have studied the fabrication of secondary bonded composite, which is doubler-plate joint, with embedded fiber Bragg grating distributed sensors. Fiber optic Bragg grating sensors were embedded into E-glass woven fabric with a nominal weight of 744 g/m^2-made of continuous glass fiber strands (Saint-Gobain Vetrotex woven roving 324). Woven composite comprises 31 layers of woven roving 324 from glass fiber. Woven fabrics layers were oriented in $0^\circ/+45^\circ/-45^\circ/0^\circ$ sequence. Longitudinal crack initiation and propagation in the doubler-plate joint are monitored under the tension loading. Fiber Optic

Bragg grating sensors were embedded in 3 different locations, one optical fiber sensor located over the top of the 20th layer, one optical fiber located over the 23rd layer and the last fiber optic sensor was located over the 26th layer. Spray adhesive is used to attach the fiber optic sensor to the woven fabric. Woven fabric layers from 1 to 24 are considered a base plate; layers from 25 to 31 are considered a doubler-plate. Vacuum assisted resin transfer molding was used to produce the composite material. Ashland Derakane vinylester resin was used.

Fiber optic Bragg grating sensors are brittle; half of the sensors were broken during the fabrication process. As mentioned previously, fiber optic Bragg grating sensors are expensive and the required interfacing and measuring devices are expensive. Durable strain monitoring system has to be robust and able to withstand all the fabrication processes. Losing sensors during the fabrication processes mean wasting resources and time, which is not suitable for system intended to last long and concern people lives.

2.9.4. Monitoring Molding Process Using GOF

Monitoring curing process during the composite fabrication process is very important. Composite mechanical properties can be affected by the difference in thermal coefficient between fiber and matrix during the cooling stage. Therefor the final quality of the composite depends on the cure time, temperature and pressure, thus monitoring curing process will lead to understanding the changes that are taking place during infusion and shed the light on issues that may be resolved to obtain high quality composites.

Kang *et al.* (77) (78) (79) have conducted studies with objective to monitoring the fabrication strain and temperature during the composite curing process. Strain during the fabrication process can cause warpage or spring back to composite sample, which cause difficulties for composite structure assembly. Optic fiber sensors were embedded into graphite/epoxy (GR/EP) composite laminate to provide on time monitoring system. Fiber Bragg grating (FBG), extrinsic Fabry-Perot interferometer (EFPI) and hybrid sensor were used. Vacuum bag autoclave molding technique was used for manufacturing the final composite samples.

Curing process composed of three steps. First stage, laminate temperature was increased to 80°C for half an hour in order to decrease the viscosity of the resin. Second stage, temperature was increased to 130°C and kept for two hours. Third stage, composite laminate was cooled to room temperature. These changes in temperature develop a fabrication strain. The fabrication strain and temperature have been simultaneously monitored through embedded two FBG/EFPI sensors (Figure 2.33) into both graphite/epoxy unidirectional and symmetric cross ply laminate. These sensors were embedded at different directions and different locations.

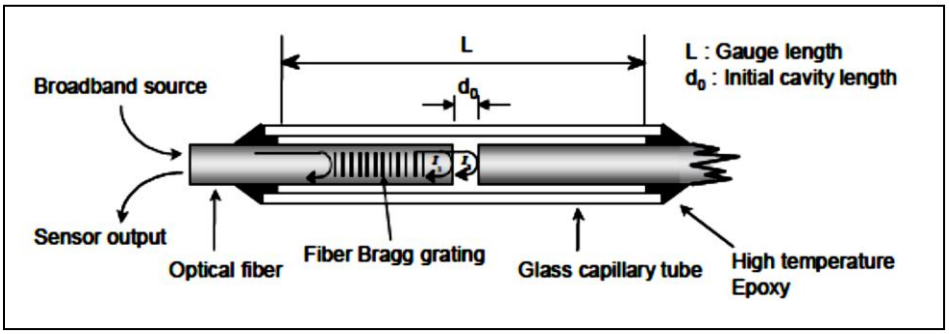

Figure 2.33 FBG/EFPI sensors (77)

Results showed that optic fiber sensors located perpendicular to the laminate show a high compressive strain than the sensor in the longitudinal direction as a result of the thermal and chemical deformation during the curing. The two sensors in the symmetric cross ply laminate shows similar compressive strain results, but higher than the compressive strain in the sensor located in the reinforcing fiber direction and lower than the compressive strain in the sensor located perpendicular to unidirectional laminate. The used system for data acquisition and data analysis are expensive and it's not a hand held system that can be easy moved from place to another. Moreover these systems cannot determine the location of the defect or the failure.

Health monitoring and curing process of the glass fiber reinforced plastic textile composite during the resin transfer molding process was studied by Kosaka *et al.* (80). Carbon fiber reinforced plastics (CFRP) and glass fiber reinforced plastics (GFRP) composites were formed and used for comparative study. Glass fabrics were used as reinforcing preforms. Because of its light weight, small size, and high strength, Bragg grating sensors were used. Resin transfer molding was used for samples fabrication, composite material made of ten layers of glass or carbon fiber with Epoxy resin. Fiber optic sensors located at the center layer of the composite. Fiber optic sensors were placed at 0° against the resin flow, dielectric sensors and thermo couples sensors were added to the composite material for measuring resin ion viscosity and temperature during the RTM and they are located near to the fiber optic sensor (Figure 2.34). Composite samples were cured for 2 hours at 100 °C and for 4 hours at 170°C in a furnace. After the curing process, samples were cooled to a room temperature. Tensile and fatigue were conducted for testing composite material properties. The curing degree, pressure, temperature, voids, defects and residual stress during molding were monitored.

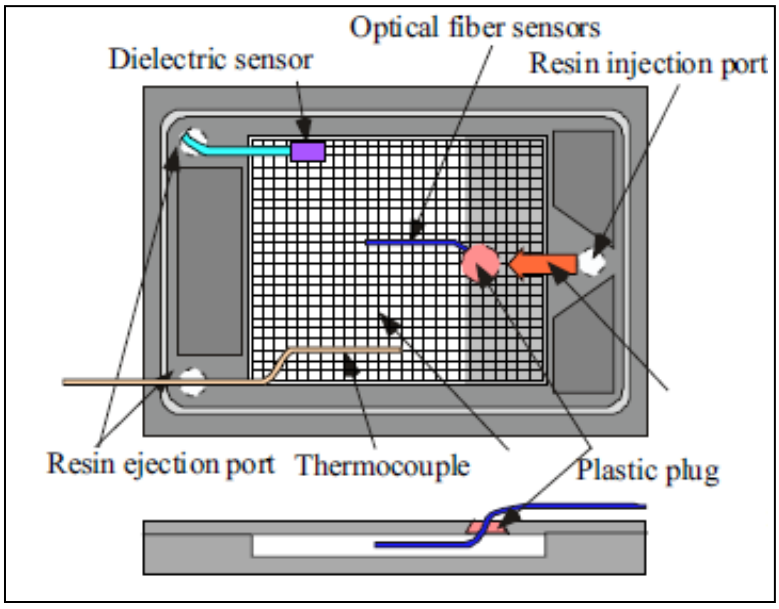

Figure 2.34 Embedded sensors during the RTM process (80)

Fiber strain sensor was connected to the strain acquisition system after finishing the resin injection process for measuring the internal strain. Dielectric sensors connected to dielectric measurement system and the strain gage was attached to both sides of the sample to measure the external strains (Figure 2.35).

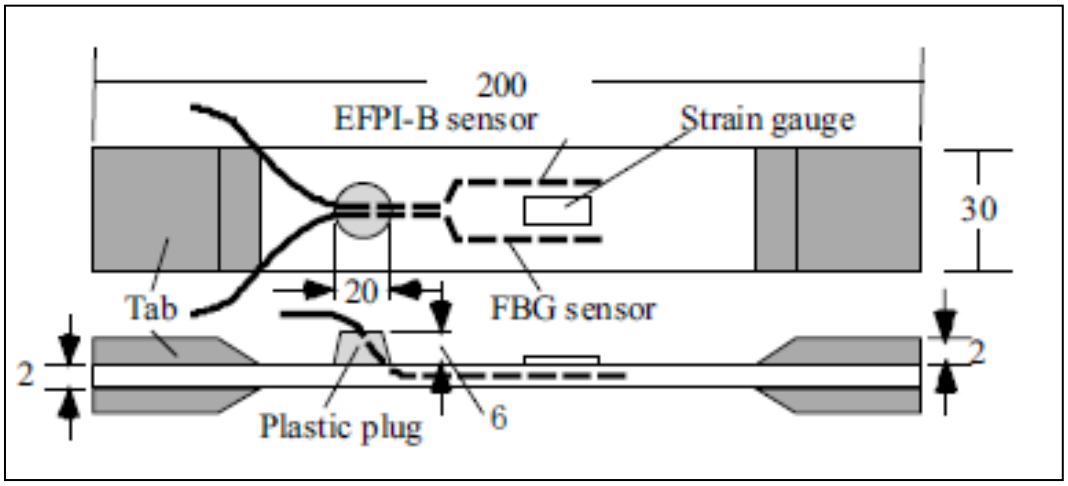

Figure 2.35 Optical fiber sensors and strain gauges (80)

Results showed that the embedded fiber optics sensors can detect the occurred fiber constrain during the curing stages. Tensile and fatigue test results showed agreements between fiber optics sensors and foil strain gage that was attached to the sample surface.

Fiber Bragg grating and Fabry-Perot optical sensors require a very high expensive and complicated signal processing devices for optical signal data analysis. These systems provide a very high measurement resolution and high quality data acquisition, which is not valuable in this type of measurement. In addition to the cost effective, these sensors are very delicate, brittle, and vulnerable to break during the installation, which means it need special care during the installation and composite fabrication.

2.10. POF Sensors

POFs sensors have many advantages; some of these advantages are comparable to these of silica optical fiber (SOF). The POFs sensors possess additional advantages such as, large core size, large numerical aperture, flexible, easy to handle, disposable and recyclable and lower compared to SOF (81). POFs also have some disadvantages such as high attenuation, which prevent it from being used for long distance sensors as SOF. POFs sensors are made of multimode optical fibers (82).

There are two types of POFs sensors, intrinsic sensors and extrinsic sensors. POFs intrinsic sensors are sensors that directly affected by the type of measurements such as temperature, pressure, or strain. These measurements depend on intensity of the light passing through optical fiber and depend on the occurred interaction inside the optical fiber itself (83). Extrinsic POFs sensors are sensors that not directly affected by the measured parameter but sensors that are used to carry or transmit light to outside of the fiber, where the light is influenced by the measurements, and receive the light to measure the change of its intensity (Figure 2.36) (84). Extrinsic sensors are used to measure vibration, rotation, displacement, velocity, acceleration, torque, and twisting, deflection and in-plane strain.

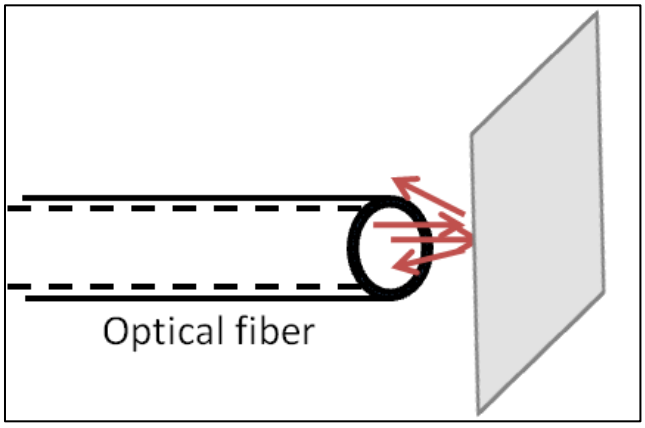

Figure 2.36 POFs Extrinsic Sensor

Intrinsic POFs sensors present the ability of sensing the change in the vicinity condition along the length of the optical fiber itself. Using Optical time Domain Reflectometer (OTDR) very useful in determining the location of that change which give the sensors more accuracy in detecting and localize the change of the condition. This performance qualifies the POFs sensors to detect strain distributer for structure health monitoring. Their physical and mechanical properties allow manufacturing them during formation of the preforms and embed them in an integrated structure along with other constituents of the preform.

Many researchers have studied the POFs sensors characteristics using the OTDR as an advanced and unique technique for measuring the change in the light intensity and determining the failure location. Husdi *et al.* (85) carried out an experimental study addressing the effect of small bending, axial strain, temperature and transverse clamping on the excess reflection and transmission loss using OTDR device. PMMA-based POF with 0.98 mm core diameter was used for conducting the study. OTDR-2000POF from Scientex Co., Japan was used in this study for signal analysis. Small bend effect was conducted by winding half turn of POF around different metal rods with different diameters. Reflection and power loss were measured using the OTDR. Results showed increase in the signal loss as the rod diameter decreased; signal loss was 1.2 dB and 3.5 dB with rod diameter 20 mm and 30 mm respectively. Signal loss was almost zero dB with rod diameter of 30 mm. Results showed a reflection only with the 8 mm rod; this reflection was greater than the intrinsic backscattering by 1dB with rod diameter 10 mm. Husdi *et al.* (85) also studied the signal reflection and loss of the POF cable and bare fiber under a clamping stress. Applied compression force controlled by the displacement of spring. The results indicated that when the force exceeded 2,500 N, the signal loss start occurring. Very small reflection occurred when the stress exceeded 2,950 N. Results data of the loss versus applied force showed different behavior between the POF cable and bare fiber. POF cable measured data was scattered after 2,500 N, which was explained by slippage between the POF and the cable jacket. Unlike the POF, bare fiber showed a slope after 2,000 N. Axial strain test results showed a small reflection under small strain and as the strain increased by 50% signal reflection increased and signal

loss increased rapidly. POF failed after the strain value reached 80%. Reflection coefficient increased from 0.09 dB to 0.30 dB as strain value increased from 5% to 40% respectively.

Results of bending test showed a signal reflection and loss with rod diameter 8 mm. Power loss without reflection occurred with rod diameter 20 mm. The authors didn't elaborate on the reason why small POF bending caused signal reflection while the large rod diameter didn't. Additionally the research was limited to angle of wrap 180 degree.

Saunders *et al.* (86) investigated the possible use of POFs sensors for measurement of PH. 20 m of POF was used; cladding was stripped out from 15 cm of the POF and located 4 m from the fiber end. Stripped part exposed to an aqueous solution of methyl red at three different values of PH 3.05, 6.35 and 9.10. Luciol ν-OTDR was used to interrogate the optical fiber at 648 nm. Results showed that the PH had an effect on the signal attenuation, as the PH value decreased the signal attenuation increased. At PH value of 3.05, 6.35 and 9.10 the light absorption at wavelength 650 nm was 0.9485, 0.042 and 0.0245 respectively. The authors didn't mention the specification of the POF. They also didn't discuss the reason behind changing the absorbance value of the light at different PH values and the relation between the absorbency and the attenuation. They could have studied the effect of exposure time on the attenuation and the effect of the core diameter on the absorbency.

Fukumoto *et al.* (87) investigated three topics in their paper: (1) performance of POF cable on detecting the deformation of wooden structure as a host material for POF sensors, (2) the ability of POF sensors to measure the applied strain after releasing the load as a function of memory effect of POFs sensors, and (3) the spatial resolution of standard PMMA-based step index POF. OTDR photon counting was used for measuring the backscattering effect and signal loss for POF deformation, memory effect and spatial resolution.

POF sensor was fixed on the top of two wooden beams by using two metal plates. Spacer plate was used between the metal plate and the wooden beams to minimize the clamping effect on the OTDR measurements. It was found that the use of spacer plate of 1.3 mm (d in

Figure 2.37) caused same effect on the backscattering of POF signal as measured by the OTDR.

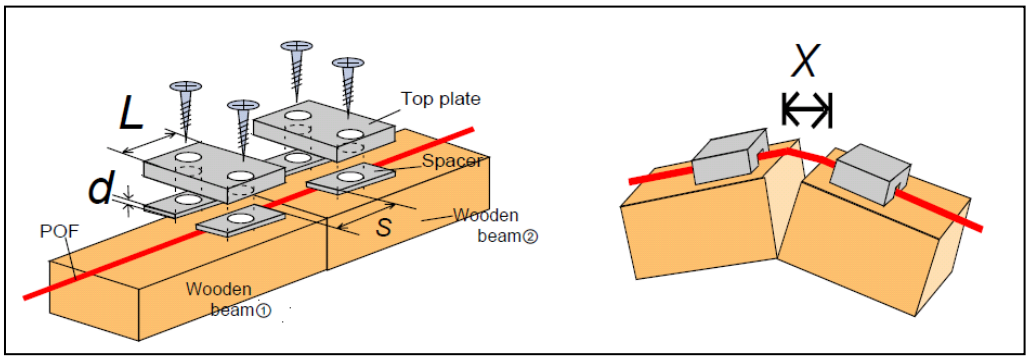

Figure 2.37 Fixing POF to the wooden beam

Experiment carried out at two different positions 15 m and 85 m from the OTDR. Wooden beam had created a 100% strain on POFs sensors and two bends occurred on the edge of the wooden beam as shown on Figure 48. Strain is measured according to Equation 14.

$$Strain = 100\ X/S\ (\%) \qquad [14]$$

Where *S* is the distance between the two plates and *X* is the distance between the two wooden parts after the break. Results showed that the occurred reflection under a 100% strain has a high magnitude at 15 m and small magnitude at 85 m.

For memory effect study, 10 cm long of POF was strained at different level and the corresponding reflections were recorded. Corresponding reflection after releasing the load were recorded as well. This feature was recommended to know whether the specimen was subjected to deformation after the effect was vanished.

Authors also studied the life of POF memory effect by leaving the POF under constant strain for some times and measure the reflection one month later after releasing the load. Results of

the constant strain showed decrease on the reflection gradually with time. Signal reflection of the released POF has showed insignificant change in reflection.

Regarding to spatial resolution, the required distance between two consecutive events that can be seen and measured correctly using the OTDR was investigated. Test was repeated 3 times at different distance between the two strained locations that are 1, 3, and 5 meters apart. Results showed that when the two strained locations are 1 m apart the two reflection peaks are overlapped and was hard to be measured. For 3 m distance the two reflection peaks are separated but the reflection can't be determined because of the distance between them is very small to be measured. 5 m distance showed two measurable reflection spikes which means the spatial resolution is 5 m.

Based on spatial resolution, authors have applied 5 points strain of 5 m apart on 100 m long POF. Backscattering was measured for the five points. Results showed decrease at the reflection magnitude as the strain point goes far from the OTDR. Memory effect was measured after releasing the load from the 5 points and results showed that the further from the OTDR the fastest the memory effect vanish.

It was decided to use a spacer plate with 1.3 mm thick based on this thickness and higher gives a less variation on the reflection, although they ignored the fact that 1.3 mm and higher caused more signal loss that affected the total distance of the POFs that can be used. Also this length would affect the spatial resolution and the number of strain points that can be measured. Each OTDR has attenuation dead zone and event dead zone, event dead zone is same as what the authors called spatial resolution. This event dead zone considers as a signature (specification) of the OTDR and the author wouldn't have to test that.

Kiesel *et al,* (88) (89) investigated the behavior of intrinsic POF sensor for large strain application. POF has an extinct flexibility properties compare to silica optical fiber which allows it to go through high degree of curvature before the occurred failure. The goal of their research was to predict the behavior of intrinsic POF sensor for large strain application and derive the associated phase shift on an intrinsic POF sensor. Axial tension test was conducted

on single mode PMMA with cladding diameter of 125 µm and numerical aperture of 0.12. Pneumatic grip was used to eliminate any deformation to the tested POF. Ten samples of 101 mm length were tested at strain rate of 0.6 mm/min. True stress (which considers change in the optic fiber diameter during test) and engineering stress was calculated. Stress-strain curve showed a linear region at the beginning of the test followed by a yielding point at 5 % strain and the fiber failed at 30% strain (Figure 2.38). Sensing performance of POSs sensors depend on yield strain more than the breaking strain because the light transmission is highly affected by fiber deformation. Compare to silica optical fiber, yield strain of tested POF is equal to ultimate strain of silica optical fiber, which is an obvious advantage to the POF.

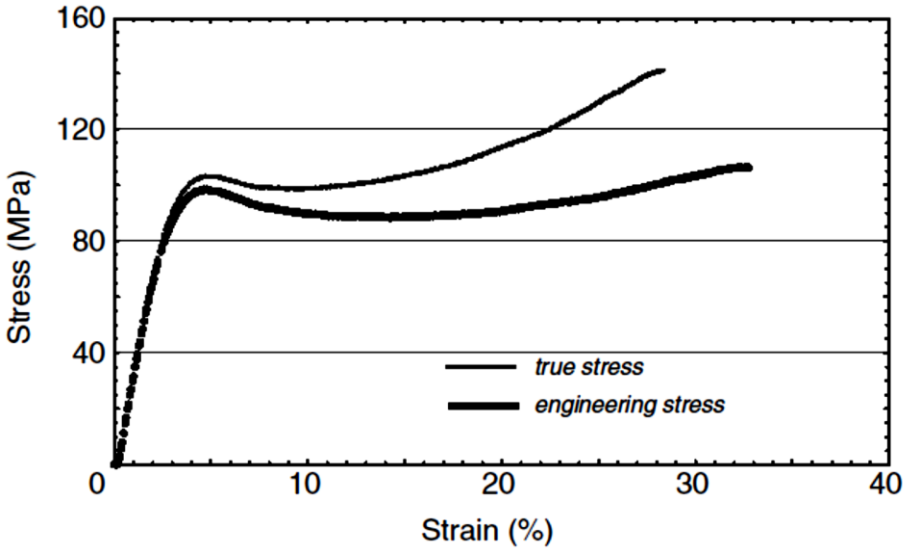

Figure 2.38 Stress-Strain curve for POF at strain rate 0.6 mm/min, true and engineering stress were shown

Effect of the strain rate on the POF mechanical properties tested under different strain rate of 0.01, 0.30, 0.90, 1.22 and 3.05 mm/min. Strain rate results showed an effect on the yield strain, as the strain rate increased the yield strain and stress increased, up to 0.3 mm/min and after this value the strain rate exhibited no effect. It was conclude that it's important for

sensing application to know the applied strain rate for accurate failure prediction since POF sensitivity at the initial linear region is low to strain rate.

Transmission test should have performed on the tested sample to verify the result from the stress strain curve and verify the effect of strain rate on the transmission and the attenuation of POF sensors. Knowing the threshold of the signal loss with the corresponding strain is very important for using the POF sensors.

2.10.1. Integrated POF Sensors for Distributed Strain Monitoring

Numerous researchers worked in embedding silica fiber optics into engineering and composite structures and only few researchers pursued work on integrated POFs sensors into such structures. Integrated silica optical fiber or POFs into the structure materials share the same purpose of providing *in situ* strain and temperature real time monitoring, however the silica optical fiber and the POFs have some advantages and disadvantages (90).

Kiesel *et al.* (91) studied the ability of integrated single mode POF sensors into structure material for *in situ* strain real time monitoring. POFs with 115 µm diameter were embedded into three separate civil structure materials casting: hydro stone, mortar and cement. POFs were pulled from the cast using a tensile strength device at rate of 2.5 mm/min. Results showed that integrated POF in mortar material was broken at 1.4 kN and the total slippage was low. Embedded POF into the hydro stone material fail at 2.5 kN and had a slippage much higher than the mortar material. POF embedded into cement specimen failed at 2.7 kN without any significant slippage. According to the author, POF didn't adhere to the hydro stone material which cause the significant slippage in the specimen while the cement provide a good host to the embedded POF due to the small cement's particles which cause the adhesion between the cement particles and POF. For mortar specimen, the slippage was relatively small because the mortar material has a large particle size which didn't bond well with the POF. Due to the large shrinkage of the concrete structure, potential signal losses in the POF may occur. To prevent this, the POF was embedded into a small pre-cast of concrete block and the block was fixed to the concrete frame before casting of the concrete reinforced

structure. No effect of cement shrinkage on the POF signal loss was recorded. The visual assessment showed no damage on the POF sensors when the concrete structure was loaded until failure.

Authors didn't measure the casting effect on the fiber optics loss associated with the casting process. Visual assessment showed no external damage on the POF while the POF core is very important because all the light transmission happen inside the POF core. Hydro stone, mortar or cement could have any chemical effect on the POF which can cause change on the refraction index which can cause signal attenuation on the POF sensors. Optical assessment is very important for evaluating the POF performance especially when cement material shrink during the curing time, which may affect the POF signal attenuation.

Nakamura *et al.* (92) investigated memory effect of POFs sensors for axial strain. PMMA-based POF with 1 mm in outer diameter was used. OTDR was used to measure the backscattering response; results showed no power loss from POFs sensors under low strain. Signal loss started after 50% strain and POFs sensors failed at 80% strain. Measurements showed that backscattering with reflection coefficient of 0.09 dB per unit % strain occurred at strain below 40% after that reflection coefficient increased to 0.3dB per unit % strain. POF is a viscoelastic material and deforms after 5% strain and doesn't return to the previous form after removing the load. 80% strain was applied to the POF for 12 minutes and the applied load was released afterward. Backscattering reflection was found at 80% strain, 50% strain (after POF cable relaxed) and after three weeks. Results showed that after three weeks reflection was reduced but didn't return to zero and transmission loss didn't significantly change. That's indication that POF cable has kept some of its deformation. In their research Nakamura et al. (93), applied strain to the same sample and kept the sample for 4 days under the applied strain. Measured reflection and transmission was slightly lower than the first time. Load was removed again; reflection was measured after releasing the stretching force and found that the reflection dropped by 3 dB. They stated that this is an indication of material ability to deform and related this phenomenon to memory effect of POFs sensors (93).

Liehr *et al.* (94) (95) studied the behavior of POF embedded into multifunctional geotextile. Since textile materials are widely used in geotextiles such as embankment, reinforcement for earthwork, drainage, and soil structure embedded POF sensors could benefit in providing real time monitoring to such important materials. Flexibility of POF gave it the ability to be woven with the textile material during fabric formation. OTDR operating with 650 nm wavelength, 35 dB dynamic range and 0.5 numerical aperture was used to measure the backscattering effect as a function of strain. Four different POF from different manufacture were evaluated for its sensitivity to the applied stain and the POF from Mitsubishi GH4001 with 1 mm diameter with PE jacket was selected for the study. Main purpose of embedded POFs sensors is detecting the soil displacement. The study was conducted on a small scale test. The test setup was made of 9 m long wooden box with 0.8 m height and 0.5 m width. The wooden box was filled with model sand in layers. Lifting cushions were placed on the bottom of the box and covered with soil. Geotextile fabrics with embedded POFs sensors was laid down and covered with soil. Lifting cushions were inflated stepwise and backscattering was measured using the OTDR. Inflated cushion caused a displacement to the soil which was monitored through the OTDR backscattering (Figure 2.39). A special signal processing algorithm was employed to process the backscattering data from the OTDR to determine the correct strain and strain distribution. It was noted that minimum of 6% strain can be detected using the POFs sensors used. This information provides good estimate of the stretched length of POFs sensors.

Figure 2.39 Experimental Test Setup

Kuang *et al.* (96) investigated the use of POF sensors for detecting cracks and monitoring deflection of concrete beams. Multi-mode step index 1 mm diameter POF was used, 7 cm of the POF was stripped from the cladding to increase the light loss when POF bent. Two types of concrete specimens were prepared, scale-model concrete and full scale reinforced concrete beams. POF sensors were attached to the bottom surface of concrete specimen after grinding the surface. A cyanoacrylate-based adhesive was used to bond the POF to the structure. End to end loss technique was used for measuring the loss in the transmitted light using ultra-high luminescent LED as a light source and light dependent resistor as a light detector.

Three and four point bending was applied to the scale-model concrete to find the ability of POF on detecting the cracks. Two specimens were tested at the peak load and crack width and corresponding light loss was measured. Remaining specimens were tested beyond the peak load to determine the ability of POF sensors of measuring the deflection. Three and four point bending were applied to the full scale reinforced concrete beams. Cracks width and light power loss were measured at different load until specimen failed.

Results showed a significant light loss at the peak load and insignificant loss prior to the peak load. When the beam is subjected to deflection the light is lost through the stripped segment

and as the deflection increased more light was escaped. Results also showed the cracks were initiated at the peak load which is corresponding to sudden loss on the transmitted light. POFs sensors were used to detect the presence of cracks on concrete structure. However, the research didn't address whether the POFs could be used for detecting the width of the crack and whether it's widely opened or small cracks. Also the results showed a loss on the transmitted light at peak load which means that small cracks before the peak load weren't detected.

2.10.2. Embedded POF in Composite

Very few researches have been conducted in embedded POF into composite material and using OTDR for power loss assessment due to loading the composites. Schukar *et al,* (97) (98) used Multi-mode POF embedded into composite material made of glass fiber and epoxy resin laminate. Effect of POF on the laminate structure and the change on POF properties were included in the study. Multi-mode POFs with 1,000, 500 and 250 µm diameter were used. OTDR was used to measure the backscattering and the power loss during the composite curing where the curing takes place at 60° C. OTDR results showed no changes happened to the POF properties (change in dimensions and chemical reaction) during the curing process of the composite since no change in power loss or reflection took place. Result also showed the POF with 1,000 µm diameter cause large voids surrounding the optic fiber. Voids around the POF of 500 and 250 µm were less than that of 1,000 µm. POF 250 µm created the least disturbance to the structure geometry. Same study has also included the tension test of produced laminate with embedded POF 500 µm diameter. Tension test were conducted to measure the bonding force between the POF and laminate structure. Results showed that POF survived and the laminate failed at 1.6% strain with increase of 0.6 dB the backscattering loss (98).

Kuang *et al,* (99) (100) investigated the use of POFs sensors for monitoring the dynamic response of cantilever and simply supported beam under dynamic load condition. POFs sensors were attached to the surface of plastic beam and embedded into carbon-fiber

composite. Civil engineering structures such as suspension bridges, elevated water tanks, and wind turbine blades experience continuous dynamic loading such as vibration, repeated forces during use by traffic, and wind. Multi-mode 1 mm POF diameter was used in the experimental, 70 mm of POF length was stripped off from the cladding using a razor blade to improve the sensitivity of the POF sensors. A sensor POF was adhered to the surface of plain acrylic specimen using a fast cure cyanoacrylate adhesive. A second POF sensor was embedded between first and the second layer of eight layers of a woven carbon-fiber reinforced epoxy beam. The composite was cured at 90° C for 6 hours under pressure of 4 bar degree.

Flexural type loading condition test was conducted on prepared cantilever with attached and embedded sensors. For the two sensors, one end of the POF was attached to light source and the other end was connected to a light detector. Cantilever vibration was created by putting different weights on its tip and was allowed to vibrate. POF sensors data signal was collected during the beam vibration. Impact test using a free weight drop test was also conducted to evaluate out of plan deflection of composite beam. Various impact energies were used with maximum 6 J with different drop height and each sample was subjected to 5 energy impacts. Results from flexure strain versus POF signal (V) showed decrease in the light intensity as flexure strain increases. Results also showed the response of the POF sensors to the dynamic flexure test frequency, POF sensors showed a low sinusoidal at low frequency (5 Hz). Authors only evaluate the impact energy that caused failure. They did not investigate other impact energy levels and study the POFs sensor response, which is useful in analyzing the survivability of the structure and assess whether failure might happen. Composite beam specifications are not well described in the paper whereas authors only mentioned that the composite beam made of 8 layers of carbon woven fabric without describing the type of carbon fibers, woven fabric specification, type of resin and composite preparation technique. The used Data acquisition system and end to end loss technique are a time consuming and these systems need to be calibrated frequently in order to acquire accurate data and takes large space.

Takeda (101) investigated using embedded POF sensors into composite structure to detect and monitor the transverse crack propagation in composite material. This study depended on the occurred local deformation of POF during the transverse crack and its effect on the optical signal loss of POFs sensors. POFs sensors were embedded into glass fiber/epoxy composite. Tensile test was conducted on the prepared sample to obtain a relation between the optical power, strain and transverse crack density. Three composite of CFRP specimens were prepared. Specimen A was composed of five layers with orientation [90°/$0°_3$/90°] and used to study the optical loss associated with multiple crack in 90°. Specimen B was five layers oriented as $[0°]_5$ and used for studying the optical loss under tension. Specimen C was 5 layers oriented as $[0°]_5$ with a prepared initial crack on the center of the top layer before the conducted test and used to study the effect of the crack propagation on the optical loss. End to end loss technique was conducted to measure the optical power in parallel with strain gauge to measure the strain. Specimen Results showed a linear decrease of optical power against the strain before the cracks start, once the crack start the optical power change to nonlinearly decrease against the strain. Results of specimen B showed a linearly decreasing on the optical power against the strain until the sample break. Specimen C with initial crack showed a different behavior, optical power showed a nonlinearly decreasing against the strain from the beginning. The crack cause deformation to the POF which cause more and fast power loss compared to specimens A and B. POFs sensors have survived and did not break after the composite specimen failed. Embedded POFs sensors were found to be a powerful way to detect and monitor the transverse crack propagation in composite laminates. The locations of the cracks were not detected due to the limitation of equipment used to detect the signal from the POF sensors.

Wong *et al.* (102) used embedded POFs sensors embedded into woven carbon fiber epoxy prepreg composite for environmental monitoring. POF sensor was embedded into mid layer of four ply woven carbon composite. Composite prepared by lay-up in picture frame mold and cured at 75°C for 8 hours under pressure of 3 bar. End to end loss technique was used to measure the power loss using an ultra-high luminescent LED (612 nm wavelength) as a light

source and light-dependent resistor (LDR) and a low-cost commercial data acquisition system (ADC-16). Change on voltage was recorded as the light intensity change due to applied strain. Tensile test results showed decrease in received light attenuation as applied load increased in a linear manner. At the beginning of the test, POF sensor showed a nonlinear increase which increases the insensitivity of the sensors at low load. Tensile tests were repeated four times on the same sample to find the effect of repeatability on the POF sensors. Repeated test results showed a good repeatability performance for second test but third and fourth test showed some scattering at the same time and the authors attributed the behavior to the interaction between the POF and the matrix polymer without elaborating on specific cause. Authors didn't mention the POF and carbon woven fabric specification. This information is important to understand the reasons behind the scattering at the third and fourth test that may depend on the change in the POF structure due to repeated test which cause the light to scatter inside the POF core.

Kuang *et al.* (103) attached POFs sensors to a composite material to assess damage and study damping control. Composite beam material was made of eight layers of woven [0/90] carbon fiber reinforced epoxy resin (EP121-C15-53) with fiber volume fraction of 40%. Prepared composite beams were left to cure at 120°C under 4 bar pressure for 90 minutes. Multi-mode, step index POF of 1 mm diameter was used in the experiment and 70 mm of POF length was stripped off from the cladding using a razor blade to improve the sensitivity of the POF sensors. A POF sensor was adhered to the surface of composite beam using a fast cure cyanoacrylate adhesive. Optical transmission efficiency was studied to check the integrity of the POF sensor after the bonding process and showed no effect on POF properties. Impact test was conducted at energies ranged from 2 to 8 J. The test was conducted away from the POF sensors to prevent damaging the sensor. Four composite specimens were tested for each impact energy test. After each impact test, residual flexure test was conducted for each damaged specimen. Results showed a significant effect of the impact test on the residual flexural test results. No optical results were reported to show the capability of the POF sensors for recognition of impact and flexural test (signal analysis). Effect of impact on the

damping ratio was studied by utilizing damaged samples from the impact test. Results revealed that POF sensors are capable of the characterizing and monitoring the damping of damaged sample. However, authors only reported a dynamic optical response comparison between undamaged and damaged samples (impacted at 8 J) and didn't mention whether the other damaged sample at impact energies 2, 4, and 6 have the same trend. Additionally, POF power loss as a result of bending during vibration weren't reported.

2.11. Conclusion

This chapter showed the importance of structural health monitoring (SHM) systems for real time monitoring of global and local response of civil engineering and composite structures under dynamic load. Dynamic response such as vibration; acceleration, strain, deformation and displacement are needed to be monitored to detect signs of failure before it occurs, a matter that saves lives and reduce maintenance cost.

Electronic sensors such as conventional strain gage are used for local structure performance, accelerometer and displacement electronic sensors such as piezoelectric transducer (PZT), piezoceramic, piezofilm (PVDF), and acoustic emission sensors AE are used for monitoring global structure performance by attaching sensors to civil engineering and composite structures. These types of sensors have some advantages such as low cost, easy to handle, and high sensitivity in detecting potential failure. However, they have numerous disadvantages: (1) they are attached to the structure surface and thus vulnerable to adverse weather conditions, (2) their large size does not allow their use as embedded sensors to monitor internal strain and structure damage, (3) they are affected by electromagnetic interference, (4) they are characterized by their low corrosion resistance, (5) they require a complicated system to triangulate the fault location, (6) Strain gage sensors cannot be multiplexed, which means that each strain gage has to be connected to a separate data acquisition port, and limited to low strain detection.

Glass optical fiber sensors have many advantages over the electrical sensors such as small size, high strength, low attenuation, immunity to electromagnetic interference, multiplexing

capability, long term strain monitoring, high measurement resolution, resistance to corrosion, easy to be embedded into structures, highly sensitive, high temperature resistance, and non-electrically conductive. GOF sensors such as Phase-Modulated Sensors and Wavelength-Modulated sensors can be used to sense pressure, temperature, strain, quasi-distributed strain and displacement. For these reasons, numerous researchers were attracted to conduct works that dealt with GOF as embedded and surface sensors. They investigated the ability of GOF in monitoring the strain of composite structures during the resin curing process and whether there is an adverse effect on the mechanical properties resulting from their existence inside the structure to be monitored.

While GOF sensors possess the advantages listed above, they are: (1) very brittle and easy to break in bending, (2) easy to break at low tensile strain (1%), which make it very difficult to handle them, (3) limited to systems with few number of measurements due to their high cost, and (4) require very precise positioning with respect to the connectors as well as the light source, which demand very expensive special tools and long time for system development.

The disadvantages of the GOF prompted fiber optic researchers and producers to develop polymer optical fiber (POF). The POF sensors are characterized by: (1) high numerical aperture, (2) extremely flexible and easy to handle, (3) inexpensive, (4) easy to splice and cleave, (5) do not require protective layer, (6) can handle high tensile strain and high fracture toughness. The POF sensors existed commercially since 1970's. Early POF sensors suffered from high attenuation (1,000 dB/km). Due to their promising applications, optic fiber producers succeeded in producing improved POF with attenuation as low as 60 dB/km (28), which is still high compared to GOF. The advantages of POF and the relatively low attenuation attracted researchers to conduct works to explore their use as replacement to the electronic and GOF sensors. Studies were conducted on the behavior of POF sensors and its ability to be used as embedded sensors into civil engineering and composite. The common feature of the POF sensor was its large diameter of 1 mm that created resin pockets between composite layers, which affect the integrity of the host material. POF with lower diameters (250 and 500 micron) showed less tendency of resin pocket formation (98). Most of these

studies employed end to end loss technique to measure the signal loss associated with the mechanical behavior of the host. Some research was conducted using low resolution OTDR, which limit the system to only detect two consecutive failures in range greater than 3 m (event dead zone = 3 m).

As indicated in the literature review, Graded index Perfluorinated POF (GI-PF-POF) is a newly developed class of optic fiber. This development advanced the POF sensors in that they are thinner and possess low attenuation. At the time of writing, the public domain did not disclose research on using such POF as embedded sensors in composite structures. Additionally, no publications dealt with incorporating POF into 3D orthogonal woven composites. Unlike 2D woven structures, in 3D woven structures yarns are straight and POF can be easily inserted during preform formation either as a replacement of constituents or between them without causing irregularity or bulkiness. As such, the recognized advantages include: (a) thin POF will not have negative impact on the composite properties, (b) POF can be inserted during formation at different layers in x-direction and can be placed over small or large area that enable monitoring stress distribution in x-y plan and/or in the z-direction. The benefits of using POF and 3D woven structure combined with the capability of recently developed high resolution OTDR that measures backscattering and signal loss of optics fiber would allow measurement of power loss due to different modes of strain and deflection (tensile, bending, pressure, torsion) and temperature. It is the target of this work to take advantage of the recent development in POF, OTDR, and 3D orthogonal woven structures in conducting research in the area of smart composites to predict failure before it occurs.

References

[1] Fink, A., Kolesnikov, B. *Hybrid titanium composite material improving composite structure coupling.* s.l. : Institute of Structural Mechanics, German Aerospace Center (DLR), 2004.

[2] Zhan-Feng, G., Yang-Liang, D., Bao-Chen, S., and Xiu-Mei, J. Strain monitoring of railway bridges using optic fiber sensors. *Journal of quality in maintenance engineering.* 2007, Vol. 13, 2, pp. 186-197.

[3] Measures, R. M., Alavie, T., Masskant, R., Huang, S., Grant, L., Guha-Thakurta, A., Tadros, G., and Rizkalla, S. Fiber optics sensing for bridges. *4th International conference on short and medium bridges.* 1994, pp. 8-11.

[4] Inaudi, D. and Glisic, B. Distributed fiber optic strain and temperature sensing for structural health monitoring. safety and management, July 16-19, 2006.

[5] Mohamed, T. S., Johnson, C. and Rizkalla, S. Behavior of Three-Dimensionally Woven Glass Fiber Reinforced Polymeric Bridge Deck. 2006, pp. 18-20.

[6] M., Mohamed, A., Bogdanovich, L., Dickinson, J., Singletary, B., Lienhart. A new generation of 3D woven fabric preforms and composites. *SAMPE Journal.* 2001, Vol. 37, 3, pp. 8-17.

[7] A., Bogdanovich, *Advancements In Manufacturing And Applications Of 3-D Woven Preforms And Composites.*. s.l. : 16th International conference on composite materials, 2007.

[8] 8. Norton, T., Hassan, T., Rizkalla, S., and Mohamed, M. Behavior of 3-D woven glass fiber reinforced polymeric bridge deck slabs. *International conference: Future vision and challenge for urban development.* December 20-22, 2004.

[9] A., Bogdanovich, D., Wigent. Fabrication of 3-D Woven Preforms and Composites with Integrated Fiber Optic Sensors. *SAMPE Journal.* 2003, Vol. 39, 4, pp. 6-15.

[10] Lee, D. G., Mitrovic, M., Stewart, A. and Garman, G. Characterization of fiber optic sensors for structural health monitoring. *Journal of Composite Materials.* 2002, Vol. 36, pp. 1349-1366.

[11] Casas, J. R. and Cruz, P. J. S. Fiber optic sensors for bridge monitoring. *Journal of bridge engineering.* Novamber 1, 2003, Vol. 8, No. 6, pp. 362-372.

[12] Krohn, D. A. *Fiber optic sensors.* 2000. pp. 2-3.

[13] Meschede, D. *Optics, Light and laser: The Practical Approach to Modern Aspects of Photonics and Laser Physics.* Germany : Wiley-VCH Verlag GmbH & CO. KGaA, 2007.

[14] Daum, W., Krauser,J., Zamzow, P. E.,Ziemann, O.,. *POF – Polymer Optical Fibers for Data Communication.* Germany : Springer-Verlag Berlin Heidelberg , 2002.

[15] Appajaiah, A. *Climatic Stability of Polymer Optical Fibers (POF).* Berlin, Germany : Bundesanstalt für Materialforschung und -prüfung (BAM), 2005.

[16] Fiber Optics For Sale Co. *Fiber Optics For Sale Co.* [Online] Fiber optics for sale Company. [Cited: June 21, 2010.] http://www.fiberoptics4sale.com/Merchant2/optical-fiber.php.

[17] Kuzyk, M. G. *Polymer Fiber Optics, Material, Physics, and Applications.* Florida : Tylor & Francis Group, 2007.

[18] Zubia, J., and Arrue, J. Plastic Optical Fibers: An Introduction to Their Technological Processes and Applications. *Optical Fiber Technology.* 2001, Vol. 7, p. 101:140.

[19] Ab-Rahman, M. S.,Guna H.,Harun, M. H. Cost-Effective Fabrication of Self-Made 1´12 Polymer Optical Fiber-Based Optical Splitters for Automotive Application. *American J. of Engineering and Applied Sciences.* 2009, Vol. 2, 2, pp. 252-259.

[20] Hundscheidt, H.H.F. *Po1ymer Optical Fibre (qualities and phenomenons).* Netherlands : Faculty of Electrical Engineering, 1994.

[21] Tanakaa, A., Sawadaa, H., Takoshimaa, T., Wakatsuki, N. New Plastic Optical Fiber Using Polycarbonate Core and Fluorescence-Doped Fiber for High Temperature Use. *Fiber and Integrated Optics.* 1987, Vol. 7, 2, pp. 139-158.

[22] Stoeffler, K., Dubois, C., Ajji, A., Guo, N., Boismenu,F., Skorobogatiy, M. Fabrication of All-Polymeric Photonic Bandgap Bragg Fibers Using Rolling of Coextruded PS/PMMA Multilayer Films. *POLYMER ENGINEERING AND SCIENCE.* 2010, pp. 1122-1127.

[23] Polishuk, P. Plastic Optical Fibers Branch Out. *TOPICS IN DESIGN AND IMPLEMENTATION.* 2006, Vols. 0163-6804, pp. 140-148.

[24] Koike, Y., Ishigure, T., and Nihei, E. High-Bandwidth Graded-Index Polymer optical fiber. *JOURNAL OF LIGHTWAVE TECHNOLOGY.* 1995, Vol. 13, 7, pp. 1475-1489.

[25] Koike, Y., Ishigure, T. Bandwidth and tranmission Distance achieved by POF. *IEICE Trans. Commun.* 1999, Vols. E 82-B, 8, pp. 1287-1295.

[26] Ishigure, T., Nihei, E., and Koike, Y. Optimum refractive index profile of the graded-index polymer optical fiber, toward gigabit data links. *APPLIED OPTICS.* 1996, Vol. 35, 12, pp. 2048-2053.

[27] Kondo, A., Ishigure, T., and Koike, Y. Fabrication Process and Optical Properties of Perdeuterated Graded-Index Polymer Optical Fiber. *JOURNAL OF LIGHTWAVE TECHNOLOGY.* Vol. 23, 8, pp. 2443-2448.

[28] Ziemann, O.,Krauser, J., Zamzow, P., E., Daum, W.,. *POF Handbook, Optical Short Range Transmission Systems.* Verlag Berlin Heidelberg : Spring, 2008. pp. 137-195.

[29] Koike, y., Ishigure, t. High-Bandwidth Plastic Optical Fiber for Fiber to the Display. *JOURNAL OF LIGHTWAVE TECHNOLOGY.* December 2006, Vol. 24, 12, pp. 4541-4553.

[30] POF Application Center. [Online] [Cited: Feb 22, 2011.] http://www.pofac.de.

[31] Kaino, T., Jinguji, K., Nara, S. Low loss poly(methylmethacrylate-d8) core optical fibers. *Appl. Phys. Lett.* April 1983, Vol. 42, 4, pp. 567-569.

[32] Emslie, c. Review Polymer optical fibres. *JOURNAL OF MATERIALS SCIENCE 23.* 1988, Vol. 23, pp. 2281-2293.

[33] Lee, L., Blyler, Jr., Arther, Jr., Salamon, t., Viriyayuthakorn, M. *Process for Fabricating Plastic Optical fiber. US 6,254,808 B1* USA, July 3, 2001.

[34] Asai, m., Hirose,r., Kondo,A., Koike, Y. High-Bandwidth Graded-Index Plastic Optical Fibe by the Dopant Diffusion Coextrusion Process. *JOURNAL OF LIGHTWAVE TECHNOLOGY.* October 2007, Vol. 25, 10, pp. 3062-3067.

[35] Asai, M., Nehashi,K., Koike, Y. Control of Refractive Index Distribution for High-Bandwidth Graded Index Plastic Optical Fiber. *JOURNAL OF LIGHTWAVE TECHNOLOGY.* August 15, 2008, Vol. 26, 16, pp. 2909 - 2918.

[36] White, W.,Blyler Jr., Ratnagiri,R., Park, M. Manufacture of Perfluorinated Plastic Optical Fibers. *Optical Fiber Communication Conference.* 2004, p. 3.

[37] Anderson, D., Johnson, L., Bell, F.,. Troubleshooting Optical-Fiber Networks. *Understanding and Using your Optical Time-Domain Reflectometer.* San Diego, California : Elsevier Academic Press, 2004.

[38] Liehr, S., Nother,N., Krebber, K. Incoherent optical frequency domain reflectometry and distributed strain detection in polymer optical fibers. *IOP PUBLISHING, Meas. Sci. Technol.* 2010, Vol. 21, p. 4.

[39] Saunders, c.,Scully, P. Distributed plastic optical fibre measurement of pH using a photon counting OTDR. *Journal of Physics: Conference Series 15.* 2005, Vol. 25, pp. 61-66.

[40] Saunders, C., Scully, P. Sensing applications for POF and hybrid fibres using a photon counting OTDR. *INSTITUTE OF PHYSICS PUBLISHING,MEASUREMENT SCIENCE AND TECHNOLOGY.* 2007, Vol. 18, pp. 615-622.

[41] Husdi, I., Nakamura, K., Ueha, S. Sensing characteristics of plastic optical fibres measured by optical time-domain reflectometry. *INSTITUTE OF PHYSICS PUBLISHING, Meas. Sci. Technol.* 2004, Vol. 15, pp. 1553-1559.

[42] AOYAMA, K., NAKAGAWA, K., ITOH, T. Optical Time Domain Reflectometry in a Single Mode fiber. *IEEE JOURNAL O F QUANTUM ELECTRONICS.* 1981, Vols. QE-17, 6, pp. 862-868.

[43] Legré, M., Thew, R., Zbinden, H., Gisin, N. High resolution optical time domain reflectometer based on 1.55mm up-conversion photon-counting module. *Optics Express,The optical Society.* 2007, Vol. 15, 13, pp. 8237-8242.

[44] Corporation, Yokogawa Electric. *Guidebook for Optical Time Domain Reflectometer.* s.l. : Communication and Measurement Business Headquarters, 2006.

[45] Danielson, B. Optical time-domain reflectometer specifications and performance testing. *APPLIED OPTICS.* 1985, Vol. 24, 15, pp. 2313-2322.

[46] Measuring fiber attenuation: optical time domain reflectometer (OTDR). *Invocom.* [Online] [Cited: 03 03, 2011.] http://www.invocom.et.put.poznan.pl/.

[47] Gagnon, J. *THE FUNDAMENTALS OF AN OTDR.* s.l. : EXFO, 2010.

[48] Beller, J. Principal of OTDR Operation. *OTDRs and Bacscattered Measurements.*

[49] Hull, D., and Clyne, T.W. *An Introduction to composite Materials.* s.l. : Cambridge University Press, Second Edition,1996.

[50] Wallenberger, T., Bingham, P. *Fiberglass and Glass Technology, Energy-Friendly Compositions and Applications.* New york : Springer Science and Business Media, 2010.

[51] Yuan, F., Tsai, L., Prakas, V., Rajendran, A. M., and Dandekar, D. P. Spall strength of glass fiber reinforced polymer composites. *International Journal of Solids and Structures.* 2007, Vol. 44, 24, pp. 7731-7747.

[52] Peter, S.T. *Hand Book of Composite material.* London, UK : Chapman & Hall, London, Second Edition, 1998.

[53] Shokrieh, M. M., and Omidi, M. J. Compressive response of glass–fiber reinforced polymeric composites to increasing compressive strain rates. *Composite Structures.* 2009, Vol. 89, 4, pp. 517-523.

[54] Fukuda, H., and Kawata, K. Young's Modulus of Short Fiber Composites. *Fiber Science and Technology.* 1974, Vol. 7, pp. 207-222.

[55] Barbero, E. J. *Introduction to Composite Material Design.* s.l. : Taylor and Francis, Inc, 1998.

[56] Smith, S.A., Emmanwori, L.L., Sadler, R.L. and Shivakumar, K.N. *Evaluation of Composite Sandwich Panels Fabricated Using Vacuum Assisted Resin Transfer Molding.* Greensboro, North Carolina A&T State University : Center for Composite Materials Research.

[57] Unrivalled Technology in Advanced Composite Materials. *Gurit, Composites Materials Technology from.* [Online] [Cited: February 11, 2010.] http://www.gurit.com.

[58] Majumder, M., Gangopadhyay, T. K., Chakraborty, A. K., Dasgupta, K. and Bhattacharya, D.K. Fibre Bragg gratings in structural health monitoring-Present status and applications. *Sensors and Actuators A.* 2008, Vol. physical 147, pp. 150-164.

[59] Li, H., Li, d., and Song, G. Recent applications offiber optic sensors to health monitoring in civil engineering. *Engineering Structures.* 2004, Vol. 26, pp. 1647–1657.

[60] Grietens, B., and Voet, M. Fiber Optic Sensors to Monitor Structural Components Made of Composite Material. *Sensors and Transducer Journal.* 2007, Vol. 80, 6, pp. 1289-1294.

[61] Hamouda, T.M., Seyam, A.M., and Saad, M.M. Prediction of Failure of 3D Woven Composite Structures using Embedded Fiber Optic Sensors. *World Journal of Engineering.* 2010, Vol. 7, 1, pp. 103-112.

[62] Sirohi, J., and Chopra, I. Fundamental Understanding of Piezoelectric Strain Sensors. *JOURNAL OF INTELLIGENT MATERIAL SYSTEMS AND STRUCTURES.* 2000, Vol. 11, pp. 246-257.

[63] *Wireless Sensors Technologies for Monitoring Civil Structure.* Mascarenas, D., Flynn, E., Todd, M., Park, G., Farrar, C. Orlando : s.n., 2008. the 26th International Modal Analysis Conference. pp. 16-20.

[64] Ide, H., Abdi,F., Miraj,R., Dang,C., Takahashi,T., Sauer,B. Wireless-Zigbee Strain Gage Sensor System for Structural Health Monitoring. *Photonics in the Transportation Industry: Auto to Aerospace II.* Vol. 7314, pp. 3-12.

[65] Rao, M., Bhat,M., Murthy,C. Structural Health Monitoring (SHM) Using Strain Gauges, PVDF Film and Structural Health Monitoring (SHM) Using Strain Gauges, PVDF Film and. *Proc. National Seminar on Non-Destructive Evaluation.* 2006, pp. 333-337.

[66] Rumsey, M., Paquette,J., White,J., Werlink,R., Beattie,A., Pitchford,C., Dam,J. Experimental Results of Structural Health Monitoring of Wind Turbine Blades. *American Institute of Aeronautics and Astronautics.* 2008, pp. 1-14.

[67] Geib, D. *Multiplexing of Extrinsic Fabry-Perot Optical Fiber Sensors for Strain Measurements.* Virginia Polytechnic Institute and State University, M.S. Thesis. 2003. Under super vision of Dr. Anbo Wang,Dr. A. Safaai, Dr. M.P. Singh.

[68] Kessler, S. *Piezoelectric-Based In-Situ Damage Detection of Composite Materials for Structural Health Monitoring Systems.* s.l. : Massachusetts Institute of Technology, P.h.D Thesis, 2002. Under super vision of Dr.Spearing,s., Cesnik,C., Atalla,M., Schoor,M..

[69] Rippert, L., Papy, J., Wevers, M., Huffel, S. Fibre optic sensor for continuous health monitoring in CFRP composite materials. *Smart structures and materials.* SPIE, 2002, Vol. 4693, pp. 312-323.

[70] Leng J., and Hao J. Damage assessment of composite laminate by using fiber optic AE sensors based on fused-tapered coupler. *Proc. of SPIE.* SPEI, 2007, Vol. 6531, pp. 1021-1025.

[71] Bullock, D. Embedded Bragg Grating fiber optic sensor for composite Flexbeam. *Fiber Optics Smart Structure and Skins V.* SPIE, 1992, Vol. 1798, pp. 253- 261.

[72] Shaaf, K., Cook, B., Ghezzo, F., Starr, A., and Nemat-Nasser, S. Mechanical properties of composite materials with integrated embedded sensor networks. *Smart structures and materials.* SPIE, 2005, Vol. 5765, pp. 781-785.

[73] Roberts, S. S. J., and Davidson, R. Mechanical Properties Of Composite Material Containing Fiber Optics Sensors. *Fiber Optics Smart Structure and Skins IV.* SPIE, 1991, Vol. 1588, pp. 326-341.

[74] Shivakumar, K., and Emmanwori, L. Mechanics Of Failure Of Composite Laminates With An Embedded Fiber Optics Sensor. *Journal of Composite Materials.* 2004, Vol. 38, pp. 669- 680.

[75] Anastasi, R. F., and Lopatin, C. *Application of a Fiber Optic Distributed Strain Sensor system to woven E-Glass Composite.* s.l. : NASA Langley Technical Report Server, 2001.

[76] Silva-Munoz, R., Lopez-Anido, R., and Nye, R. Fabrication of Secondary Bonded VARTM Composite Doubled-Plate Joint Panel with Embedded Fiber Bragg Grating Strain Sensors for Fatigue Crack Monitoring. *COMPOSITES & POLYCON* . 2007, pp. 1-12.

[77] Kang, H., Hoon Kang, D. Hong, C. and Gon-Kim, C. Monitoring of fabrication strain and temperature during composite cure using fiber optic sensors. *SPIE.* 2001, Vol. 4336, pp. 211-218.

[78] Kang, H., Hoon Kang, D. Hong, C. and Kim, C. Cure monitoring of composite laminates using fiber optic sensors. *INSTITUTE OF PHYSICS PUBLISHING, SMART MATERIALS AND STRUCTURES.* 2002, Vol. 11, pp. 279–287.

[79] *Simultaneous monitoring of strain and temperature during and after cure of unsymmetric composite laminate using fibre-optic sensors.* Kang, H., Hoon Kang, D.

Hong, C. and Kim, C. 2003, INSTITUTE OF PHYSICS PUBLISHING, SMART MATERIALS AND STRUCTURES, Vol. 12, pp. 29–35.

[80] Kosaka, T., Osaka, K., Nakakita, S., and Fukuda, T. Fiber Optic strain Monitoring of Textile GFRP during RTM Molding and Fatigue Tests by Using Embedded FBG Sensors. *Smart Structure and Materials.* SPIE, 2003, Vol. 5056, pp. 73- 80.

[81] CHANG, X., LI,M., HAN,X. Recent development and applications of polymer optical fiber sensors for strain measurement. *Front. Optoelectron. China.* 2009, Vol. 2, 4, pp. 362-367.

[82] *Plastic Optical Fibres (POF) in sensing – current status and prospects.* Kalymnios, D. Bellingham : SPIE, 2005. 17th International Conference on Optical Fibre Sensors. Vol. 5855.

[83] Zubia, J., Arrue, J. Plastic Optical Fibers: An Introduction to Their Technological Processes and Applications. *Optical Fiber Technology.* 2001, Vol. 7, pp. 101-140.

[84] Grattan, K., Sun, T. Fiber optic sensor technology: an overview. *Sensors and Actuators.* 2000, Vol. 82, pp. 40-61.

[85] Husdi, I., Nakamura, K., Ueha, S. Sensing characteristics of plastic optical fibres measured by optical time-domain reflectometry. *MEASUREMENT SCIENCE AND TECHNOLOGY, INSTITUTE OF PHYSICS PUBLISHING.* 2004, Vol. 15, pp. 1553–1559.

[86] Saunders, C., Scully, P. Distributed plastic optical fibre measurement of pH using a photon counting OTDR. *Sensors & their Applications XIII, Journal of Physics.* 2005, Vol. 15, pp. 61-66.

[87] Fukumoto, T., Nakamura, K.,Ueha, S. A POF-based distributed strain sensor. *Proc. of SPIE.* 2007, Vol. 6770, pp. 1-9.

[88] Peters K., Kiesel, S., Abdi, O., Hassan, T., Kowalsky, M. Intrinsic polymer optical fibers for large deformation strain sensors. *News Room.* 2008, Vol. 10.1117/2.1200802.1065.

[89] Kiesel, S., Peters K., Hassan T., and Kowalsky, M. Behaviour of intrinsic polymer optical fibre sensor for large-strain applications. *MEASUREMENT SCIENCE AND TECHNOLOGY, IOP PUBLISHING.* 2007, Vol. 18, pp. 3144 – 3154.

[90] Merzbacher, C.I., Kersey A.D., Friebele, E.J. Fiber optic sensors in concrete structures: a review. *SMART MATERIALS AND STRUCTURES, IOP PUBLISHING.* 2011, Vol. 20.

[91] Kiesel, S., Van Vickle, P., Peters, K., Abdi, O., Hassan, T., Kowalsky, M.,. Polymer optical fiber sensors for the civil infrastructure. *Mechanical, and Aerospace Systems, SPIE Sensors and Smart Structures.* 2006, Vol. SPIE 6174, pp. 1-12.

[92] Nakamura, K., Husdi,I., Ueha, S. Memory effect of POF distributed strain sensor. *Second European Workshop on Optical Fibre Sensors, Proceedings of SPIE.* Vol. 5502, pp. 144-147.

[93] Nakamura, K., Husdi, I., Ueha, S. A distributed strain sensor with the memory effect based on the POF OTDR. *17th International Conference on Optical Fibre Sensors, Proceedings of SPIE.* 2005, Vol. 5855, pp. 807-810.

[94] Liehr, S., Lenkea,P., Krebbera,K., Seegerb,M., Thieleb,E., Metschiesb,H., Gebreselassie, B., Münich, J., Stempniewski, L. Distributed strain measurement with polymer optical fibers integrated into multifunctional geotextiles. *Optical Sensors, Proc. of SPIE.* Vol. 7003.

[95] Liehr, S., Lenke,P., Wendt,M., Krebber,K., Seeger,M., Thiele,E., Metschies, H., Gebreselassie,B., Münich, J. Polymer Optical Fiber Sensors for Distributed Strain Measurement and Application in Structural Health Monitoring. *IEEE SENSORS JOURNAL.* 2009, Vol. 9, 11, pp. 1330-1338.

[96] Kuang, K., Akmaluddin, Cantwell, W., Thomas, C. Crack detection and vertical deflection monitoring in concrete beams using plastic optical fibre sensors. *MEASUREMENT SCIENCE AND TECHNOLOGY, INSTITUTE OF PHYSICS PUBLISHING.* 2003, Vol. 14, pp. 205-216.

[97] Peters, K. Polymer optical fiber sensors- a review. *Smart Materials and Structures, IOP science.* 2011, Vol. 20, pp. 1-17.

[98] Krebber, K.,Lenke,P., Liehr,S.,Schukar,M., Wendt,M., Witt, J. DISTRIBUTED POF SENSORS – RECENT PROGRESS AND NEW CHALLENGES. *Invited Paper Inernational conference on Plastic optical Fiber.* Yokohama, Japan : s.n., 2010.

[99] Kuang, K., Cantwell, W. The use of plastic optical fibre sensors for monitoring the dynamic response of fibre composite beams. *MEASUREMENT SCIENCE AND TECHNOLOGY, INSTITUTE OF PHYSICS.* 2003, Vol. 14, pp. 736–745.

[100] Kuang, K.,Quek,S.,Koh,C.,Cantwell,W., Scully,P. Plastic Optical Fibre Sensors for Structural HealthMonitoring:A Reviewof Recent Progress. *Journal of Sensors, Hindawi Publishing Corporation.* 2009, Vol. 2009, p. 13.

[101] Takeda, N. Characterization of microscopic damage in composite laminates and real-time monitoring by embedded optical fiber sensors. *International Journal of Fatigue 24, Elsevier Science Ltd.* 2002, Vol. 24, pp. 281–289.

[102] Wong, Y., Scully, P., Bartlett, R., Kuang, k., Cantwell, W. Plastic Optical Fibre Sensors for Environmental Monitoring: Biofouling and Strain Applications. *Blackwell Publishing Ltd.* 2003, Vol. 39, pp. 115-119.

[103] Kuang, K., Cantwell,W. The use of plastic optical fibres and shape memory alloys for damage assessment and damping control in composite materials. *MEASUREMENT SCIENCE AND TECHNOLOGY, INSTITUTE OF PHYSICS PUBLISHING.* 2003, Vol. 14, pp. 1305–1313.

[104] Kiesel S., Van Vickle P., Peters K., Abdi O., Hassan T., and Kowalsky M.,. Polymer optical fiber sensors for the civil infrastructure. *Proc. SPIE Smart Mater. Struct. Symp.* Vol. 6174, pp. 996–1007.

CHAPTER 3

3. Objectives

It was indicated in the literature review chapter that the prior research in monitoring composite structure while subjected to strain of different modes did not take advantage of the recently developed GI-PF-POF, 3D orthogonal woven structure, and high resolution OTDR that measures backscattering and signal loss of optics fiber would allow measurement of power loss due to different modes of strain and deflection (tensile, bending, pressure, torsion) and temperature. Choosing the optimum sensors that can be embedded in any structure should consider many parameters. In order to cover more area of the host structure, Optic sensors has to be embedded in continuous manner which cause optic fiber to bend at the edges. Resulting loss at these bending points should not cause signal loss to have a qualified sensor. Effect of composite constituents such as preform structural parameters and resin type on embedded POF is very critical. These must be designed or selected to ensure proper functioning of the sensor without the loss of its sensitivity or negatively impact the host structure integrity. Sensing characterization of embedded POF sensors in 3D orthogonal woven composite during manufacturing process, under bending and impact damage helps to understand composite behavior and predict structures failure. The lack of research in this area is the inspiration behind undertaking the current research.

The main goal of this research is to evaluate different types of optic fibers and identify their potential use as sensors for predicting composite structure failure. The target is to develop systems based on 3D orthogonal woven composite structures with embedded optic fiber sensors in order to monitor and identify the location of structure failure before it takes place.

Range of experiments was conducted to achieve the goal of the proposed research. The experiments are structured to:

1- Evaluate different types of GOF and GI-PF-POF sensors to identify their capabilities in detecting bending deflection using end to end power loss technique
2- Investigate effect of resin type on the integrity of POF sensors based on change on backscattering level and induced signal attenuation during the curing time

3- Evaluate the effect of embedded POF in 3D orthogonal woven composites on host structure integrity.

4- Sensing characterization of embedded newly developed GI-PF-POF in monitoring 3D orthogonal woven composites manufacturing process. Also investigate the response of embedded POF to increment load and repeated impact throughout OTDR backscattering level and induced signal attenuation.

CHAPTER 4

4. Evaluation of Optic Fibers as Embedded Sensors for Structure Health Monitoring of Fiber Reinforced Composites

Abstract

Advantages of optical sensors whether Silica optic fiber (SOF) or Polymer optical fiber (POF) over conventional electronic sensors have attracted the attention of numerous researchers for using them as sensors for structure health monitoring. SOFs established themselves in signal for communicating digital data for many applications. SOFs are, however, exhibit drawbacks such as brittleness, low strain, and attenuation due to bending. These drawbacks limit the use of SOF in fiber reinforced composites as embedded sensors. Unlike SOF, the newly developed POF do not possess such drawbacks and they provide opportunity for monitoring the health of fiber-based composite structures. Bending in optical fiber is a major concern due to fiber attenuation at bending points resulting from preform structure during formation.

The main objective of the present study is to evaluate the effect of the macrobending of SOF and POF on signal power integrity to identify their capability as integrated sensors into composites from textile preforms. Two types of SOFs and a newly developed Perfluorinated POF (PF-POF) were evaluated in 3-point macrobending test bed using laser light source. The relationships between the optic fibers signal loss and bending radius, bending deflection and wrap angle were established. Our research identified the range of capabilities of the studied optic fibers as embedded sensors in fiber-based composites using the developed test bed. The results showed that POF provides higher sensitivity and range of bending deflection compared to SOF. The work also unveiled the bending radius at which no signal loss occurred.

4.1 Introduction

High maintenance, heavy weight and corrosion of steel have opened research areas to replace steel with much lighter fiber reinforced composite (FRC), which are known to be stronger,

lighter than steel and resistant to corrosion. The advantages of composite materials have opened the door for them to replace steel and alloy metals in numerous markets and applications like aerospace, automotive, windmill, military, bridges, and constructions. During their use, structures are subjected to stresses and they may unpredictably fail and cause loss in lives and resources. The exterior of structures in areas of disasters (such as storms and earthquakes) may seem undamaged while the interior structure elements are failing. System that are able to predict such problems before damages take place are obviously desirable so measures can be taken to reinforce the structure and avoid failure. The development of these systems has been recently the subject of extensive research.

Conventional sensors such as strain gage, accelerometer and displacement are used for structures (such as civil engineering and composite) health monitoring (1) (2) (3) (4). They are attached to the structure surface and thus negatively affected by adverse weather conditions, characterized by their large size that does not allow their use as embedded sensors to monitor internal strain and structure damage, affected by electromagnetic interference, and possess low corrosion resistance. Additionally, they require complicated systems to triangulate the fault location and cannot be multiplexed. On the other hand, optical fiber sensors have many advantages over the conventional sensors. Optic fibers advantages include small size, high strength, low attenuation, immunity to electromagnetic interference, multiplexing capability, resistance to corrosion, easy to be embedded into structures, highly sensitive, and high temperature resistance. Silica optical fiber (SOF) sensors can be used to sense pressure, temperature, strain, quasi-distributed strain and displacement (5). For these reasons, numerous researchers used SOF as embedded and surface sensors (6) (7) (8) (9). While SOF sensors possess the advantages listed above, they are not without drawbacks. SOF are very brittle and require very precise positioning with respect to the connectors as well as the light source, which demand very expensive special tools and long time for system development (10).

The disadvantages of the SOFs prompted fiber optic researchers and producers to develop polymer optical fiber (POF) sensors, which are characterized by high numerical aperture,

extremely flexible and easy to handle, inexpensive, easy to splice and cleave, do not require protective layer, and can handle high tensile strain and high fracture toughness (106). Studies were conducted on the behavior of POF sensors and its ability to be used as embedded sensors into geotextile, civil engineering and composite structures (12) (13) (14) (15) (16) (17).

Three-dimensional (3D) textile structures preforms are formed using different technologies such as nonwoven, stack of two-dimensional (2D) woven, and 3D orthogonal and stitched woven. Due to their integral bounded structures, 3D woven fabric preforms are known for their advantages over the nonwoven and 2D woven preforms in that they provide higher resistance to crack propagation, eliminate delamination, faster in resin transfer, and could be formed with very low to very high fiber volume fraction (18). One class of 3D woven preforms is 3D orthogonal woven preforms. 3D orthogonal woven preforms (Figure 4.1) are integrated structures with three yarn systems that are combined without interlacing resulting in no crimp in yarns (19). SOF and POF are characterized by its small diameters, which ease their integration between layers of stacked 2D fabrics, or integrated in 2D and 3D preforms during weaving process to be part of the preform (20). Fiber optic can be integrated in 3D orthogonal woven preforms in y-direction and/or x-direction; these two directions maintain the optical fiber straight inside the 3D preform (Figure 4.1). Unlike the 3D orthogonal structures, 2D woven preforms may cause bending of yarns as a result of interlacing as it can be seen from Figure 4.2. Continuous insertion of the optical fiber is required to cover large area of the preform, which requires the optical fiber to be bent at the preforms edges (Figure 4.1).

Bending of SOF or POF is a major concern due to fiber attenuation in power signal at bending points. Since integration of optical fiber in 2D preform and continuous insertion techniques causing macrobending in integrated optical fiber, studying bending loss of optical fiber is essential to identify the range of applicability of such sensors and the stability of their integration in 2D and 3D preforms. The main objective of the present study is to evaluate the effect of the macrobending of SOF and POF on signal power integrity to identify their

capability as integrated sensors into composites from textile preforms. Macrobending loss parameters such as bending radius, bending deflection and wrap angle are addressed.

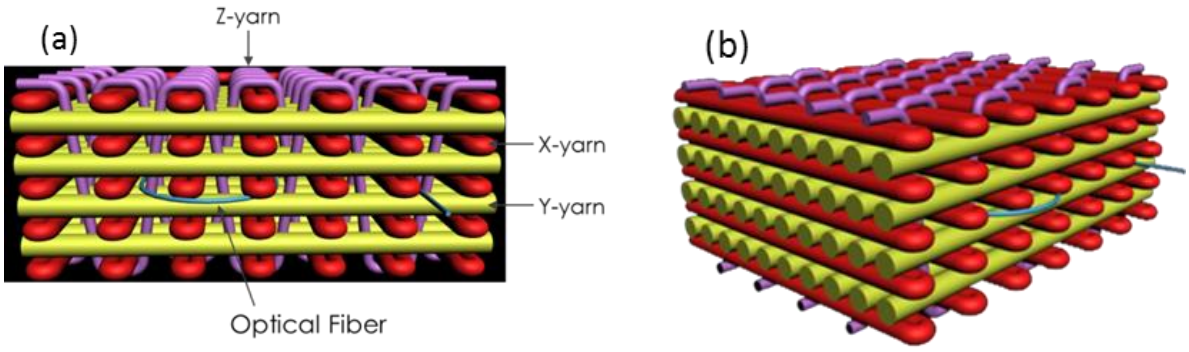

Figure 4.1 Schematic of thick, integral 3D orthogonal woven structure

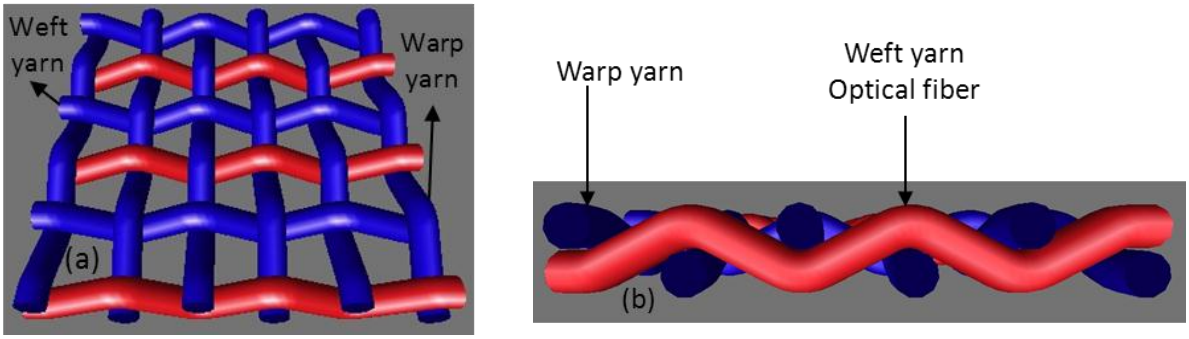

Figure 4.2 Figure 2 Schematic of 2D woven with embedded optical fiber

4.1.1 Bending loss in optical fiber

An optical fiber consists of at least two optically dissimilar materials; the core and the cladding. The cladding is low reflective index material and the core is made of high reflective index material (21). Difference in refractive index between optical fiber core and cladding cause the light to propagate along the optical fiber length throughout the total internal reflection. Signal attenuation occurs as light propagate along the optical fiber as a result of

imperfection, absorption, scattering, and bending. Macrobending and microbending are two types of bending that cause attenuation on power signal. Macrobending (bending radius is much greater than optical fiber radius) of optical fiber will causes signal loss and this loss on optical power will lead to a reduction on fiber performance. Light propagate from one end of the fiber to the other end through the total internal reflection at the interface between core and cladding. This internal reflection occurs at a critical angle that keeps the light reflected along the axis of the optical fiber. Macrobending of optical fiber may cause the incident light to reflect at an angle greater than the critical angle. Figure 4.3(a) shows a trace of light rays indicated on black arrows reflected at angels' Θ_1 and Θ_2 as a result of weaving the optical fiber in 2D woven structure as an example. These angles are greater than the critical angle Θ_c, which cause some of the light to refract out of the optical fiber core through the cladding and cause signal attenuation. Microbending (bending with small curvature) loss is caused by the imperfection and irregularity of the optical fiber material during the manufacturing process (22). These irregularity or imperfection of the core or cladding will cause deviation from perfect total internal reflection. Figure 4.3(b) shows a light rays reflect with angle Θ_3 and Θ_4, these angles are greater than critical angle Θ_c and causes the light to refract out of the optical fiber core through the cladding and the signal loss will occur (23).

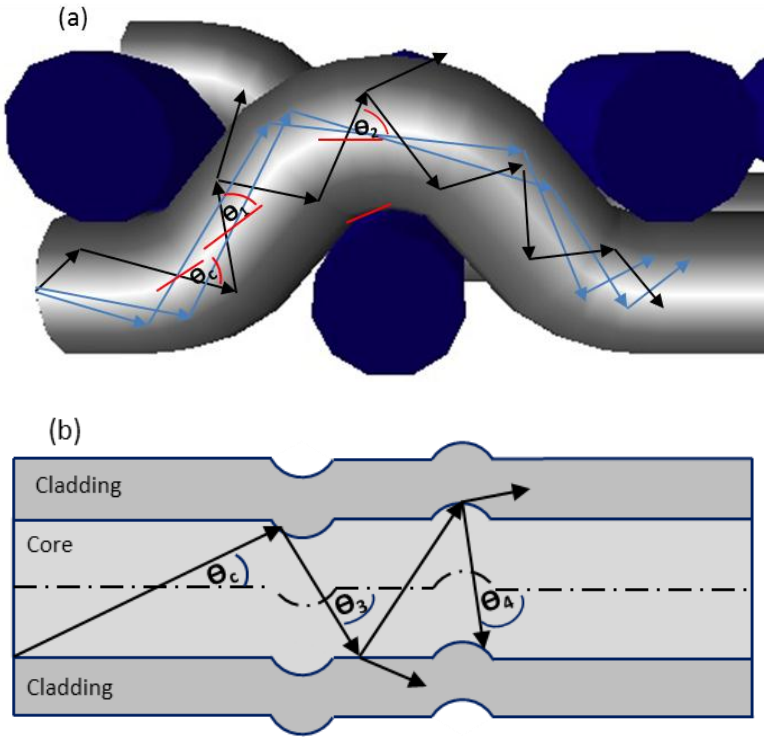

Figure 4.3 Optical fiber bending loss a) macrobending loss b) microbending loss

4.2 Experimental

4.2.1 Materials

Materials used to form 3D orthogonal woven composites include fiber glass (supplied by PPG Industries, Shelby, NC, USA) to manufacture the preforms, fiber optic, and polyester resin. The advantageous characteristics (high tensile strength, high heat and chemical resistance, and dimensional stability, low cost) of glass fibers promoted their use in FRC. Three different linear densities of fiber glass were acquired for the x, y, and z yarns. The linear densities are 735 tex, 2275 tex, and 276 tex, respectively.

A SOF per each 3D woven sample produced was placed in the middle of the preforms in the y-direction. Two types of Multimode fiber optic (which is an optical fiber whose core diameter is large compared to the optical wavelength and consequently, a large number of light modes are capable of propagation) were used; namely MLD and MFD. Table 4.1 shows

the specifications of the two optic fibers obtained from the supplier's catalog (NewPort). MFD consists of a core surrounded by a cladding layer. These two layers are surrounded by the acrylate coating layer to protect the fiber optic.

Table 4.1 SOF specifications

Model	Operating Wavelength (nm)	NA	Core Diameter (µm)	Cladding Diameter (µm)	Coating Diameter (µm)	Attenuation @850/1300 nm (dB/km)	Bandwidth @850/1300 nm (MHz/km)
F-MFD	850/1300	0.275	62.5 ±3	125 ±2	250 ±15	3.2/0.9	160/500
F-MLD	850/1300	0.29	100 ±4	140 ±3	250 ±15	4.0/1.5	100/100

Second type of optical fiber is POF (GigaPOF-50SR), which is recently developed by Chromis Fiber Optics, was selected to investigate its response and characterize its sensitivity to bending. This type of POF is characterized by low attenuation, IR-transparent, high bandwidth, graded refractive index, multi-mode. This optic fiber is bare fiber (does not need protective jacket) with core and cladding material made of Perfluorinated polymer. Table 4.2 depicts the fiber specifications.

Table 4.2 GigaPOF-50SR specification

Model	Core Diameter (µm)	Cladding Diameter (µm)	Max. Tensile load (N)	Attenuation at 850 nm (dB/km)
POF-50SR	50 ± 5	490 ±5	7.0	< 60

4.2.2 Formation of 3D Woven Preforms and Composites

Four 3D orthogonal specimens were woven using four layers of y-yarns. 3D weaving machine donated by 3TEX, Inc. and available at the College of Textiles, NCSU was used to form the samples with two different pick densities. Linear loom speed is 12 picks/min with 5 simultaneous insertions (total picks/min is 60 x 2 = 120 since the process is set for double insertion per shed). Two samples were woven with pick density of 3.14 picks/cm/layer (or total 15.7 picks/cm), the other two samples were woven with pick density of 5.5 picks/cm/layer (or total 27.5 picks/cm). Warp yarns (y-direction) are split to four sheets to form the multi-sheds (Figure 4.4). Five filling yarns (x- direction) were inserted from one side. The five filling yarns were inserted through five sheds. Three sheds are formed between the four y-yarns and two sheds are formed at the top and bottom of the four layers of y-yarns and two z-yarns layers (very top and bottom sheds).

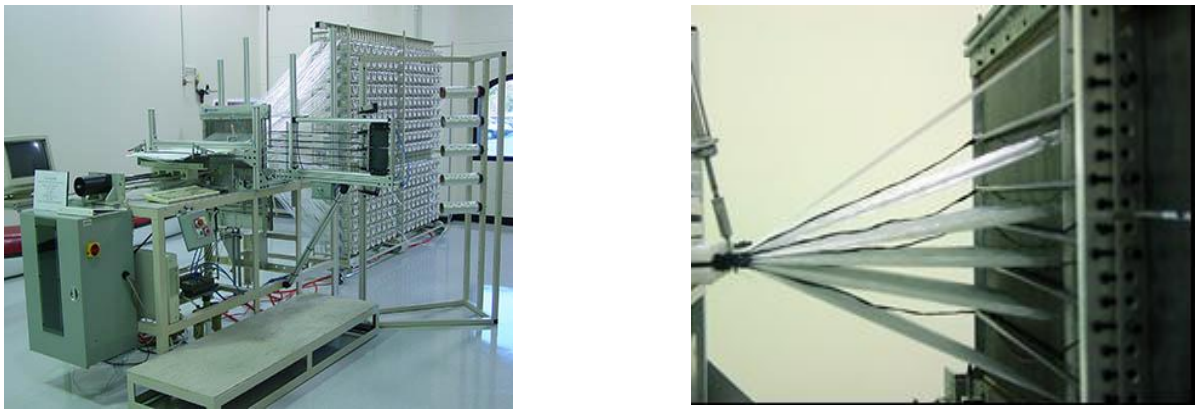

Figure 4.4 Left shows overall view of the 3D weaving machine and right shows the machine during multi-insertion of filling yarns (x-yarns) through multi-shed formed of warp yarns (y-yarns) and z-yarns (top and bottom sheets)

Optic fibers were embedded in the 3D orthogonal woven structure during weaving. Each fiber optic was placed in the second layer in the y-direction (middle layer). Figure 4.5 shows an optic fiber placed in the sample center. To produce composites (solidify the preforms),

Vacuum Assisted Resin Infusion Molding technique was employed. In this process a vacuum pressure is used to remove air from the sample and pull resin into the preforms. The process increases the compaction of the structure and produces composites with low resin content. Figure 4.6 - Figure 4.8 illustrate the steps of the resin infusion process. Figure 4.6 shows an image of 3D woven laid on heavy smooth surface prior to the application of resin. Figure 4.7 shows the samples after covering with impermeable polymeric sheet and vacuum was applied. Once a complete vacuum is achieved, resin is pulled through the laminate via carefully placed tubing, impregnating the entire preform (Figure 4.8).

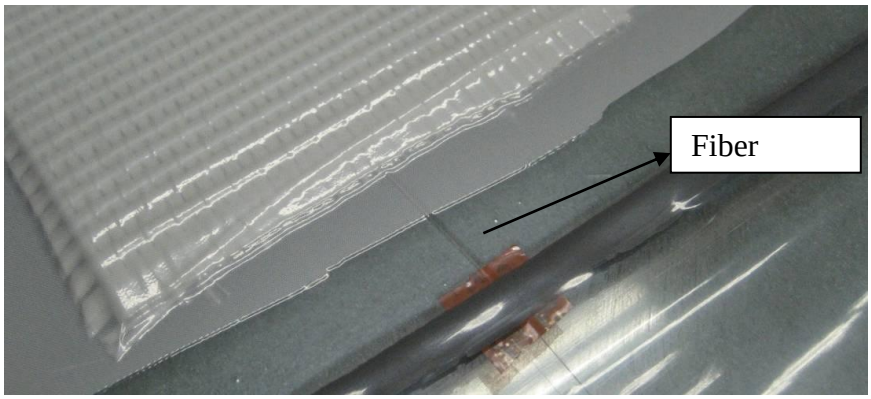

Figure 4.5 3D woven sample with an embedded fiber optic

Figure 4.6 3D woven samples before resin infusion

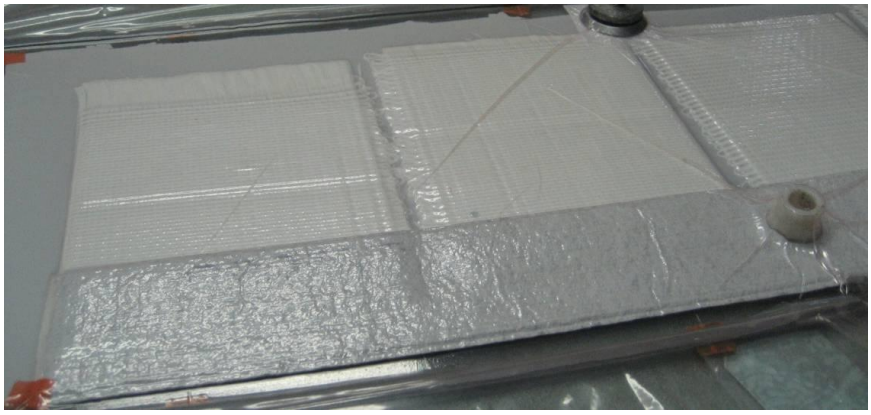

Figure 4.7 3D woven samples subjected to vacuum before resin infusion

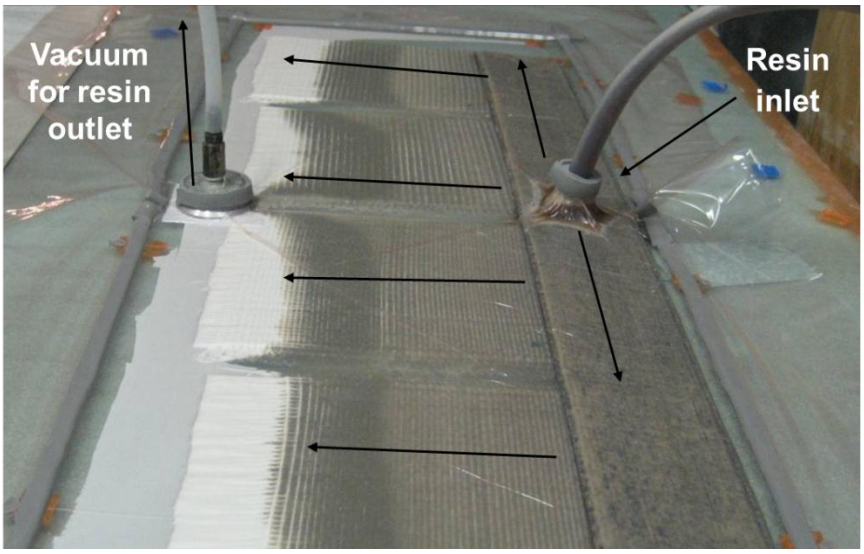

Figure 4.8 3D woven samples during resin infusion process with (arrows indicate the resin flow direction)

4.2.3 Fiber Optic/Laser Based Test Bed

A set up was developed to assess signal loss at different bending deflection and span lengthic length. The system consists of light source (Laser), single mode couplers, fiber optic mount,

and sample stage and receiver unit as detector (Figure 4.9 and Figure 4.10). Helium-Neon (HeNe) Laser was used as a light source with low Output Power of 2.0 mw and beam diameter 0.81 mm with wave length of 633 nm. Cylindrical Laser Mount assembly (rod and rod clamp) provides a heavy construction to prevent movement of the light source during measurements. Single mode couplers are used to accurately adjust the laser beam height and angle of the optical fiber that allow its alignment with the light source. The receiver units consist of detector and optical power meter. The detector detects the light power which transmits through the fiber optic, whereas, the detector is connected to the optical power meter. The power meter is suitable for applications requiring the measurement of low-power, high-power or energy of continuous or pulsed light sources. Light source, single mode coupling, fiber optic mount, and sample stage and receiver unit are attached to Grade Breadboard to provide rock-solid stability and rigidity to support the different parts of the system and prevent any vibration since any movement would affect the power detection and cause errors.

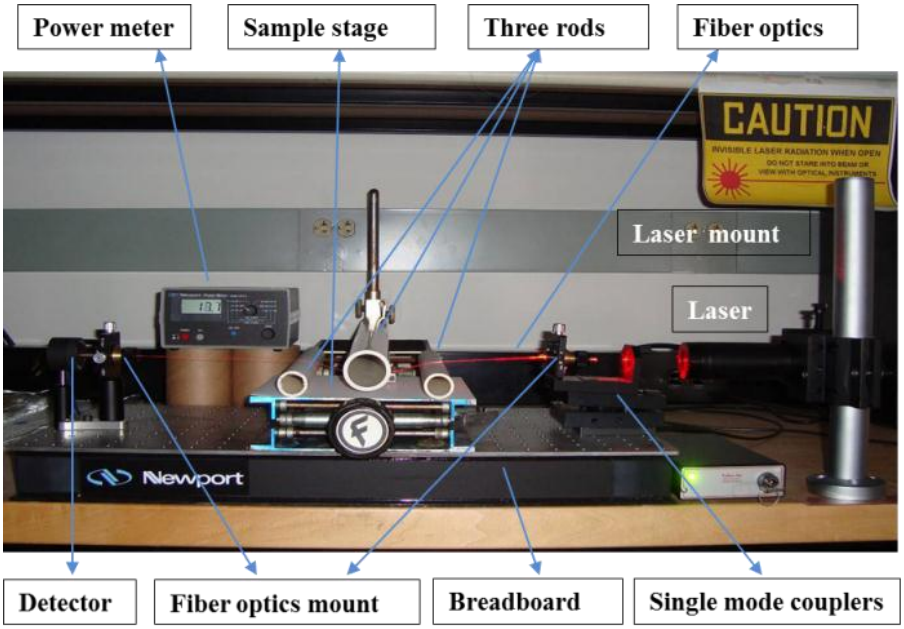

Figure 4.9 Fiber Optic/Laser Based Test Bed

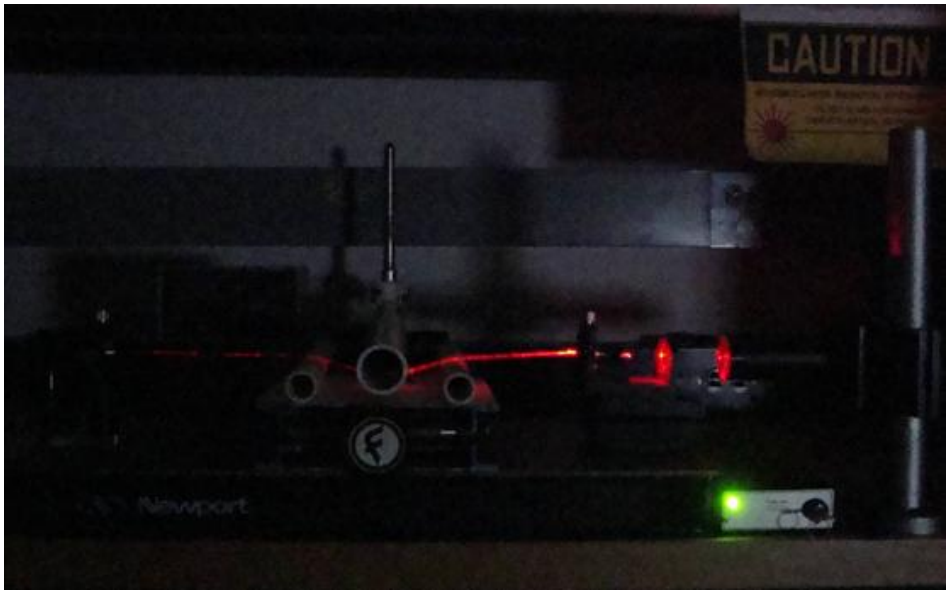

Figure 4.10 Fiber Optic/Laser Based Test Bed in the dark

4.2.4 SOF Setting and Measurement

As a first step, the optical power meter is calibrated. The calibration was performed in dark to get a zero reading. The light source (laser) is then turned on and the laser detector is moved very close to the laser source (so the loss is negligible) and the power is indicated on the power meter display. A value of power of 2 mw (laser power) should be detected since the maximum power of the laser is 2 mw. The distance between the laser source and the fiber optic mount (that is fixed on the single mode couplers) is selected to be 80 mm. The length of the fiber optic which is embedded in the sample is 550 mm and this length was kept constant for all samples. The distance between the fiber optic mount and the detector which is connected to the optical power meter is 3 mm.

The SOF to be tested is prepared by stripping 50 mm acrylate coating layer from each end of the fiber. Then the ends of the fiber must be carefully cleaved to create a perfectly flat end face. The two ends of the fiber optic after stripping and cleaving are settled in the fiber chucks or the fiber holder. The holders keep the fiber optic straight and protect the two ends

from any damage that could affect the accuracy of the measurement. The laser source and the power meter are turned on. The single mode couplers are adjusted using three-axis positioner to align the fiber optic with the laser beam.

Three rods were mounted on the stage (Figure 4.9) to bend the fiber in three point bending mode. The outer rods' diameter was 27 mm and the middle rod diameter was 41 mm. Two variables were considered, namely the span length and bending deflection (defined as the vertical distance deflected from the horizontal center of fiber optic) of the fiber optic. The span length levels selected were 80 mm, 120 mm, and 160 mm and the bending deflection levels chosen were 0 mm, 4 mm, 8 mm, 12 mm, 16 mm, and 20 mm. For all tests the fiber optic length was kept constant (550 mm). Changing the span length or bending deflection required movement of the single mode couplers and the laser source and alignment of the laser beam with the fiber optic.

4.2.5 POF Setting and Measurement

Effect of bending deflection on the power loss of POF using three point bending mode was studied. The test setup shown schematically in Figure 4.11and Figure 4.12 were constructed to conduct the investigation. The setup of Figure 4.11was designed for initial experiment to determine the bottom rods critical radii. Rods with critical radius or higher do not cause power loss. This enabled the construction of three point bending set up of Figure 4.12so that the power loss is only due to POF deflection created from the movable middle rod. The initial experiment revealed that the critical radius is 19 mm. Based on this finding the three point bending set up was constructed with two bottom rolls of radius 41.5 mm each. Three different middle rod radii were chosen 3.2 mm, 4.75 mm, 6.35 mm, 13.25 mm, and 19 mm (which is the critical radius). Deflections values investigated were 0 mm, 5 mm, 10 mm, 15 mm, 20 mm, 25 mm, 30 mm, 35 mm, 40 mm, 45 mm, 50 mm, and 70 mm. Output power were recorded at each deflection for each rod radius.

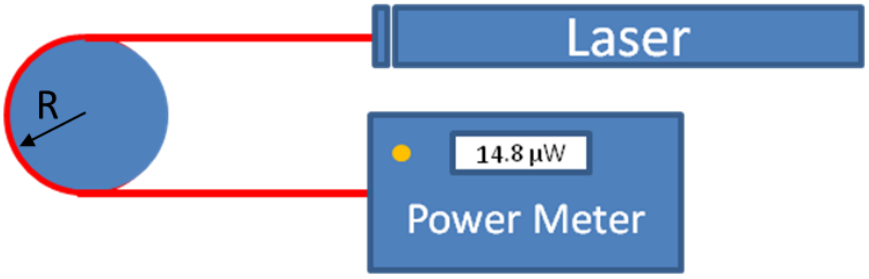

Figure 4.11 wrapped POF at 180 degree on rods

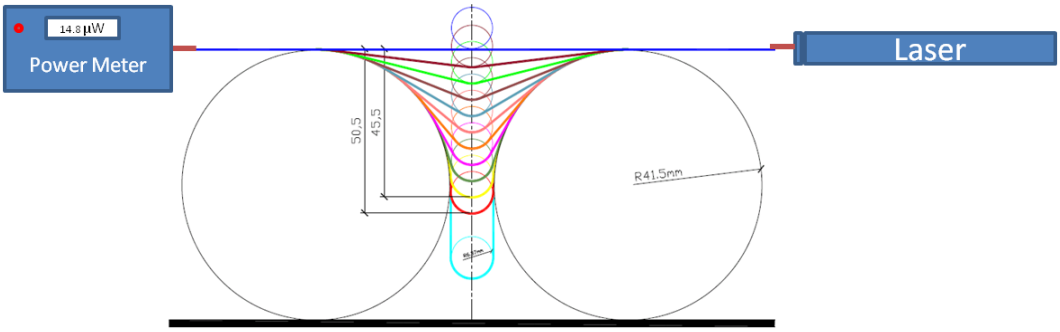

Figure 4.12 Effect of deflection height and bending angle on POF power loss %

4.2.6 Determination of Power Loss

The power loss (in percent) of the laser transmitted through the fiber optic as a result of bending deflection was determined from the following equation:

$$P_l = \frac{100\,(P_s - P_d)}{P_s}$$

Where P_l is the power loss, P_s is the power measured for straight fiber optic, and P_d is the power measured for deflected fiber optic of the same length. The power transmitted through a straight fiber optic of 550 mm long is 25.2 µw (micro watt).

4.3 Results and Discussion

4.3.1 Effect of bending deflection and middle rod radius for SOF

Figure 4.13 show the results of power transmitted through straight SOF in free state (before embedding in the preforms), 3D orthogonal woven preform, and final composite. The results indicate that there is no power loss of the three cases which supports the fact that 3D orthogonal woven preforms keep their y-yarns in straight configuration, which is an advantage over the other preform structure. Figure 4.14- Figure 4.16 illustrate the relationships between the bending deflection and the power loss of two different types of multimode SOF optical fiber MLD and MFD with 3 different span lengths 80, 120 and 160 respectively. The results of the figures show that as the fiber optic bending deflection increases the power loss increases at all levels of span lengths. The rate of power loss is higher for bending deflection range of 0 mm to 8 mm than bending deflection range of 8 mm to 20 mm. The power loss tends to level off with high bending deflection for short span length. The sensor is useful (sensitive) for deflections of up to 8 mm for span length of 80 mm. For composites tested at such span length that fail at deflection of 8 mm or higher, the sensor would not be qualified for health monitoring of such structures.

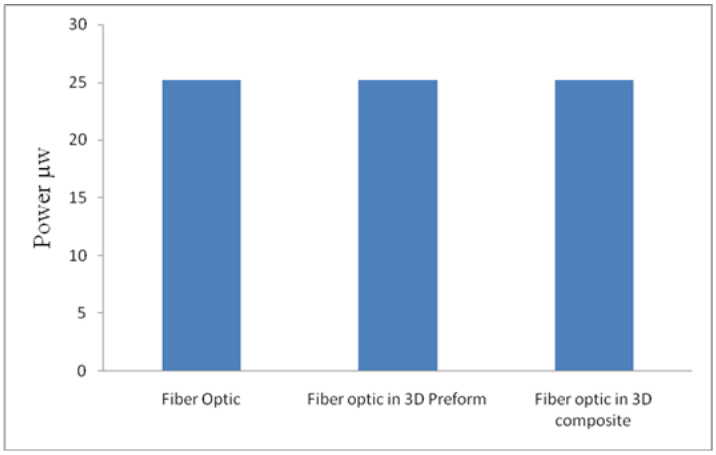

Figure 4.13 Comparison of power measured at the outlet of SOF (MFD) in free state, inside 3D woven preform and inside 3D woven composite

Figure 4.14- Figure 4.16 revealed also that fiber optic of type MFD caused high power loss than fiber optic of type MLD. The data of Figure 4.14- Figure 4.16 are presented in different way in Figure 4.17and Figure 4.18 to illustrate the effect of span length for a given fiber optic type. It is clear from Figure 4.14- Figure 4.18 that as the span length increases the power loss decreases. This is expected since for the same bending deflection in mm, the deflection angle of a fiber optic is lower for long span length compared to deflection angle of fiber optic of short span length. The deflection angle was calculated for data of Figure 4.17and Figure 4.18 and the results are shown in Figure 4.19 and Figure 4.20. The results of deflection angle support the explanation that as the span length increases deflection angle is lower for the same deflection.

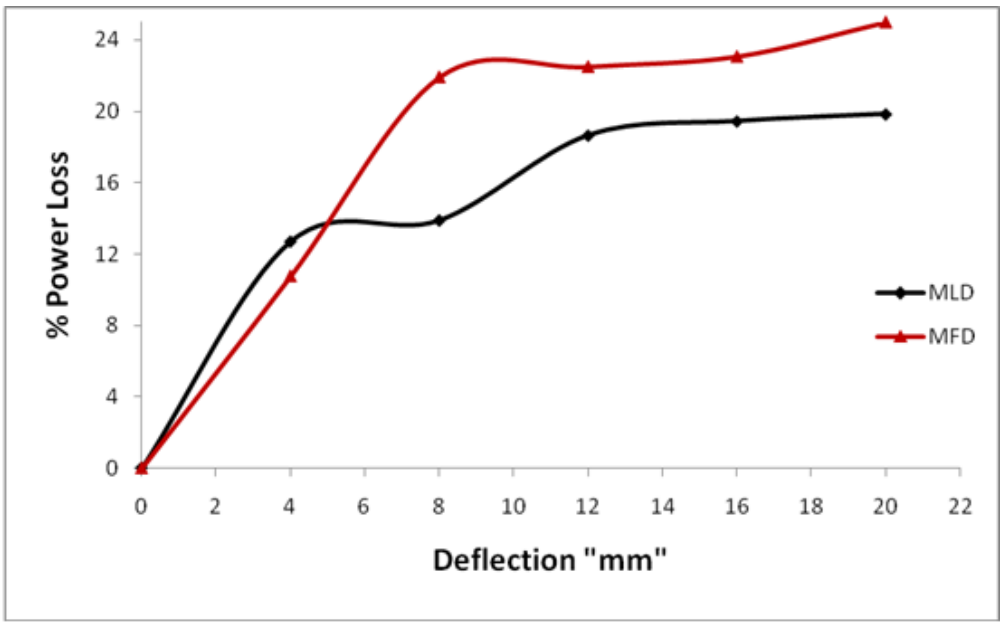

Figure 4.14 Deflection vs. power loss of fiber optic type MLD & MFD with span length 80 mm

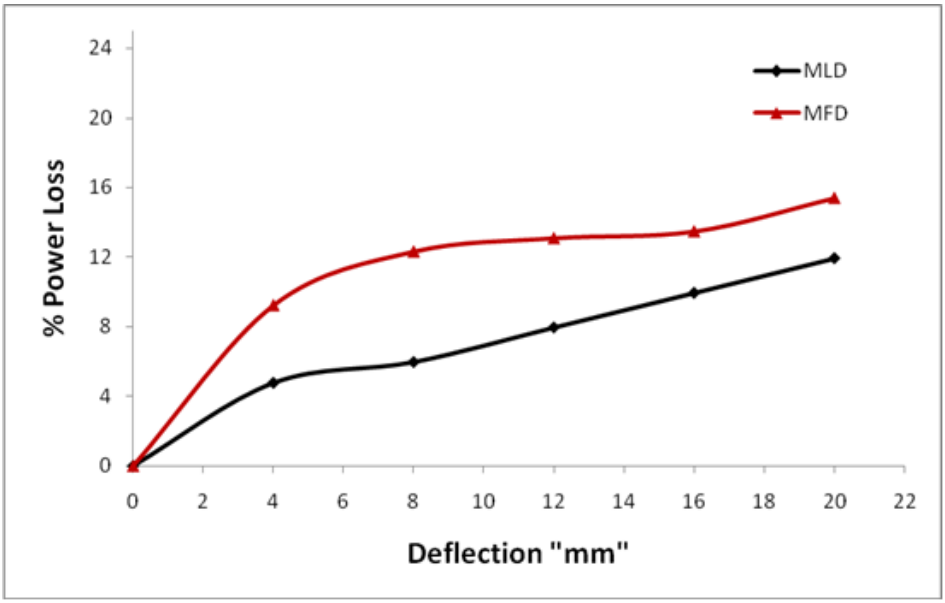

Figure 4.15 Deflection vs. power loss of fiber optic type MLD & MFD with span length 120 mm

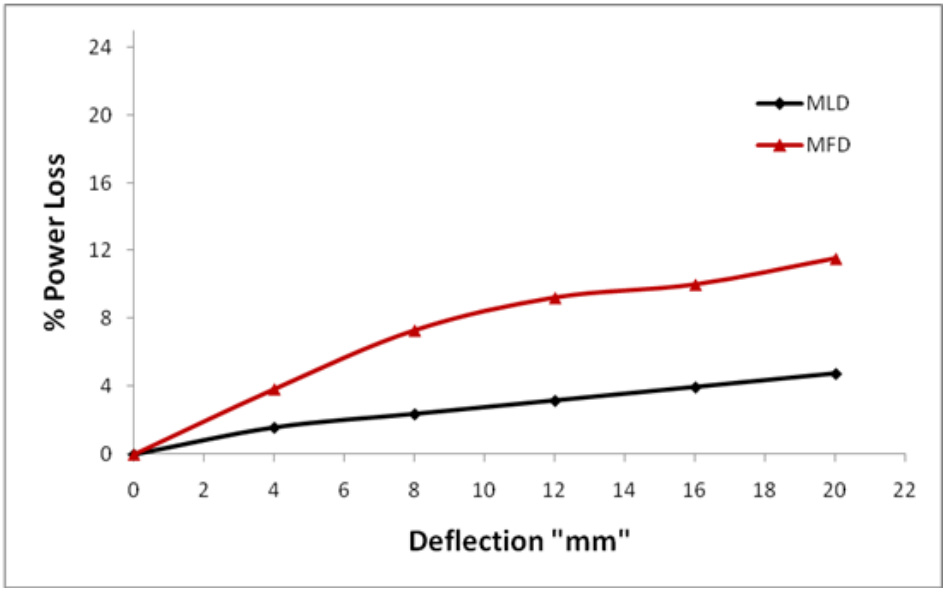

Figure 4.16 Figure 15 Deflection vs. power loss of fiber optic type MLD & MFD with Span length 160 mm

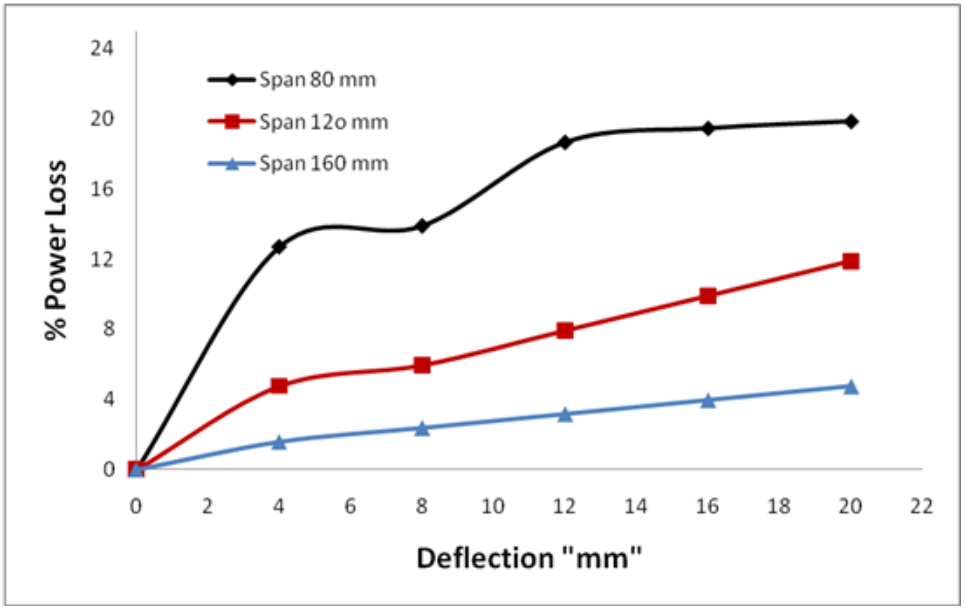

Figure 4.17 Deflection-power loss relationships using MLD fiber optic at different span lengths

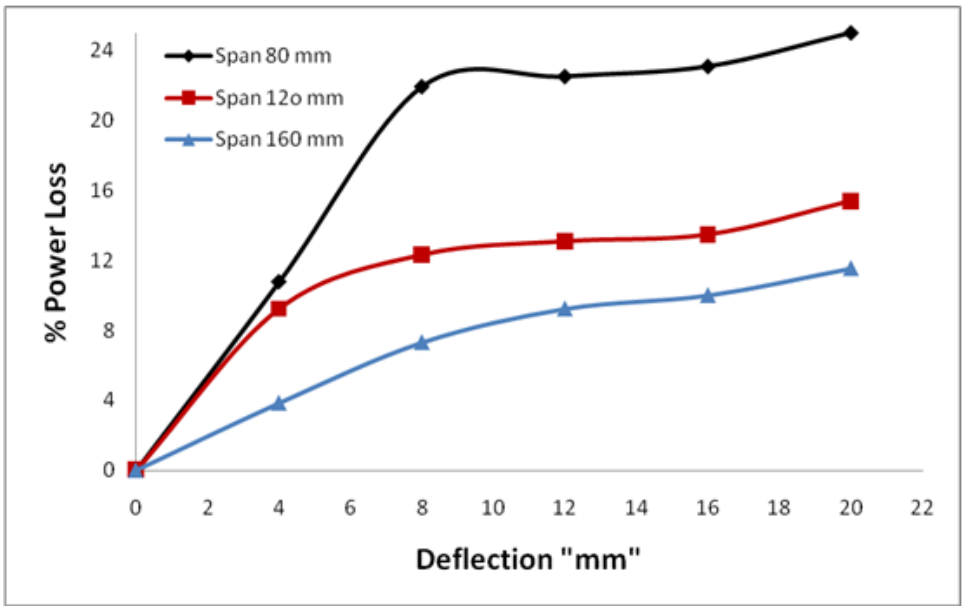

Figure 4.18 Deflection-power loss relationships for MFD fiber optic type at different span lengths

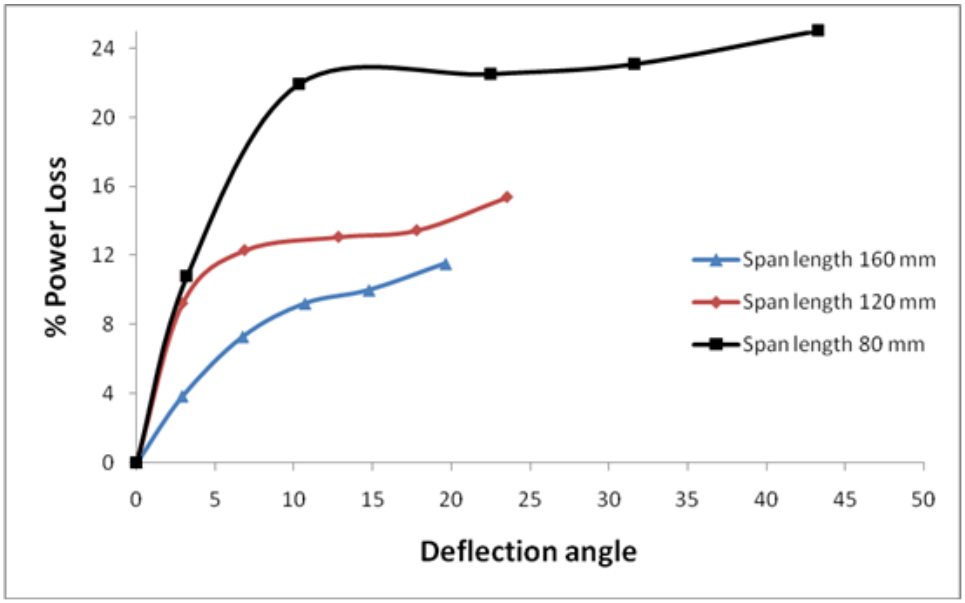

Figure 4.19 Effect of deflection angle on power loss of MFD fiber optic at different span lengths

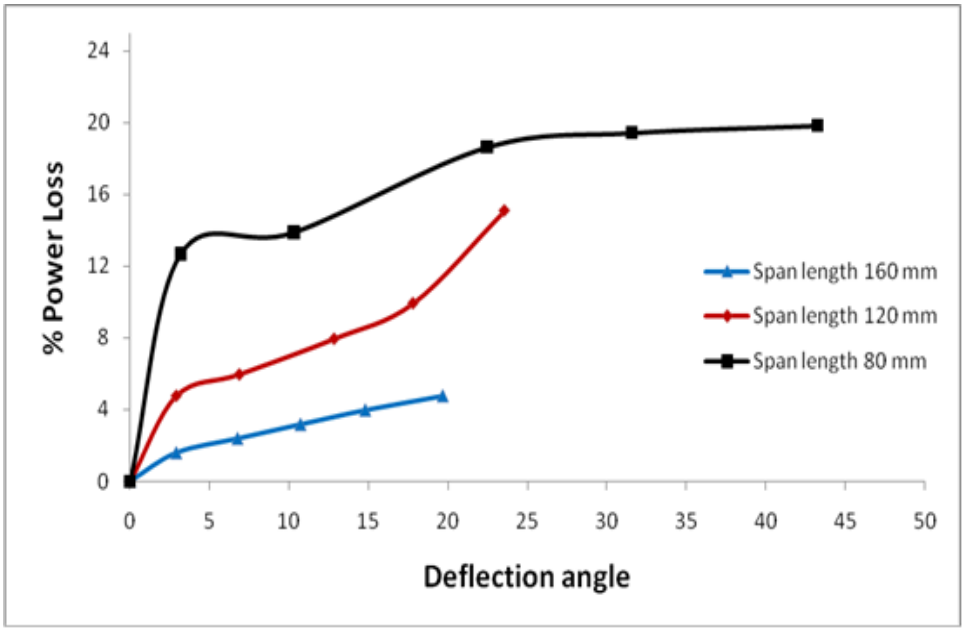

Figure 4.20 Effect of deflection angle on power loss of MLD fiber optic at different span lengths

4.3.2 Critical Radius

We define the critical radius as the bending radius at which the optic fiber exhibits no loss in signal. Bending a fiber optic to the critical radius or higher does not cause signal loss. It is essential to find out the critical radius associated with each optic fiber and consider this value in constructing and designing sensors.

Figure 4.21 illustrates the effect of bending radius on optical power loss of the investigated three optic fibers. Different rods were used to create the data of the figure. Each optic fiber were wraped half turn around each rod (180º wrap angle) as seen in Figure 6, which simulates the bending at the seleveges of the compsoite structure. Results show that as the rod radius increases optical power loss decreases, which indicate that small radius is accosiated with more light reflection beyond the critical angle and more light rayes were escaped from the optic fiber core through the cladding and caused the attenuation. Resluts also indicate that no power loss has occured at bending radius 19.00 mm and higher for the POF. Figure 4.21 also shows results of signal loss at wrap angle of 180º of the two types of SOF-MFD and SOF-MLD. For these fibers the power loss at radius 19 mm was 15 % and 7% respectively. The power loss data of SOFs suggest that the SOFs will continue to exihibit power loss even with rod radius higher than those used in this experiment. However, the loss is very small for bending radius of 40 mm and higher.

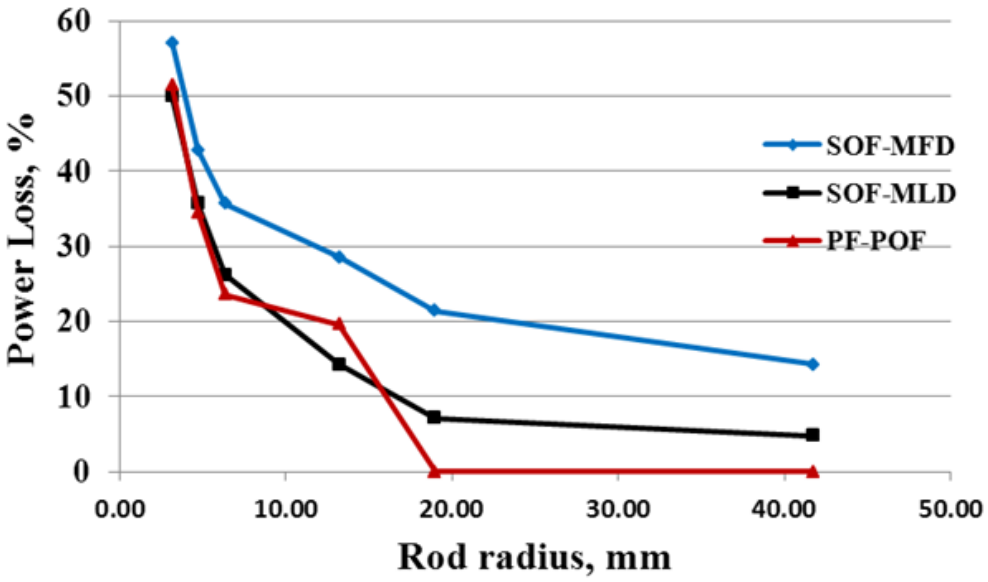

Figure 4.21 Effect of bend radius at 180º wrap angle on POF and SOF optical power loss

The data of Figure 4.21 can be used to avoid or minimize optic signal loss as a result of integrating SOF and/or POF into 2D or 3D preforms. For example, to integrate POF into 3D preform in continous manner, the POF has to be inserted in x-direction every 38 mm or more so the bending radius at the edges will be equal or higher than 19 mm and no power loss will occure and hence more area of the preform can be covered by the sensor if so desired (Figure 4.22).

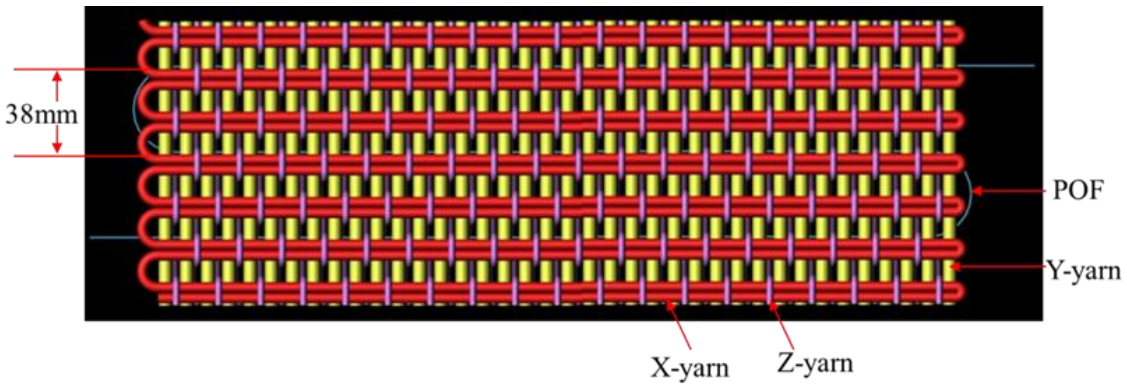

Figure 4.22 Top view of 3D preform with integrated POF in continous matter every 38 mm

4.3.3 Effect of bending deflection and middle rod radius for POF

This part of the investigation was conducted on the POF using the test bed set up to find out its potential as embedded sensor in fiber reinforced composites without the need to manufacture the composite structures. Figure 4.23 shows the effect of bending deflection and middle rod radius on the power loss. The results indicate that for a given middle rod radius, the power loss increases with the bending deflection up to certain value after which the power loss is leveled off. The power loss increases with the reduction of the radius of the movable rod. It is worth noting from the results that the signal attenuation of the POF at different bending radii tends to be constant at 40 mm and higher values of deflection. At this range of deflections the POF was wrapped an exact half turn around the rods (or 180º wrap angle). This result concludes that maximum signal attenuation was at wrap angle 180º (Figure 4.24) for the range of moving rod diameter and angle of wrap investigated. Regardless of the value of the diameter of moving rod the rate of power loss is the same at range of deflection from 0 mm to 20 mm indication of same sensitivity. Beyond this point (20 mm), the rate of change of power loss in terms of deflection gets higher as the middle rod radius decreases. When deflection increased to 40 mm and higher, the power loss leveled off for all range of rod diameter investigated. It is worth noting that the sensitivity of this sensor is high for bending deflection of up to 40 mm. It is clear from the results of power loss of

POF and SOF that POF critical bending loss radius is smaller than SOF (Figure 4.21). Thus, POFs are better qualified as embedded sensors in compsites structures due to their high senstitivty to bending deflection and conformability.

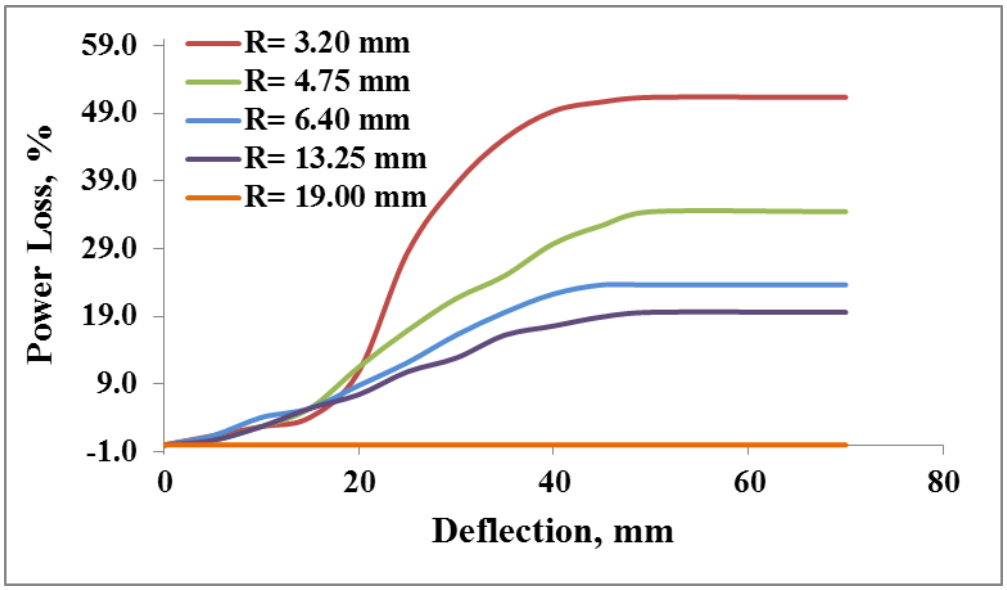

Figure 4.23 Deflection-power loss relationships for POF at different rods radii

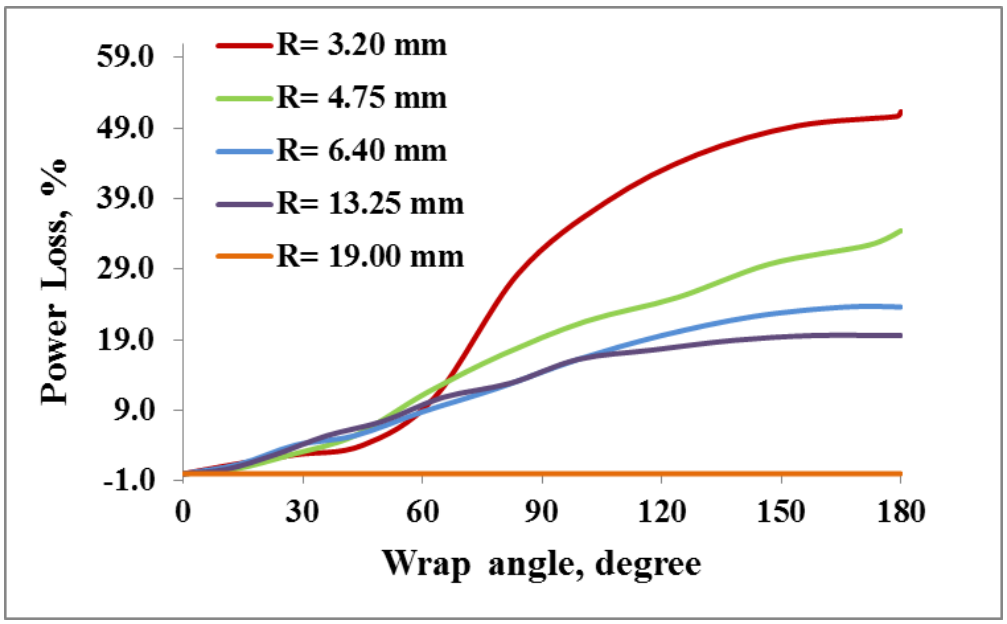

Figure 4.24 Wrap angle-power loss relationships for POF at different rods radii

4.4 Conclusions

We constructed a test bed system based on fiber optic/laser with the goal that it can be used to predict failure of structure subjected to bending. The results revealed that SOF in free state, embedded in 3D woven preform, and imbedded in 3D composite show same power transmitted through them without power loss. This is an important finding that led to the fact that there is no need to conduct failure test on 3D orthogonal woven composite to determine the critical bending deflection. As expected the power loss was influenced by the span length, bending deflection, deflection angle and type of fiber optic. As the bending deflection increases, the power loss increased at a fixed span length due to the escape of the light form the optical fiber core through the cladding at the macrobending points. For the same bending deflection, an increase in the span length caused a reduction in power loss.

The SOF types tested are MFD and MLD. MFD fiber showed higher power loss and is thus a better candidate for detection of bending since it provided more sensitivity. Caution must be

practiced when the relationship between deflection and power loss is not sensitive (power loss does not vary by changing the bending deflection). Two sets of experiments were conducted. The first was structured to reveal the critical radius, which is the bending radius at which (or higher value) no signal loss occurs, in order to find out the initial configuration of the fiber optic in the composite structure. The second experiment was designed to assess the sensors sensitivity while in the composite structure to monitor its health. It was found that critical radius of the investigated POF was 19 mm while neither SOFs showed critical radius. The SOFs continued to lose power at high bending radius of 40 mm and the data indicate no sign of reaching to zero power loss regardless of bending radius. However, the power loss of SOFs is small at bending radius of 40 mm or higher. POF showed increase of power loss as the middle rod radius decreased, bending deflection increased, or wrap angle increased. Increase of bending deflection beyond 40 mm did not cause further power loss indication of at a given span length there is a bending deflection after which the sensor has no sensitivity and does not respond to further deflection. Results can be used in designing smart sensors with high sensitivity for health monitoring of composite made of 2D or 3D preform.

Our research identified the range of capabilities and sensitivities of the studied optic fibers as embedded sensors in fiber-based composites to monitor their bending using the developed test bed. The results of this study showed that POF provides higher sensitivity and range of bending deflection compared to SOFs. The work also unveiled the bending radius at which minimum or no signal loss occurred.

References

[1] Sirohi, J., and Chopra, I. Fundamental Understanding of Piezoelectric Strain Sensors. *Journal of Intelligent Material Systems and Structures.* 2000, Vol. 11, pp. 246-257.

[2] Ide, H., Abdi,F., Miraj,R., Dang,C., Takahashi,T., Sauer,B. Wireless-Zigbee Strain Gage Sensor System for Structural Health Monitoring. *Photonics in the Transportation Industry: Auto to Aerospace II.* Vol. 7314, pp. 3-12.

[3] Rao, M., Bhat,M., Murthy,C. Structural Health Monitoring (SHM) Using Strain Gauges, PVDF Film and Structural Health Monitoring (SHM) Using Strain Gauges, PVDF Film and. *Proc. National Seminar on Non-Destructive Evaluation.* 2006, pp. 333-337.

[4] Rumsey, M., Paquette,J., White,J., Werlink,R., Beattie,A., Pitchford,C., Dam,J. Experimental Results of Structural Health Monitoring of Wind Turbine Blades. *American Institute of Aeronautics and Astronautics.* 2008, pp. 1-14.

[5] Lee, D. G., Mitrovic, M., Stewart, A. and Garman, G. Characterization of Fiber Optic Sensors for Structural Health Monitoring. *Journal of Composite Materials.* 2002, Vol. 36, 11, pp. 1349-1366.

[6] Zhan-Feng, G., Yang-Liang, D., Bao-Chen, S., and Xiu-Mei, J. Strain monitoring of railway bridges using optic fiber sensors. *Journal of quality in maintenance engineering.* 2007, Vol. 13, 2, pp. 186-197.

[7] Leng J., and Hao J. Damage assessment of composite laminate by using fiber optic AE sensors based on fused-tapered coupler. *Proc. of SPIE.* SPEI, 2007, Vol. 6531, pp. 1021-1025.

[8] Rippert, L., Papy, J., Wevers, M., Huffel, S. Fibre optic sensor for continuous health monitoring in CFRP composite materials. *Smart structures and materials.* SPIE, 2002, Vol. 4693, pp. 312-323.

[9] Shaaf, K., Cook, B., Ghezzo, F., Starr, A., and Nemat-Nasser, S. Mechanical properties of composite materials with integrated embedded sensor networks. *Smart structures and materials.* SPIE, 2005, Vol. 5765, pp. 781-785.

[10] Ishigure, T., Nihei,E., and Koike, Y. Optimum refractive-index profile of the graded-index polymer optical fiber, toward gigabit data links. *APPLIED OPTICS.* 1996, Vol. 35, 12, pp. 2048-2053.

[11] Merzbacher C I, Kersey A D and Friebele E J 1996 Fiber optic sensors in concrete structures: a review *Smart Material and Structures* 5 196-208

[12] Kiesel, S., Van Vickle, P., Peters, K., Abdi, O., Hassan, T., Kowalsky, M.,. Polymer optical fiber sensors for the civil infrastructure. *Mechanical, and Aerospace Systems, SPIE Sensors and Smart Structures.* 2006, Vol. SPIE 6174, pp. 1-12.

[13] Nakamura, K., Husdi,I., Ueha, S. Memory effect of POF distributed strain sensor. *Second European Workshop on Optical Fibre Sensors, Proceedings of SPIE.* Vol. 5502, pp. 144-147.

[14] Liehr, S., Lenkea,P., Krebbera,K., Seegerb,M., Thieleb,E., Metschiesb,H., Gebreselassie, B., Münich, J., Stempniewski, L. Distributed strain measurement with polymer optical fibers integrated into multifunctional geotextiles. *Optical Sensors, Proc. of SPIE.* Vol. 7003.

[15] Liehr, S., Lenke,P., Wendt,M., Krebber,K., Seeger,M., Thiele,E., Metschies, H., Gebreselassie,B., Münich, J. Polymer Optical Fiber Sensors for Distributed Strain Measurement and Application in Structural Health Monitoring. *IEEE SENSORS JOURNAL.* 2009, Vol. 9, 11, pp. 1330-1338.

[16] Kuang, K., Akmaluddin, Cantwell, W., Thomas, C. Crack detection and vertical deflection monitoring in concrete beams using plastic optical fibre sensors. *MEASUREMENT SCIENCE AND TECHNOLOGY, INSTITUTE OF PHYSICS PUBLISHING.* 2003, Vol. 14, pp. 205-216.

[17] Kuang, K.,Quek,S.,Koh,C.,Cantwell,W., Scully,P. Plastic Optical Fibre Sensors for Structural HealthMonitoring:A Reviewof Recent Progress. *Journal of Sensors, Hindawi Publishing Corporation.* 2009, Vol. 2009, p. 13.

[18] Yi, H., Ding, X. Conventional Approach on Manufacturing 3D Woven Preforms Used for Composite. *Journal of Industrial Textiles.* 2004, Vol. 34, 1, p. 34: 39.

[19] Mohamed, T. S., Johnson, C. and Rizkalla, S. Behavior of Three-Dimensionally Woven Glass Fiber Reinforced Polymeric Bridge Deck. *Composites Research Joumal.* 2007, Vol. 1, pp. 27-42.

[20] Grillet, A., Kinet, D., Witt, J., Schukar, M., Krebber, K., Pirotte, F., and Depre, A. Optical fiber Sensors Embedded into Medical Textiles for Healthcare Monitoring. *IEEE Sensors Journal.* 2008, Vol. 8, 7, pp. 1215-1222.

[21] Casas, J. R. and Cruz, P. J. S. Fiber optic sensors for bridge monitoring. *Journal of bridge engineering.* 2003, Vol. 8, 6, pp. 362-372.

[22] Zendehnam, A., Mirzaei, M., Farashiani, A., Farahani, L. Investigation of bending loss in a single-mode optical fiber. *Pramana-Journal of physics.* 2010, Vol. 74, 4, pp. 591-603.

[23] Gupta, S. C. *Textbook on optical fiber communication and its applications.* s.l. : PHI Learning Pvt. Ltd., 2004. pp. 44-45.

[24] Hamouda, T.M., Seyam, A.M., and Saad, M. (2010). Predict of Failure of of 3D woven composite Structures using Embedded Fiber Optic Sensors. *World Journal of Engineering*, 7(1), 103-112.

CHAPTER 5

5. Effect of Resin Type on the Signal Integrity of Embedded Perfluorinated Polymer Optical Fiber

Abstract

Polymer optical fibers (POF) hold many advantages for embedded sensing, such as their low cost, flexibility, high tensile strain limits and high fracture toughness. POF sensors may therefore be integrated into fiber reinforced composite structures for monitoring structural behavior. Since POFs do not require a protective coating, it is critical to verify that the resin system does not negatively impact the noise level or performance of POF sensors during the composite manufacturing. This study measured the effect of Vinylester and Epoxy resin systems on the signal loss of embedded perfluorinated, graded index POFs. Photon counting Optical Time Domain Reflectometer (OTDR) was used to monitor the signal attenuation and backscattering level of the POFs throughout the resin curing cycle. Fourier Transform Infrared Spectrometry (FTIR) and cross section analyses using scanning electronic microscope (SEM) images were also conducted to investigate whether the resin system caused chemical and physical changes of the POF. This study showed that Vinylester resin caused a significant increase in the backscattering level of POF sensors and therefore induced high fiber signal losses. On the other hand, the POF treated with Epoxy showed no change in backscattering level indicating no chemical or physical change had occurred to POF.

5.1 Introduction

Sensors written into silica optical fibers (SOF) have been broadly implemented as sensors for smart structures (1-3). While the strength of SOFs is relatively high, they are very brittle and therefore cannot be bent to a small radius of curvature. This limitation makes it hard for them to conform around small microstructural features when embedded in fiber reinforced composite structures. The brittleness of SOFs also dictates the use of multi-layer of cables or relatively stiff coatings to protect the silica SOF (4). . In contrast, multi-mode POFs are relatively flexible, easy to handle, and easier to handle, splice and cleave as compared to SOFs, which translates to a low preparation cost when fabricating composite structures with

embedded POFs. Additionally, POFs requires no additional protective layers surrounding the fiber to prevent water ingress into the fiber (4). For these reasons, POFs have great potential as a relatively inexpensive embedded sensor for textile composites. While SOF core diameters range from 10 μm to 100 μm, multi-mode POF core diameters range from 50 μm to 1,000 μm (5). Using a large diameter core simplifies the coupling of light waves into the fiber; however it also increases the perturbation to the surrounding composite material due to the larger diameter.

Organic polymer polymethylmethacrylate (PMMA), polystyrene (PS) and polycarbonate (PC) are the most commonly used polymer as a core material for multimode POFs. These POFs have a high attenuation of 1,000 dB/Km, which limits their use to short distance communications (6) (7). One of the main reasons behind the high attenuation of PMMA, PS and PC is the C-H bond vibration absorption, which can be reduced by replacing hydrogen atoms with heavier atoms such as fluorine, chlorine and deuterium (4) (5) (6). This perfluorination (PF) and deuteration of polymers decreases the attenuation to less than 50 dB/km in the visible region of the spectrum.

There are many current fields of applications that do utilize POFs such as telecommunications, image scanners, shape-defect detectors, temperature sensors, humidity sensors, navigation systems, and liquid-level detectors (3) (8) (9) (10). POFs have also been applied to detect color, brightness, opacity, density, and turbidity (6). POFs are also characterized by their high strain, which can reach more than 30% of its original length (11) (12). For these reasons, POF sensors have been integrated into civil engineering and composite structures to detect initial cracks, monitor crack propagation, identify structural failures, and measure dynamic responses, structural deflections and strain distributions (13) (14) (15) (16) (17) (18) (19) (20).

While POF sensors present these many advantages for embedment into composite smart structures, the POF must also be resistant to chemical reactions resulting from the resin system constituents during infusion and curing to be successful as a sensor. As POFs do not

require the same protective coatings as SOFs, this resistance to chemical reactions is critical. Physical and/or chemical changes in a POF would result in a change in the backscattering level. When an embedded length of POF is utilized as a sensor, this increase in backscattering would decrease the signal to noise ratio and potentially decrease the sensor lifetime. As POFs already demonstrate high attenuation levels, minimizing the losses induced by embedment is important. To our knowledge there is no published research that addresses this issue. Therefore, in this paper, the effects of resin type on the integrity of perfluorinated graded index POFs during resin infusion and curing was studied using optical time domain reflectometry (OTDR) to measure attenuation and localized structural defects. Vinylester and Epoxy resins were used in this work, as these are the most common resin types used for textile composites. These two resin types present different final properties of the composite material system: Vinylester resins are distinguished by their high corrosion resistance while Epoxy resins provide higher strength properties.

5.2 Experimental Methods

The optical fiber used in this study was a low attenuation, IR-transparent POF with a higher bandwidth graded index (GI), acquired from Chromis Fiberoptics, Inc. (GigaPOF-62LD). The POF fiber diameter is 750 μm, while the core and cladding are made of Perfluorinated polymer (PF) (Polyperfluoro-butenyvinyleether). The specifications along with tolerance of the POF are shown in Table 5.1(as provided by manufacturer).

Table 5.1 GI-PF-POF specifications

Property	Value
Core diameter	62.5 ± 5 µm
Cladding diameter	750 ± 5 µm
Numerical aperture	0.185 ± 0.015
Max. tensile load	15.0 N
Long-term bend radius	7.0 mm
Core refractive index	1.357
Cladding refractive index	1.342
Backscatter coefficient	-57 dB

Two different types of resin were used to conduct the study. The first was DERAKANE® 8084 Epoxy Vinylester resin donated by Ashland, Inc. This resin system is suitable for resin transfer molding RTM, hand lay-up, spray-up, filament winding and many other fiber reinforced polymer (FRP) applications. This resin system also provides a high chemical and corrosion resistance to the composite product. Table 5.2 shows the cured resin properties supplied by the manufacturer.

Table 5.2 Cured resin properties for Vinylester resin

Property	Value
Tensile strength	76 Mpa
Tensile modulus	2.9 Gpa
Flexural strength	130 Mpa
Density	1.14 g/m^3
Glass transition temp. (Tg)	115° C
Mixed viscosity at 25°C	400 cp

DERAKANE® 8084 Epoxy Vinylester resin system requires the use of an initiator to initiate the cross linking reaction that cause the resin curing, as well as promoters and accelerators to speed up and enhance the curing process. Methylethylketone peroxide (MEKP) was used as an initiator and Cobalt Naphthenate-6 % (CoNap6 %), Dimethylaniline (DMA) was used as the promoter and accelerator. The gel time depends on the working area conditions and the amount of each constituent. In this study, the gel time was chosen to be 60 minutes with a working temperature maintained at 21°C. The amount of MEKP, CoNap6%, and DMA were 2.5, 0.4, and 0.1 phr (part per hundred resin compound) by weight respectively.

The second resin system tested was the Epoxy 2000 resin acquired from Fibre Glast Developments Corporation and made of a multifunctional acrylate. Epoxy 2000 resin is characterized by its medium viscosity and is suitable for fabricating parts and other composite structural applications. Additionally, it is used to fabricate high performance composite parts. The hardener (Hardener 2120) which is made of modified amine mixture was used to provide a longer working time that is required for vacuum bagging and for preparing larger parts before the resin has gelled. This hardener-resin system has a pot life of 2 hours and a curing time of 12 hours at room temperature (about 21º C). Resin and hardener mixing ratio was 100:27 by weight or 3:1 by volume. Table 5.3 lists the properties of system 2000 Epoxy resin and 2120 hardener.

Table 5.3 System 2000 Epoxy resin and 2120 hardener properties

Property	Value
Tensile strength	316.2 Mpa
Tensile modulus	17.37 Gpa
Flexural strength	459.65 Mpa
Density	1.134 g/m^3
Glass transition temp. (Tg)	90° C
Mixed viscosity at 25°C	925 – 975 cp

To investigate the effect of resin type on the light scattering attenuation properties of the POF, a technique was developed to embed the optical fiber in resin without the need for preforms. The goal was to separate out only the effect of the resin on the POF and not the role of reinforcements. In this technique, a three meter long POF was used for each test. The POF was inserted in the middle of a 12 mm diameter PVC tube so that 31 cm of POF was inside the tube and 148 cm was protruding out from one end of the tube and 121 cm from the other end of the tube (Figure 5.1). Then, the prepared resin system was poured inside the tube and left to cure. The end of the 148 cm long portion of the POF was connected to the OTDR to collect the attenuation data.

In total, three samples were prepared. Sample 1 was prepared using DERAKANE® 8084 Epoxy Vinylester resin system. Samples 2 and 3 were prepared using system 2000 Epoxy resin. Sample 1 and 2 were prepared and cured at room temperature for 24 hours, while sample 3 was prepared at room temperature for 30 minutes and cured at 27° C for 8 hours and then 2.5 hours at room temperature. POF attenuation data was collected from each sample before and after applying the resin, during the curing time and after the curing time.

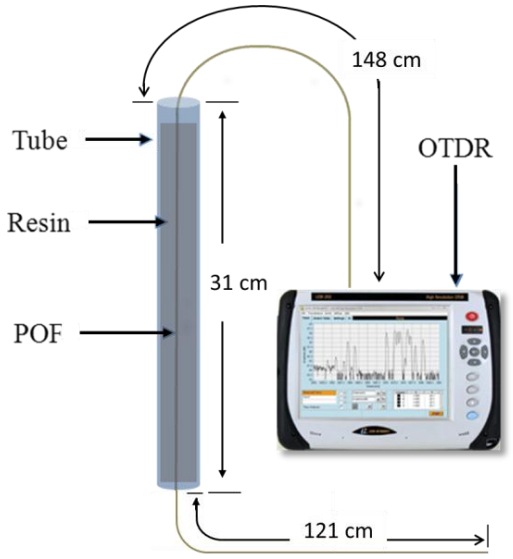

Figure 5.1 POF attenuation test setup

The local attenuation in the POF, both throughout the section embedded in the resin and at the ingress and egress from the resin, was measured using OTDR. OTDR is an advanced equipment that is commonly used to measure optical fiber transmission losses, determine the location of defects, and measure the optical fiber length (15). OTDR is also used for testing optical fibers during the installation, maintenance and restoration of optical fiber sensor based systems (21). The principal of OTDR is that the light source launches a short pulse, with a specific pulse width, into an optical fiber. This light pulse scatters along the optical fiber due to the impurities and the fiber imperfection. A portion of the launched light is backscattered to the light input direction, which will be detected at the input to the optical fiber with a time delay equal to the time required for the light wave to travel from the input to reflection source and back to the input again (22). The backscatter is therefore recorded as a function of time. By applying the speed of the light in the optical fiber (i.e. knowing the index of refraction in the POF) and the backscatter coefficient, the time delay of the backscattered signal is converted to a distance along the optical fiber.

OTDR is sensitive to any change that may occur along the optical fiber that induces optical fiber attenuation. Additionally, different types of defects affect the light backscattering in different ways and can therefore be separated in the backscattered signal. To demonstrate, Figure 5.2 shows a schematic of an OTDR waveform (signal trace), i.e. a plot of the backscatter light level (amplitude as y-axis) along the optical fiber (x-axis). The slope of the curve (caused by Rayleigh scattering) determines the backscattering level (attenuation) as a function of distance along the fiber length. Defects in the optical fiber at specific locations appear as sudden increases or decreases in the amplitude. Reflections and losses are shown in the graph as two different features along the fiber length (23). Reflections cause a sharp increase in the curve, whereas sudden decreases in signal are caused by losses. The sudden increases in amplitude at the beginning and ending of the optical fiber are caused by the termination of the optical fiber at the front panel of the OTDR and the end of the optical fiber respectively, which are always detected (24). These known locations are then used as reference distances for other defects. Dynamic Range (DR), which is an important specification of OTDR, is defined as the difference between the initial power level of the fiber under test and the noise floor level of the detector (Figure 5.2). OTDR has previously been applied to measure optical fiber attenuation in distributed SOF and POF sensors (25) as well as micro bending, temperature changes, mechanical stress, and strain in these sensors (26). In this study a photon-counting OTDR (LOR-220, LUCIOL), with DR of 12 dB, was used to measure the backscatter light level along the POF. This type of photon-counting module converts one photon at 670 nm to one visible photon and detects this visible photon with a silicon photon-counting device, providing extremely high sensitivity (27). The OTDR was configured to emit a wavelength of 670 nm, with a time step resolution of 1.25 ns and signal pulse width of 1 ns.

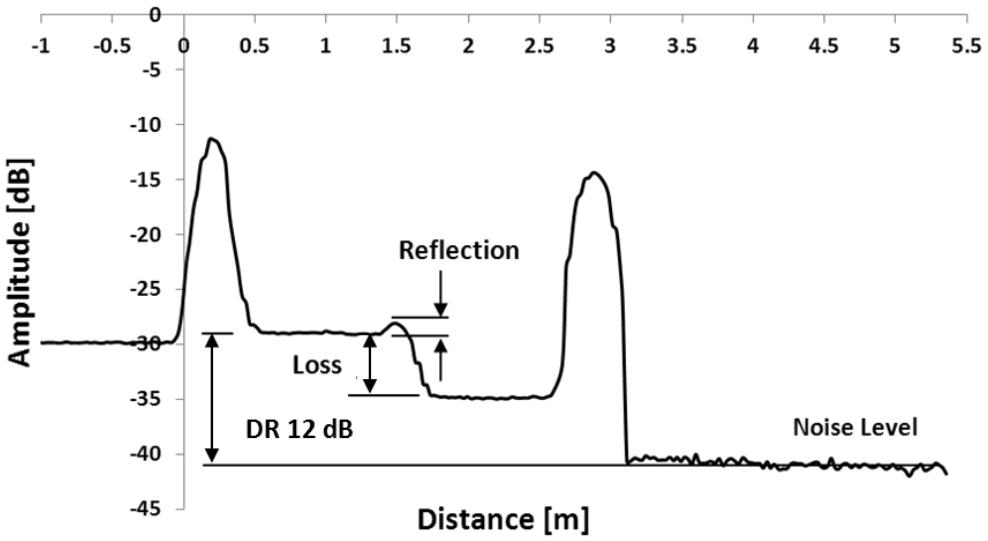

Figure 5.2 Schematic of a typical OTDR waveform

5.3 Measurements Results

5.3.1 Backscattering level

The first experiment was conducted to reveal the effects of the Vinylester resin on the POF structure and performance. The levels of backscattering in the POF samples were measured before adding the Vinylester resin and after adding the resin hourly. The measurements for the initial (before adding resin) and selected times after adding the resin are plotted in Figure 5.3 and 5.4. A decrease in the backscattering level of the POF was observed as the curing time increased. Fiber before treatment, 1 hour, and 2 hours after treatment showed same drop in the initial power level and the noise floor level of the detector. The DR for these three cases was 12 dB, which is the characteristics of the OTDR used (Figure 5.3). After 4 hours of curing, the measurements show a noticeable drop of 1dB in the backscattering level at 1.58 m (at a point that is embedded in the resin) into the POF with no change on the noise level. The POF signal attenuation reached its maximum loss of 4.0 dB along the POF fiber length after 12 hours. These drops in the backscattering level continued until the sample solidified, which indicates a significant change on the POF structure at this location that led to the loss in DR. Fourier Transform Infrared Spectrometry and cross section analysis were conducted on the

POF to find out the cause of this attenuation (as described in the following section), indicating that a significant increase in the POF diameter was visible. Figure 5.4 shows the change in backscattering level with the curing time. POF loss along the tested fiber before treatment with the Vinylester resin was 0.37 dB and backscattering level was -29.48 dB (measured at the start Rayleigh backscattering signal). Resin was fully consolidated after 12 hours and the crosslinks between the resin chains were almost completed, indicated by the fact that there was no further increase in fiber signal loss beyond this point. POF signal loss and change in attenuation must be considered when design sensors. After treating POF with vinylester resin, residual DR was 8 dB and fiber attenuation was increased from 144 dB/Km to 223 dB/km (measured for the protruded length after resin). These changes limit the distance that POF sensors can cover.

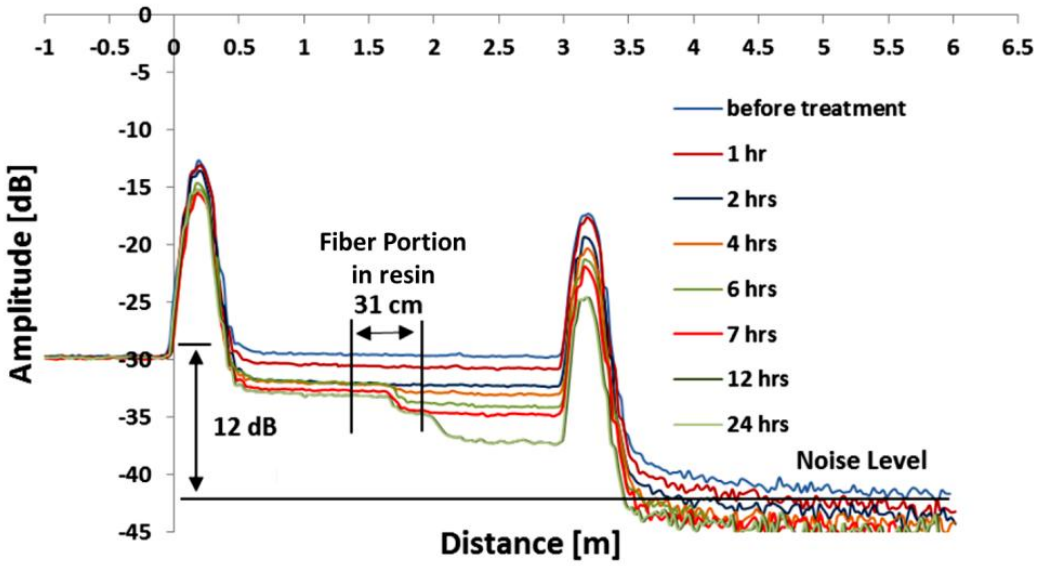

Figure 5.3 Backscattering level measurements for GI-PF-POF embedded in DERAKANE® 8084 Epoxy Vinylester resin

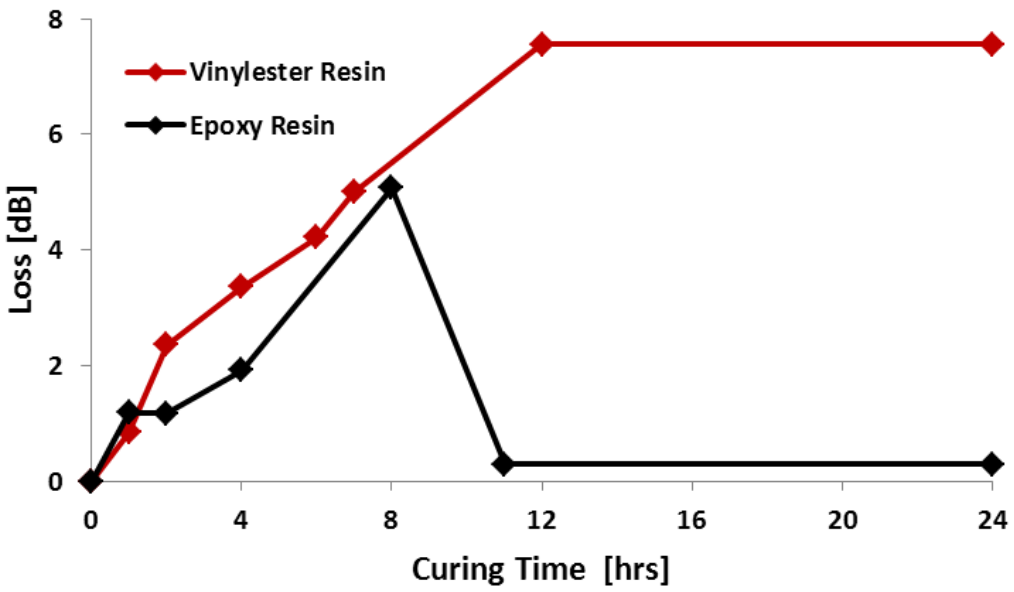

Figure 5.4 Fiber loss (dB) of POF treated with Vinylester and Epoxy resins during curing time (time = 0 is before resin was added)

Backscattering data from the POF embedded in the system 2000 Epoxy at room temperature were also collected throughout the curing time (Figure 5.5). The POF backscattering level decreased as the curing time increased with no change in the dynamic range. The maximum decrease in POF backscattering level occurred after 8 hours and was -33.75 dB, a decrease by 4.5 dB in the backscattering level compared to the level before resin treatment. The resin was fully cured and reached the solidification state after 12 hours. The backscattering level of the POF sensors after 12 and 24 hours showed a return to the same level as the initial case before resin treatment.

The increase in attenuation or POF signal loss during the curing time is also plotted in Figure 5.4. After mixing the Epoxy resin with the hardener, cross linking between polymer chains was initiated and continued until the resin solidified (which may take 12 to 24 hours). Crosslinking reaction is an exothermic reaction generating a significant amount of heat, which could have affected the physical properties of the POF. When the resin cured and most

of the crosslinking between the polymer chains was completed and the heat dissipated, the fiber attenuation returned back to its initial state (Figure 5.4). After the resin cure cycle, the signal loss in the POF embedded in the Epoxy resin was orders of magnitude less than that of the POF embedded in the Vinylester resin.

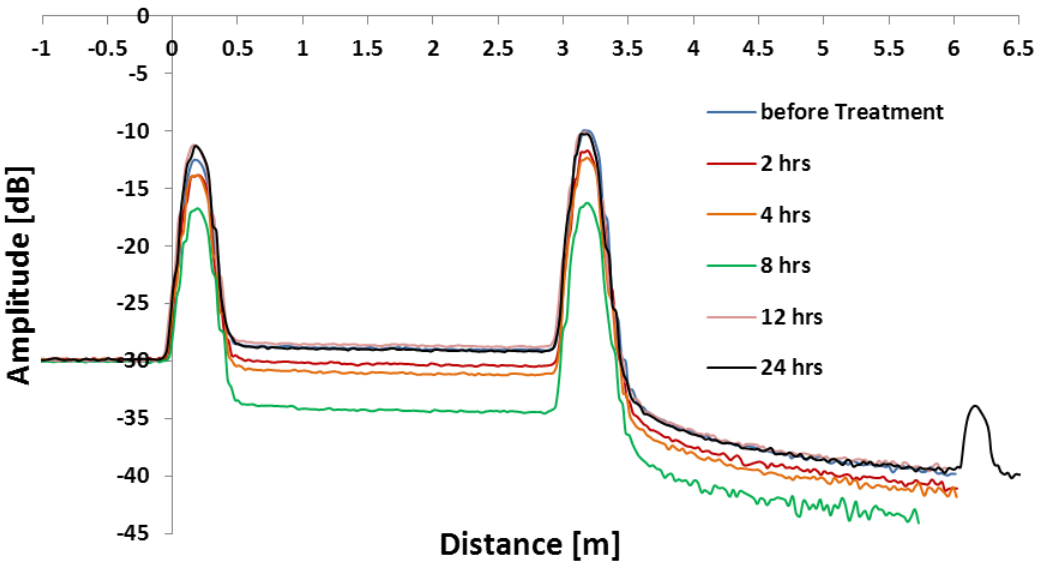

Figure 5.5 Backscattering level measurements for GI-PF-POF embedded in system 2000 Epoxy resin

Figure 5.6 depicts the backscattering data for the POF treated with Epoxy resin with an elevated 27° C curing temperature. The results showed no significant effect on backscattering level of the POF sensors when a higher temperature was used to expedite the curing time. On the other hand, the curing time was decreased using a curing temperature of 27º C as compared to 21º C. Curing at a higher temperature caused faster building of the cross links between the polymer chains, however the effect of utilizing a higher temperature on the backscattering level of the POF was insignificant.

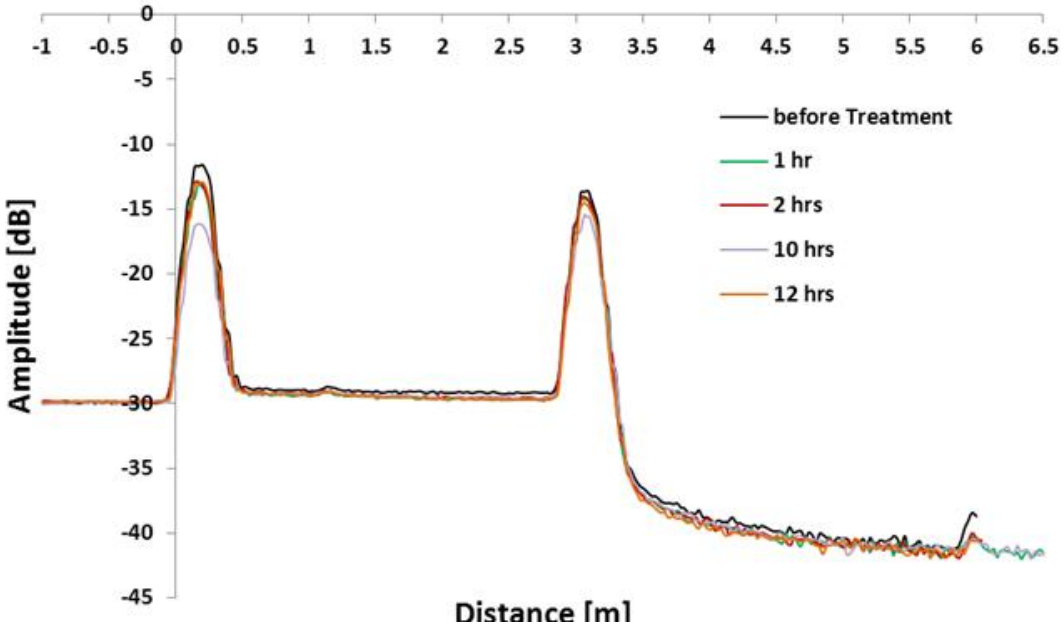

Figure 5.6 Backscattering level measurements for GI-PF-POF embedded in system 2000 Epoxy resin at 27º C

5.3.2 Fourier Transform Infrared Spectrometry

The previous OTDR testing showed a significant drop in the backscattering level of the POF embedded in the Vinylester resin at a location of 1.58 m along the fiber, while the POF embedded in the Epoxy resin showed no change in the backscattering level even after full curing. The large magnitude of the drop in the backscattering level of POF/Vinylester indicates a change in the POF condition, not simply a difference in residual stresses on the POF between the two systems. To investigate the source of the increase in signal loss in the POF embedded in the Vinylester, we first performed Fourier Transform Infrared Spectrometry (FTIR) to determine if a chemical reaction had occurred between the POF and the Vinylester resin.

FTIR is a method where IR radiation is passed through a sample [28]. Some of the infrared radiation is absorbed by the sample and some of it is passed through (transmitted). The

resulting spectrum represents the molecular absorption creating a molecular fingerprint of the sample. Figure 5.7shows the results of the FTIR analysis for the POF used in this study, a pure Vinylester resin sample and a Vinylester resin sample with an embedded POF. The FTIR analysis of the combined POF treated with Vinylester showed no presence of any new active group, which is evidence that no chemical reaction occurred between the POF and the Vinylester resin.

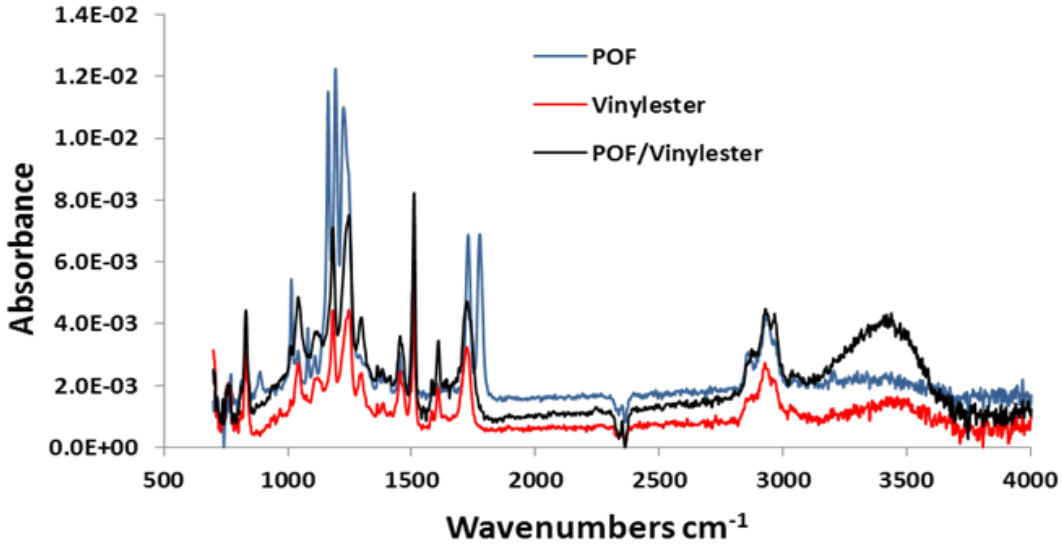

Figure 5.7 FTIR absorbance analyses of Vinylester resin, POF, and POF/Vinylester samples

5.3.3 Cross section analysis

A cross section analysis was conducted on POF, POF/Vinylester, and POF/Epoxy samples to investigate if any physical changes in the POF caused the drop in backscattering level of the POFs embedded in the Vinylester resin. Figure 5.8 shows SEM cross section images POF treated with Vinylester (Figure 5.8(b)) and untreated POF (Figure 5.8(a)). The POF/Vinylester sample was prepared by dipping the POF into Vinylester resin mixed with MEKP. After 2 hours, before the resin fully consolidated, the POF was freed from the resin using a sharp blade without causing any damage. The original POF and POF/Vinylester

samples were saturated in liquid nitrogen and a segment of both samples was cut using a sharp blade and placed on SEM sample holder using double sided adhesive tape. The images indicate that the fiber diameter increased from 750 µm to 811.38 µm (a 61.38 µm or 8.2% increase).Therefore, swelling of the POF occurred due to penetration of the POF by the Vinylester resin during cure. This penetration into the POF of a foreign substance is most likely the cause of the decreased backscatter level observed earlier.

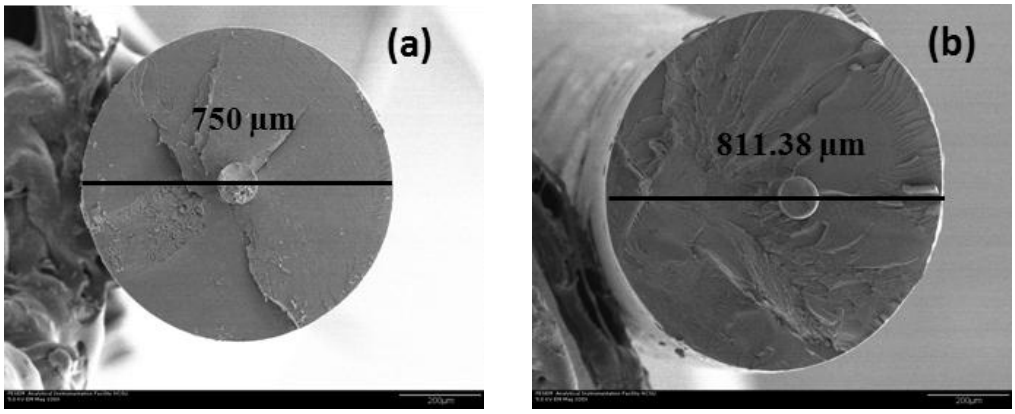

Figure 5.8 (a) Scanning Electron Microscope (SEM) image of original GI-PF-POF, (b) POF after embedment in Vinylester resin.

Further study of the untreated POF, POF treated with Vinylester, and POF treated with Epoxy cross sections were conducted using stereomicroscopy. This type of microscopy has the capability of imaging the POF cross section using two separate optical paths. Two different images of each sample were therefore obtained, first when the light passes through the cross section (transmission), and second when the light reflects from the sample surface (reflection). Figure 5.9 shows the transmission and reflection images of the pristine POF. The POF cross section was first cleaved with a razor blade. Since the POF is made of an optically transparent polymer, the transmitted light image shows a bright cross section (Figure 5.9a) and the reflected light image appears dark (Figure 5.9b).

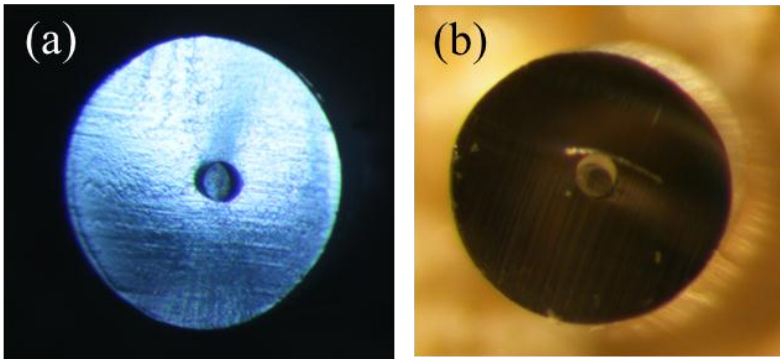

Figure 5.9 (a) Transmitted light image for POF, (b) reflected light image for POF

Figure 5.10 shows similar images obtained for a POF cross section after it was embedded in the Vinylester resin and full cure was achieved. The POF/ Vinylester sample was extracted from the Vinylester resin before it fully consolidated. The POF/Vinylester sample was then inserted into a small piece of cork and a segment of the cork and the POF/Vinylester was cut using a sharp blade. Figure 5.10(a) and Figure 5.10 (b) show different cross sections of the POF/Vinylester imaged in transmission. Figure 5.10 (a) shows a partial penetration of the Vinylester resin into the POF, while Figure 5.10(b) shows a full penetration of the Vinylester resin into POF sensors. Figure 5.10(a) and Figure 5.10 (b) also show vinylester resin didn't penetrate through the core whereas the light was transmitted through the core during the light guiding properties analysis. The penetration is visible due to the decrease in light transmitted through the POF. This penetration explains why swelling of the POF fiber occurred (increasing the POF diameter). The cross section image in reflection shown in Figure 5.10(c) supports this finding, as the POF/Vinylester image is not opaque indicating that the POF with Vinylester is no longer transparent.

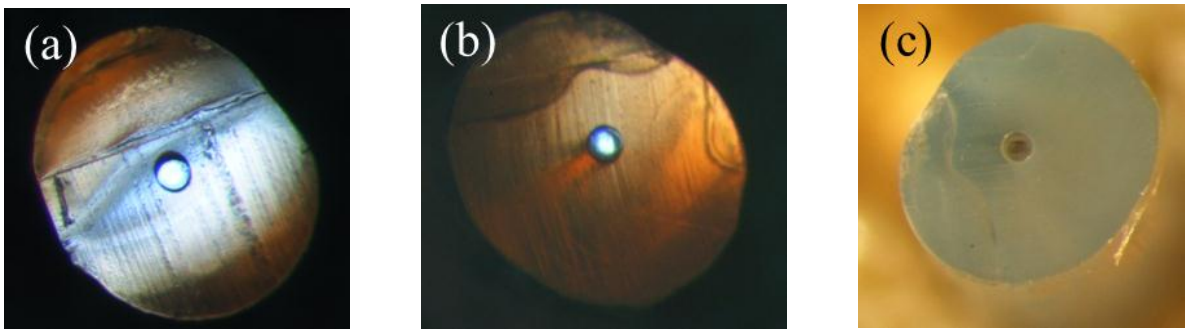

Figure 5.10 (a), (b) Transmitted light image for cross section of POF/Vinylester, (c) reflected light image for cross section of POF/Vinylester

On the other hand the POF treated with Epoxy cross section images (as seen in Figure 5.11) show the same behavior as the original POF, which indicated no resin penetration of the Epoxy into the POF. The primary reason for the penetration of the Vinylester resin into the POF is most likely its relatively low viscosity (400 cp at 25 ºC) as compared to that of the Epoxy resin (900-975 cp at 25 ºC). This lower viscosity of the Vinylester permitted the resin to penetrate though the POF and cause swelling of the POF.

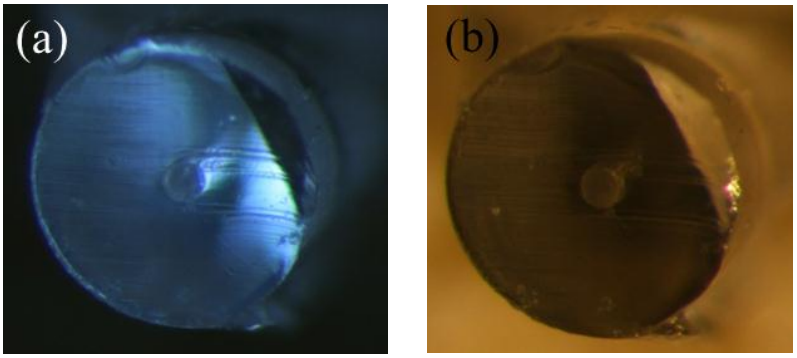

Figure 5.11 (a) Transmitted light image for cross section of POF/Epoxy, (b) reflected light image for cross section of POF/Epoxy.

5.4 Conclusion

In any composite material system, the choice of resin plays a major role in the final material properties. In this study we evaluated the effect of common resins type on the integrity of embedded POFs. The choice of resin may clearly affect the performance or sensitivity of embedded POF sensors for detecting structure damage. POFs are already limited for long distance transmission due to their high signal loss; therefore any further increase in fiber signal loss would further limit their use. While we only considered the two most common resin types, this work provides a research protocol to reveal whether POF integrity is affected by a resin system of interest.

This study showed that Vinylester resin caused a significant increase in the backscattering level of POF sensors and therefore induced high fiber signal losses. FTIR analysis showed that no chemical reaction between the POF and Vinylester resin had occurred. Cross section analysis showed a significant increase in the diameter of the POF treated with Vinylester, while stereomicroscope images showed evidence of the presence of the Vinylester inside the POF cross section. Penetration of the Vinylester inside the POF affected the light propagation inside the POF because the Vinylester resin has a higher refractive index than the core of the POF, resulting in attenuation of the light signal. On the other hand, the POF treated with Epoxy showed no change in backscattering level indicating no chemical or physical change had occurred to POF. Further, cross section analyses showed no penetration of the Epoxy resin into the POF. Epoxy resin systems are therefore preferred for textile composites if embedded POF sensors are to be implemented. In situations where a Vinylester resin is required, an additional protective coating or treatment to the POF may be required.

References

[1] Kersey A D 1996 A Review of recent developments in fiber optic sensor technology *Optical Fiber Technology* **2** 291–317

[2] Lee B 2003 Review of the present status of optical fiber sensors *Optical Fiber Technology* **9** 57–79

[3] Merzbacher C I, Kersey A D and Friebele E J 1996 Fiber optic sensors in concrete structures: a review *Smart Material and Structures* **5** 196-208

[4] Kuzyk M G 2007 Polymer Fiber Optics: Material, Physics, and Applications (Boca Raton, FL: CRC/Taylor & Francis)

[5] Appajaiah A 2005 Climatic Stability of Polymer Optical Fibers (POF) *Dissertation Bundesanstalt für Materialforschung und -prüfung (BAM)* (Berlin, Germany)

[6] Zubia J and Arrue J 2001 Plastic optical fibers: an introduction to their technological processes and applications *Optical Fiber Technology* **7** 101-140

[7] Ab-Rahman M S, Guna H and Harun M H 2009 Cost-effective fabrication of self-made 1x12 polymer optical fiber-based optical splitters for automotive application *American Journal of Engineering and Applied Sciences* **2** 252-259

[8] Seibel E, Johnston S and Melville C 2006 A full-color scanning fiber endoscope *Optical Fibers and Sensors for Medical Diagnosis and Treatment Applications Proceedings of SPIE* 6083 at no. 608303

[9] Kuang K, Quek S and Maalej M 2008 Remote flood monitoring system based on plastic optical fibres and wireless motes *Sensors and Actuators A: Physical* 147 449–455

[10] Bartlett R J, Philip-Chandy R, Eldridge P, Merchant D F, Morgan R and Scully P J 2000 Plastic optical fibre sensors and devices *Transactions of the Institute of Measurement and Control* 22 431–457

[11] Kiesel S, Peters K, Hassan T and Kowalsky M 2007 Behaviour of intrinsic polymer optical fibre sensor for large-strain applications *Measurement Science and Technology* 18 3144 – 3154

[12] Kiesel S, Peters K, Hassan T and Kowalsky M 2008 Large deformation in-fiber polymer optical fiber sensor *IEEE Photonics Technology Letters* 20 416-418

[13] Liehr S, Lenke P, Krebber K, Seeger M, Thiele E, Metschies H, Gebreselassie B, Münich J C and Stempniewski L 2008 Distributed strain measurement with polymer optical fibers integrated into multifunctional geotextiles Optical Sensors *Proceedings of the Society of Photo-Optical Instrumentation Engineers SPIE* 7003 art no. 700302

[14] Liehr S, Lenke P, Wendt M, Krebber K, Seeger M, Thiele E, Metschies H, Gebreselassie B and Münich J 2009 Polymer optical fiber sensors for distributed strain measurement and application in structural health monitoring *IEEE Sensors Journal* 9 1330-1338

[15] Liehr S, Nother N and Krebber K 2010 Incoherent optical frequency domain reflectometry and distributed strain detection in polymer optical fibers *Measurement Science and Technology* 12 art no. 017001

[16] Grillet A, Kinet D, Witt J, Schukar M, Krebber K, Pirotte F and Depre A 2008 Optical fiber sensors embedded into medical textiles for healthcare monitoring *IEEE Sensors Journal 8* 1215-1222

[17] Kuang K S C and Cantwell W J 2003 The use of plastic optical fibre sensors for monitoring the dynamic response of fibre composite beams *Measurement Science and Technology* 14 736–745

[18] Kuang K S C and Cantwell W J 2003 The use of plastic optical fibres and shape memory alloys for damage assessment and damping control in composite materials *Measurement Science and Technology* 14 1305–1313

[19] Kuang K S C, Akmaluddin, Cantwell W J and Thomas C 2003 Crack detection and vertical deflection monitoring in concrete beams using plastic optical fibre sensors *Measurement Science and Technology* 14 205-216

[20] Kuang K S C, Quek S, Koh C, Cantwell W J and Scully P 2009 Plastic optical fibre sensors for structural health monitoring: a review of recent progress *Journal of Sensors* 2009 1-13

[21] Anderson D A, Johnson L and Bell F G 2004 Troubleshooting Optical-Fiber Networks: Understanding and Using your Optical Time-Domain Reflectometer (London, UK: Academic Press)

[22] Saunders C and Scully P J 2005 Distributed plastic optical fibre measurement of pH using a photon counting OTDR *Sensors & Their Applications XIII: Journal of Physics Conference Series* 15 61-66

[23] Yokogawa Electric 2006 Guidebook for Optical Time Domain Reflectometer Communication and Measurement

[24] Danielson B L 1985 Optical time-domain reflectometer specifications and performance testing *Applied Optics* 24 2313-2322

[25] Saunders C and Scully P J 2007 Sensing applications for POF and hybrid fibres using a photon counting OTDR *Measurement Science and Technology* 18 615-622

[26] Husdi I R, Nakamura K and Ueha S 2004 Sensing characteristics of plastic optical fibres measured by optical time-domain reflectometry *Measurement Science and Technology* 15 1553-1559

[27] Legré M, Thew R, Zbinden H and Gisin N 2007 High resolution optical time domain reflectometer based on 1.55 □m up-conversion photon-counting module *Optics Express* 15 8237-8242

[28] Smith B C 2011 Fundamentals of Fourier Transform Infrared Spectroscopy (Second Edition) (Boca Raton, FL: CRC)

CHAPTER 6

6. Evaluation of the Integrity of 3D Orthogonal Woven Composites with Embedded Polymer Optical Fiber

Abstract

Due to their high flexibility, high tensile strain and high fracture toughness, polymer optical fibers (POF) are excellent candidates to be utilized as embedded sensors for structure health monitoring of fiber reinforced composites. In 3D orthogonal woven structures yarns are laid straight and POF can be easily inserted during preform formation either as a replacement of constituents or between them. The results of the previous paper indicated how an optic fiber sensor can be integrated into 3D orthogonal woven preforms with no signal loss. This paper addresses whether incorporating POF into 3D orthogonal woven composites affects their structure integrity and performance characteristics. Range of 3D orthogonal woven composites with different number of layers and different weft densities was fabricated. The samples were manufactured with and without POF to determine the effect of embedding POF on composite structure integrity. Bending, tensile strength tests, and cross section analysis were conducted on the composite samples. Results revealed that integrity of 3D orthogonal woven composite was not affected by the presence of POF. Due to its high strain, embedded POF was able to withstand the stresses without failure as a result of conducting destructive tests of the composite samples. Micrograph of cross-section of composite samples showed that minimum distortion of the tow yarn cross-section in vicinity of POF and no presence of air pocked around the embedded POF which indicates that 3D woven preform provided a good host for embedded POF.

Keywords:

A. Polymer Fiber Optic (PFO)

A. Embedded FOP Sensor

B. 3D Orthogonal Woven Preform

B. Fiber Reinforced Composite

C. VARTM

6.1 Introduction

Composite materials offer potential structure that is high strength and stiffness at lower weight compared to conventional structural materials. Because of these advantages, composite materials are being used for building, bridges, aircraft, windmill, sports goods, and automobiles. 3D textile structures preforms are formed using different technologies such as nonwoven, stack of 2D woven, and 3D integrated woven (orthogonal and stitched structures). 3D woven fabric preforms are known for their advantages over the nonwoven and 2D woven preforms in that they provide higher resistance to crack propagation, eliminate delamination, faster in resin transfer, and higher fiber volume fraction (1). Optical fibers whether silica optical fiber (SOF) or polymer optical fiber (POF) can be integrated into composite structure during the manufacturing process and provide a reliable structure diagnostic system. Due to its advantages over the electronic sensors such as small size, light weight, immunity to electromagnetic interference, and sensitivity, optical fibers are used as embedded sensors (2). Embedded optical fiber can be used to monitor the composite fabricating process, internal strain, force, pressure, temperature, and bending (3). Optical fibers can be integrated into 3D woven preform during the preform formation process or can be embedded between layers of prepreg plies (4). However, embedding optic fibers in composite structures should not affect composite structure integrity and performance.

Laminate thickness, orientation of embedded optical fiber, optical fiber diameter, and type of protective coating on optical fiber are parameters that may cause degradation of strength and modulus of composite structure (5). Many studies have been conducted to evaluate effect of embedded optical fibers parameters on the mechanical properties of composite structure. Embedded SOF in the mid-plane of 8 to 20 plies of unidirectional carbon/epoxy laminate with orientation varied from 0 to 90º created resin pockets. The resin pockets disturbed composite structure and caused premature failure initiation (5). Degradation of optical fiber coating layer at high temperature caused reduction in the interlaminate shear strength of composite structure (6). Bending strength of orthogonal woven glass/epoxy prepreg laminate with embedded SOF was investigated (7). 24 plies of laminates were prepared with

embedded SOF between first and second layers. The number of embedded optical fibers ranged from 0 to 50. Reduction in bending stress of the laminates was observed as the number of embedded optical fibers increased.

SOF possess many disadvantages such as (1) very brittle and easy to break in bending, (2) easy to break at low tensile strain (1%), which make it very difficult to handle them, (3) limited to systems with few number of measurements due to their high cost, and (4) require very precise positioning with respect to the connectors as well as the light source, which demand very expensive, skills, special tools and long time for system development. While POF sensors are characterized by high numerical aperture, extremely flexible and easy to handle, inexpensive, easy to splice and cleave, do not require protective layer, and can handle high tensile strain and high fracture toughness (8). Studies were conducted on the behavior of POF sensors and its ability to be used as embedded sensors into geotextile, civil engineering and composite structures (9) (10) (11). High strain properties and ductile behavior of POF allow their utilization as a distributed strain sensors for measuring the strain distribution, detecting cracks, and vertical deflection of the hosting material (12) (13) (14). As the research in integration of POF in civil engineering and composite structures is growing, there is a need for evaluating the effect of embedded POF on host structure integrity.

Bond strength of embedded POF in civil engineer material (mortar, hydrostone, and cement paste) was studied (15) (16). Pullout test on POF was conducted on prepared samples to determine the bond strength between the POF and civil engineer material. Small particles of cement material provided a good host of POF due to good bond between both. Unlike the cement, smooth surface of hydrostone decrease the bond strength with the POF and cause high slippage. On the other hand, rough particle surface of mortar caused a good bond with POF and low slippage was observed. Three different POF (PMMA) diameters of 1 mm, 500 µm, and 250 µm were embedded into glass fiber- epoxy laminate. POF with 1 mm diameters caused large air pockets around the POF which caused disturbance to the laminate geometry, while the other two diameters caused less air pockets. Bending strength of woven glass/epoxy prepreg with embedded number of silicon optic fiber (SOF) was studied to

reveal its effect on composite structures (17). Increasing numbers of embedded SOF increased composite rigidity. Embedded SOF along the reinforced direction has no significant effect on composite flexure strength and modulus. However, composite performance decreased with embedded SOF when measured at 45^{o} angle.

Unlike 2D woven structures, yarns in 3D orthogonal woven structures are straight and POF can be easily inserted during preform formation either as a replacement of constituents or between them without causing irregularity or bulkiness that lead to resin rich areas and air pockets. As such, the recognized advantages include: (a) thin POF will not have negative impact on the composite properties, (b) POF can be inserted during formation at different layers in x-direction and can be placed over small or large area that enable monitoring stress distribution in x-y plane and/or in the z-direction. While the 3D orthogonal woven structures possess such advantages, none of previous publications considered incorporating POF into 3D orthogonal woven composites to investigate the effect of their presence on the performance of the final composites to be monitored. The current research main goal is to make use of the advantages of the 3D orthogonal woven composites and POF in structure health monitoring. The health monitoring of structures will be addressed in the next paper. This part of the study deals with investigation of the effect of presence of POF on the performance of the composites as a first step to check whether the performance is negatively impacted by the presence of the POF. To achieve the goal range of 3D orthogonal woven composites from glass fiber/epoxy with embedded POF and without POF in weft direction were constructed and tested for their bending and tensile properties. The bending and tensile data were statistically treated to unveil the parameters (number of y- and x-layers, weft density, and presence of POF) of significant effect and their interactions.

6.2 Experimental Methods

6.2.1 Materials

The POF used in this study was a low attenuation, IR-transparent POF with a high bandwidth graded index (GI), acquired from Chromis Fiberoptics, Inc. The POF fiber diameter is 750

μm, while the core and cladding are made of Perfluorinated polymer (PF) (Polyperfluoro-butenyvinyleether). The specifications along with tolerance of the POF are shown in Table 6.1. Core diameter is 62.5 μm, which is the common multi-mode core diameter.

Table 6.1 GI-PF-POF specifications

Property	**Value**
Core diameter	62.5 ± 5 μm
Cladding diameter	750 ± 5 μm
Numerical aperture	0.185 ± 0.015
Max. tensile load	15.0 N
Long-term bend radius	7.0 mm
Core refractive index	1.357
Cladding refractive index	1.342

Materials used to form 3D orthogonal woven composites were fiber glass (E-glass), supplied by PPG Industries. The advantageous characteristics (high tensile strength, high heat and chemical resistance, and dimensional stability, low cost) of glass fibers promoted their use in FRC. Three different linear densities of fiber glass were acquired for the x-, y-, and z-yarns. The linear densities are 735 (g/km or tex), 2275 (g/km or tex), and 276 (g/km or tex), respectively. Figure 6.1 shows 3D orthogonal woven preform with x-, y-, and z-yarns identification.

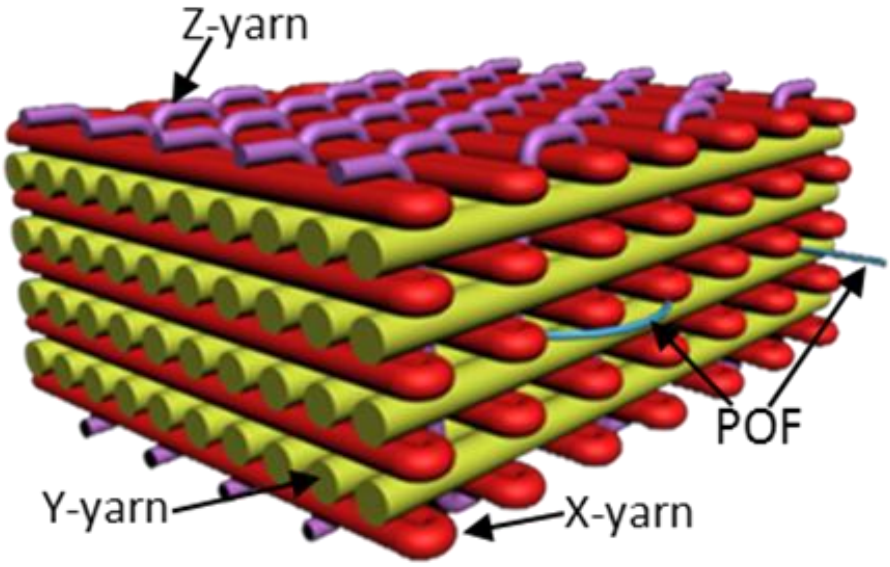

Figure 6.1 Simulation of 3D woven preform with embedded POF.

The resin used was a two part system consisted of Epoxy 2000 and Hardener 2120 acquired from Fibre Glast Developments Corporation. This system has a pot life and curing time of 2 hours and 12 hours, respectively, at room temperature (about 21º C). Mixing ratio of resin : hardener was 100:27 by weight or 3:1 by volume. Table 6.2 depicts the properties of resin system. This resin was selected for its high tensile strength and modulus. Another significant reason for the selection is its harmless effect on the POF as it was revealed in (18).

Table 6.2 Resin system properties.

Property	Value
Tensile strength	316.2 Mpa
Tensile modulus	17.37 Gpa
Flexural strength	459.65 Mpa
Density	1.134 g/m^3
Glass transition temp. (Tg)	90° C
Mixed viscosity at 25°C	925 – 975 cp

6.2.2 Experimental Design

Table 6.3 depicts samples specifications of 3D orthogonal preforms. Three variables namely number of y-yarn layers (3 levels), x-yarn density/layer (2 levels), and presence of the POF (two levels for presence and absent of POF) were considered. In total 12 preforms were manufactured. The '0' and '1' in Table 6.3 denote absence and presence of POF respectively. The fixed architecture parameters of the 3D orthogonal woven preforms are shown in

Table 6.4.

Table 6.3 3D orthogonal woven preform specification.

Sample ID	Presence or absence of POF	Pick density (yarns/cm/layer)	y-yarn layers (x-yarn layers)
1	0	1.57	2 (3)
2	1	1.57	2 (3)
3	0	4.72	2 (3)
4	1	4.72	2 (3)
5	0	1.57	3 (4)
6	1	1.57	3 (4)
7	0	4.72	3 (4)
8	1	4.72	3 (4)
9	0	1.57	4 (5)
10	1	1.57	4 (5)
11	0	4.72	4 (5)
12	1	4.72	4 (5)

Table 6.4 Fixed architecture parameters.

Parameters	Value
Number of y-yarns/layer	102
Total number of z-yarns	102
Reed Number, dents/cm	2.36
Z-yarns/dent	1
Y-yarn/layer/dent	1
Preform width, cm	43.18
Weave structure (double insertion/shed)	Plain

6.2.3 Formation of Preforms with Embedded POF and Composites

3D weaving machine (Figure 6.2), which is donated by 3TEX, Inc., was used for preforms formation. Figure 6.2 shows the machine while weaving a preforms with 4 layers of y-yarns and 5 layers of x-yarns, which are being inserted simultaneously during one weaving cycle. The binding yarns (z-yarns) are the top and bottom layers in Figure 6.2.

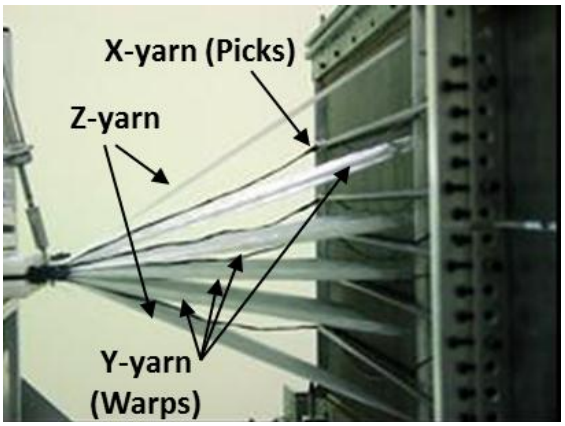

Figure 6.2 3D weaving machine (donated by 3TEX, Inc.) during multi-insertion of filling yarns (x-yarns) through multi-shed formed of warp yarns (y-yarns) and z-yarns (top and bottom sheets)

Optic fibers were embedded in the 3D woven preform structures during the weaving process. Figure 6.3 shows the location of the POF in 3D woven preforms of 2-, 3-, and 4-layers of y-yarns. The POF was inserted in x-direction. The preforms were treated with resin system using vacuum assisted resin transfer molding (VARTM) technique. The vacuum pressure of 100 kPa was used and kept constant for all samples.

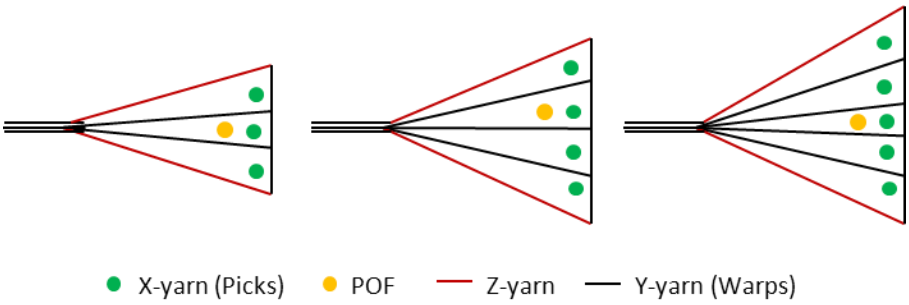

Figure 6.3 Schematic diagram embedded POF location and orientation in 3D woven preform

6.3 Testing and Statistical Analyses

Density and constituent contents of 3D woven composite were measured according to ASTM D792-08 and ASTM D3171-11 respectively. MTS Landmark Servo hydraulic Test System with 370.25 Load Frame was used to conduct tensile test on prepared samples according to ASTM D3039. Laser extensometer was used to measure samples strain during the test. The tensile tests were performed in the x-yarn direction, which is also the direction of the POF.

The bending tests (3-point mode) were performed using TESTRESOUCES model 130Q1000 load frame with QS Controller. The flexural test machine is a customized dual column load frame with 500 mm clearance between the two columns to test large specimen. The span length is adjustable and ranges from 30 mm to 470 mm. Five specimens of 25 mm wide and 80 mm long from each of the 12 composites of Table 6.3 were loaded at a rate of 4 mm/min. The specimen length was in the direction of x-yarns, which is the direction of the POF. Each specimen for bending or tensile contained one POF.

For the bending and tensile tests, the thickness of each specimen was measured and considered in the determination of the bending strength and modulus and tensile stress and modulus.

General Linear Model (GLM) statistical analysis was performed to find out whether there is significant effect of the variables and their interactions on each property considered. The statement of the GLM used:

$$y = x1 \quad x2 \quad x3 \quad x1*x2 \quad x1*x3 \quad x2*x3$$

Where y is the response or property, x1 is '0' or '1' for absence or presence of POF, x2 is x-yarn density/layer, and x3 is the number of y-yarn layers. X1*x2, x1*x3, x2*x3 are first order interactions of the main effect x1, x2, and x3.

Additionally, Tukey's multiple mean comparison was performed to differentiate between the 12 means of the experimental design of Table 3 for each property considered. The confidence level used was 95% for both GLM and Tukey multiple mean comparison.

6.4 Results and Discussion

6.4.1 Composite Physical Properties

Table 6.5 depicts physical properties of the 12 composite samples. The data indicates that the fiber weight fraction (Wr), fiber volume fraction (Vr), and volume density are not significantly different. The table reports also the values of the total linear density (g/km or tex) of the reinforcement (glass fibers), which is proportional to the cross-section area (perpendicular to x-direction) of the fibers in a given sample. These are the fibers that were torn in the bending and tensile testing.

Table 6.5 Physical properties of composite samples

Sample ID	Total Linear Density (g/km) in x-direction/sample of width 25 mm	Thickness (mm)	Wr (%)	Vr (%)	Density (g/cm^3)
1	8,270	1.55	71.79	55.56	1.93
2	8,214	1.61	69.08	52.11	1.88
3	24,641	2.00	68.28	51.65	1.89
4	24,387	2.03	69.44	52.58	1.89
5	10,771	2.04	65.71	47.71	1.81
6	10,879	2.05	63.69	45.99	1.89
7	33,019	2.86	69.25	52.41	1.83
8	33,208	2.95	66.08	48.62	1.91
9	13,540	2.45	70.00	53.48	1.81
10	13,585	2.47	65.31	47.39	1.86
11	41,069	3.21	67.52	50.45	1.82
12	40,704	3.25	66.37	48.57	1.93

6.4.2 Mechanical Properties

GLM statistical analysis showed the presence or absence of the POF has no significant effect on flexural strength regardless of the number of layers or x-yarn density. Comparable samples with or without POF exhibited about the same flexural strength. Using POF as embedded sensor in 3D orthogonal woven composite structures has no negative effect on their integrity judged by the bending strength. Statistical analysis using Tukey's multiple mean comparison supported the GLM finding in regards to the effect of presence/absence of POF. The results of flexural strength along with error bars of the 12 composite samples are shown graphically in Figure 6.4. Selected typical flexural strength-strain diagrams are shown in Figure 6.6 Visual inspection of Figure 6.4 and Figure 6.5 supports the GLM and Tukey’s

statistical analyses. Bending stress-strain curves for all tested samples are shown in appendix A section A.1.

GLM indicated that the x-yarn density and number of layers had significant effect on the flexural strength due to thickness increase (Table 6.5 and Figure 6.10) with these two parameters. In general, as the number of layers (or x-yarn density) increased the bending strength increased. Additionally the interaction of number of layers and x-yarn density had significant effect on the flexural strength. Figure 6.6 shows the results of the flexural modulus of the 12 composite samples. GLM and Tukey statistical analyses showed that the flexural modulus followed exact same pattern as the flexural strength. Again the presence of POF did not cause deterioration of the flexural modulus of the composite structures. Optical analysis (discussed later) showed that the presence of the POF did not cause voids and distorted only the x-yarn in contact with the POF. Flexural strength and flexural modulus raw data and statistical analysis are shown in appendix A section A.2 and A 3.

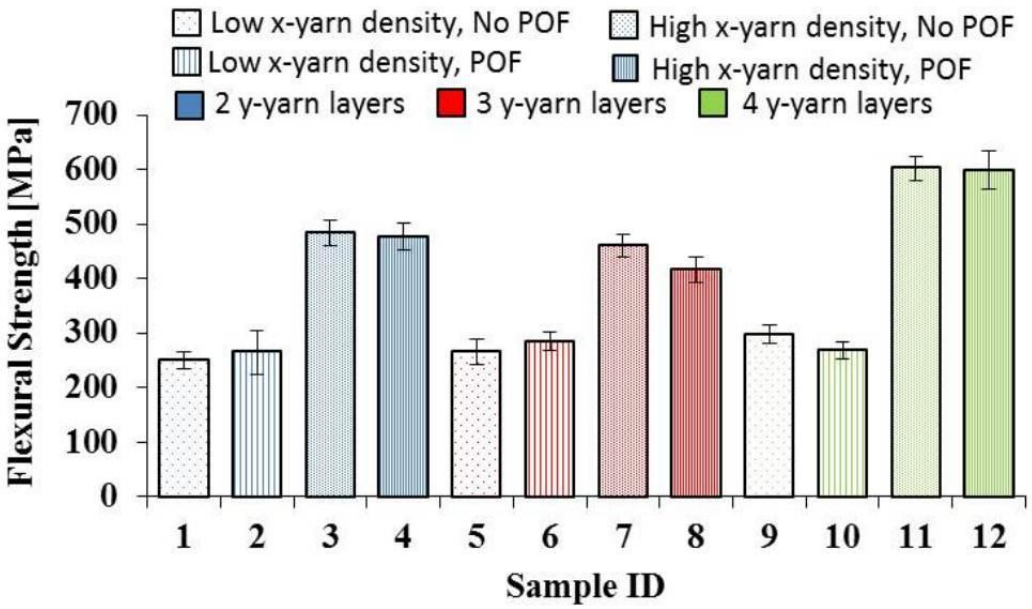

Figure 6.4 Flexural strength of 3D orthogonal woven composite samples

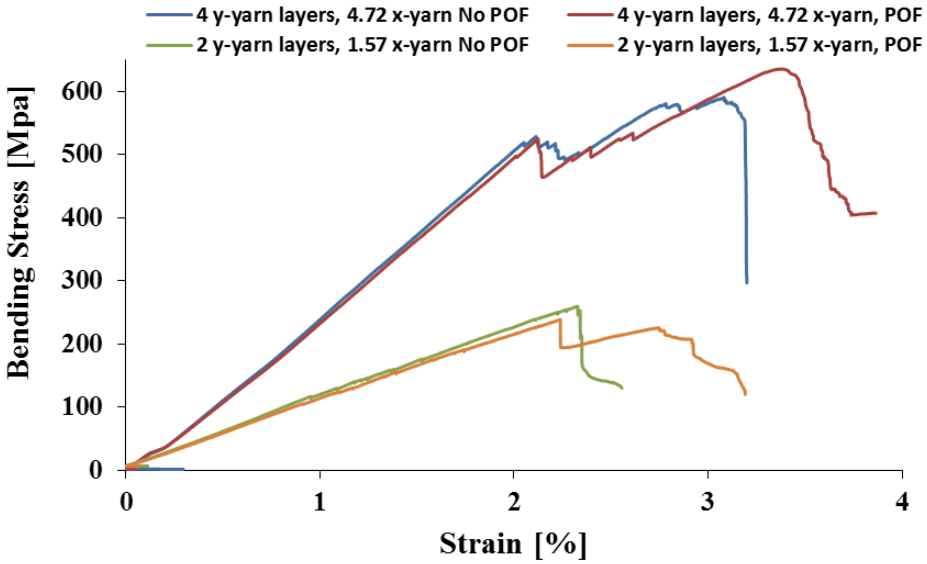

Figure 6.5 Typical bending stress-strain curves of composites of different layers with and without the presence of POF

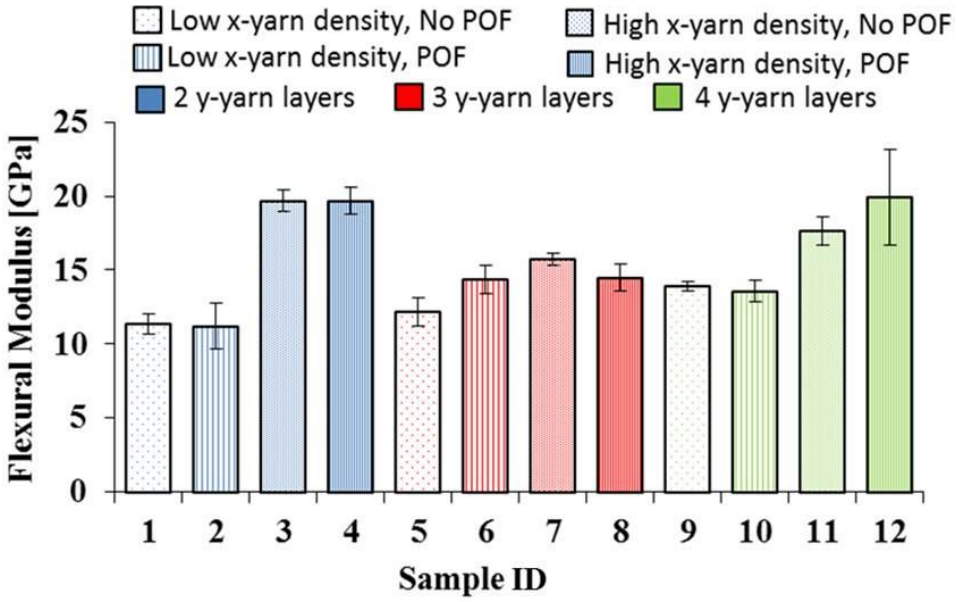

Figure 6.6 Flexural modulus of 3D orthogonal woven composite samples

GLM and Tukey's multiple mean comparison statistical analyses showed that embedded POF has no significant effect on tensile strength and modulus regardless of the number of layers or x-yarn density (Figure 6.7- Figure 6.8). Comparable samples with or without POF exhibited about the same tensile strength. Using POF as embedded sensor in 3D orthogonal woven a composite structure has no negative effect on their integrity in terms of tensile strength and modulus.

The results of Figure 6.7 and Figure 6.8 indicate that the tensile strength and modulus are not equal for all samples. The variation of the samples thickness (Figure 6.10) in terms of number of layers and x-yarn density is not linear due to variation of the compressible yarn cross-section with the number of layers and x-yarn density. Additionally, VARTM process is known to produce composite panels with thickness variation (19). For this reason, it was thought to use a different way of expressing the tensile strength using different units. The load carrying constituents for this test are the x-yarns. The total tex of x-yarns (tex is defined as g/km of yarn, which is proportional to material cross section area) of each tested sample was calculated and the strength was expressed in cN/tex. The total tex is an independent parameter of composite thickness and does not get affected by the VARTM process variables. Figure 6.11 shows the results of tensile strength of the 12 composite samples in (cN/tex). Tukey's multiple mean comparisons on the data of Figure 6.11 shows that the strength of samples 1-9 are not significantly different. The difference of the other samples (10-12) from the rest may be attributed to the inherent variability of the fibers and resin infusion process. Tensile strength and tensile modulus raw data and statistical analysis are shown in appendix A section A.5 to A.7.

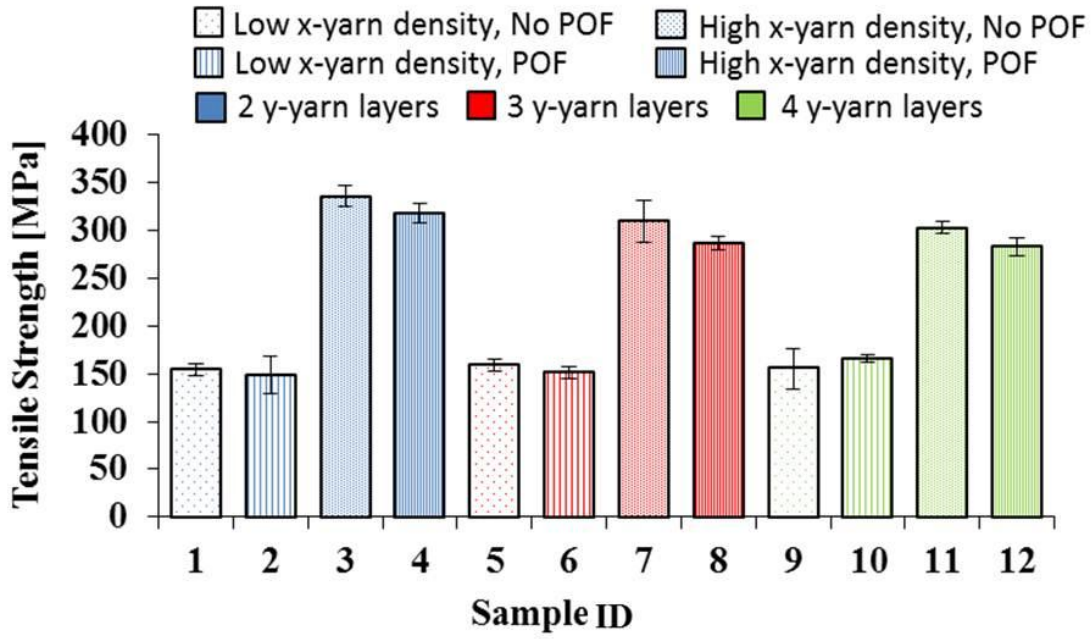

Figure 6.7 Tensile stress of 3D orthogonal woven composite samples

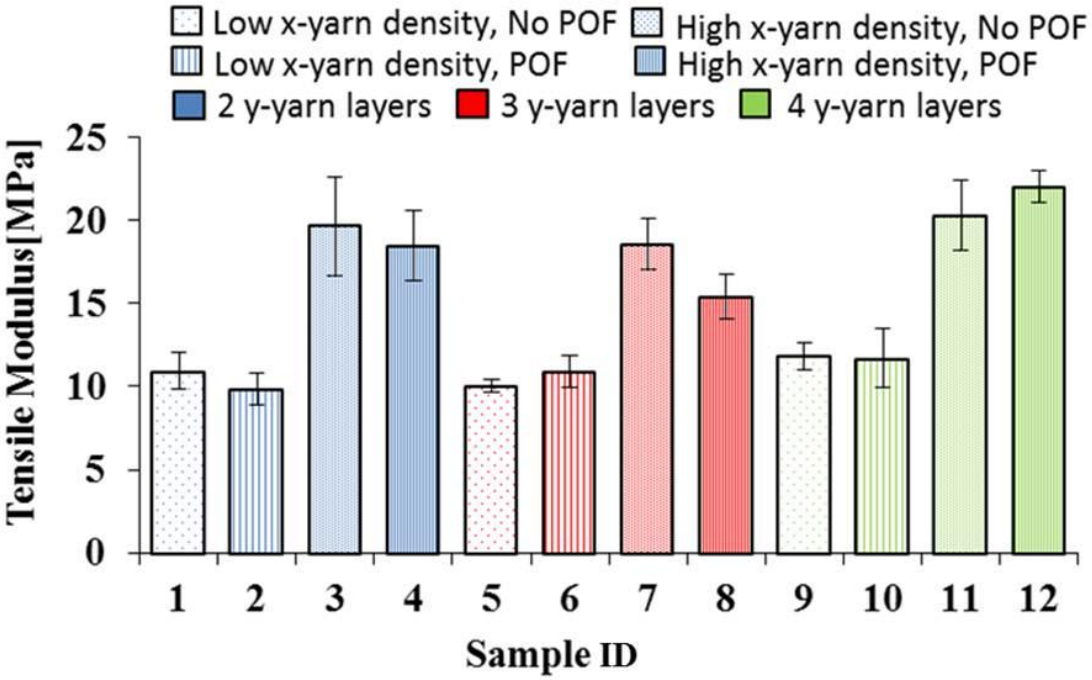

Figure 6.8 Tensile modulus of 3D orthogonal woven composite samples

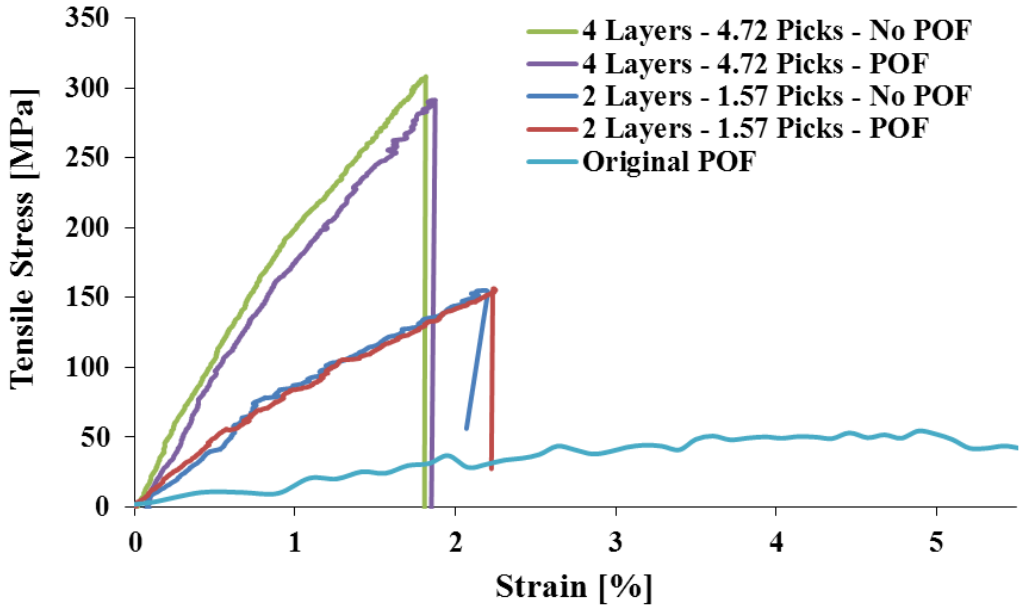

Figure 6.9 Typical tensile stress-strain curves of composites of different layers with and without the presence of POF

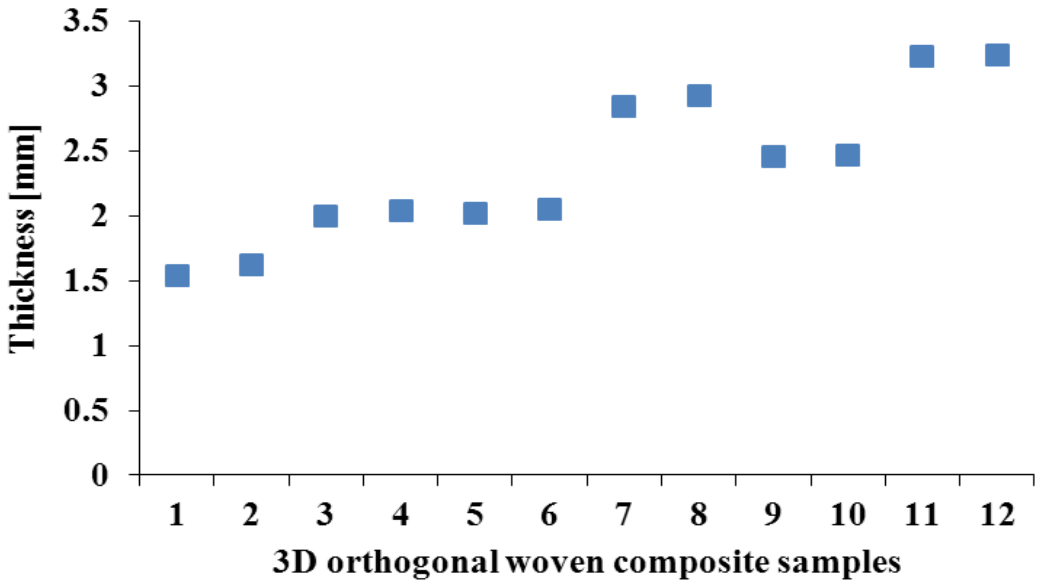

Figure 6.10 Thickness of the composite samples

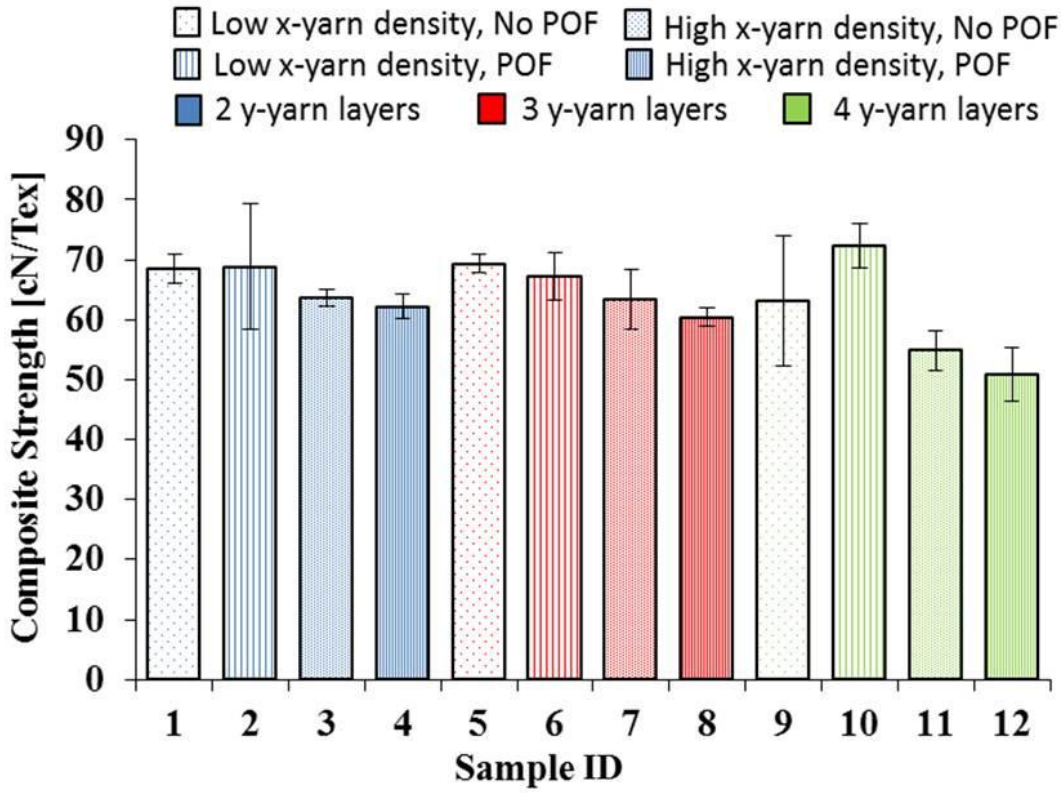

Figure 6.11 Composite strength in normalized units (cN/tex)

It is worth mentioning that the POF sensor, which is characterized by its high strain, was not broken (observed in all specimens bending and tensile tests) even though the host composite sample was failed at 2 % strain as it can be seen from Figure 6.12. This indicates that the POF sensor will not break before the composite from 3D orthogonal woven composites. In a separate tensile testing, the POF exhibited yield strain 4.9% and strain at peak load 5.4%, which is higher than the host material strain at failure (Figure 6.9). Tensile stress-strain curves for all samples are shown in appendix A section A.4.

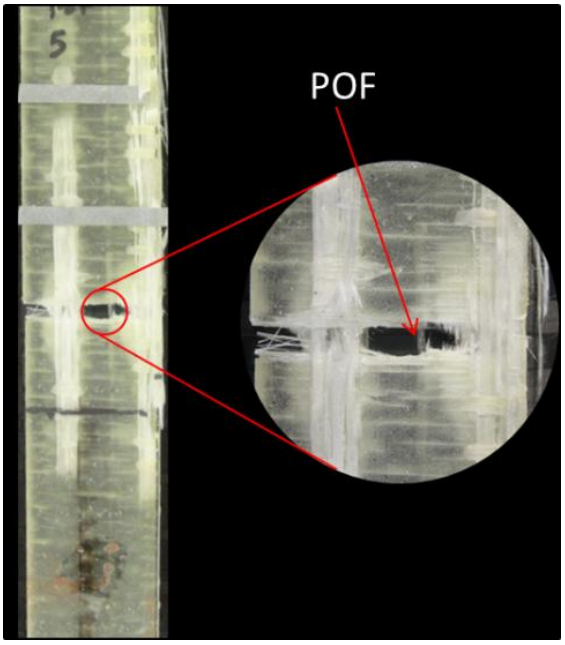

Figure 6.12 Unbroken embedded POF after composite sample failed under tensile test

6.4.3 Optical Analysis

Optical analysis was thought to investigate the effect of the presence of the POF on the composite structures. Samples for optical imaging were prepared using four level of grinding followed by one level of polishing. The abrasive papers made of silicon carbide with different grade were used and all abrasive paper grades level were according to Federation of European Producers of abrasive (FEPA) and noted by P-grade abrasive grit size. Composite samples were cut and mounted in middle castable mounting mold ring with 25 mm diameter. Acrylic resin was used for casting and holding specimens. The entire process of preparing samples, grinding and polishing are presented in appendix A section A.8. Figure 6.13 and Figure 6.14 show stereomicroscopic images for polished samples. Presence of POF caused resin pockets as a result of creation of space between the y-yarns surrounding the POF. However, the space was filled with resin and no void formation in most cases. All composites with low x-yarn density (1.57 threads/cm/layer) showed partial lenticular shape for the resin pockets. As the x-yarn density increased to 4.72 threads/cm/layer the shape and

size of resin pockets decreased due to presence of more yarns under z-yarn float. The presence of the POF caused distortion of the x-yarn in contact with it. This localized distortion did not cause deterioration of the mechanical properties as discussed earlier. Cross section images for all samples are shown in appendix A (Figure A.26 to Figure A.32).

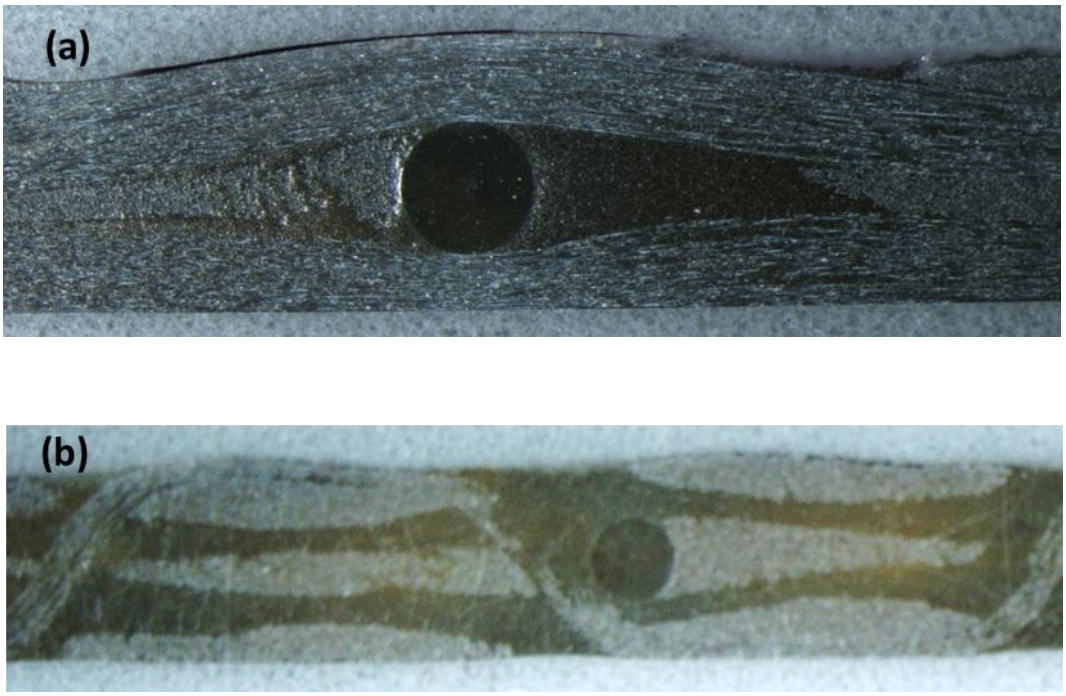

Figure 6.13 Cross-section of composites with ID 2 (top) and 4 (bottom)

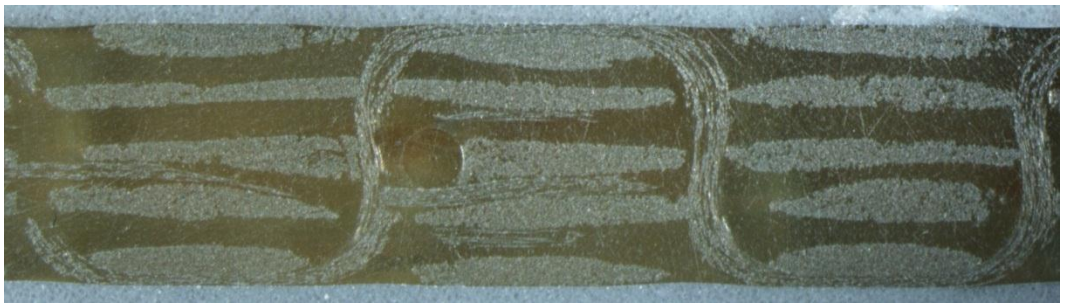

Figure 6.14 Cross-section of composite with ID 12

6.5 Conclusion

We conducted systematic investigation with main goal to find out whether embedding POF sensor in 3D orthogonal woven composites negatively affect the performance of the composites. In total twelve composite samples were manufactured with three variables namely presence/absence of POF, number of y-yarn/x-yarn layers, and x-yarn density. The performance of 3D woven composites was assessed for bending and tensile properties. It was found that the performance of the samples containing POF sensor were not significantly different from those without sensor. Optical images of cross-section of composite samples unveiled that the presence of POF did not cause much change in the structure. The presence of POF caused resin pockets beside the fiber optic at the side of z-yarn and caused minor distortion of the x-yarn in contact with POF. The resin pockets and x-yarn distortion were reduced for structures with high x-yarn density compared to those with low x-yarn density. The minor resin pockets and x-yarn distortion did not cause negative impact on the composite samples performance.

It was shown in (18) the epoxy resin system did not affect the POF signal integrity and did not cause any signal loss after the resin infusion process was completed. Additionally, it was shown in (20) unlike Silica Optic Fiber (SOF), POF can be configured in 3D orthogonal woven composite without losing any of its signal sensitivity. The findings reported here and in (18) and (20) indicated that POF is a viable sensor that can be embedded in 3D orthogonal woven composite for Structural health monitoring.

References

[1] Mohamed, T. S., Johnson, C. and Rizkalla, S. Behavior of Three-Dimensionally Woven Glass Fiber Reinforced Polymeric Bridge Deck. *Composites Research Joumal.* 2007, Vol. 1, pp. 27-42.

[2] Pan, X., Liang,D., Li, D. Optical fiber sensor layer embedded in smart composite material and structure. *Smart Materials and Structures.* 2006, Vol. 15, pp. 1231-1234.

[3] Rogers, C.A. Intelligent Material Systems and Structures US/Japan Working on Smart/Intelligent Materials and Systems. pp. 11–18.

[4] Bogdanovich, A., E., Wigent III, D., E., and Whitney, T., J. Fabrication of 3-D Woven Preforms and Composites with Integrated Fiber Optic Sensors. *SAMPE Journal*. 2003, Vol. 39, 4, pp. 6-15.

[5] Shivakumar, K., and Emmanwori, L. Mechanics of Failure of Composite Laminates with an Embedded Fiber Optic Sensor. *Journal of Composite Materials*. 2004, Vol. 38, pp. 669-680.

[6] Roberts, S. S. J., and Davidson, R. Mechanical properties of composite materials containing embedded fibre optic sensors. *Fiber Optic Smart Structures and Skins IV*. 1991, Vol. 1588, pp. 326–341.

[7] Liu, R., Liang, D. Experimental study of optical fibers influence on composite. *Proc. of SPIE*. Vol. 7522, pp. 1-8.

[8] Merzbacher, CI, Kersey AD, Friebele EJ. Fiber optic sensors in concrete structures: a review. Smart Mater Struct 1996;5(2):1-7.

[9] Liehr, S., Lenkea,P., Krebbera,K., Seegerb,M., Thieleb,E., Metschiesb,H., Gebreselassie, B., Münich, J., Stempniewski, L. Distributed strain measurement with polymer optical fibers integrated into multifunctional geotextiles. *Optical Sensors, Proc. of SPIE*. Vol. 7003.

[10] Kiesel, S., Van Vickle, P., Peters, K., Abdi, O., Hassan, T., Kowalsky, M.,. Polymer optical fiber sensors for the civil infrastructure. *Mechanical, and Aerospace Systems, SPIE Sensors and Smart Structures.* 2006, Vol. SPIE 6174, pp. 1-12.

[11] Nakamura, K., Husdi,I., Ueha, S. Memory effect of POF distributed strain sensor. *Second European Workshop on Optical Fibre Sensors, Proceedings of SPIE*. Vol. 5502, pp. 144-147.

[12] Liehr, S., Lenke,P., Wendt,M., Krebber,K., Seeger,M., Thiele,E., Metschies, H., Gebreselassie,B., Münich, J. Polymer Optical Fiber Sensors for Distributed Strain Measurement and Application in Structural Health Monitoring. *IEEE SENSORS JOURNAL*. 2009, Vol. 9, 11, pp. 1330-1338.

[13] Kuang, K., Akmaluddin, Cantwell, W., Thomas, C. Crack detection and vertical deflection monitoring in concrete beams using plastic optical fibre sensors.

MEASUREMENT SCIENCE AND TECHNOLOGY, INSTITUTE OF PHYSICS PUBLISHING. 2003, Vol. 14, pp. 205-216.

[14] Kuang, K.,Quek,S.,Koh,C.,Cantwell,W., Scully,P. Plastic Optical Fibre Sensors for Structural HealthMonitoring:A Reviewof Recent Progress. *Journal of Sensors, Hindawi Publishing Corporation.* 2009, Vol. 2009, p. 13.

[15] Kiesela, S., Vicklea, P., Petersa, K., Abdib, O., Hassanb,T., Kowalskyb, M. Polymer optical fiber sensors for the civil infrastructure. *Smart Structures and Materials.* 2006, Vol. 6174, pp. 1-12.

[16] Peters, K. Polymer Optical fiber sensors: A review. *Smart Material and Structures.* 2011, Vol. 20, pp. 1-17.

[17] Liu, R., Liang, D. Experimental study of optical fibers influence on composite. *Fourth International Conference on Experimental Mechanics.* 2010, Vol. 7522, pp. 1-8.

[18] Hamouda. T., Peters, K., and Seyam, M., A. Effect of Resin type on the signal Integrity of an embedded Perfluorinated Polymer Optical fiber. *Smart Mater. struct.* 2012, Vol. 21, pp. 1-8.

[19] Andersson, H. M., Lundstrom, T. S., Gebart B. R. and Synnergren, P. Application of Digital Speckle Photography to Measure Thickness Variation in the Vacuum Infusion Process. *Polymer Composites.* 2003, Vol. 24, 3, pp. 448-455.

[20] Hamouda, T., Smart Textiles: Embedded Fiber Optic Sensors in 3D Orthogonal Composite Structures, Ph.D. Theis, North Carolina State University, Raleigh, NC, USA 2012.

CHAPTER 7

7. Sensing Characteristic of Embedded POF into 3D Orthogonal Woven Composite using OTDR during the Manufacturing and Under Bending and Impact Testing

Abstract

The work reported in Chapters 5 and 6 indicate POF sensors can be configured in 3D orthogonal woven composites keeping excellent sensitivity suitable for sensing system for health monitoring of structures. Additionally, the presence of POF in 3D woven composites did not have any negative effect on their performance characteristics. This part addresses a study to evaluate the sensing characteristic of embedded POF in 3D orthogonal woven preforms before and during resin infusion steps and the final composites when subjected to bending stresses and repeated impact. Different composite samples with embedded POF were fabricated with different 3D orthogonal woven composite parameters namely number of y-/x-layers and x-yarn density. The signal of POF was not affected significantly by the preform structure. During application of resin using VARTM technique, significant drop in backscattering level was observed due to pressure caused by vacuum. Measurements of POF signal while in the final composites after resin curing indicated that the backscattering level almost returned to the original level of un-embedded POF. The POF responded to application of bending load to the composite with reduction in the backscattering level. The backscattering level almost returned back to its original level after removing the bending load. However, the POF backscattering level increased with bending deflection and then dropped to its maximum level (Dynamic Range) when bending load caused composite failure despite the POF did not break. Repeated impact was conducted on composite samples to assess the potential of using POF in assessing composite damage after each impact test. Results showed increase in POF signal loss with number of impacts. Continuation of impact tests caused the area of damage to propagate in the composite samples and total loss of the POF signal as indicated by zero DR response. The results indicated POF responded well to repeated impact and can be used to assess the damage propagation of composite structures subject to impact.

7.1 Introduction

Civil engineering infrastructure such as bridges, dams, skyscrapers, airports, highways, wind mill, railways, and tunnels are must for civilization. These infrastructures are heavy and take long time to be built and expensive to construct and maintain. On the other hand the infrastructure has a lifetime which depends on, age, usage, the location, surrounding atmosphere (earthquakes, tornadoes, etc.) and also frequent maintenance needed to keep it safe for use (1). Thus, there is an increase need for structural health monitoring systems (SHM) that able to detect any change on the structure that may indicate damage or failure (2) (3). SHM includes sensing systems (electrical or optical), data processing unit, and evaluation and analysis systems (4). Growth of undetected hidden damage may unnoticeable and may increase and cause sudden failure to the structure. Thus, finding a SHM system that able to monitor the internal hidden failure and determine failure location is desired (5).

Because of its lightweight, easy to build, long life, less maintenance needed and high strength, textile composite materials are excellent candidates for replacing traditional material in infrastructure such as steel and concrete. These advantages of textile composites have led to a numerous applications such as aircrafts, automobile, military, wind turbine blade (6). In addition to the advantages of textile woven composite, optical fiber can be integrated into 3D woven preform during the weaving process, different direction, between different layers, and cover more area of the composite using only one length of the fiber optic. 3D textile structures preforms are formed using different technologies such as nonwoven, stack of 2D woven, and 3D woven. 3D woven fabric preforms are known for their advantages over the nonwoven and 2D woven preforms in that they provide higher resistance to crack propagation, eliminate delamination, faster in resin transfer, and higher fiber volume fraction (7). Presence of embedded optics sensors into textile structures will provide a good monitoring system that can monitor composite manufacturing parameters, internal strain, force, pressure, temperature, Impact damage and bending during the composite manufacturing process (8) (9).

POF sensors are characterized by, high numerical aperture, extremely flexible and easy to handle, inexpensive, easy to splice and cleave, do not require protective layer, and can handle high tensile strain and high fracture toughness (10). Studies were conducted on the behavior of POF sensors and its ability to be used as embedded sensors into geotextile, civil engineering and composite structures (11) (12) (13). High strain properties and ductile behavior of POF allow their utilization as a distributed strain sensors for measuring the strain distribution, detecting cracks, and impact of the hosting material (14) (15) (16). Changing in POF signal under different impact velocity were studied using end to end loss to determine structure deflection by attaching POF to structure surface (17). Optical Time Domain Reflectometer (OTDR) is a method that commonly applied to measure optical fiber transmission losses, determine the location of defects, and measure the optical fiber length (18). OTDR has previously been used to measure optical fiber attenuation in distributed SOF and POF sensors (19) (20) as well as micro bending, temperature changes, mechanical stress, and strain in these sensors (21). Previous impact studies were conducted on 2D woven laminate with POF sensors attached to composite surface. Change in POF signal under different impact velocity was studied using end to end loss to determine structure deflection by attaching POF to structure surface (22).

As indicated earlier, previous research did not take advantages of the 3D orthogonal woven composites as a viable host that do not get negatively impacted by embedding optic fibers and maintain the sensitivity of the optic fiber sensor. This research addresses the lack of previous work and focus in evaluating the sensing behavior of POF embedded in range of 3D orthogonal woven composites while subjected to bending and repeated impact.

7.2 Experimental Methods

7.2.1 Materials

The POF used in this study was a low attenuation, IR-transparent POF with a high bandwidth graded index (GI), acquired from Chromis Fiberoptics, Inc. The POF fiber diameter is 750 µm, while the core and cladding are made of Perfluorinated polymer (PF) (Polyperfluoro-

butenyvinyleether). The specifications along with tolerance of the POF are shown in Table 7.1. Core diameter is 62.5 µm, which is the common multi-mode core diameter.

Table 7.1 GI-PF-POF specifications.

Property	Value
Core diameter	62.5 ± 5 µm
Cladding diameter	750 ± 5 µm
Numerical aperture	0.185 ± 0.015
Max. tensile load	15.0 N
Long-term bend radius	7.0 mm
Core refractive index	1.357
Cladding refractive index	1.342
Backscatter coefficient	-57 dB
Dynamic Range	16 dB

Materials used to form 3D orthogonal woven composites were fiber glass (E-glass), supplied by PPG Industries. The advantageous characteristics (high tensile strength, high heat and chemical resistance, and dimensional stability, low cost) of glass fibers promoted their use in FRC. Three different linear densities of fiber glass were acquired for the x-, y-, and z-yarns. The linear densities are 735 (g/km or tex), 2275 (g/km or tex), and 276 (g/km or tex), respectively. Figure 6.1 shows 3D orthogonal woven preform with x-, y-, and z-yarns identification.

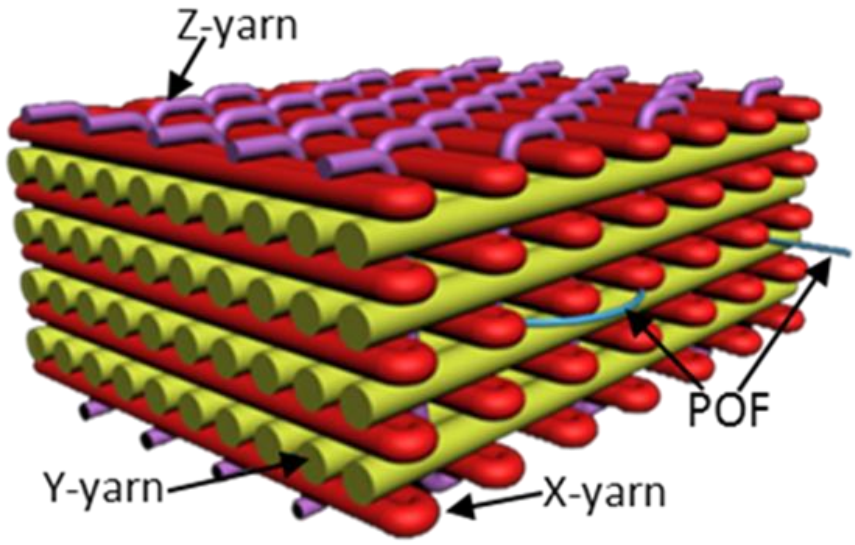

Figure 7.1 Schematic diagram of 3D woven preform with embedded POF.

The resin used was a two part system consisted of Epoxy 2000 and Hardener 2120 acquired from Fibre Glast Developments Corporation. This system has a pot life and curing time of 2 hours and 12 hours, respectively, at room temperature (about 21º C). Mixing ratio of resin : hardener was 100:27 by weight or 3:1 by volume. Table 7.2 depicts the properties of resin system. This resin was selected for its high tensile strength and modulus. Another significant reason for the selection is its harmless effect on the POF as it was revealed in (23).

Table 7.2 System 2000 Epoxy resin and 2120 hardener properties.

Property	Value
Tensile strength	316.2 Mpa
Tensile modulus	17.37 Gpa
Flexural strength	459.65 Mpa
Density	1.134 g/m3
Glass transition temp. (Tg)	90 ° C
Mixed viscosity at 25°C	925 – 975 cp

7.2.2 Experimental Design

Table 7.3 depicts experimental design of prepared 3D orthogonal woven composite for bending test. Three variables namely number of y-yarn layers (3 levels), x-yarn density/layer (3 levels), and increment bending load of 5 levels that differ in value depending on sample thickness or number of layers. In total 9 preforms were manufactured. All preforms were manufactured with embedded POF in the middle layer. The fixed architecture parameters of the 3D orthogonal woven preforms are shown in

Table **7.4**.

Table 7.3. Experimental design of bending tests

Parameter	Levels
y-yarn layers (x-yarn layers)	2(3), 3(4), 4(5)
x-yarn density (yarns/cm/layer)	1.57, 4.72
Number of bending loads	5
Total Number of Treatments	6

Table 7.4 Fixed architecture parameters

Parameters	Value
Number of y-yarns/layer	102
Total number of z-yarns	102
Reed Number, dents/cm	2.36
Z-yarns/dent	1
Y-yarn/layer/dent	1
Preform width, cm	43.18
Weave structure (double insertion/shed)	Plain

For repeated impact test, 6 samples were selected as shown in Table 7.5. Repeated impact test was conducted on selected samples at constant potential energy of 9 J. Fixed parameter to acquire this potential energy was 70 mm drop height, 1.310 Kg drop weight, and impact speed of 3.71 m/s. Impact test was repeated 30 times or until POF signal loss reached its maximum.

Table 7.5 Experimental design of Impact tests

Parameter	Levels
y-yarn layers (x-yarn layers)	2(3), 3(4), 4(5)
x-yarn density (yarns/cm/layer)	1.57, 4.72
Number of Impacts	Up to 30

7.3 Samples Fabrication

7.3.1 Formation of 3D Woven Preforms with Embedded POF

3D weaving machine (Figure 7.2(a)), which is donated by 3TEX, Inc., was used for preforms formation. Figure 7.2(b) shows the machine while weaving a preform with 4 layers of y-yarns and 5 layers of x-yarns, which are being inserted simultaneously during one weaving cycle. The binding yarns (z-yarns) are the top and bottom layers in Figure 7.2(b).

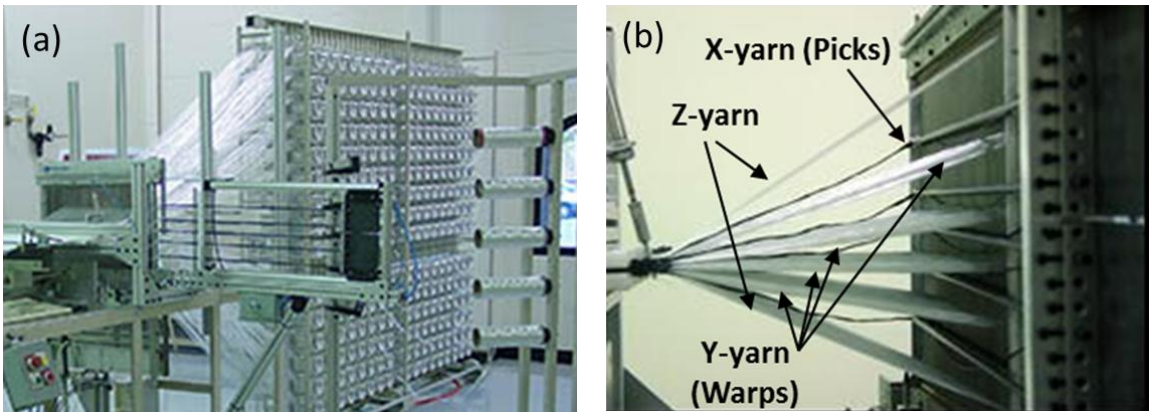

Figure 7.2 a) 3D weaving machine b) multi-insertion of filling yarns (x-yarns) through multi-shed formed of warp yarns (y-yarns) and z-yarns (top and bottom sheets)

POFs were inserted in the middle shed (between the 2nd and 3rd layers of y-yarns in case of 4-y yarn layers) in x-direction. Figure 7.3 shows an example of preform of 4-y yarn layers with the location of the POF indicated. One POF was inserted every 3.8 cm to cover large area of the 3D orthogonal woven preform. The inserted POF was bent at both selvedges of the 3D orthogonal preform to a radius of 1.9 cm (Figure 7.4) According to the finding in chapter 4, the critical bending radius at which the optic fiber exhibits no loss in signal was 1.9 cm. Therefore, this distance between the embedded POF was maintained constant for all fabricated preforms. The total length/sample of POF was approximately 5 meters, 135 cm was embedded in the preform and the remaining length was protruded from both sides of the preform to allow connecting to the OTDR. Table 7.6 list samples ID, y-yarn layers (x-yarn layers), and x-yarn density. Figure 7.5 shows the location of the POF in 3D woven preforms of 2-, 3-, and 4-layers of y-yarns.

Table 7.6 Sample identification and specifications

Sample ID	x-yarn density (yarns/cm/layer)	y-yarn layers (x-yarn layers)
I	1.57	2 (3)
II	3.14	2 (3)
III	4.72	2 (3)
IV	1.57	3 (4)
V	3.14	3 (4)
VI	4.72	3 (4)
VII	1.57	4 (5)
VIII	3.14	4 (5)
IX	4.72	4 (5)

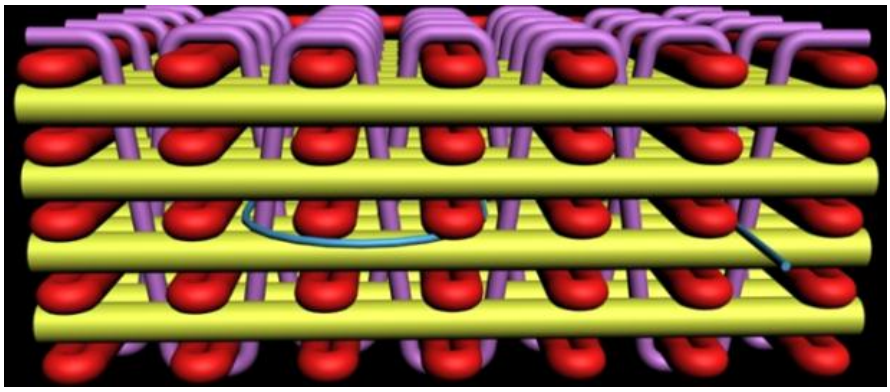

Figure 7.3 Side view of schematic diagram of embedded POF into 3D preform with 4-y yarn layers

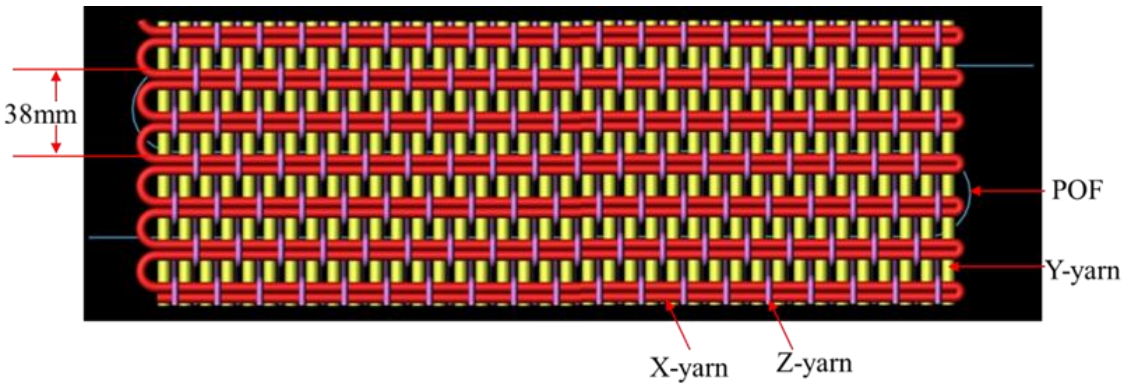

Figure 7.4 Embedded POF into 3D preform

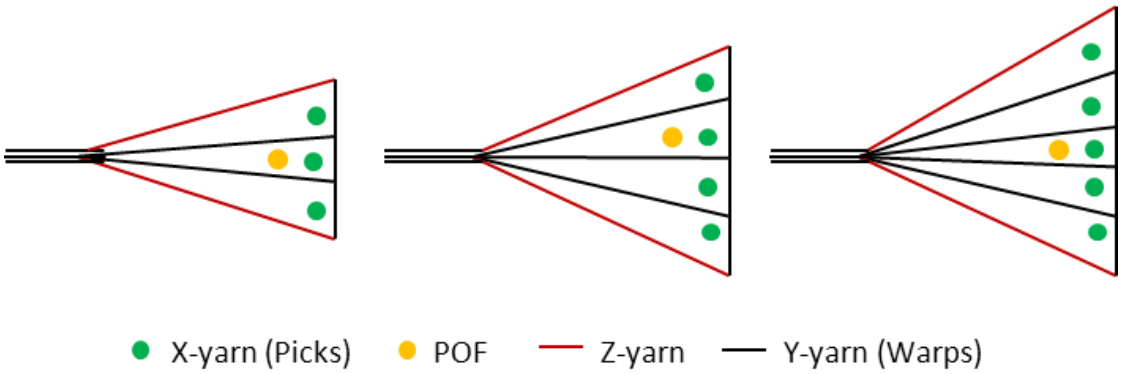

Figure 7.5 Schematic diagram embedded POF location and orientation in 3D woven preform

7.3.2 Resin Treatment

3D orthogonal woven preforms were treated with resin system using vacuum assisted resin transfer molding (VARTM) technique. Protruded POF was threaded into 2 mm furcation tube to provide extra protection to the protruded length of the POF. Furcation tube was placed carefully on top of the sticky tape and additional small piece of sticky tape was placed on top of the furcation tube to prevent any air leakage during the resin treatment process (Figure 7.6). The vacuum pressure of 100 kPa was used and kept constant for all samples. After applying the vacuum and before the infusion, one end of the embedded POF was connected to the OTDR to monitor the vacuum effect on POF signal loss (Figure 7.9). Prepared resin mixture placed in a vacuum desiccator for degasing to removes the air bubbles

that were created during stirring the mixture. Removing air bubbles from the resin mixture before the infusion decrease the potential void in the prepared composite and improve the performance of the produced composite. Figure 7.12 shows 3D orthogonal woven preform and 3D orthogonal woven composite with embedded POF. After a sample was cured, effect of curing on POF signal loss was measured at two different times (24 hours and 60 days). More details of 3D orthogonal woven composite preparation are provided in appendix B. Prepared sample size was 47 cm length and 15 cm width.

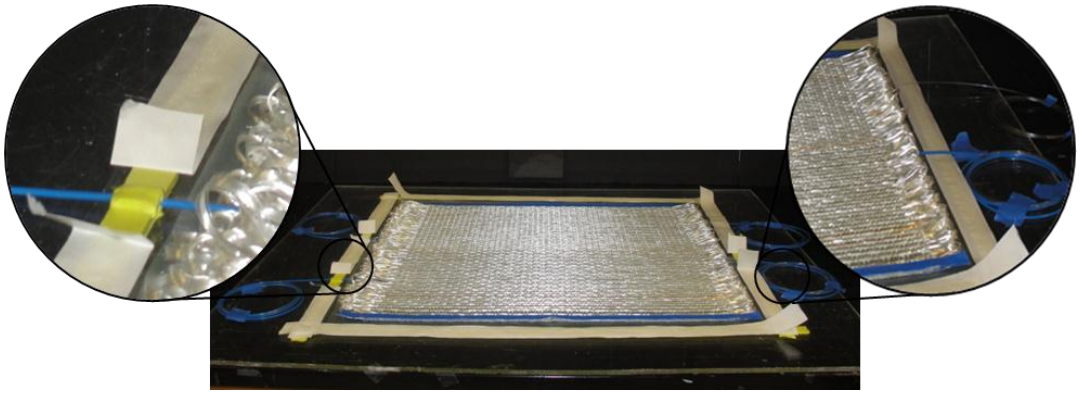

Figure 7.6. Sticky tape placed around 3D preform

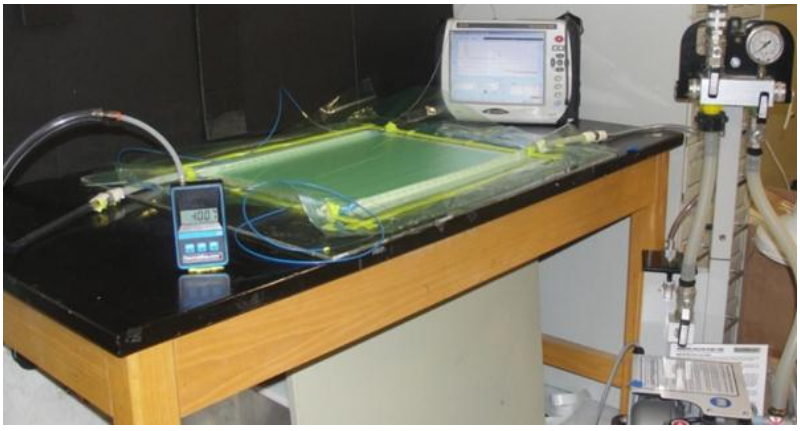

Figure 7.7. Sample preparation for resin infusion process and POF data collection by OTDR

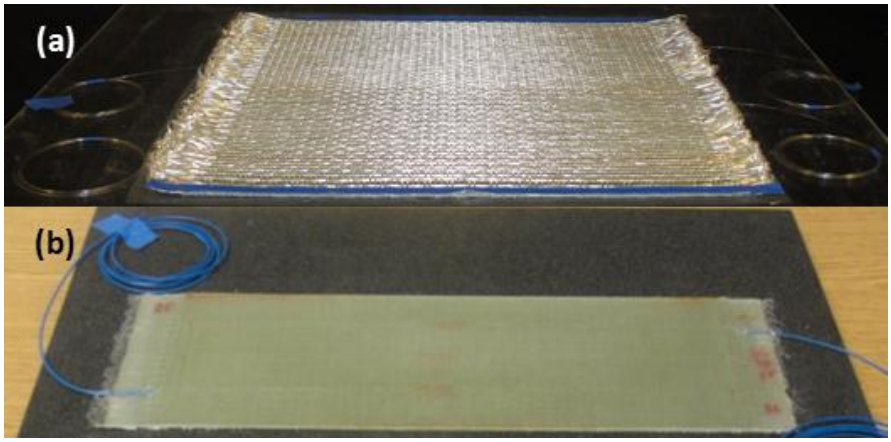

Figure 7.8. 3D orthogonal woven preform (a) and 3D orthogonal woven composite (b) with embedded POF

7.4 Testing and Evaluation

7.4.1 Attenuation Measurement

The principal of OTDR is that the light source launches a short pulse, with a specific pulse width, into an optical fiber; this light pulse will scatter along the optical fiber due to the impurities and the fiber imperfection. A portion of the launched light is backscattered to the input direction, which will be detected at the input to the optical fiber with a time delay equal to the time required for the light wave to travel from the input to reflection source and back to the input again (24). The backscatter is therefore recorded as a function of time. By applying the speed of the light in the optical fiber (i.e. knowing the index of refraction in the POF), the time delay of the backscattered signal is converted to a distance along the optical fiber.

OTDR is sensitive to any change that may occur along the optical fiber that induces optical fiber attenuation. Additionally, different types of defects affect the light backscattering in different ways and can therefore be separated in the backscattered signal. To demonstrate, Figure 7.9 shows a schematic of an OTDR waveform (signal trace), i.e. a plot of the backscatter light level (amplitude) along the optical fiber. The slope of the curve (caused by

Rayleigh scattering) determines the backscattering level (attenuation) as a function of distance along the fiber length. Defects in the optical fiber at specific locations appear as sudden increases or decreases in the amplitude. Reflections and losses are shown in the graph as two different features along the fiber length (25). Reflections cause a sharp increase in the curve, whereas sudden decreases in signal are caused by losses. The sudden increases in amplitude at the beginning and ending of the optical fiber are caused by the termination of the optical fiber at the front panel of the OTDR and the end of the optical fiber respectively, which are always detected (26)(27). These known locations are then used as reference distances for other defects. In this study a photon-counting OTDR (LOR-220, LUCIOL) was used to measure the backscatter light level along the POF. This type of photon-counting module converts one photon at 670 nm to one visible photon and detects this visible photon with a silicon photon-counting device, providing extremely high sensitivity (28)(29)(30). The OTDR was configured to emit a wavelength of 670 nm, with a time step resolution of 1.25 ns and signal pulse width of 1 ns.

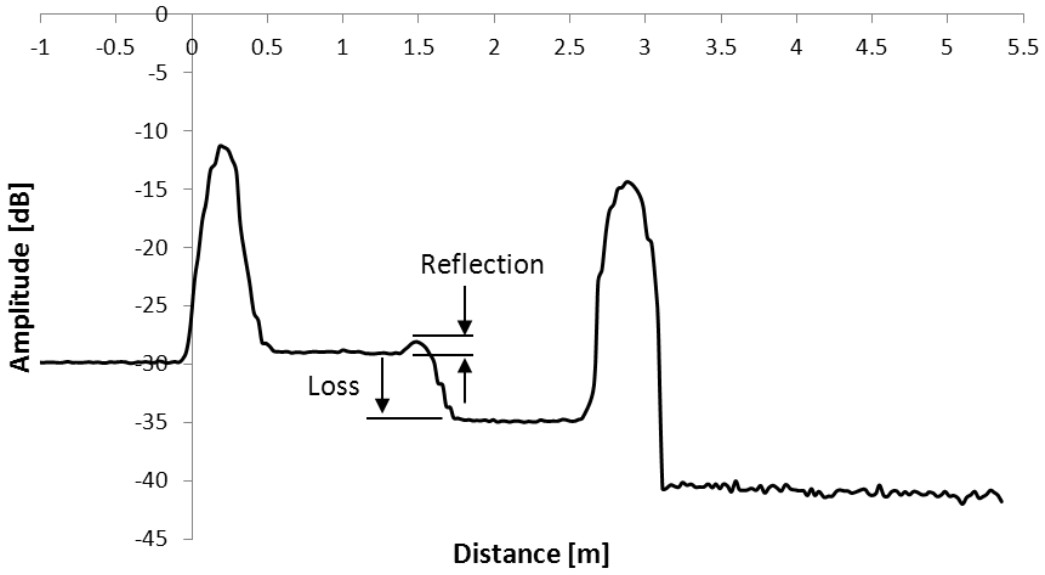

Figure 7.9 Schematic of a typical OTDR waveform.

7.4.2 Flexural test

The bending test (3-point mode) was performed using TESTRESOUCES model 130Q1000 load frame with QS Controller (Figure 7.10). The flexural test machine is a customized dual column load frame with 500 mm clearance between the two columns to test large specimen. The span length is adjustable and ranges from 30 mm to 470 mm. The bending test was conducted at a rate of 4 mm/min bending deflection and 65 mm span length. The specimen length was 45 cm in the x-direction, which is the direction of the POF, and 15 cm width. One end of the POF was connected to the OTDR to measure the backscattering level and induced signal attenuation under applied load and after releasing the load.

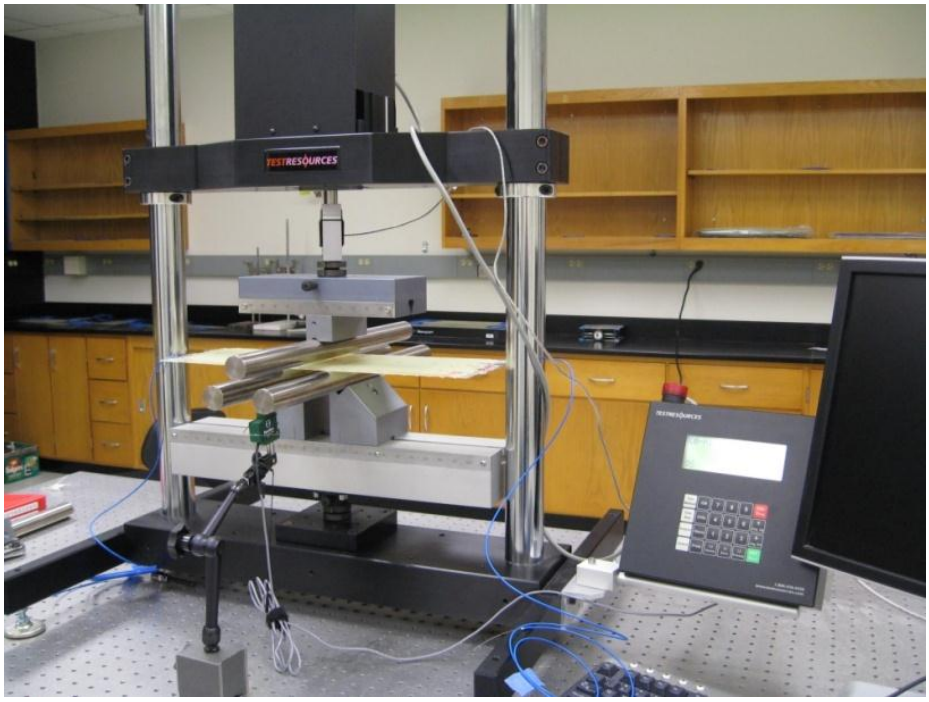

Figure 7.10 TESTRESOURCES bending tester and OTDR during measurements

7.4.3 Drop Weigh Impact test

Impact test was conducted on 3D orthogonal woven composite using CEAST 9310, Bench Top Falling Weight Impact Tester. CEAST 9310 is a low energy impact tester with maximum energy 21 Joules, maximum dropping mass of 3.510 kg, maximum drop height of 700 mm, and maximum impact speed of 3.71 m/s. One protruded end of POF was connected to the OTDR to measure backscattering level and signal loss before the impact (control sample) and after each impact. Samples were fixed between the sample holders and placed on impact device (Figure 7.11).

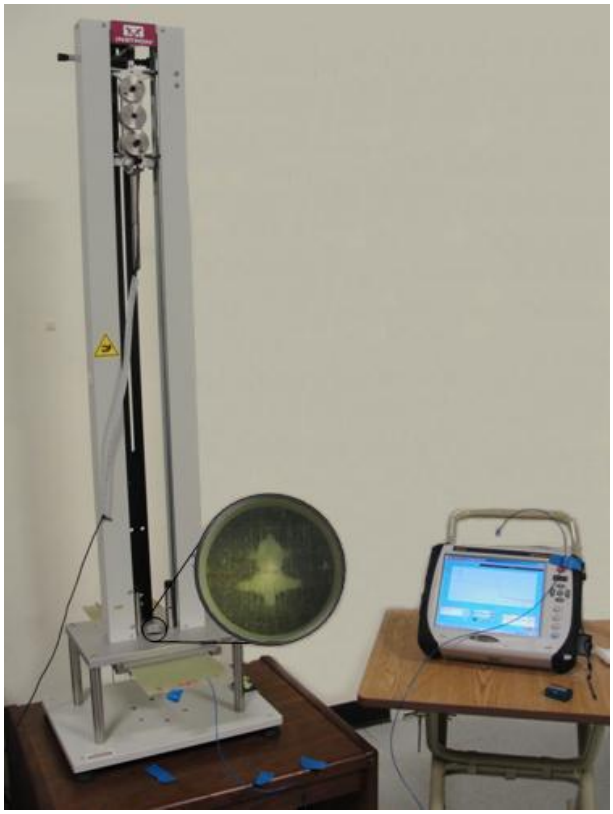

Figure 7.11 Impact CEAST 9310 (Bench Top Falling Weight Tester) and OTDR during measurements

7.5 Results and Discussion

7.5.1 Attenuation measurement during fabrication

Backscattering level was measured for as supplied POF (control). The backscattering level was measured for the embedded POF after preform formation, after applying vacuum of resin infusion, and after 24 hours of resin treatment monitored from the time of start the infusion. This would allow the identification of the cause of signal loss if any. Figure 7.12 illustrate typical OTDR trace of sample VII (4 layers and 1.57 x-yarns/cm/layer). Embedded POF length was 1.369 cm, POF entered 3D composite at length of 1.452 m and exited at length of 2.821 m. Noticeable drop on the backscattering level at distance of 2.13 m occurred after applying 100 Kpa vacuum pressure. The backscattering level after 24 hours of infusion is the same as that of after vacuum. This drop indicates significant effect of the vacuum pressure on POF resulting from fiber distortion, which was not recovered after resin curing. It is clear from the results that weaving process didn't cause any damage to the POF. The distributed loss in dB/km of the original POF was 177 dB/km and remained the same after weaving, which indicates that formation and architecture of preform did not cause distortion of POF.

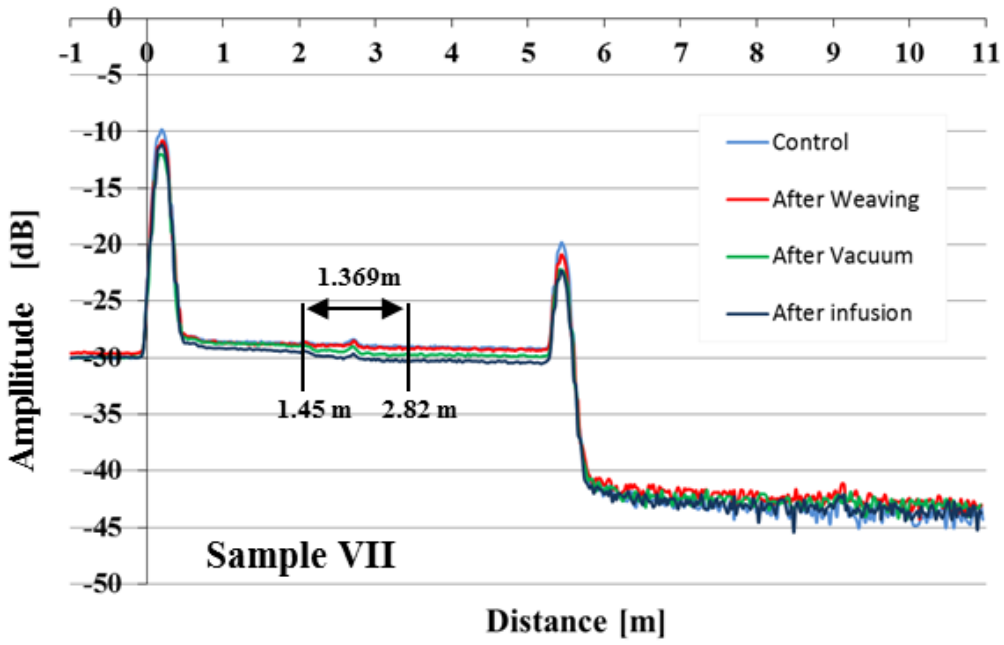

Figure 7.12 Backscattering of embedded POF into composite sample with 4 y-yarn layers and 1.57 x-yarns/cm/layer for different fabrication processes

Figure 7.13 shows another example of OTDR signal trace of embedded POF in sample IX (4 layers and 4.72 x-yarn/cm/layer). OTDR trace shows a drop on backscattering level at 2.69 m from the entry of POF to 3D composite, this drop start after applying the vacuum and did not change after the sample was cured.

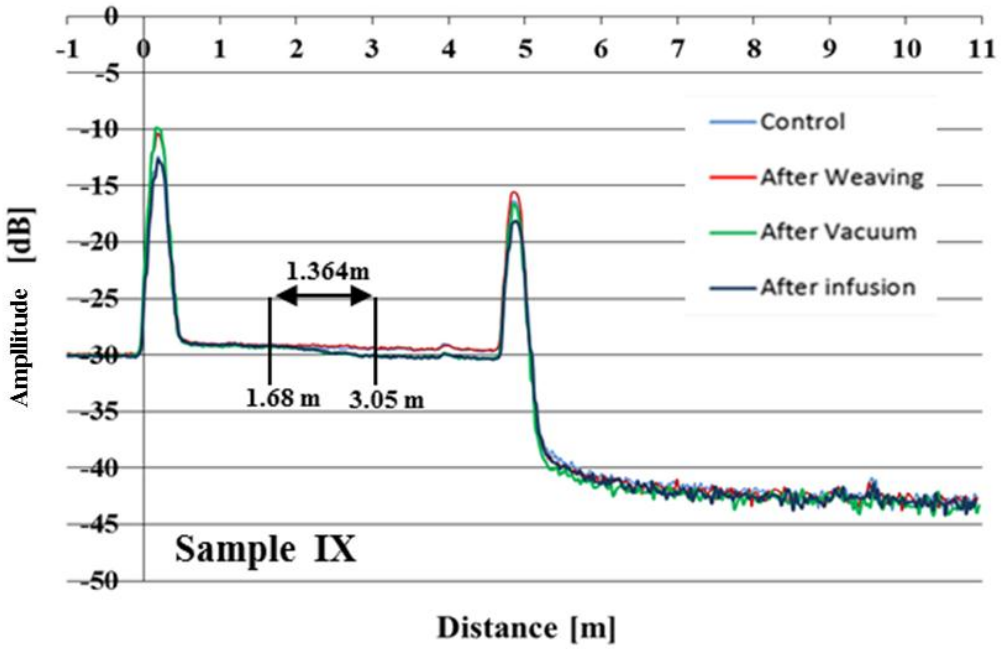

Figure 7.13 Backscattering of embedded POF into composite sample with 4 y-yarn layers and 4.72 x-yarn/cm/layer for different fabrication processes

Figure 7.14 shows backscattering level of embedded POF section of sample IX. This embedded section of POF located between 1.68 m and 3.04 m along its length. Backscattering levels of original POF before and after weaving show approximately same results. Further, the OTDR traces of POF after vacuum application and resin infusion are about the same. Figure 7.14 also shows the OTDR traces with locations where drops on the backscattering level occurred for the stages after vacuum application and 24 hours after resin infusion. Total signal loss for the entire embedded section of POF is only 0.76 dB, which is minor compared to 177 dB/km. The drops of the signal are related to the distortion/flattening and waviness of the POF as a result of contact with preform yarns and vacuum pressure.

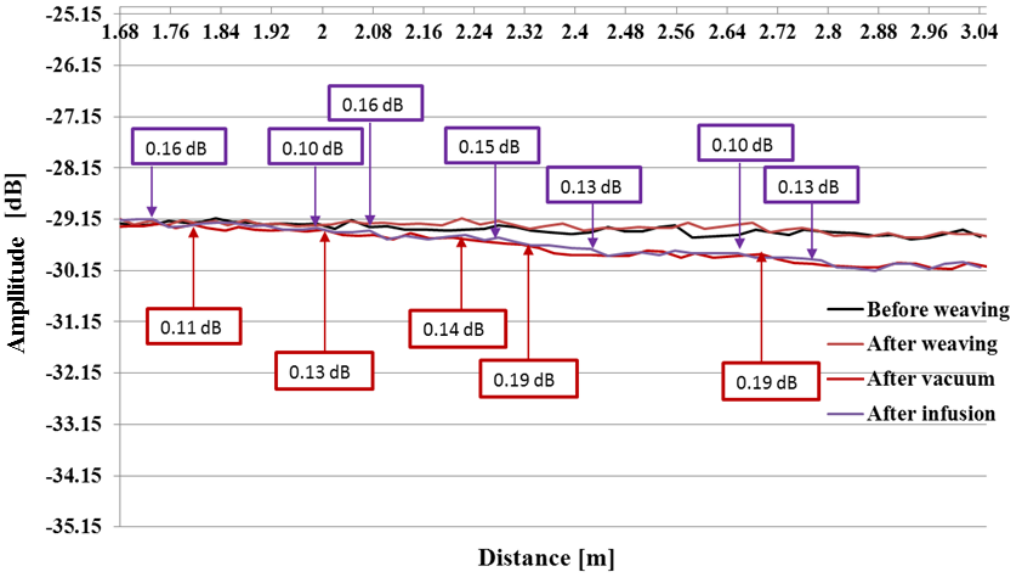

Figure 7.14 Backscattering of POF embedded in composite sample IX (4 y-yarn layers and 4.72 x-yarns/cm/layer) at different formation stages

Figure 7.15 shows a complied data of signal attenuation after each process of fabricating 3D woven composite. All embedded POF into samples of 2 y-yarn layers showed attenuation after weaving process (0.14 dB-0.22 dB) while POF in samples of 3 and 4 y-yarn layers did not exhibit significant signal attenuation. Samples of 2 y-yarn layers possess open and more flexible structure that may cause the embedded POF to be easily distorted at the contact points with preform yarns and during sample handling. Waviness of POF in such structure was noticed. The results of signal attenuation after vacuum application indicate that open structure samples with low number of y-yarn layers and x-yarn densities did not provide support for the POF a matter that caused more signal loss. However, after 24 hours from resin infusion the signal attenuation of all samples is about the same, which is evidence of distortion recovery of the POF.

To investigate the effect of aging, signal attenuations of all the nine composite samples were collected after 60 days after curing or 61 days from resin infusion (Figure 7.16). The highest signal loss after 60 days is only 0.4 dB (=1.0 dB-0.6 dB) for sample IX to after resin

infusion. The results of Figure 7.12 - Figure 7.16 indicate that the embedded POF maintained high DR after processing and thus the POF is a suitable sensor for SHM.

It is worth mentioning here that 3 replications of the samples were produced and tested for backscattering. While the replication results are generally the same, there is variation from replica to another. However, the POF in each sample exhibited reasonable DR that is potentially good for SHM.

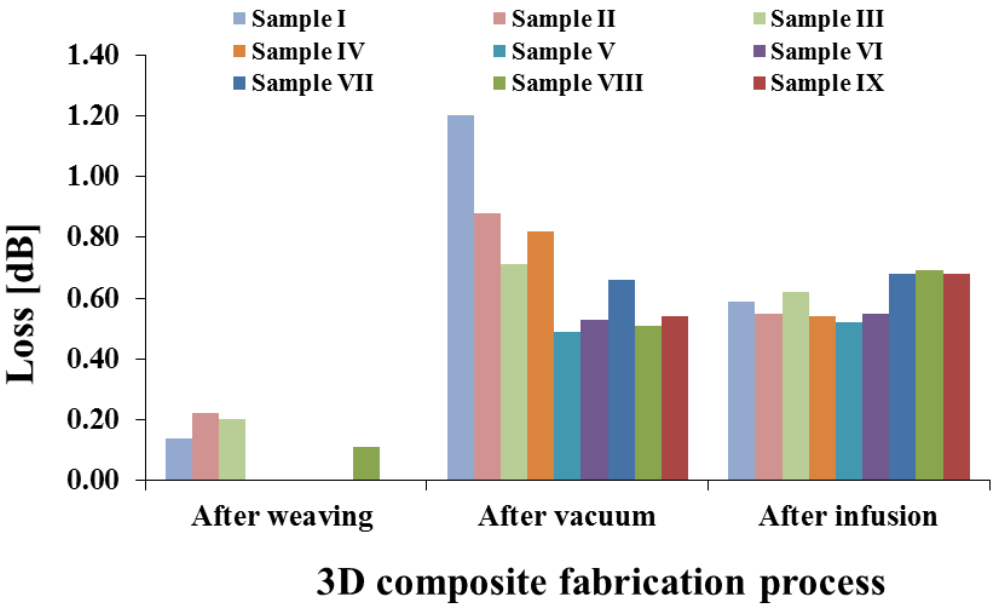

Figure 7.15 Signal attenuation of embedded POF after each process of fabricating 3D woven composite

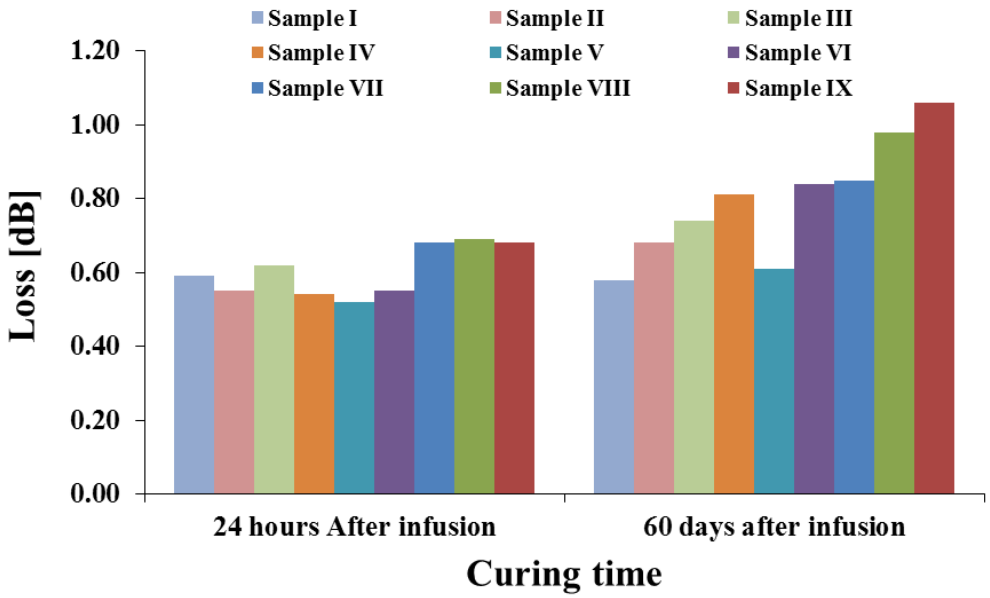

Figure 7.16 Signal attenuation of embedded POF after infusion

7.5.2 Attenuation of POF Signal due to Bending

One protruded end of the embedded POF was connected to OTDR and backscattering and signal attenuation was collected while 3D composite samples experienced different bending loads. Bending load was applied to the required level, then the test was paused and backscattering signal was collected. The load was released and signal was measured. Signal was also measured for all samples at failure load and after releasing the load.

Figure 7.17 shows OTDR signal trace of embedded POF in composite of 4 y-yarn layers with x-yarn density 1.57 (sample VII) under different bending loads. No signal loss on embedded POF was recorded under bending load 605 N. Loads/strain 1,210 N/1.6%, 1,815 N/2.3%, 2,303 N/2.9%, and 2,460 N/3.0% caused drop in POF backscattering at three different locations of 1.75 m, 2.24 m, and 2.70 m, which are the three contact points of composite sample with the upper rod. Signal loss at these locations is due to bending and flattening of the POF. Change in cross-section shape leads to change in the refractive index of POF, which result in drop in backscattering level at these locations. After applying load of 2,460 N

(breaking load) it was noticed that signal loss of POF is substantial. The OTDR signal showed both loss and reflection indication of structure damages (may be necking) to POF under very high bending stress.

The backscattering level of POF after removing the load/strain is shown in Figure 7.18. OTDR trace showed a good recovery of POF after releasing the applied bending load up to 2,303 N, whereas backscattering level returned to the original levels of backscattering. After releasing the load of 2,460 N (breaking load), the reflection part of the signal vanished and the signal loss of POF decreased from 10.43 dB to 2.9 dB.

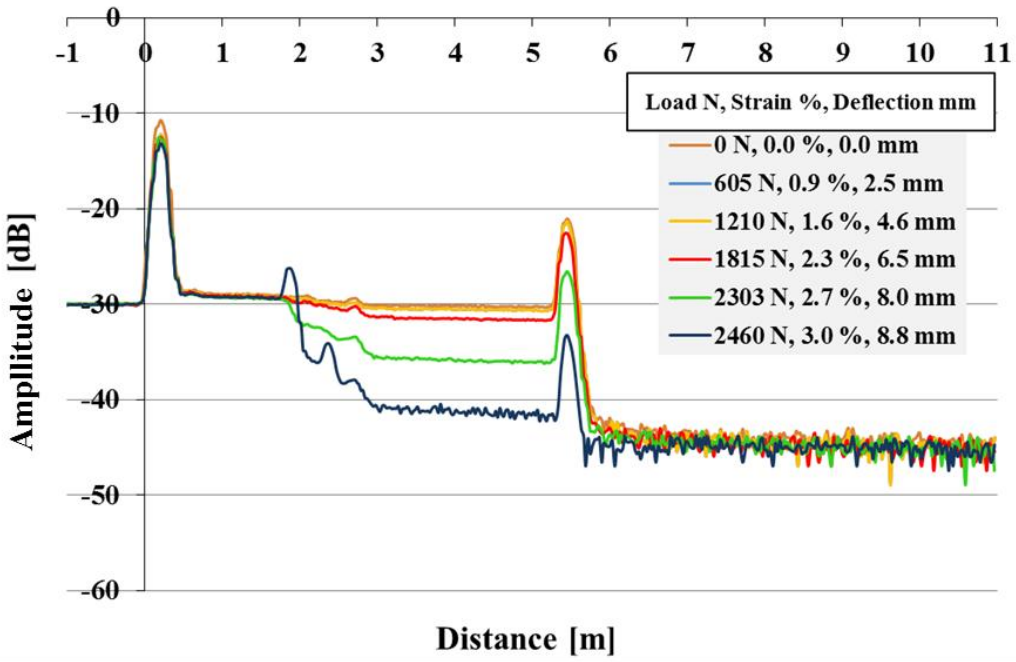

Figure 7.17 Backscattering of embedded POF into composite sample VII with 4-yarn layers and 1.57 x-yarn/cm/layer of different bending loads

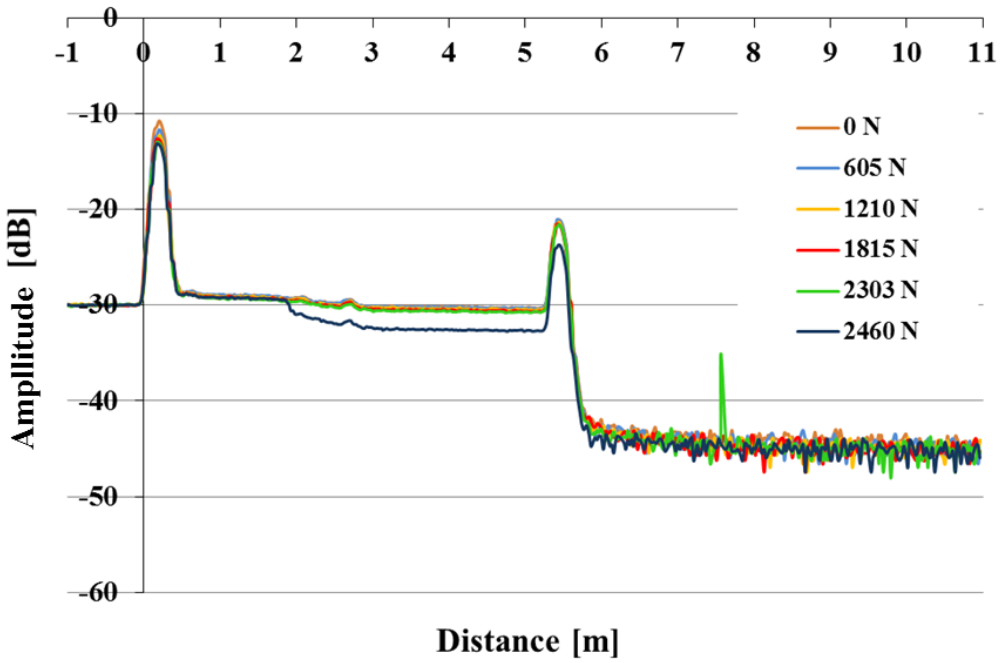

Figure 7.18 Backscattering of POF embedded in composite sample VII with 4-yarn layers and 1.57 x-yarn/cm/layer after unloading

Table 7.7 depicts the loss associated with each of the three contact location with the upper rod for each bending load Figure 7.19. Signal loss increased with applied load increased.

Table 7.7 Loss under increment load at the three contact locations for sample VII

Distance / Load, Strain	1.75 m	2.24 m	2.70 m
1210 N, 1.6 %	0.26 dB	0.50 dB	0.34 dB
1815 N, 2.3 %	0.45 dB	0.75 dB	0.68 dB
2303 N, 2.7 %	2.75 dB	1.43 dB	1.34 dB
2460 N, 3.0 %	6.21 dB	2.02 dB	2.21 dB

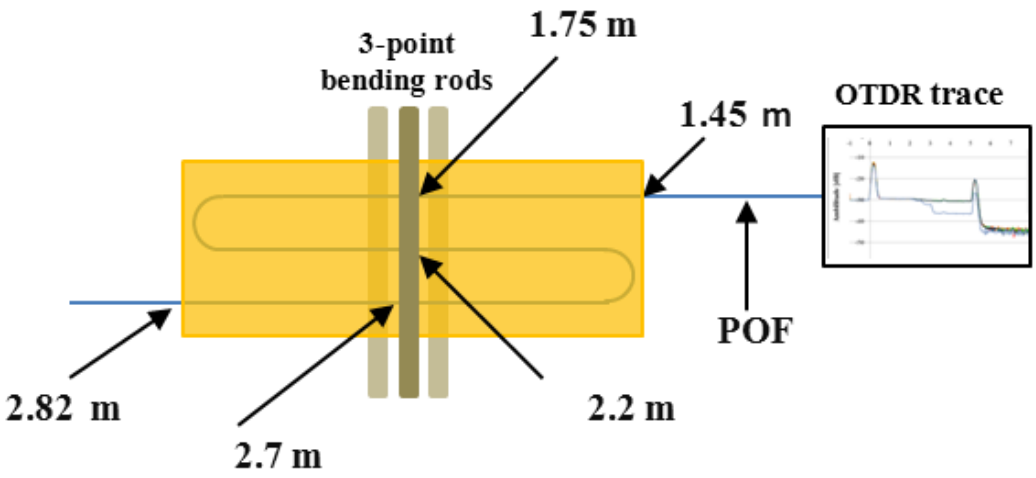

Figure 7.19. Schematic of composite sample and POF being tested for bending

Figure 7.20 and Figure 7.21 illustrate another example of OTDR trace of embedded POF in 3D woven composite made of 4 y-yarn layers and x-yarn density 4.72 (sample IX) after loading and unloading respectively. In Figure 7.20, POF trace showed signal loss between 1.6 m and 3.0 m at the three contact points with the upper rod (2.1 m, 2.5 m, and 2.9 m). Table 7.8 shows the signal loss at the three locations in terms of bending load. Comparing the results of Figure 7.17 and Figure 7.18 to those of Figure 7.20 and Figure 7.21, one notice that the signal loss of sample IX at the breaking bending load was highly significant compared to sample VI. The POF of sample IX lost all DR at the location 2.5 m indication of severe damage at this location. Sample IX is stiffer than sample VI that caused severe damage to the POF to the degree that it did not recover much of its lost signal after load removal as it can be seen from Figure 7.21. Flexural stress-strain curves for all samples under different loads are shown in appendix B section B.1. Backscattering level of all tested sample under increment loads and after unloading are shown in appendix B section B.2 (Figure B.15 to Figure B.32).

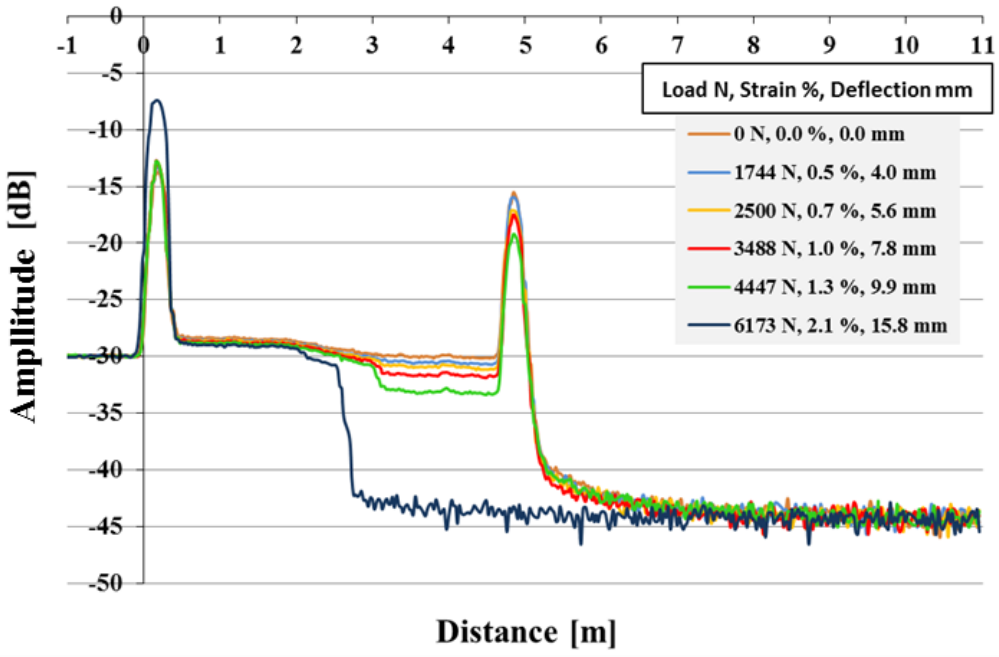

Figure 7.20 Backscattering level of embedded POF in sample IX with 4-yarn layers and 4.72 x-yarn/cm/layer for different bending loads

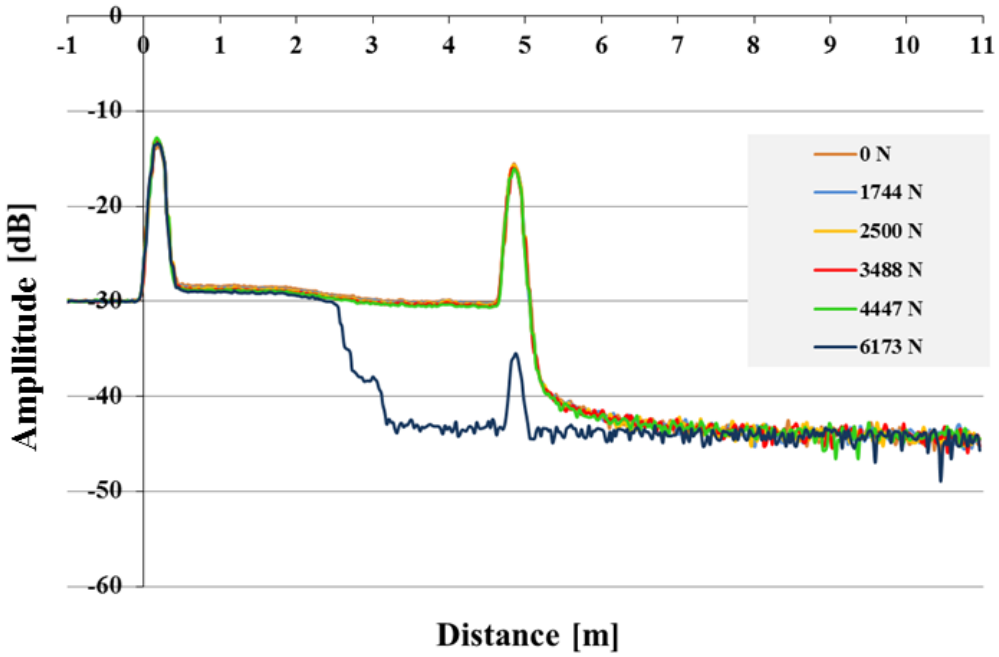

Figure 7.21 Backscattering level of embedded POF in sample IX with 4-yarn layers and 4.72 x-yarn/cm/layer after unloading

Figure 7.22 and Figure 7.24 show the bending load-signal loss and corresponding bending stain-signal loss relationships for all fabricated 3D woven composite samples. Figure 7.23 shows the signal loss after removing the bending load (the bending loads are identified in the figure for reference). The results of the 9 samples are in line with the two above examples in that as the bending load/stain increases the signal loss increases. The interesting point to note here is that the signal loss of POF was recovered for all levels of loading except at the breaking load. Again these results support the viability of using the POF as sensors for SHM. However, the signal loss of POF corresponding to the permissible bending strain level, which depends on the member role in the structure to be monitored, needs to be identified from bending trials. The signal loss beyond the permissible bending strain shall trigger the action to be taken before failure of the member that may lead to failure of the structure takes place.

Table 7.8 Loss under increment load at the three contact locations for sample IX

Distance / load, Strain	2.1 m	2.5 m	2.9 m
1744 N, 0.5 %	0.65	0.31	0.55
2500 N, 0.7 %	0.52	0.56	0.65
3488 N, 1.0 %	0.44	0.60	1.29
4447 N, 1.3 %	0.71	0.74	2.20
6173 N, 2.1 %	1.45	11.93	N/A

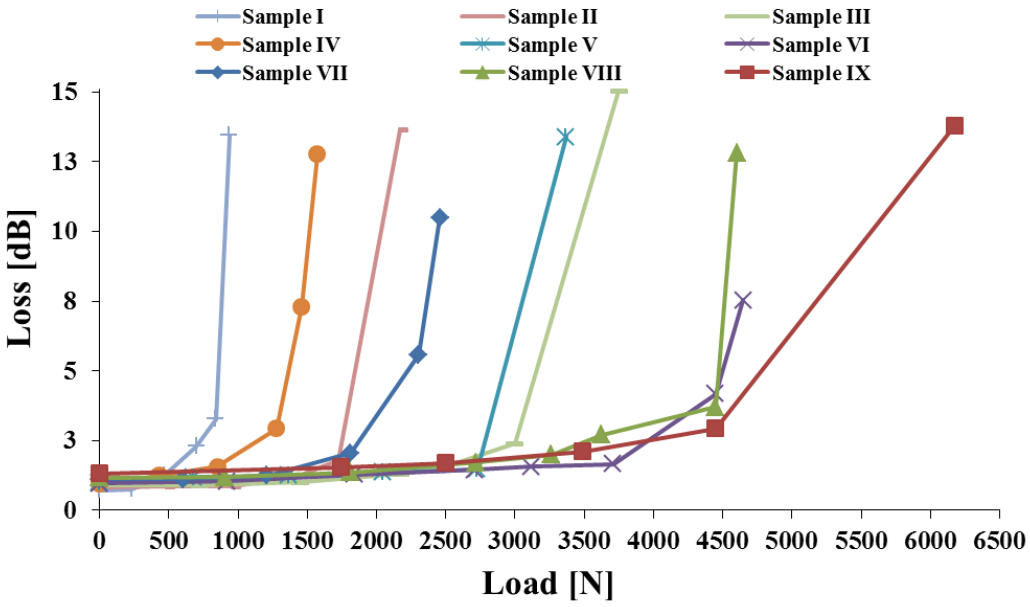

Figure 7.22 Total loss of embedded POFs in 3D woven composites under increment bending loads

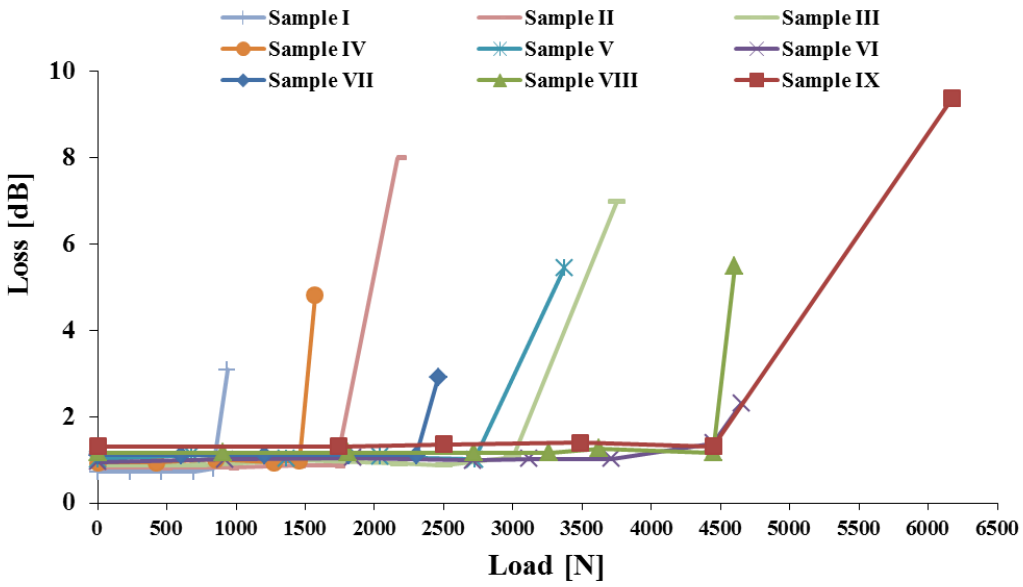

Figure 7.23 Total loss of embedded POFs in 3D woven composites after releasing loads

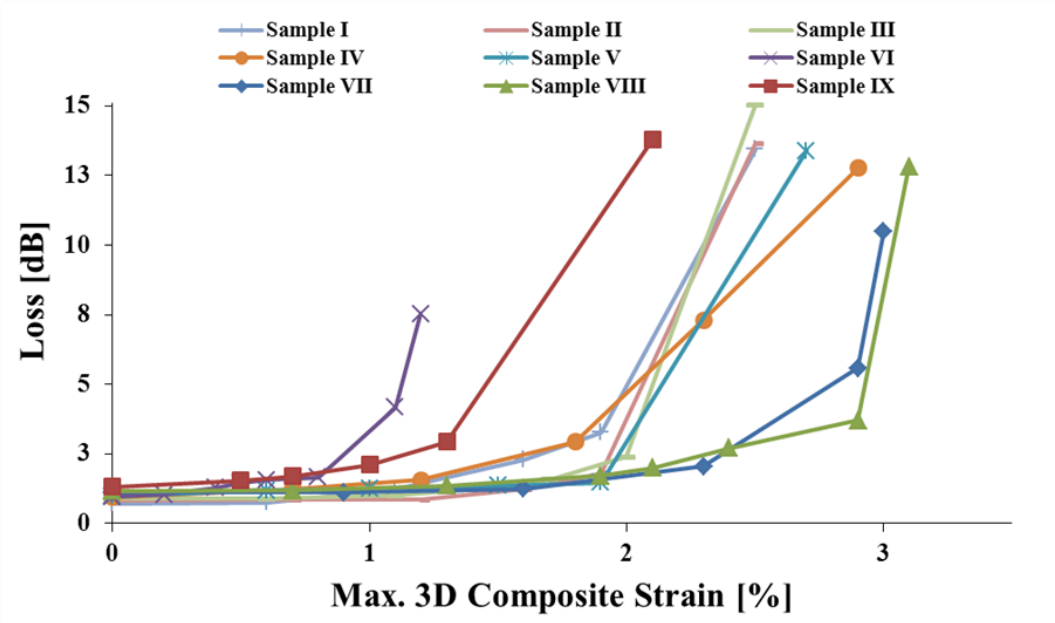

Figure 7.24 Total signal loss vs samples strain %

7.5.3 Attenuation of POF Signal due to Impact

Before performing the impact test on each sample, one the end of POF protruding out of the sample was connected to the OTDR. Figure 7.25 shows a sample prepared for the impact test. The sample was located in the sample holder so that the impact sticker hits the sample at position shown.

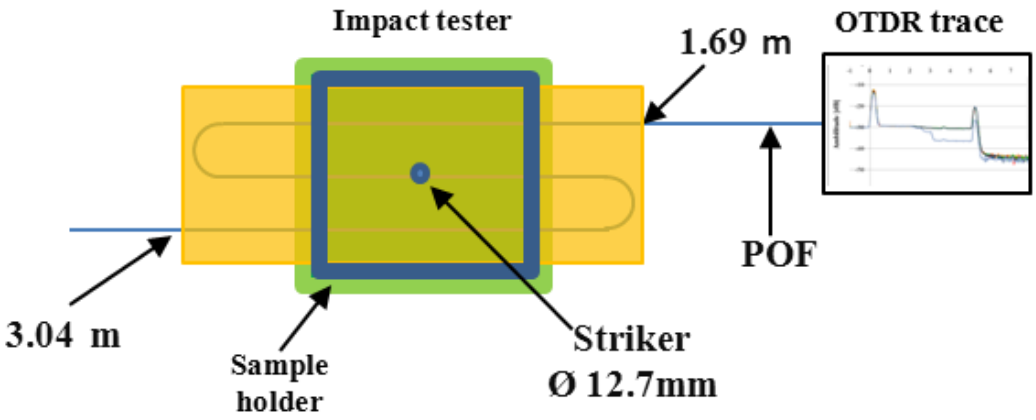

Figure 7.25. Schematic of composite sample being tested for impact

Table 7.9 depicts the number of conducted impacts and POF response status for all sample tested. Samples VI and IX, which structured with highest x-yarn density and 3 and 4 y-yarn layers, were impacted 30 times and POF maintained DR of 9 dB and 11 dB respectively. The POFs embedded in the other samples (I, III, IV, and VII) lost their DR completely because these samples possess less resistance to impact. While none of the samples were punctured, visual examination of the impacted area showed damage that propagated with increase in the number of impacts.

Table 7.9. POF signal loss in terms of repeated impact tests

Sample ID	Pick density (yarns/cm/layer)	y-yarn layers (x-yarn layers)	Number of impacts	POF DR (dB)
I	1.57	2 (3)	3	0.0
III	4.72	2 (3)	9	0.0
IV	1.57	3 (4)	3	0.0
VI	4.72	3 (4)	30	9.0
VII	1.57	4 (5)	14	0.0
IX	4.72	4 (5)	30	11.0

Figure 7.26 shows OTDR trace of impacted 4 y-yarn layer and x-yarn density of 1.57 (sample VII). Impact test was repeated 14 times until POF signal loss reached the maximum; the DR reached zero. Backscattering level before starting the impact test was -28.18 dB. After first impact, backscattering level experience significant drop and POF signal loss was 4.87 dB and located at 2.48 m. This drop on the backscattering indicates that embedded POF experienced high stress or deformation at this impacted point. Drop on backscattering level continued until 4th impact with POF signal loss of 6.34 dB, which indicate that the stress and deformation on the POF continued up to this impact level. From the 4th impact until the 8th impact, no significant change was noticed on backscattering level, which indicates that no further stress, deformation or damage occurred to POF. After the 8th level of impact and until the 14th level of impact, backscattering continued to drop until it reached the noise level and POF signal loss reached the full DR, which indicates that POF was completely damaged. Figure 7.26 shows small reflection at the impact location, which is indication of POF experienced crack or small strain. Figure 7.27 shows images of impacted sample at different number of impacts. Visual examination of the images indicates that the damage area is propagating as number of impacts increases. Image of sample back side showed structure protrusion at the impacted location.

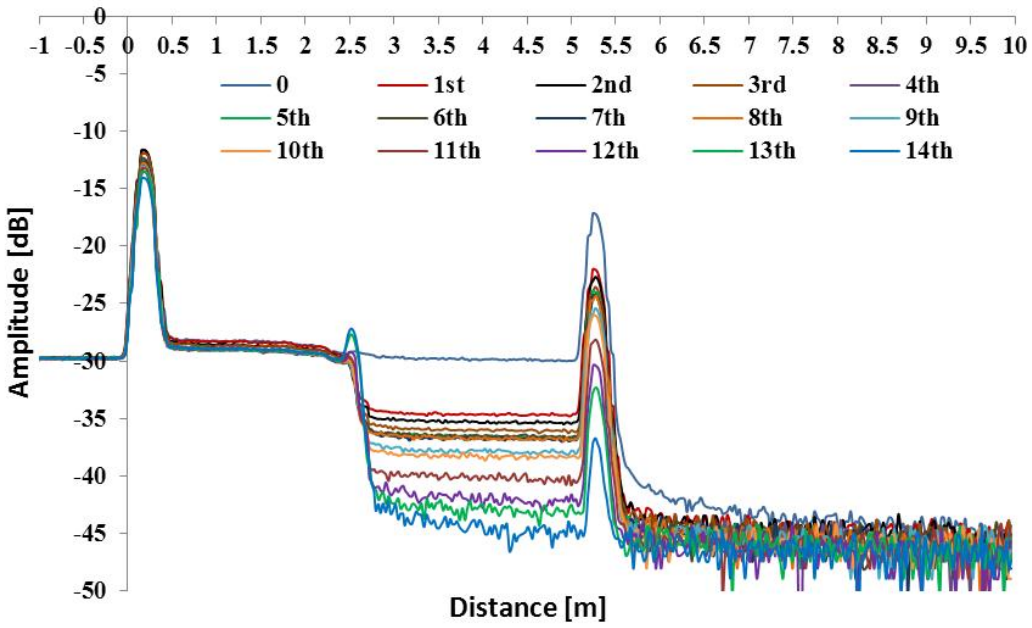

Figure 7.26 OTDR traces of embedded POF in sample VII after impact tests

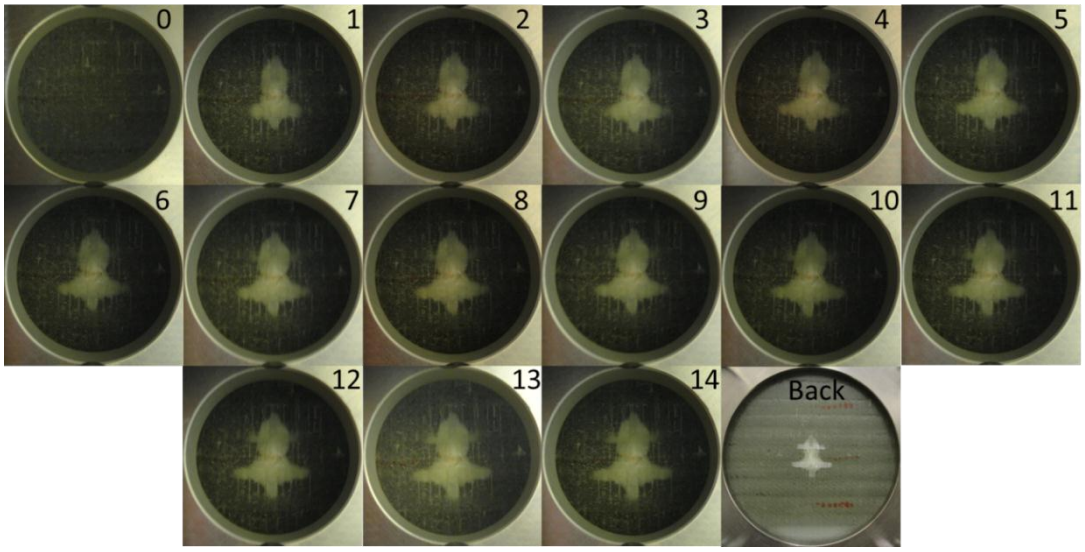

Figure 7.27 Images of sample VII, before, after repeated impacts, and back of the sample

As mentioned earlier, embedded POF in 4 and 3 y-yarn layers woven composite samples with x-yarn density of 4.72 maintained DR of 9 dB after 30 repeated impacts. Figure 7.28 shows backscattering levels of POF in composite sample VI. After the first impact, backscattering level of POF dropped at 2.5 m (impact location) and signal loss was 1.67 dB. As the impact test was repeated up to 30 times, the level of POF backscattering dropped causing signal loss of 4.0 dB. Figure 7.28 shows images of sample VI before, after each of the 30 tests, and the back of the sample after 30 impacts. While the impacted area was damaged and the damage progressed, the damage was not sever enough to completely damage the POF. The structural difference between the two extreme samples (VI and VII) was reflected in the behavior of the OTDR trace (Figures 7.25 and 7.27) and the damage progress (Figures 7.26 and 7.28) of these samples. Backscattering levels and impact images for all six samples are shown in appendix B (Figure B.33 to Figure B.44).

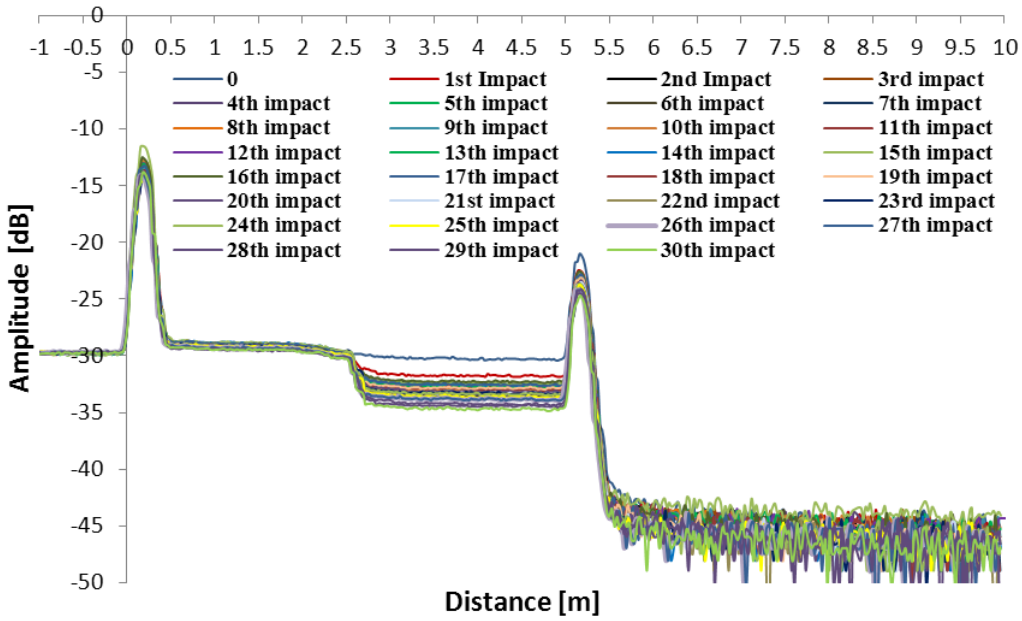

Figure 7.28 OTDR trace of POF in sample VI after impact tests

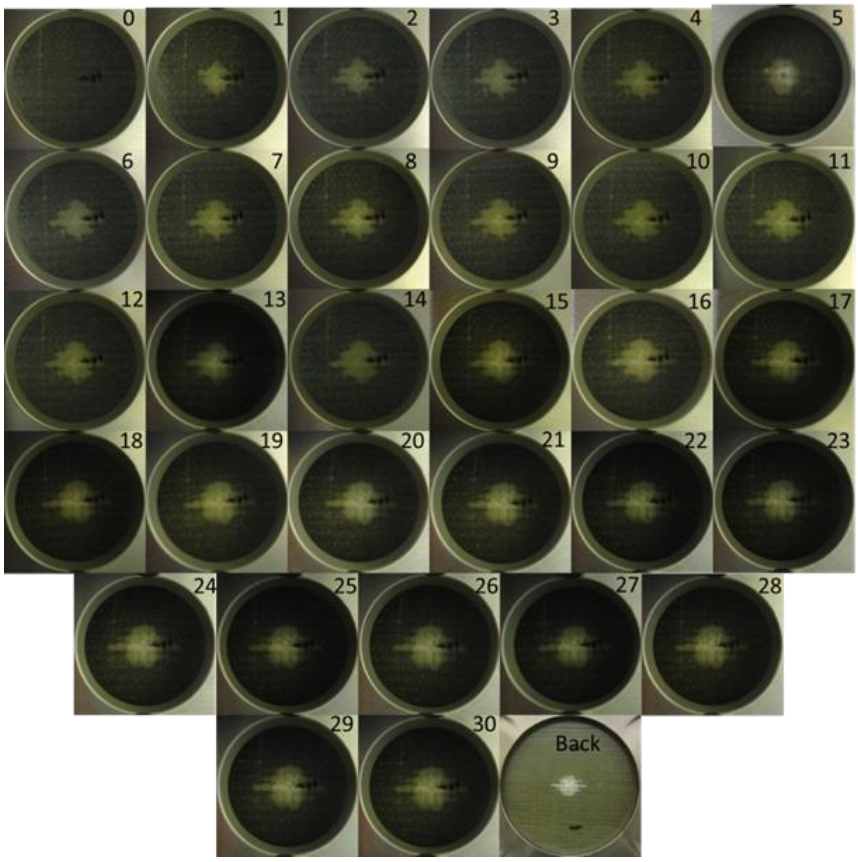

Figure 7.29 Images of sample VI, before, after repeated impacts, and back of the sample

Embedded POF signal loss versus number of impacts is shown in Figure 7.30. Samples I, III, IV, and VII showed increase in POF signal loss as number of impacts increase until backscattering levels reached the full DR (full signal loss). POF in samples VI and IX showed increase in signal loss after first impact and insignificant loss after further increase in number of impacts. The POF in samples VI and IX also showed lowest signal loss value compared to POF embedded in the other samples. While the damage due to impact propagated significantly (Figure 7.28), the POF signal did not reflect the level of damage. This is related to the position of the POF which is in the middle of the thick samples VI and IX. For such samples the POF sensor need to be configured differently. Additionally, Assessment of structure performance (bending, compression, tensile) after impact is a must to correlate the POF signal loss to objective evaluation.

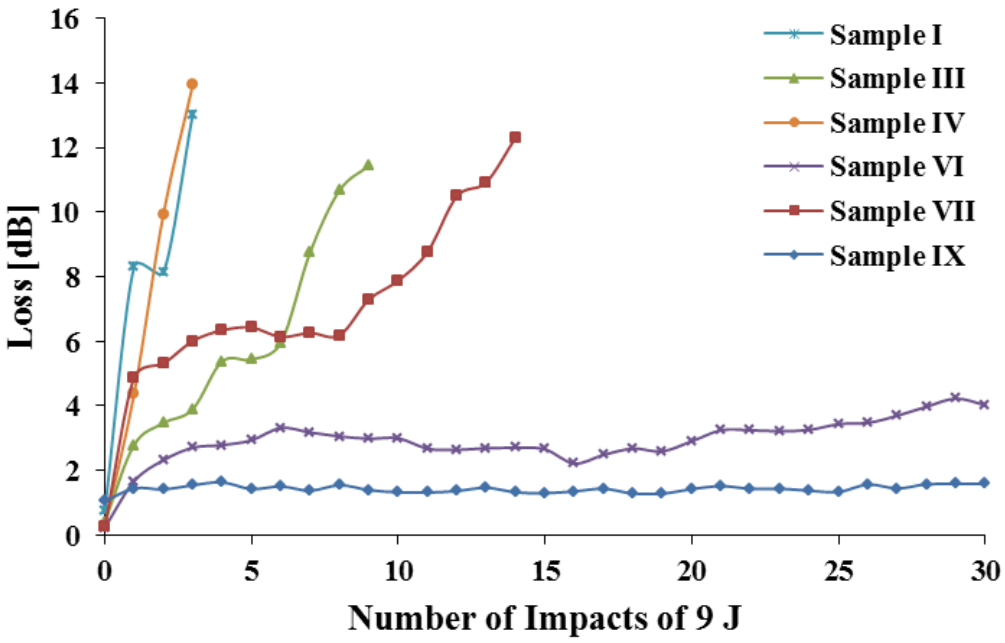

Figure 7.30 POF loss with repeated impact

Figure 7.31 to Figure 7.34 illustrate samples deformation, peak impact force, total impact energy, and energy at peak load versus number of repeated impact respectively. Sample I, IV, and VII with x-yarn density of 1.57 showed high total energy at first impact. These two figures show no significant change in peak impact force and energy at peak impact force value after repeated impacts. Total energy graph shows the relation between peak force and impact deformation.

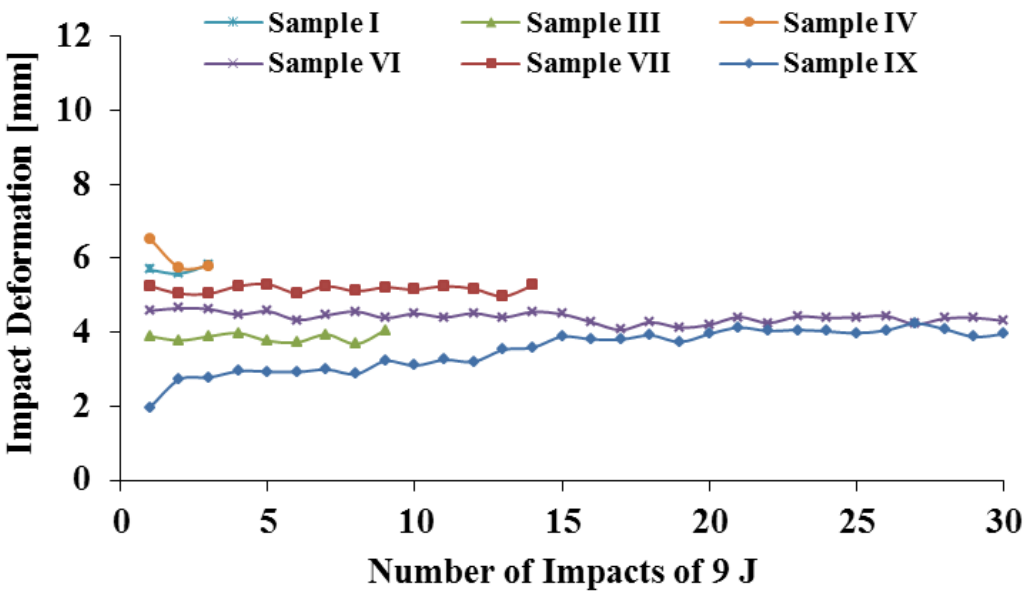

Figure 7.31 Deformation vs number of impacts.

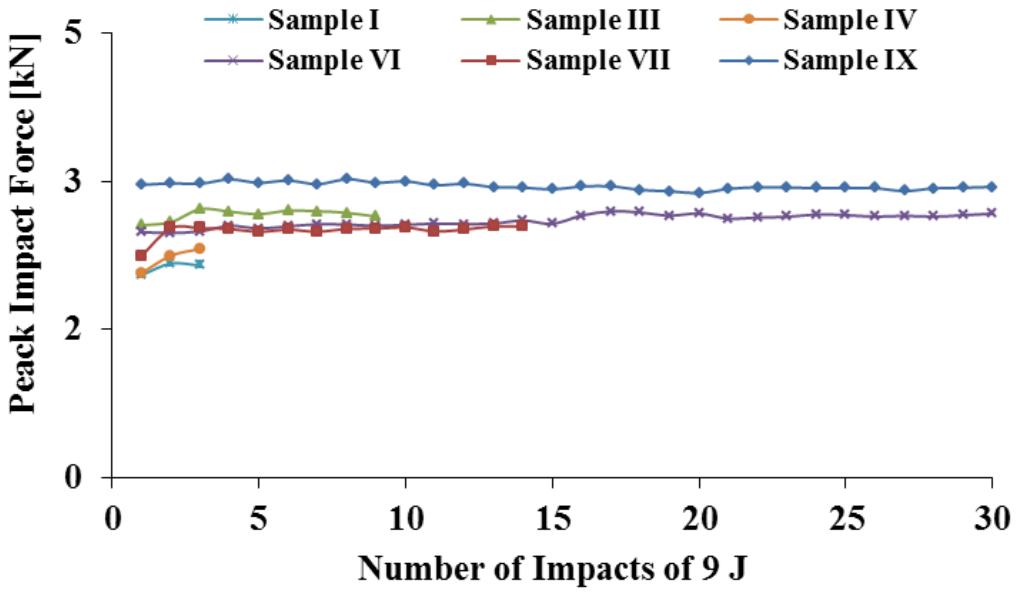

Figure 7.32 Peak force vs number of impacts.

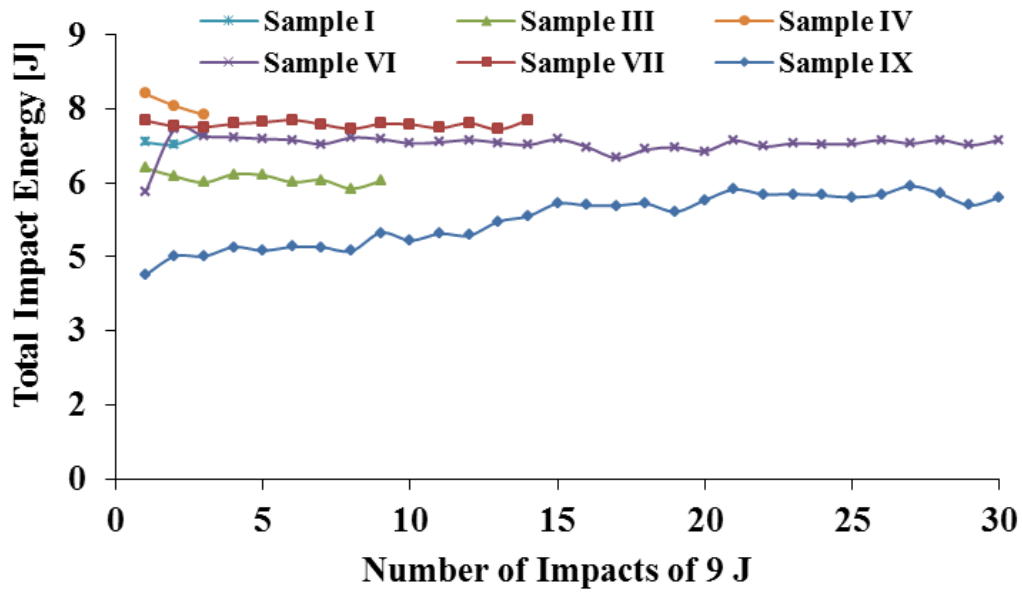

Figure 7.33 Energy vs number of impacts

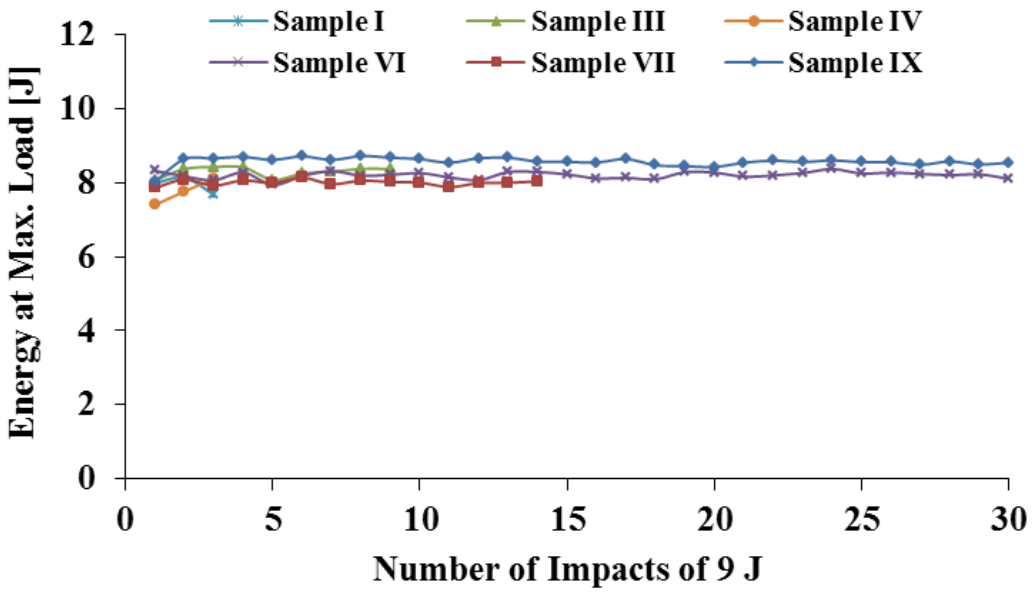

Figure 7.34 Peak energy vs number of impacts

Figure 7.35 and Figure 7.36 were created to understand the interrelationship between the architecture of composite, impact parameters, and POF signal loss due to repeated impact. The graphs depict the interrelationship for the first and final impacts for the six samples under investigation. The graphs show composite sample thickness, deformation due to impact, energy at peak impact force, and peak impact force, and POF signal loss. In general, POF signal loss increased with composite sample deformation. Samples I, VII, and IV with x-yarn density of 1.57 showed the highest signal loss (8.30 dB, 4.87 dB, and 4.36 dB respectively) after first impact. These three samples are the thinnest and thus the easiest to deform and cause high distortion to the POF. Samples VI and IX (3 and 4 y-yarn layers and x-yarn density of 4.72) possess highest thickness and lowest deformation that translated to lowest distortion of the POF and hence low signal loss after first and 30th impacts.

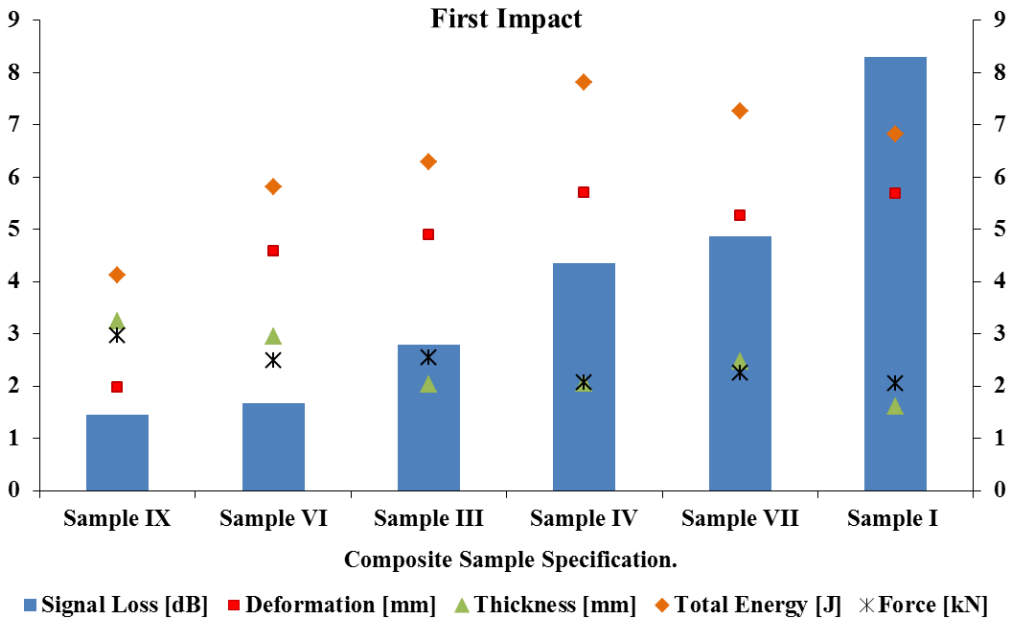

Figure 7.35 The interrelationship POF signal loss, total deformation, thickness, total energy, and peak force after first impact

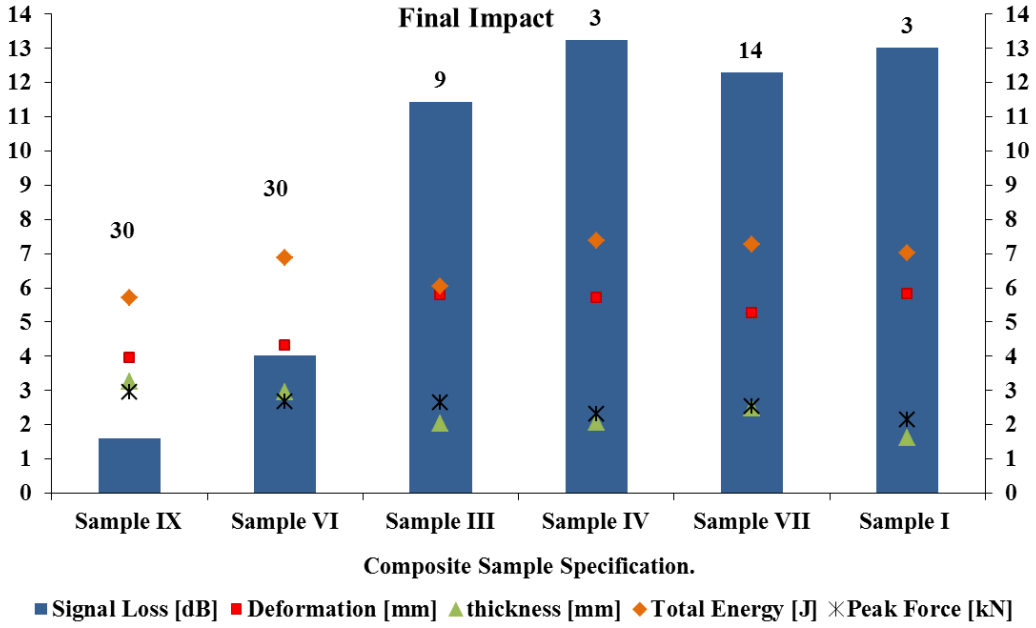

Figure 7.36 The interrelationship POF signal loss, total deformation, thickness, total energy, and peak force after final impact

7.6 Conclusion

This part addresses a study to evaluate the sensing characteristic of embedded POF in 3D orthogonal woven preforms before and during resin infusion steps and the final composites when subjected to bending stresses and repeated impacts. Different composite samples with embedded POF were fabricated with different 3D orthogonal woven composite parameters namely number of y-/x-yarn layers and x-yarn density.

All embedded POF into samples of 2 y-yarn layers showed small attenuation after weaving process while POF in samples of 3 and 4 y-yarn layers did not exhibit significant signal attenuation. Samples of 2 y-yarn layers possess open and more flexible structures that may cause the embedded POF to be easily distorted at the contact points with preform yarns and during sample handling. Bowing of POF in such structure was noticed. The results of signal attenuation after vacuum application indicate that open structure samples with low number of

y-yarn layers and x-yarn densities did not provide support for the POF a matter that caused more signal loss. However, after 24 hours from resin infusion the signal attenuation of all samples is about the same, which is evidence of distortion recovery of the POF.

Results of bending load-signal loss and corresponding bending strain-signal loss relationships for all fabricated 3D orthogonal woven composite samples show increase in POF signal loss as bending load/strain increased. The interesting point to note here is that the signal loss of POF was recovered for all levels of loading except at the breaking load.

Repeated impact was conducted on selected samples. Interrelationship between the architecture of composite, impact parameters, and POF signal loss due to repeated impact showed that POF signal loss increased with composite sample deformation. Samples with x-yarn density of 1.57 showed the highest signal loss due to its thin structure and thus were easy to deform and cause high distortion to the POF. Samples that possess highest thickness and lowest deformation that translated to lowest distortion of the POF and hence low signal loss after first and 30^{th} impacts.

Overall, POF showed good response for sensing the stresses during composite fabrication process, bending load, and repeated impacts. After preform formation and composite fabrication, embedded POF exhibited reasonable DR that makes them viable sensors for SHM. While sensing bending load/strain is obviously clear, the assessment of impact damage in this work is subjective and more assessment of performance after impact is required to be able to relate the signal loss to mechanical properties of composites after impact.

References

[1] Chang P., Flata A., Liu S.C. Review Paper: Health Monitoring of Civil Infrastructure. *Structural Health Monitoring.* Vol. Vol 2 , 3, pp. 0257–267.

[2] Housner G. W., Bergman L.A., Caughey T.K., Chassiakos A.G., Claus R.O., Masri S.f., Skelton, R.E., Soon, T.T., Spencer, B.F., Yao J.T.P. STRUCTURAL CONTROL:

PAST, PRESENT, AND FUTURE. *Journal of Engineering Mechanics.* 1997, Vol. 123, 9, pp. 897-971.

[3] Yan-liang D., Bao-Chen S., Xiu-mei J. Strain monitoring of railway bridges using optic fiber sensors. *Journal of quality in Maintenance Engineering.* 2007, Vol. 13, 2, pp. 186-197.

[4] Li H., Li D., Song G. Recent applications offiber optic sensors to health monitoring in civil engineering. *Engineering Structures.* 2004, Vol. 26, pp. 1647–1657.

[5] Mal A., Ricci F., Banerjee S., Shih F. A Conceptual Structural Health Monitoring system based on Vibration and wave Propagation. *Structural Health Monitoring.* 2005, Vol. 4, 3, pp. 283-293.

[6] X.M, Tao. Integration of Fiber-optic Sensors in Smart Textile Composites: Design and Fabrication. *Journal of Textile Institute.* 2000, Vol. 91, 3, pp. 448-459.

[7] Mohamed, T. S., Johnson, C. and Rizkalla, S. Behavior of Three-Dimensionally Woven Glass Fiber Reinforced Polymeric Bridge Deck. *Composites Research Joumal.* 2007, Vol. 1, pp. 27-42.

[8] Kang H., Kang D., Hong C., Kim C. Monitoring of Fabrication strain and temperature During Composite cure Using Fiber Optic Sensors. *Nondestructive Evaluation of Materials and Composites.* 2001, Vol. 4336, pp. 211-218.

[9] Kosaka T., Osaka K., Nakakita S., Fukuda T. Fiber optic strain monitoring of textile GFRP during RTM molding and fatigue tests by using embedded FBG sensors. *Smart Structures and Materials.* 2003, Vol. 5056, pp. 73-80.

[10] Merzbacher C I, Kersey A D and Friebele E J 1996 Fiber optic sensors in concrete structures: a review *Smart Material and Structures* 5 196-208

[11] Liehr, S., Lenkea,P., Krebbera,K., Seegerb,M., Thieleb,E., Metschiesb,H., Gebreselassie, B., Münich, J., Stempniewski, L. Distributed strain measurement with polymer optical fibers integrated into multifunctional geotextiles. *Optical Sensors, Proc. of SPIE.* Vol. 7003.

[12] Kiesel, S., Van Vickle, P., Peters, K., Abdi, O., Hassan, T., Kowalsky, M.,. Polymer optical fiber sensors for the civil infrastructure. *Mechanical, and Aerospace Systems, SPIE Sensors and Smart Structures.* 2006, Vol. SPIE 6174, pp. 1-12.

[13] Nakamura, K., Husdi,I., Ueha, S. Memory effect of POF distributed strain sensor. *Second European Workshop on Optical Fibre Sensors, Proceedings of SPIE.* Vol. 5502, pp. 144-147.

[14] Liehr, S., Lenke,P., Wendt,M., Krebber,K., Seeger,M., Thiele,E., Metschies, H., Gebreselassie,B., Münich, J. Polymer Optical Fiber Sensors for Distributed Strain Measurement and Application in Structural Health Monitoring. *IEEE SENSORS JOURNAL*. 2009, Vol. 9, 11, pp. 1330-1338.

[15] Kuang, K., Akmaluddin, Cantwell, W., Thomas, C. Crack detection and vertical deflection monitoring in concrete beams using plastic optical fibre sensors. *Measurement Science And Technology, Institute Of Physics Publishing*. 2003, Vol. 14, pp. 205-216.

[16] Kuang, K.,Quek,S.,Koh,C.,Cantwell,W., Scully,P. Plastic Optical Fibre Sensors for Structural HealthMonitoring:A Reviewof Recent Progress. *Journal of Sensors, Hindawi Publishing Corporation.* 2009, Vol. 2009, p. 13.

[17] Kuang, K., Cantwell, W. The use of Plastic Optical Fiber Sensors for Monitoring the dynamic Response of fiber Composite beams. *Measurement Science and Technology*. 2003, Vol. 14, pp. 736-745.

[18] Liehr, S., Nother,N., Krebber, K. Incoherent optical frequency domain reflectometry and distributed strain detection in polymer optical fibers. *IOP PUBLISHING, Meas. Sci. Technol.* 2010, Vol. 21, p. 4.

[19] Anderson, D., Johnson, L., Bell, F.,. Troubleshooting Optical-Fiber Networks. *Understanding and Using your Optical Time-Domain Reflectometer*. San Diego, California : Elsevier Academic Press, 2004.

[20] Saunders, C., Scully, P. Sensing applications for POF and hybrid fibres using a photon counting OTDR. *Institute of Physics Publishing, Measurement Science And Technology*. 2007, Vol. 18, pp. 615-622.

[21] Husdi, I., Nakamura, K., Ueha, S. Sensing characteristics of plastic optical fibres measured by optical time-domain reflectometry, *Meas. Sci. Technol.* 2004, Vol. 15, pp. 1553-1559.

[22] Kuang, K., Cantwell, W. The use of Plastic Optical Fiber Sensors for Monitoring the dynamic Response of fiber Composite beams. *Measurement Science and Technology.* 2003, Vol. 14, pp. 736-745.

[23] Hamouda. T., Peters, K., and Seyam, M., A. Effect of Resin type on the signal Integrity of an embedded Perfluorinated Polymer Optical fiber. *Smart Mater. struct.* 2012, Vol. 21, pp. 1-8.

[24] M., Mohamed, A., Bogdanovich, L., Dickinson, J., Singletary, B., Lienhart. A new generation of 3D woven fabric preforms and composites. *SAMPE Journal.* 2001, Vol. 37, 3, pp. 8-17.

[25] A., Bogdanovich. *Advancements In Manufacturing And Applications Of 3-D Woven Preforms And Composites.* s.l. : 16th International conference on composite materials, 2007.

[26] Saunders, c.,Scully, P. Distributed plastic optical fibre measurement of pH using a photon counting OTDR. *Journal of Physics: Conference Series 15.* 2005, Vol. 25, pp. 61-66.

[27] Corporation, Yokogawa Electric. *Guidebook for Optical Time Domain Reflectometer.* s.l. : Communication and Measurement Business Headquarters, 2006.

[28] Danielson, B. Optical time-domain reflectometer specifications and performance testing. *Applied Optics.* 1985, Vol. 24, 15, pp. 2313-2322.

[29] Legré, M., Thew, R., Zbinden, H., Gisin, N. High resolution optical time domain reflectometer based on 1.55mm up-conversion photon-counting module. *Optics Express,The optical Society.* 2007, Vol. 15, 13, pp. 8237-8242.

[30] Pan, X., Liang,D., Li, D. Optical fiber sensor layer embedded in smart composite material and structure. *Smart Materials and Structures.* 2006, Vol. 15, pp. 1231-1234.

CHAPTER 8

8. Overall Conclusion and Suggestion for Future Work

This research deals with sensing characterization of relatively newly developed Graded Index Perfluorinated Polymer Optic Fiber (GI-PF-POF) as promising sensors for Structural Health Monitoring (SHM). Range of 3D orthogonal woven composites were used as host structures to evaluate the ability of embedded POF to detect structure damage and thus plan for preventive maintenance and avoid sudden structure failure. Developed test bed to measure end to end loss and backscattering using OTDR techniques was used to assess the results and reveal the interrelationships between structural stresses and POF signal loss. Four different but interrelated studies were carried out to design POF sensors with high sensitivity and assess the viability of the sensors in detecting different mode of stresses. These are:

1- **Evaluation of optic fibers to reveal its initial configuration as embedded sensors to avoid initial signal loss before the sensor use**

The study led to the correct configuration of optic fiber that could be used to include one sensor to embed in composite structure of large area with minor or no loss in signal of the POF. This work set a protocol and set a test bed to evaluate fibers without the need to form composite structures and could be used to further evaluation of other type of optic fibers since every fiber has its own characteristics.

2- **Investigation of the effect resin type on the signal integrity of POF to find out whether the resin treatment would chemically or physical interact with the polymeric material and cause any damage to its structure and signal**

This investigation revealed that epoxy resin has no negative effect on POF integrity compare to vinylester resin. Simple study protocol was used to investigate resin effect with no need for embedding POF in composite structures. Vinylester resin penetration into POF structure requires more and further investigations in addition to investigation of other resins types and different fiber specification.

3- **Studying of the effect of presence of the POF in the composite structure integrity and whether the POF has negative impact on mechanical properties of the host materials**

This part of the study unveiled that no negative effect on composite mechanical properties was caused by the presence of POF. Statistical and optical analyses results supported this finding. Further study on effect of multi POF integration on composite structure mechanical structure needs to be investigated.

4- **Evaluation of the POF sensor viability in response to bending and repeated impacts**

Results of this evaluation showed good response of POF in sensing the stresses during composite fabrication process, bending load, and repeated impacts. Backscattering technique was viable method in detecting changes on POF under different stresses modes. This assessment of impact damage in this work is subjective and more assessment of performance after impact is required to be able to relate the signal loss to mechanical properties of composites after impact.

In general, this study establishes a foundation of viability and promising opportunity for POF sensors to be applied on SHM.

APPENDICES

A. Mechanical test on samples of chapter 5

A.1 3-point bending test

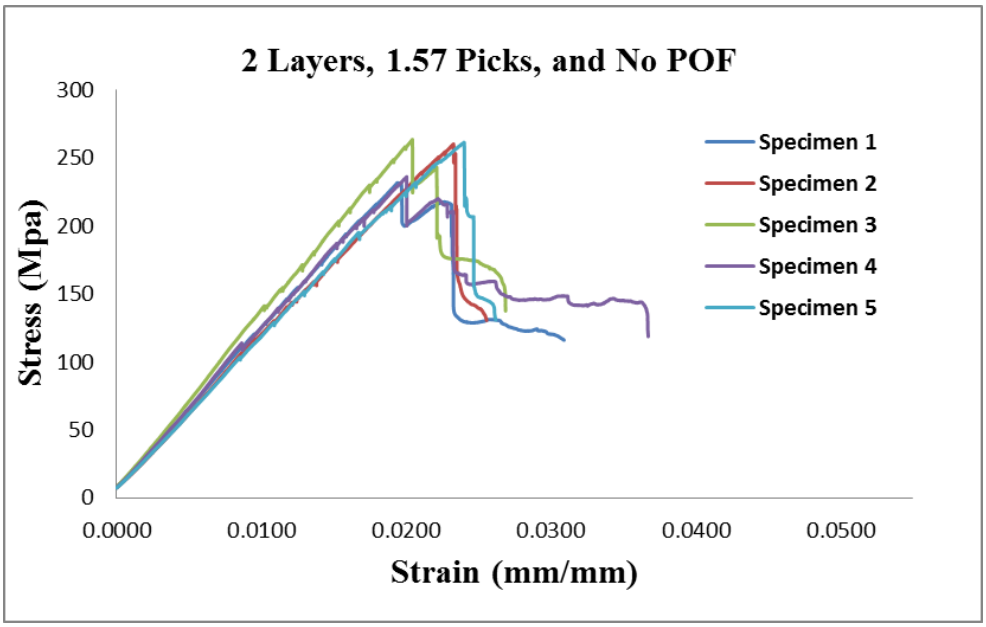

Figure A.1 Typical stress-strain for sample 1

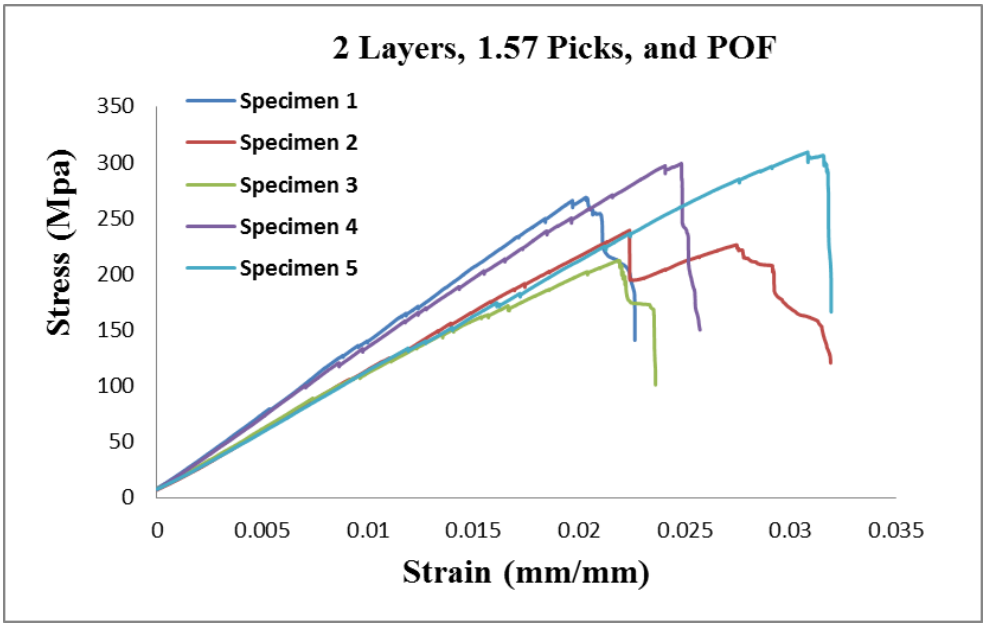

Figure A.2 Typical stress-strain for sample 2

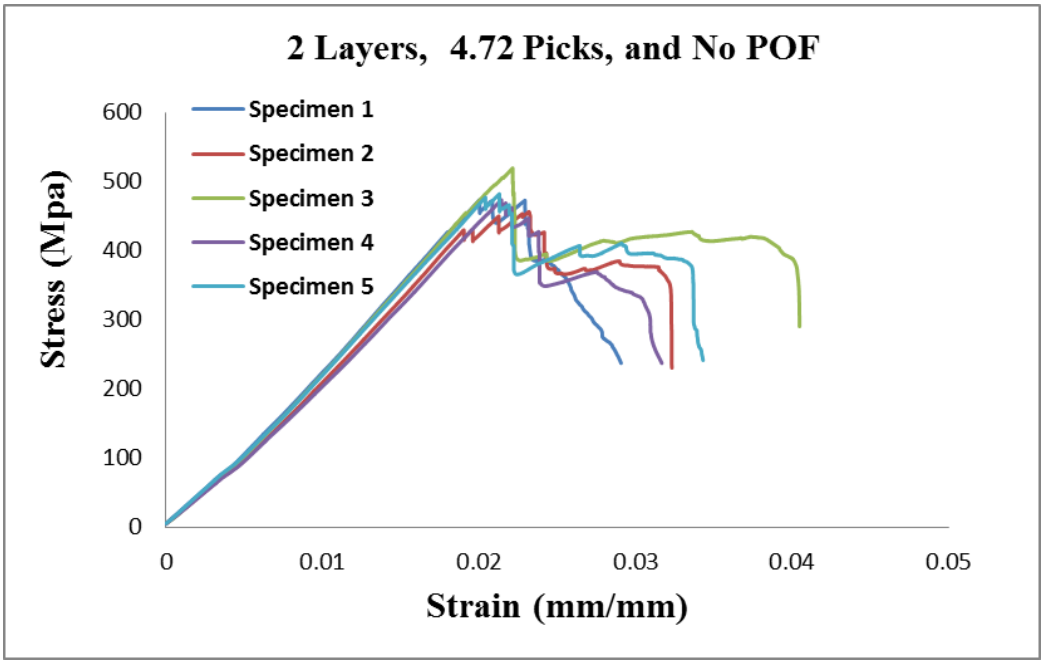

Figure A.3 Typical stress-strain for sample 3

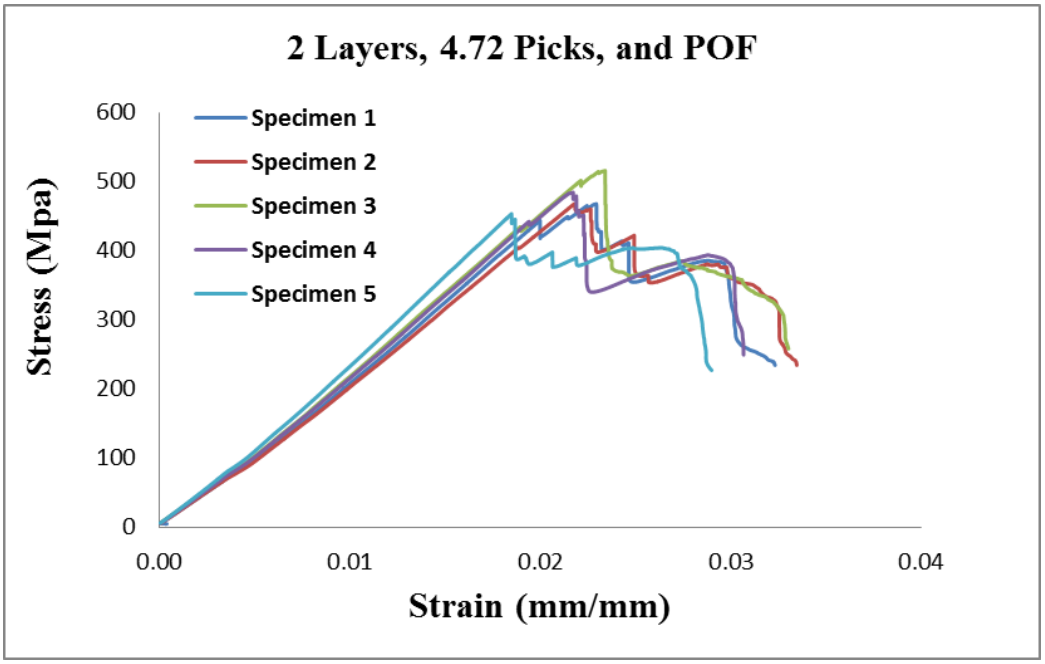

Figure A.4 Typical stress-strain for sample 4

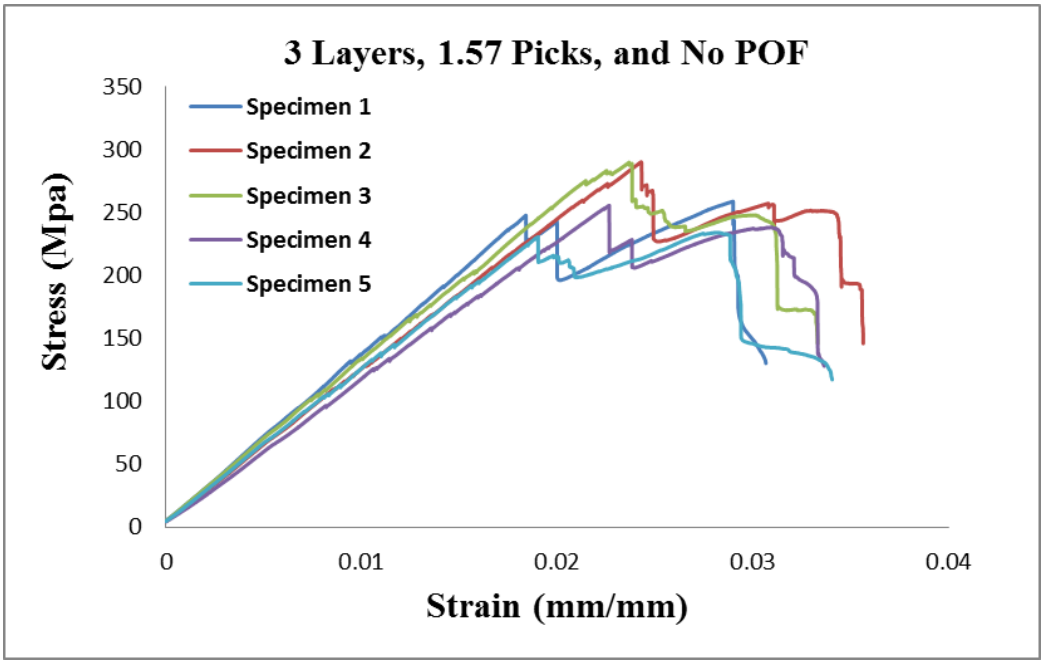

Figure A.5 Typical stress-strain for sample 5

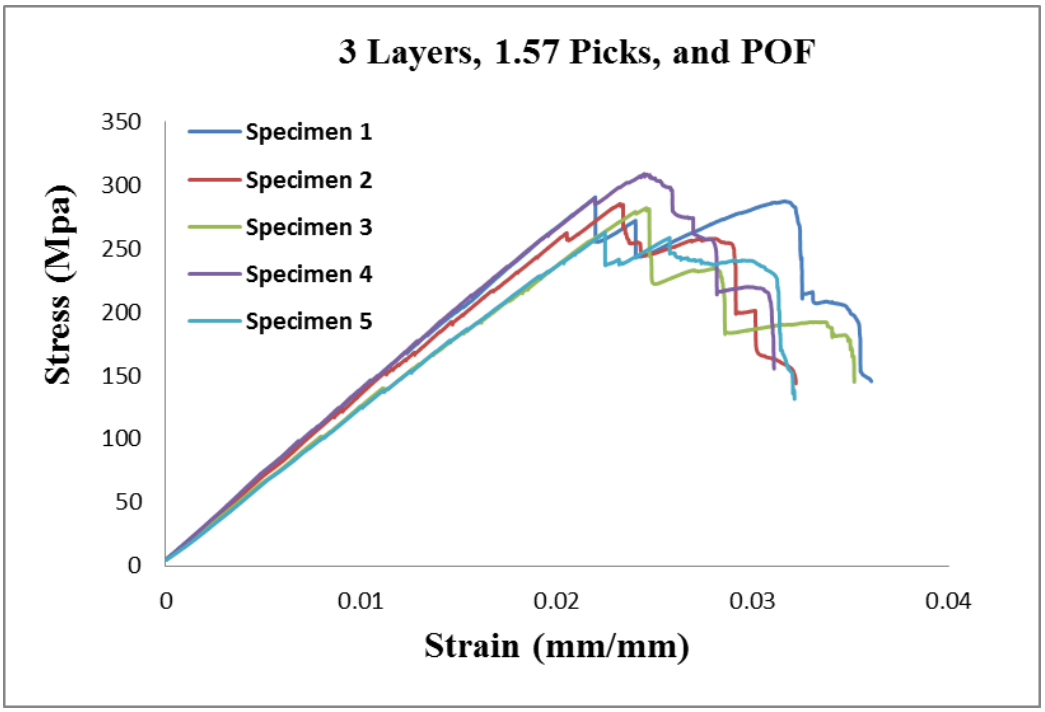

Figure A.6 Typical stress-strain for sample 6

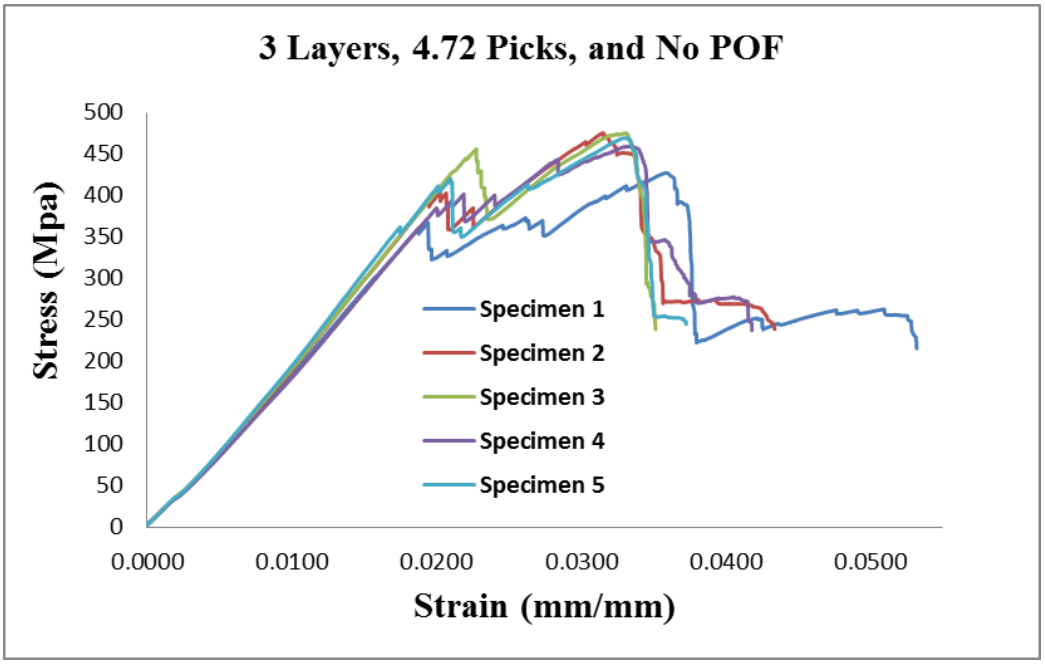

Figure A.7 Typical stress-strain for sample 7

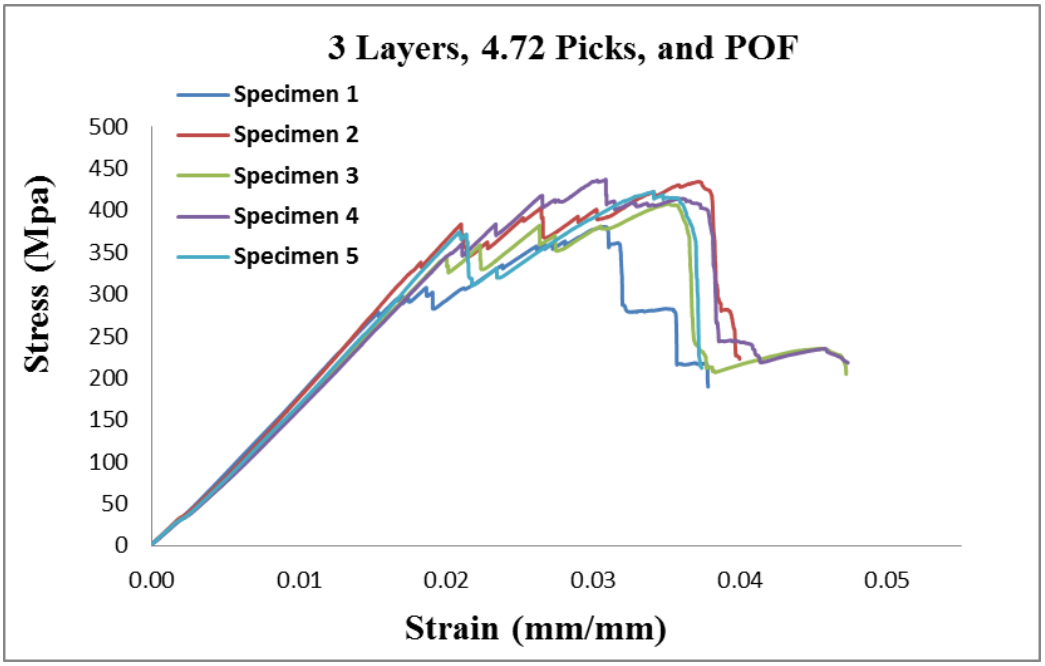

Figure A.8 Typical stress-strain for sample 8

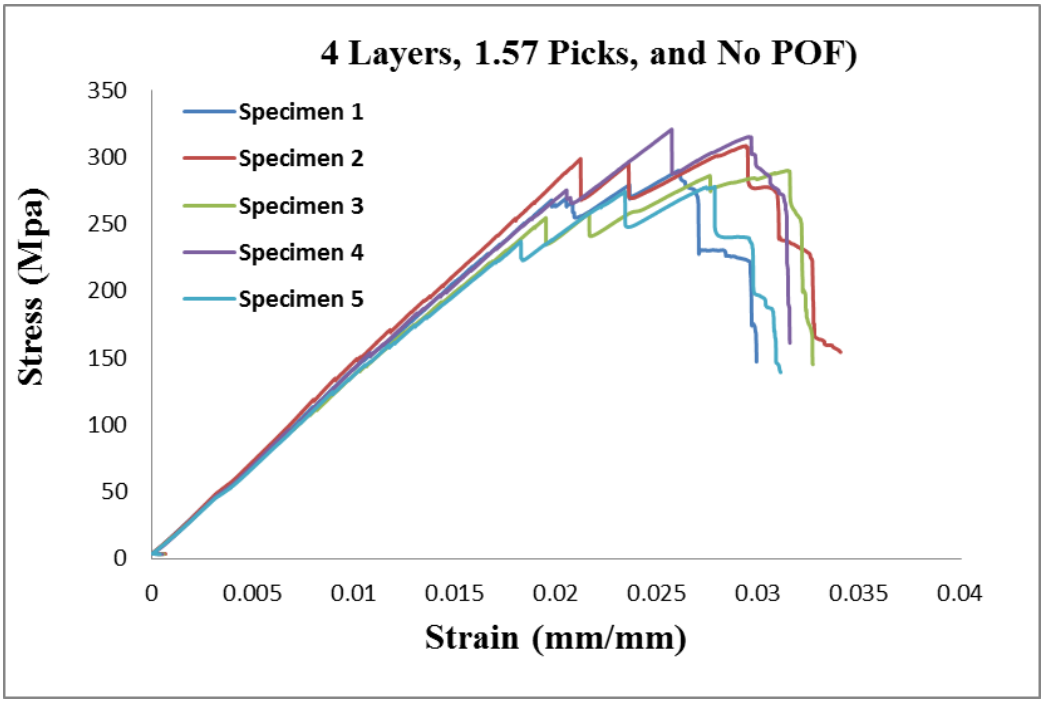

Figure A.9 Typical stress-strain for sample 9

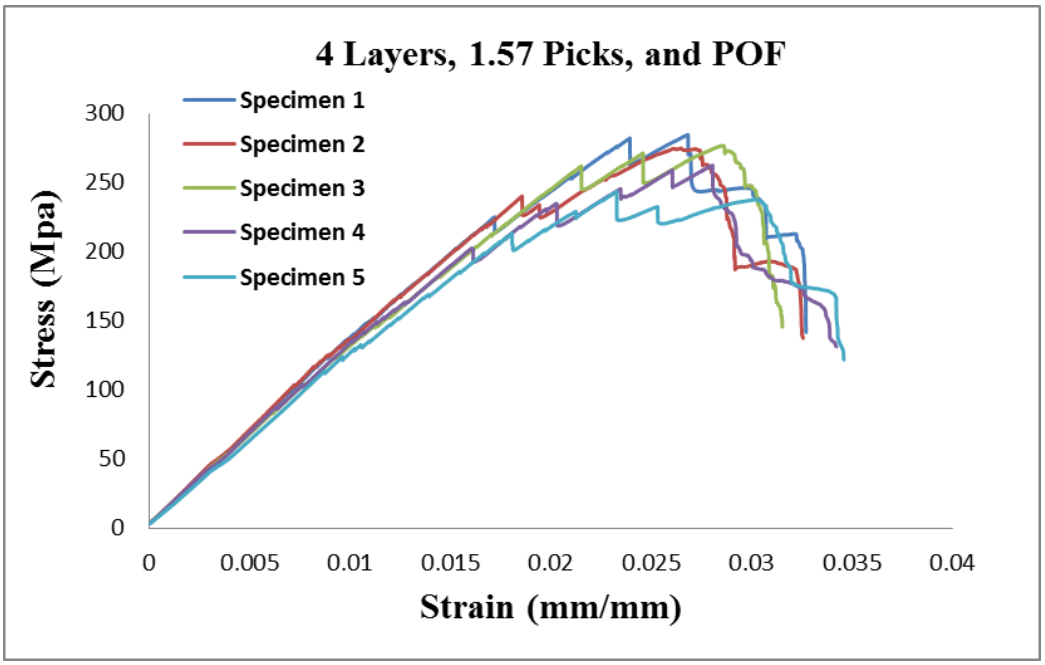

Figure A.10 Typical stress-strain for sample 10

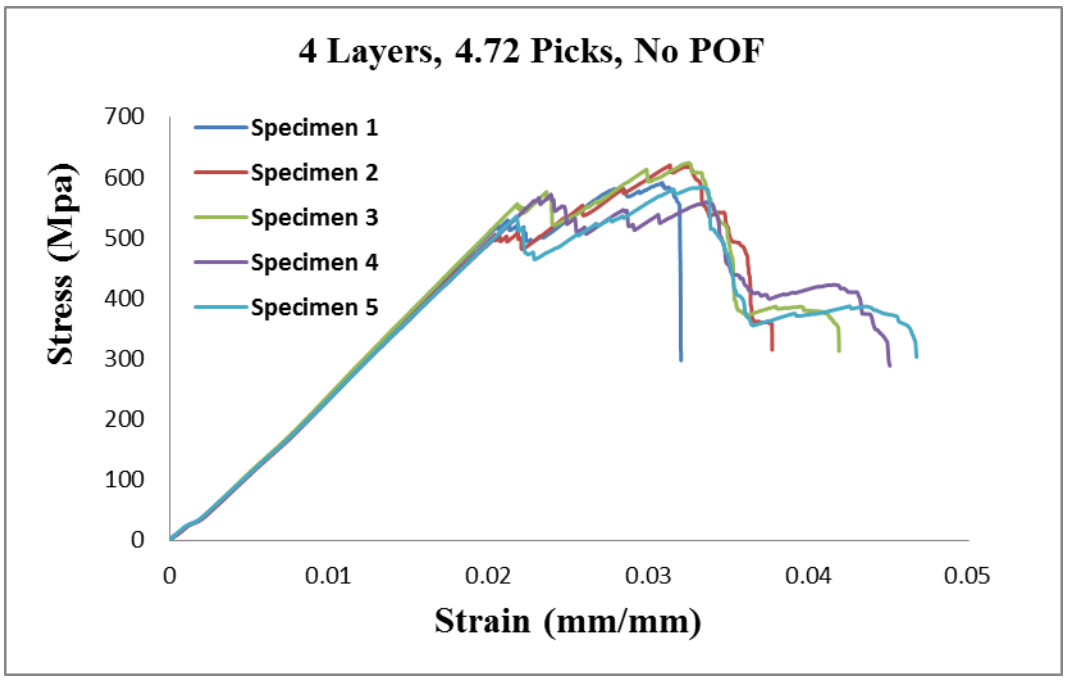

Figure A.11 Typical stress-strain for sample 11

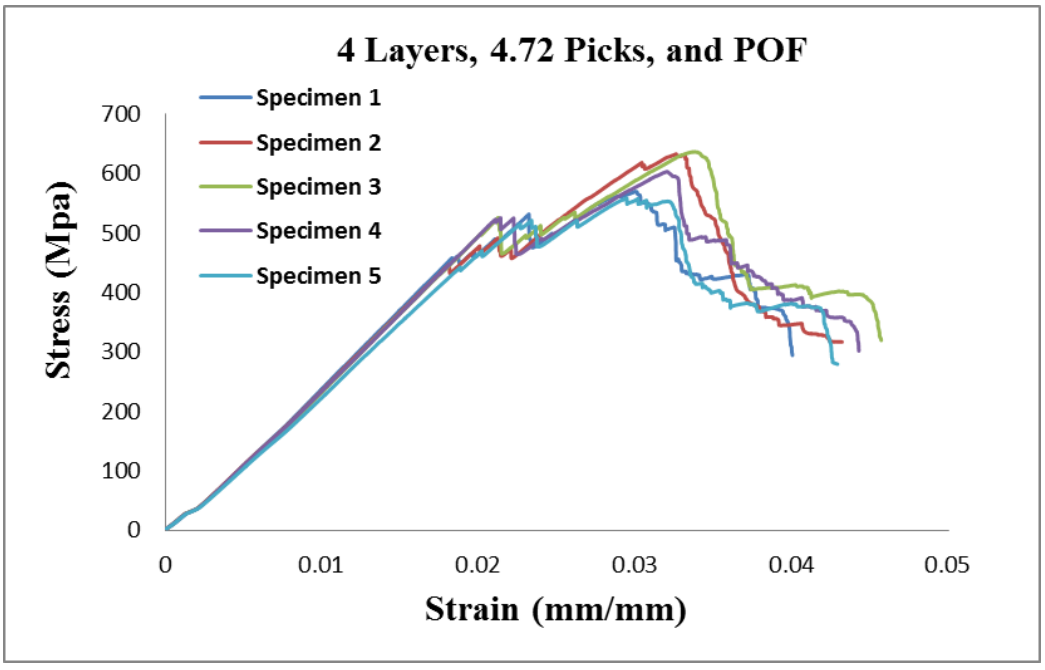

Figure A.12 Typical stress-strain for sample 12

Analyses:

A.2 Flexural strength statistical analysis

Table A.1 Raw data of bending test

Sample ID	Presence of POF	x-yarn density	# of y-yarn layers	Bending strength MPa
1	0	1.57	2 (3)	231.67
2	0	1.57	2 (3)	260.05
3	0	1.57	2 (3)	263.40
4	0	1.57	2 (3)	235.99
5	0	1.57	2 (3)	261.30
6	1	1.57	2 (3)	211.97
7	1	1.57	2 (3)	238.99
8	1	1.57	2 (3)	268.43
9	1	1.57	2 (3)	298.82
10	1	1.57	2 (3)	308.93
11	0	4.72	2 (3)	473.31
12	0	4.72	2 (3)	456.15
13	0	4.72	2 (3)	519.04
14	0	4.72	2 (3)	487.19
15	0	4.72	2 (3)	481.75
16	1	4.72	2 (3)	467.55
17	1	4.72	2 (3)	467.52
18	1	4.72	2 (3)	515.48
19	1	4.72	2 (3)	484.09
20	1	4.72	2 (3)	453.09
21	0	1.57	3 (4)	258.47
22	0	1.57	3 (4)	289.87
23	0	1.57	3 (4)	289.45
24	0	1.57	3 (4)	255.27
25	0	1.57	3 (4)	233.73
26	1	1.57	3 (4)	290.09
27	1	1.57	3 (4)	284.91
28	1	1.57	3 (4)	281.49
29	1	1.57	3 (4)	262.31
30	1	1.57	3 (4)	308.39
31	0	4.72	3 (4)	426.87
32	0	4.72	3 (4)	474.99
33	0	4.72	3 (4)	475.11
34	0	4.72	3 (4)	458.69

35	0	4.72	3 (4)	468.91
36	1	4.72	3 (4)	380.84
7	1	4.72	3 (4)	434.59
38	1	4.72	3 (4)	408.17
39	1	4.72	3 (4)	437.33
40	1	4.72	3 (4)	422.64
41	0	1.57	4 (5)	289.68
42	0	1.57	4 (5)	289.78
43	0	1.57	4 (5)	277.67
44	0	1.57	4 (5)	308.11
45	0	1.57	4 (5)	320.55
46	1	1.57	4 (5)	284.53
47	1	1.57	4 (5)	274.68
48	1	1.57	4 (5)	276.48
49	1	1.57	4 (5)	262.30
50	1	1.57	4 (5)	243.35
51	0	4.72	4 (5)	590.65
52	0	4.72	4 (5)	619.71
53	0	4.72	4 (5)	623.80
54	0	4.72	4 (5)	571.07
55	0	4.72	4 (5)	607.87
56	1	4.72	4 (5)	569.17
57	1	4.72	4 (5)	632.22
58	1	4.72	4 (5)	635.75
59	1	4.72	4 (5)	602.42
60	1	4.72	4 (5)	557.78

Table A.2 Flexural strength means and standard deviation for sample with and without POF

Sample ID	**Presence of POF**	**x-yarn density**	**# y-yarn layers**	**Bending strength MPa**	
				Mean	**Std.**
1	0	1.57	2 (3)	250.48	15.32
2	1	1.57	2 (3)	265.43	40.54
3	0	4.72	2 (3)	483.49	23.09
4	1	4.72	2 (3)	477.54	23.88
5	0	1.57	3 (4)	265.35	24.14
6	1	1.57	3 (4)	285.43	16.58
7	0	4.72	3 (4)	460.91	20.17
8	1	4.72	3 (4)	416.71	23.13
9	0	1.57	4 (5)	297.16	17.01
10	1	1.57	4 (5)	268.26	16.04
11	0	4.72	4 (5)	602.62	21.83
12	1	4.72	4 (5)	599.46	35.54

Table A.3 Bending Strain means' and standard deviation

Sample ID	Displacement mm		Strain %	
	Mean	Stdv.	Mean	Stdv.
1	9.71	0.70	2.14	0.19
2	9.93	0.82	2.27	0.21
3	7.25	0.38	2.05	0.10
4	7.36	0.61	2.11	0.18
5	7.41	0.86	2.16	0.27
6	7.67	0.45	2.23	0.14
7	5.02	0.39	2.05	0.13
8	4.74	0.42	2.00	0.17
9	5.67	0.36	1.97	0.10
10	5.39	0.59	1.88	0.18
11	4.76	0.23	2.15	0.11
12	4.53	0.35	2.10	0.16

Table A.4 GLM of flexural strength for parameters and interaction

Source	DF	Sum of Squares	Mean Square	F Ratio	Prob > F
POF	1	926.63	926.6	1.3898	0.2440
Picks	1	826754.85	826754.8	1239.998	<.0001*
Layers	2	84070.52	42035.3	63.0460	<.0001*
POF*Picks	1	1471.81	1471.8	2.2075	0.1436
POF*Layers	2	1185.14	592.6	0.8888	0.4176
Picks*Layers	2	61112.66	30556.3	45.8295	<.0001*

Table A.5 GLM of flexural strength for parameters

Source	DF	Sum of Squares	Mean Square	F Ratio	Prob > F
POF	1	926.63	926.6	1.3644	0.2480
Picks	1	826754.85	826754.8	1217.373	<.0001*
Layers	2	84070.52	42035.3	61.8957	<.0001*
Picks*Layers	2	61112.66	30556.3	44.9933	<.0001*

Table A.6 Flexural strength analysis of Variance (ANOVA)

Source	DF	Sum of Squares	Mean Square	F Ratio	Prob > F
Factor	11	824387.5	74944.3	14.8875	<.0001*
Error	48	241634.0	5034.0		
C. Total	59	1066021.5			

Table A.7 Flexural strength mean's comparisons using Tukey-Kramer HSD

Level					Mean
4Layers 4.72P without POF	A				602.62003
4Layers 4.72P with POF	A	B			506.07877
2Layers 4.72P without POF	A	B			483.49003
2Layers 4.72P with POF	A	B			477.54400
3Layers 4.72P without POF	A	B			460.91394
3Layers 4.72P with POF		B	C		416.71585
4Layers 1.57P without POF			C	D	297.15957
3Layers 1.57P with POF			C	D	285.43818
4Layers 1.57P with POF			C	D	268.26793
2Layers 1.57P with POF			C	D	265.42848
3Layers 1.57P without POF			C	D	265.35648
2Layers 1.57P without POF				D	250.48093

A.3. Flexural Modulus Analysis

Table A.8 Raw data of flexural modulus

Sample ID	Presence of POF	x-yarn density	# of y-yarn layers	Bending Modulus GPa
1	0	1.57	2 (3)	11.52
2	0	1.57	2 (3)	10.63
3	0	1.57	2 (3)	12.30
4	0	1.57	2 (3)	11.59
5	0	1.57	2 (3)	10.67
6	1	1.57	2 (3)	13.06
7	1	1.57	2 (3)	10.05
8	1	1.57	2 (3)	10.35
9	1	1.57	2 (3)	12.66
10	1	1.57	2 (3)	9.89
11	0	4.72	2 (3)	20.16
12	0	4.72	2 (3)	18.71
13	0	4.72	2 (3)	20.01
14	0	4.72	2 (3)	19.08
15	0	4.72	2 (3)	20.44
16	1	4.72	2 (3)	18.72
17	1	4.72	2 (3)	18.85

18	1	4.72	2 (3)	19.98
19	1	4.72	2 (3)	19.88
20	1	4.72	2 (3)	21.02
21	0	1.57	3 (4)	13.03
22	0	1.57	3 (4)	11.83
23	0	1.57	3 (4)	12.98
24	0	1.57	3 (4)	10.64
25	0	1.57	3 (4)	12.26
26	1	1.57	3 (4)	14.94
27	1	1.57	3 (4)	14.70
28	1	1.57	3 (4)	13.75
29	1	1.57	3 (4)	13.05
30	1	1.57	3 (4)	15.44
31	0	4.72	3 (4)	15.41
32	0	4.72	3 (4)	15.59
33	0	4.72	3 (4)	16.17
34	0	4.72	3 (4)	15.25
35	0	4.72	3 (4)	16.08
36	1	4.72	3 (4)	15.82
37	1	4.72	3 (4)	15.01
38	1	4.72	3 (4)	13.83
39	1	4.72	3 (4)	13.78
40	1	4.72	3 (4)	13.86
41	0	1.57	4 (5)	14.12
42	0	1.57	4 (5)	13.69
43	0	1.57	4 (5)	13.41
44	0	1.57	4 (5)	14.24
45	0	1.57	4 (5)	13.97
46	1	1.57	4 (5)	14.15
47	1	1.57	4 (5)	14.28
48	1	1.57	4 (5)	13.35
49	1	1.57	4 (5)	13.72
50	1	1.57	4 (5)	12.48
51	0	4.72	4 (5)	18.30
52	0	4.72	4 (5)	18.04
53	0	4.72	4 (5)	18.60
54	0	4.72	4 (5)	16.54
55	0	4.72	4 (5)	16.65
56	1	4.72	4 (5)	23.17
57	1	4.72	4 (5)	23.78
58	1	4.72	4 (5)	17.76
59	1	4.72	4 (5)	17.61

60	1	4.72	4 (5)	17.26

Table A.9 Flexural Modulus mean and standard deviation for sample with and without POF

Sample ID	Presence of POF	x-yarn density	# of y-yarn layers	Bending Modulus GPa	
				Mean	Std.
1	0	1.57	2 (3)	11.34	0.70
2	1	1.57	2 (3)	11.20	1.53
3	0	4.72	2 (3)	19.68	0.74
4	1	4.72	2 (3)	19.69	0.94
5	0	1.57	3 (4)	12.15	0.98
6	1	1.57	3 (4)	14.37	0.96
7	0	4.72	3 (4)	15.70	0.41
8	1	4.72	3 (4)	14.46	0.92
9	0	1.57	4 (5)	13.89	0.34
10	1	1.57	4 (5)	13.60	0.72
11	0	4.72	4 (5)	17.63	0.97
12	1	4.72	4 (5)	19.91	3.26

Table A.10 GLM of Flexural modulus for parameters and interaction

Source	DF	Sum of Squares	Mean Square	F Ratio	Prob > F
POF	1	3.40015	3.4002	1.6896	0.1996
Picks	1	388.18908	388.1891	192.8929	<.0001*
Layers	2	44.39408	22.1970	11.0298	0.0001*
POF*Picks	1	0.22564	0.2256	0.1121	0.7391
POF*Layers	2	2.83633	1.4182	0.7047	0.4991
Picks*Layers	2	108.78444	54.3922	27.0277	<.0001*

Table A.11 GLM of flexural modulus for parameters

Source	DF	Sum of Squares	Mean Square	F Ratio	Prob > F
POF	1	1	3.40015	3.4002	1.7380
Picks	1	1	388.18908	388.1891	198.4283
Layers	2	2	44.39408	22.1970	11.3463
Picks*Layers	2	2	108.78444	54.3922	27.8033

Table A.12 Flexural modulus analysis of Variance (ANOVA)

Source	DF	Sum of Squares	Mean Square	F Ratio	Prob > F
Factor	11	571.00922	51.9099	32.1741	<.0001*
Error	48	77.44344	1.6134		
C. Total	59	648.45267			

Table A.13 Flexural modulus mean's comparisons using Tukey-Kramer HSD

Level						Mean
4Layers 4.72P with POF	A					19.92
2Layers 4.72P with POF	A					19.69
2Layers 4.72P without POF	A					19.68
4Layers 4.72P without POF	A	B				17.63
3Layers 4.72P without POF		B	C			15.70
3Layers 4.72P with POF			C	D		14.46
3Layers 1.57P with POF			C	D		14.38
4Layers 1.57P without POF			C	D	E	13.89
4Layers 1.57P with POF			C	D	E	13.60
3Layers 1.57P without POF				D	E	12.15
2Layers 1.57P without POF					E	11.34
2Layers 1.57P with POF					E	11.20

A.4. Tensile test

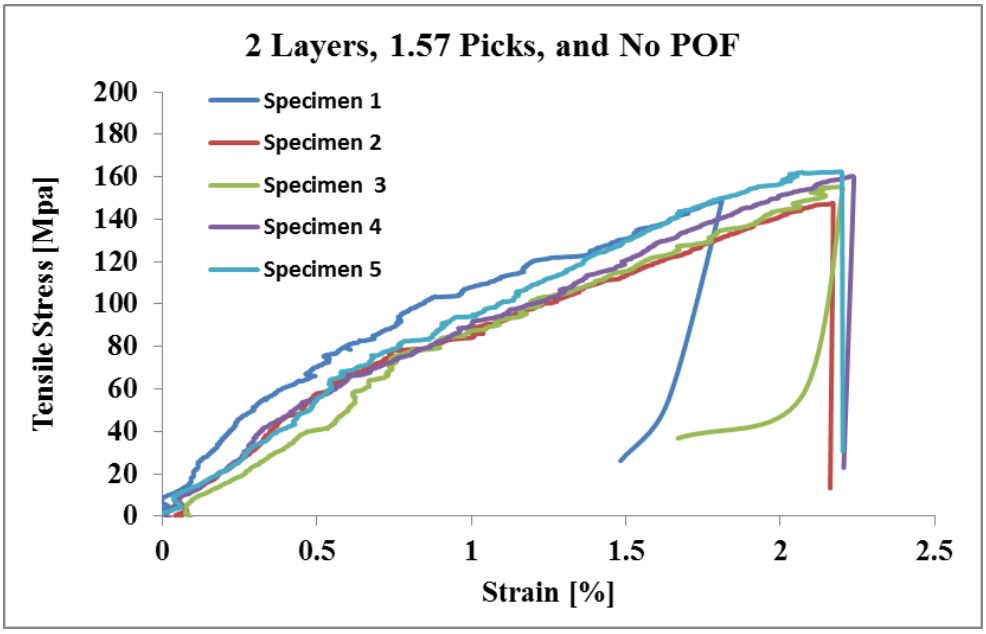

Figure A.13 Typical tensile stress-strain for sample 1

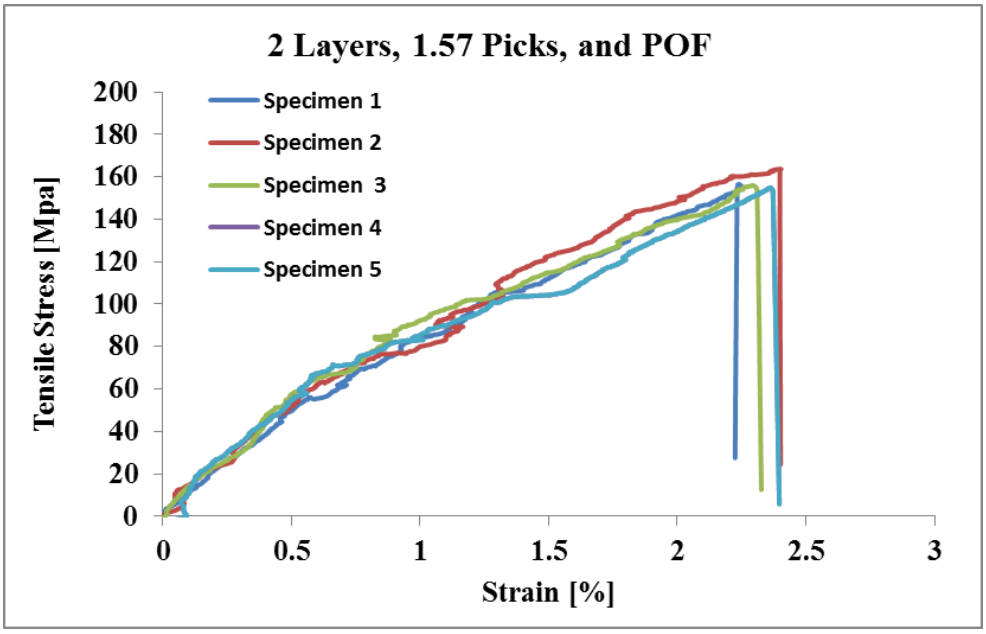

Figure A.14 Typical tensile stress-strain for sample 2

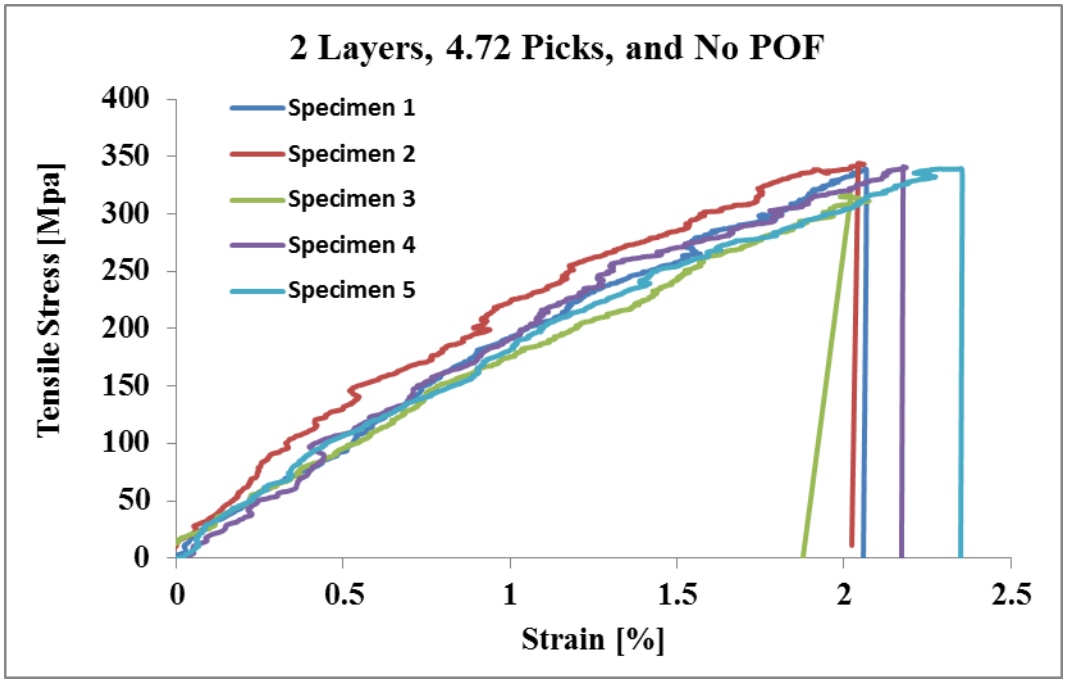

Figure A.15 Typical tensile stress-strain for sample 3

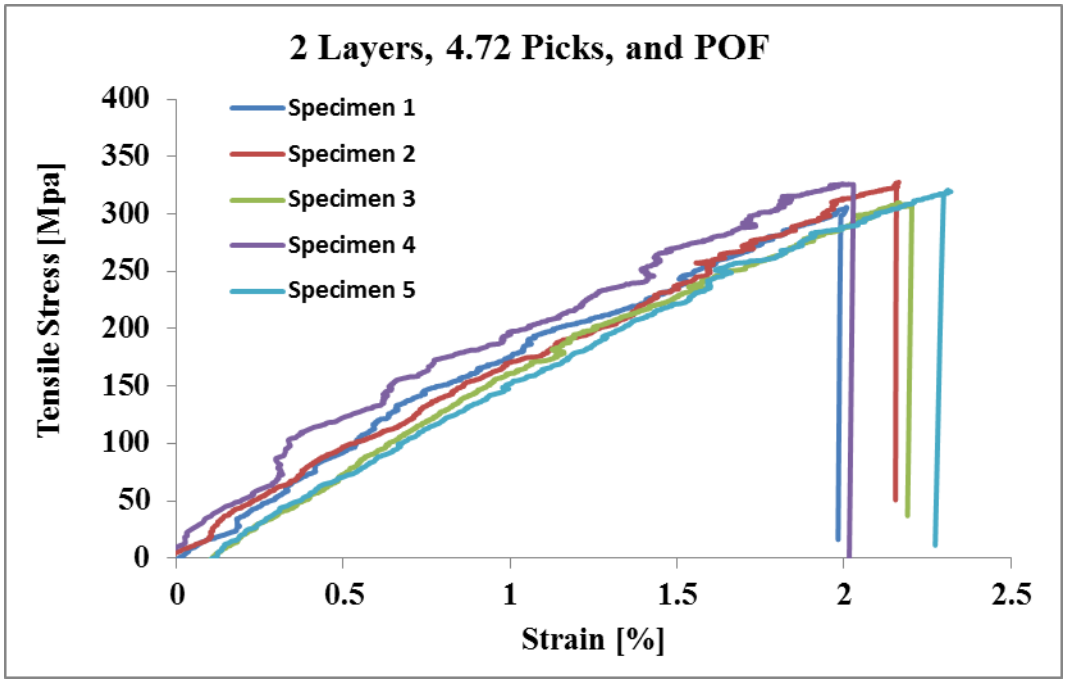

Figure A.16 Typical tensile stress-strain for sample 4

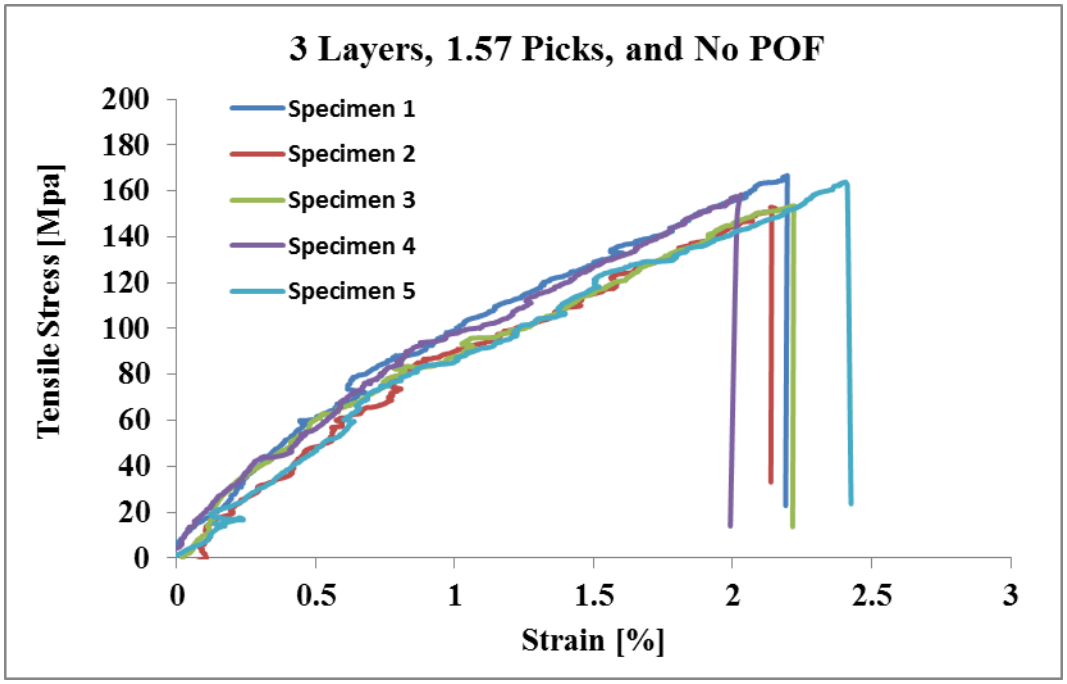

Figure A.17 Typical tensile stress-strain for sample 5

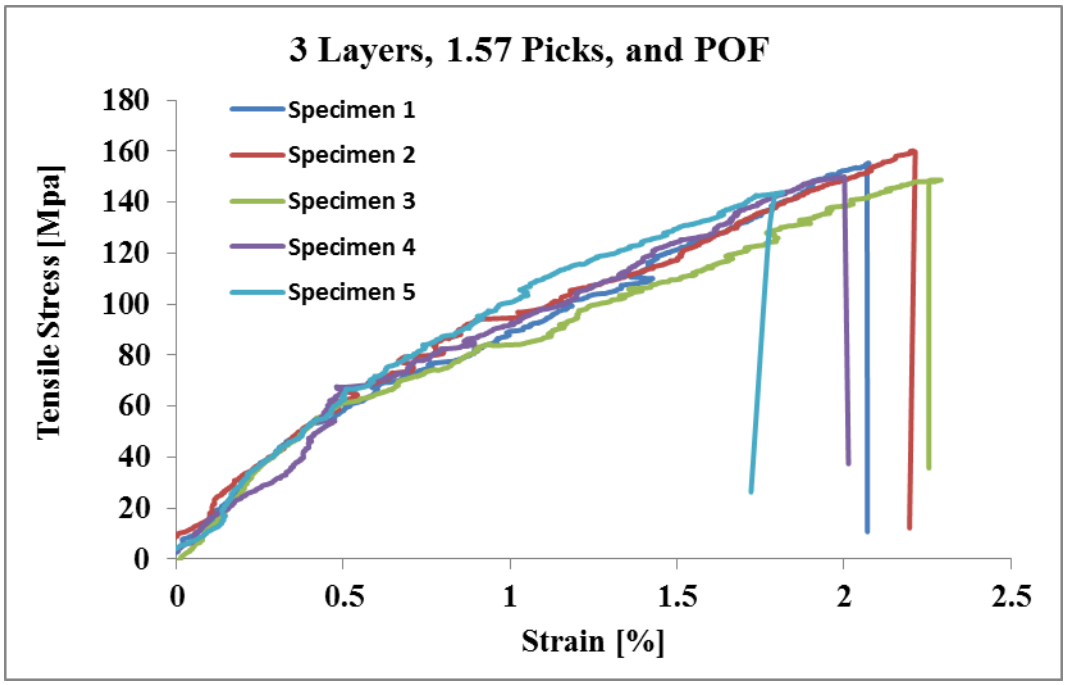

Figure A.18 Typical tensile stress-strain for sample 6

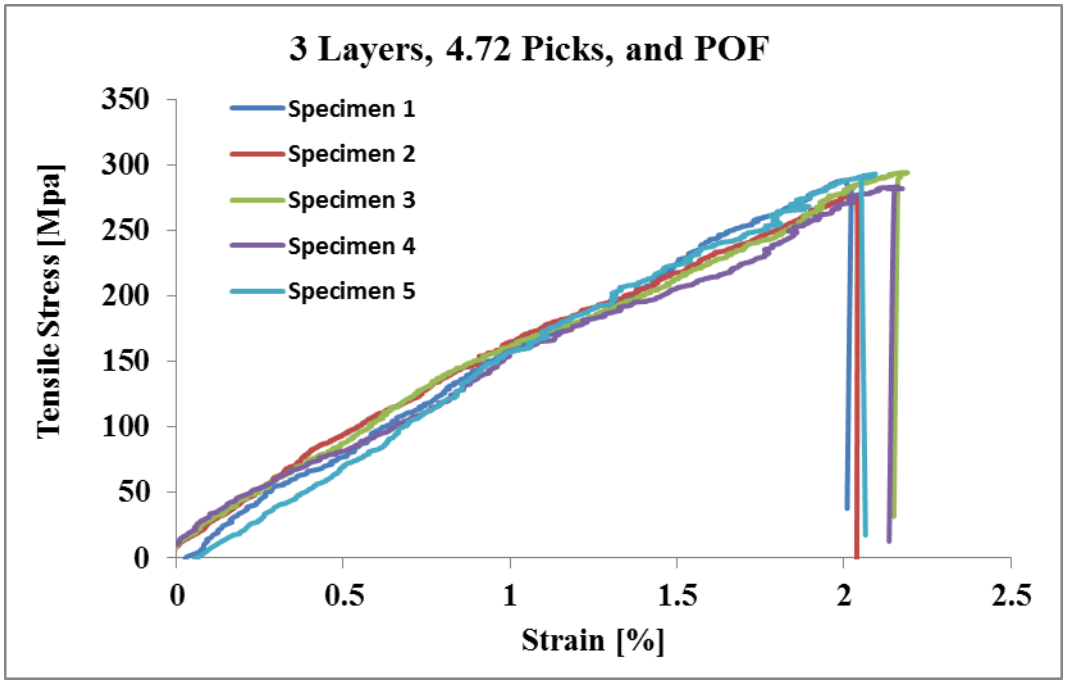

Figure A.19 Typical tensile stress-strain for sample 8

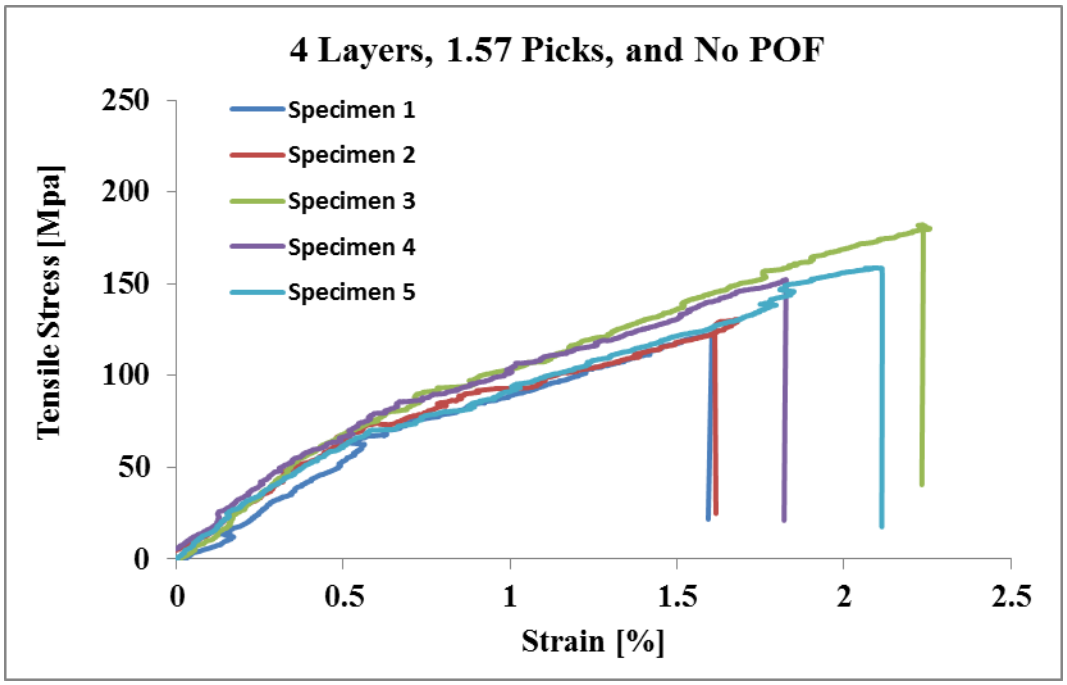

Figure A.20 Typical tensile stress-strain for sample 9

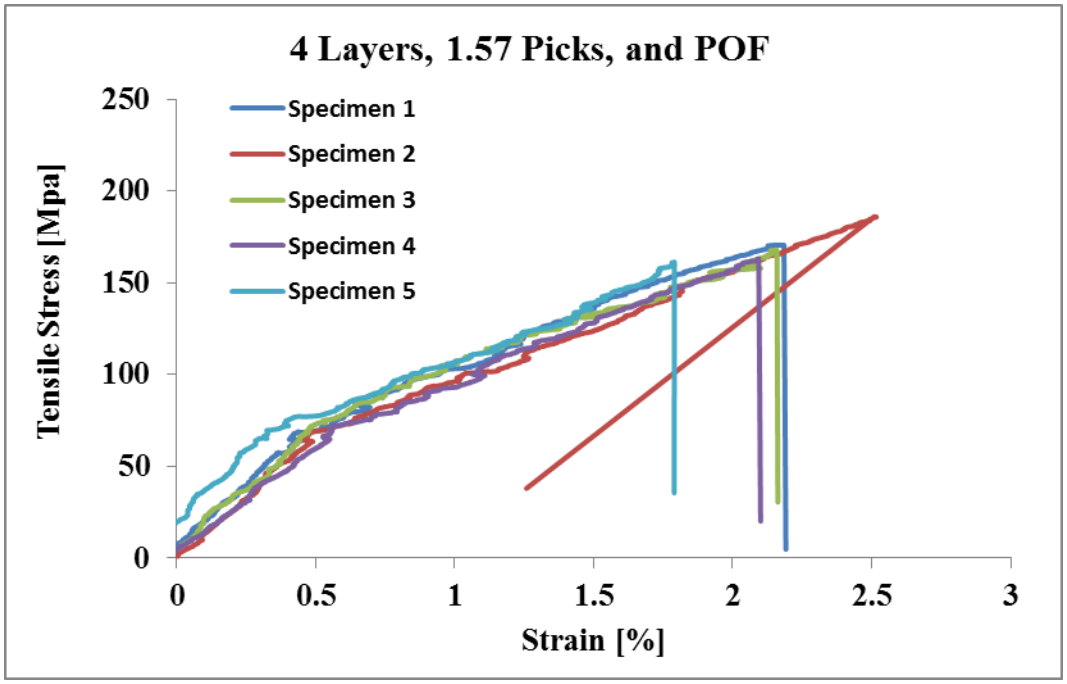

Figure A.21 Typical tensile stress-strain for sample 10

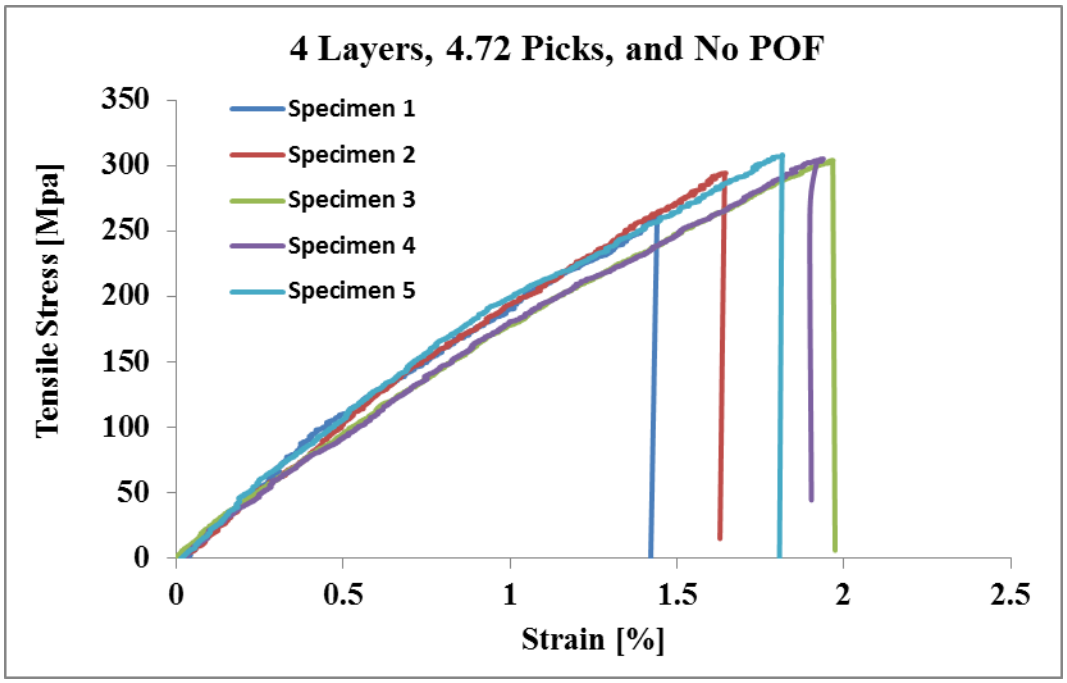

Figure A.22 Typical tensile stress-strain for sample 11

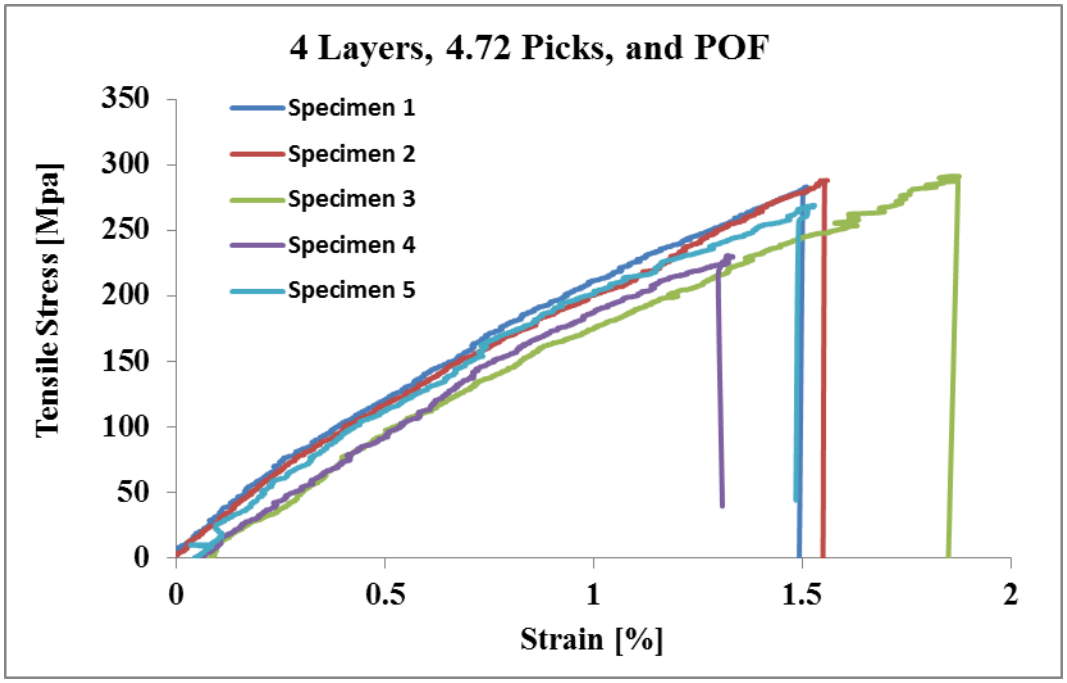

Figure A.23 Typical tensile stress-strain for sample 12

A.5 Tensile strength statistical analyses

T**able A.14** Raw data of tensile test

Sample ID	Presence of POF	x-yarn density	# of y-yarn layers	Tensile stress MPa
1	0	1.57	2 (3)	148.86
2	0	1.57	2 (3)	147.50
3	0	1.57	2 (3)	155.21
4	0	1.57	2 (3)	160.30
5	0	1.57	2 (3)	162.40
6	1	1.57	2 (3)	156.48
7	1	1.57	2 (3)	163.66
8	1	1.57	2 (3)	155.99
9	1	1.57	2 (3)	154.75
10	1	1.57	2 (3)	115.15
11	0	4.72	2 (3)	338.55
12	0	4.72	2 (3)	344.16

13	0	4.72	2 (3)	316.63
14	0	4.72	2 (3)	341.25
15	0	4.72	2 (3)	339.26
16	1	4.72	2 (3)	305.85
17	1	4.72	2 (3)	327.69
18	1	4.72	2 (3)	309.78
19	1	4.72	2 (3)	325.88
20	1	4.72	2 (3)	320.86
21	0	1.57	3 (4)	166.79
22	0	1.57	3 (4)	152.85
23	0	1.57	3 (4)	153.52
24	0	1.57	3 (4)	158.41
25	0	1.57	3 (4)	163.88
26	1	1.57	3 (4)	155.42
27	1	1.57	3 (4)	160.17
28	1	1.57	3 (4)	148.74
29	1	1.57	3 (4)	149.97
30	1	1.57	3 (4)	143.81
31	0	4.72	3 (4)	280.58
32	0	4.72	3 (4)	324.58
33	0	4.72	3 (4)	327.17
34	0	4.72	3 (4)	325.16
35	0	4.72	3 (4)	292.98
36	1	4.72	3 (4)	288.14
37	1	4.72	3 (4)	276.12
38	1	4.72	3 (4)	294.07
39	1	4.72	3 (4)	283.22
40	1	4.72	3 (4)	292.92
41	0	1.57	4 (5)	122.62
42	0	1.57	4 (5)	130.56
43	0	1.57	4 (5)	181.93
44	0	1.57	4 (5)	152.13
45	0	1.57	4 (5)	158.60
46	1	1.57	4 (5)	170.57
47	1	1.57	4 (5)	186.01
48	1	1.57	4 (5)	167.88
49	1	1.57	4 (5)	163.09
50	1	1.57	4 (5)	161.27
51	0	4.72	4 (5)	262.97

52	0	4.72	4 (5)	294.29
53	0	4.72	4 (5)	304.09
54	0	4.72	4 (5)	305.16
55	0	4.72	4 (5)	308.24
56	1	4.72	4 (5)	302.78
57	1	4.72	4 (5)	301.19
58	1	4.72	4 (5)	291.48
59	1	4.72	4 (5)	305.78
60	1	4.72	4 (5)	281.45

Table A.15 Tensile strength mean and standard deviation for sample with and without POF

Sample ID	**Presence of POF**	**x-yarn density**	**# of y-yarn layers**	**Tensile Stress MPa**	
				Mean	**Std.**
1	0	1.57	2 (3)	154.86	6.46
2	1	1.57	2 (3)	149.21	19.35
3	0	4.72	2 (3)	335.97	11.02
4	1	4.72	2 (3)	318.01	9.73
5	0	1.57	3 (4)	159.09	6.17
6	1	1.57	3 (4)	151.62	6.31
7	0	4.72	3 (4)	325.64	1.36
8	1	4.72	3 (4)	286.87	7.37
9	0	1.57	4 (5)	155.81	21.14
10	1	1.57	4 (5)	165.70	4.27
11	0	4.72	4 (5)	302.95	6.03
12	1	4.72	4 (5)	283.01	9.77

Table A.16 Tensile strain mean and standard deviation

Sample ID	Strain %	
	Mean	Stdv.
1	1.94	0.34
2	2.13	0.47
3	2.10	0.18
4	2.12	0.12
5	2.19	0.16
6	2.05	0.21
7	2.07	0.09
8	2.08	0.06
9	1.88	0.29
10	1.90	0.39
11	1.83	0.22
12	1.54	0.20

Table A.17GLM of tensile strength for parameters and interaction

Source	**DF**	**Sum of Squares**	**Mean Square**	**F Ratio**	**Prob > F**
POF	1	429.22	429.2	2.2865	0.1368
Picks	1	344097.70	344097.7	1833.052	<.0001*
Layers	2	2004.27	1002.1	5.3385	0.0079*
POF*Picks	1	922.33	922.3	4.9133	0.0312*
POF*Layers	2	2057.83	1028.9	5.4812	0.0070*
Picks*Layers	2	4259.97	2130.0	11.3467	<.0001*

Table A.18 Tensile strength analysis of Variance (ANOVA)

Source	**DF**	**Sum of Squares**	**Mean Square**	**F Ratio**	**Prob > F**
Factor	11	353799.37	32163.6	164.9789	<.0001*
Error	48	9357.88	195.0		
C. Total	59	363157.25			

Table A.19 Tensile strength mean's comparisons for using Tukey-Kramer HSD

Level					Mean
2Layers 4.72P without POF	A				335.97000
2Layers 4.72P with POF	A	B			318.01192
3Layers 4.72P without POF	A	B	C		310.09388
4Layers 4.72P with POF		B	C		296.53608
4Layers 4.72P without POF		B	C		294.95062
3Layers 4.72P with POF			C		286.89440
4Layers 1.57P with POF				D	169.76209
3Layers 1.57P without POF				D	159.08869
2Layers 1.57P without POF				D	154.85520
3Layers 1.57P with POF				D	151.62116
2Layers 1.57P withPOF				D	149.20633
4Layers 1.57P without POF				D	149.16907

A.6. Tensile modulus statistical analyses

Table A.20 Raw data of tensile modulus

Sample ID	Presence of POF	x-yarn density	# of y-yarn layers	Tensile stress GPa
1	0	1.57	2 (3)	12.59
2	0	1.57	2 (3)	11.45
3	0	1.57	2 (3)	9.87
4	0	1.57	2 (3)	10.20
5	0	1.57	2 (3)	10.63
6	1	1.57	2 (3)	8.69
7	1	1.57	2 (3)	9.00
8	1	1.57	2 (3)	9.95
9	1	1.57	2 (3)	10.85
10	1	1.57	2 (3)	10.67
11	0	4.72	2 (3)	18.89
12	0	4.72	2 (3)	24.16
13	0	4.72	2 (3)	16.82
14	0	4.72	2 (3)	21.05
15	0	4.72	2 (3)	17.49
16	1	4.72	2 (3)	19.97

17	1	4.72	2 (3)	16.62
18	1	4.72	2 (3)	18.33
19	1	4.72	2 (3)	21.19
20	1	4.72	2 (3)	16.38
21	0	1.57	3 (4)	10.53
22	0	1.57	3 (4)	9.66
23	0	1.57	3 (4)	10.47
24	0	1.57	3 (4)	9.82
25	0	1.57	3 (4)	9.81
26	1	1.57	3 (4)	10.01
27	1	1.57	3 (4)	10.06
28	1	1.57	3 (4)	10.57
29	1	1.57	3 (4)	11.86
30	1	1.57	3 (4)	12.10
31	0	4.72	3 (4)	17.43
32	0	4.72	3 (4)	20.26
33	0	4.72	3 (4)	18.78
34	0	4.72	3 (4)	16.58
35	0	4.72	3 (4)	19.87
36	1	4.72	3 (4)	15.71
37	1	4.72	3 (4)	16.17
38	1	4.72	3 (4)	15.79
39	1	4.72	3 (4)	13.05
40	1	4.72	3 (4)	16.38
41	0	1.57	4 (5)	11.46
42	0	1.57	4 (5)	12.25
43	0	1.57	4 (5)	12.46
44	0	1.57	4 (5)	12.48
45	0	1.57	4 (5)	10.53
46	1	1.57	4 (5)	11.56
47	1	1.57	4 (5)	9.94
48	1	1.57	4 (5)	12.36
49	1	1.57	4 (5)	11.23
50	1	1.57	4 (5)	14.76
51	0	4.72	4 (5)	22.88
52	0	4.72	4 (5)	21.30
53	0	4.72	4 (5)	17.86
54	0	4.72	4 (5)	18.33
55	0	4.72	4 (5)	21.18
56	1	4.72	4 (5)	22.56
57	1	4.72	4 (5)	22.18
58	1	4.72	4 (5)	20.65

59	1	4.72	4 (5)	20.86
60	1	4.72	4 (5)	23.87

Table A.21 Tensile modulus mean and standard deviation for sample with and without POF

Sample ID	Presence of POF	x-yarn density	# of y-yarn layers	Tensile Stress GPa	
				Mean	Std.
1	0	1.57	2 (3)	10.95	1.09
2	1	1.57	2 (3)	9.83	0.97
3	0	4.72	2 (3)	19.68	2.98
4	1	4.72	2 (3)	18.50	2.09
5	0	1.57	3 (4)	10.06	0.41
6	1	1.57	3 (4)	10.92	0.99
7	0	4.72	3 (4)	18.59	1.57
8	1	4.72	3 (4)	15.42	1.35
9	0	1.57	4 (5)	11.83	0.84
10	1	1.57	4 (5)	11.97	1.79
11	0	4.72	4 (5)	20.31	2.14
12	1	4.72	4 (5)	22.02	1.32

Table A.22 GLM of tensile modulus for parameters and interaction

Source	DF	Sum of Squares	Mean Square	F Ratio	Prob > F
POF	1	3.16618	3.1662	1.0930	0.3008
Picks	1	998.69424	998.6942	344.7579	<.0001*
Layers	2	79.75480	39.8774	13.7660	<.0001*
POF*Picks	1	2.62713	2.6271	0.9069	0.3455
POF*Layers	2	14.34793	7.1740	2.4765	0.0943
Picks*Layers	2	21.10840	10.5542	3.6434	0.0333*

Table A.23 GLM of tensile modulus for parameters

Source	DF	Sum of Squares	Mean Square	F Ratio	Prob > F
POF	1	3.16618	3.1662	1.0370	0.3131
Picks	1	998.69424	998.6942	327.1069	<.0001*
Layers	2	79.75480	39.8774	13.0612	<.0001*
POF*Picks	2	21.10840	10.5542	3.4569	0.0388*
Picks*Layers	1	3.16618	3.1662	1.0370	0.3131

Table A.24 Tensile modulus analysis of variance (ANOVA)

Source	DF	Sum of Squares	Mean Square	F Ratio	Prob > F
Factor	11	1140.4636	103.679	40.1094	<.0001*
Error	48	124.0750	2.585		
C. Total	59	1264.5386			

Table A.25 Tensile modulus mean's comparisons using Tukey-Kramer

Level						Mean
4Layers 4.72P with POF	A					22.02
4Layers 4.72P without POF	A	B				20.31
2Layers 4.72P without POF	A	B				19.68
3Layers 4.72P without POF	A	B	C			18.59
2Layers 4.72P with POF		B	C			18.50
3Layers 4.72P with POF			C	D		15.42
4Layers 1.57P with POF				D	E	11.97
4Layers 1.57P without POF					E	11.83
2Layers 1.57P without POF					E	10.95
3Layers 1.57P with POF					E	10.92
3Layers 1.57P without POF					E	10.06
2Layers 1.57P with POF					E	9.83

A.7 Normalized tensile stress (cN/Tex) statistical analyses

Table A.26 Total tex ANOVA

Source	DF	Sum of Squares	Mean Square	F Ratio	Prob > F
Factor	11	2110.7674	191.888	6.9929	<.0001*
Error	48	1317.1399	27.440		
C. Total	59	3427.9073			

Table A.27 Total tex mean's comparisons using Tukey-Kramer

Level					Mean
4Layers 1.57P with POF	A				72.313120
3Layers 1.57P without POF	A	B			69.353620
2Layers 1.57P with POF	A	B			68.771560
2Layers 1.57P without POF	A	B			68.461340
3Layers 1.57P with POF	A	B			67.136540
2Layers 4.72P without POF	A	B	C		63.628420
3Layers 4.72P without POF	A	B	C		63.373160
4Layers 1.57P without POF	A	B	C		63.244660
2Layers 4.72P with POF	A	B	C	D	62.208860
3Layers 4.72P with POF		B	C	D	60.437040
4Layers 4.72P without POF			C	D	54.857920
4Layers 4.72P with POF				D	50.876700

A.8. Composite sample cross section preparation

Composite samples with embedded POF were prepared for the optical analysis by rough grinding and polishing. Grinding is a required step to removes large cracks, micro cracks, and mounting resin debris. Grinding process also can be used to adjust the sample level to acquire the desired information. Grinding was followed by rough polishing to acquire better surface quality with less surface roughness. **Figure A.24** shows optical picture for sample before and after preparation. Four level of grinding were conducted on samples followed by one level of polishing. Abrasive papers made of silicon carbide with different grade were

used. All presented abrasive paper grades level were according to Federation of European Producers of abrasive (FEPA) and noted by P-grade abrasive grit size. Composite samples were cut and mounted in middle castable mounting molds ring with 1 inch diameter. Acrylic resin was used for casting and holding specimens.

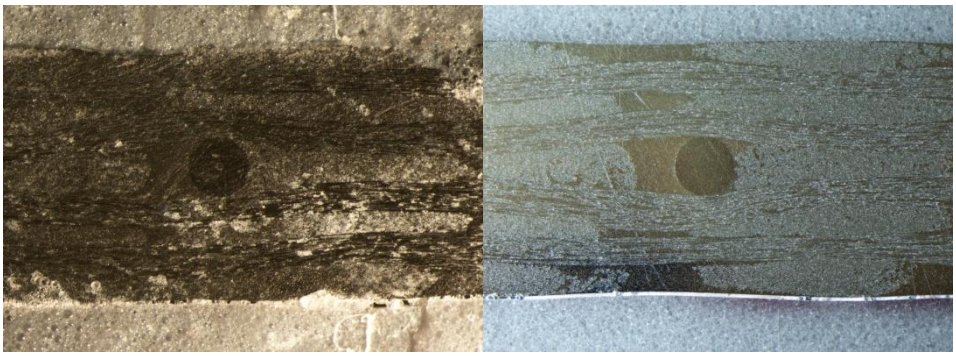

Figure A.24 Composite sample before preparation (Left) and after preparation (Right)

All grinding process performed manually, for stages of grinding process starts with low grit (more aggressive) and ends with high grit (finer). First stage of grinding was conducting on prepared specimens using aggressive abrasive silicon carbide paper grit P-120. Aggressive grade was used to remove the excess acrylic resin and to acquire flat surface quickly without inducing any damage to the prepared samples. Water was used during all grinding process to cool the samples, to remove grinding debris, and serve as a lubricant. Grit size of the abrasive paper was increased to P-280, P-400, and P-1200. Finer grit sizes reduce the scratches on the surface and prepare the sample for polishing. After grinding process, samples was polished using micro cloth and polishing suspension 0.05 µ. Polishing suspension was used to produce excellent surface finishes and reduce staining of the samples. **Figure A.25** shows all grinding and polishing stages.

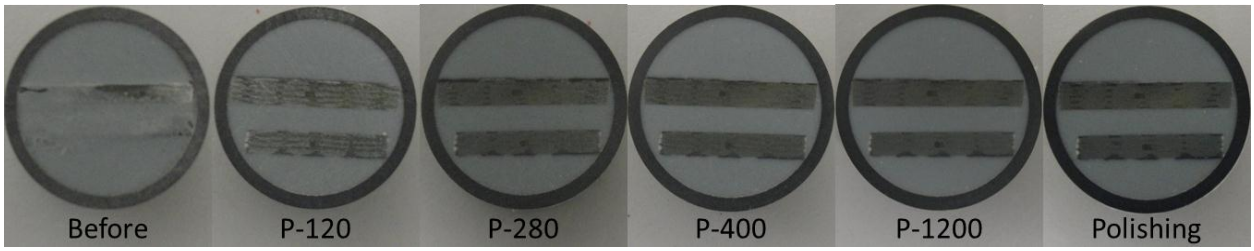

Figure A.25 Grinding and polishing stages with used abrasive silicon carbide paper

Figure A.26 - Figure A.32 show stereomicroscopic images for polished samples. Presence of embedded POF between the 3D preform layers caused the appearance of resin pockets. No presence of voids was notices in all samples except the four layers sample with pick density 1.57. All preforms with low pick density of 1.57 picks/cm/layer showed an eye shape for the resin pockets. As the pick density increases as the shape and size of resin pockets decrease. Z-yarn was located between each y-yarn; **Figure A.31**shows decrease on resin size next to embedded POF. Bending and tensile tests showed no significant reduction on samples stress on most of tested samples. Presented images also showed the presence of resin pockets in different location where the POF was absent. All images showed no occurred damage or change on embedded POF.

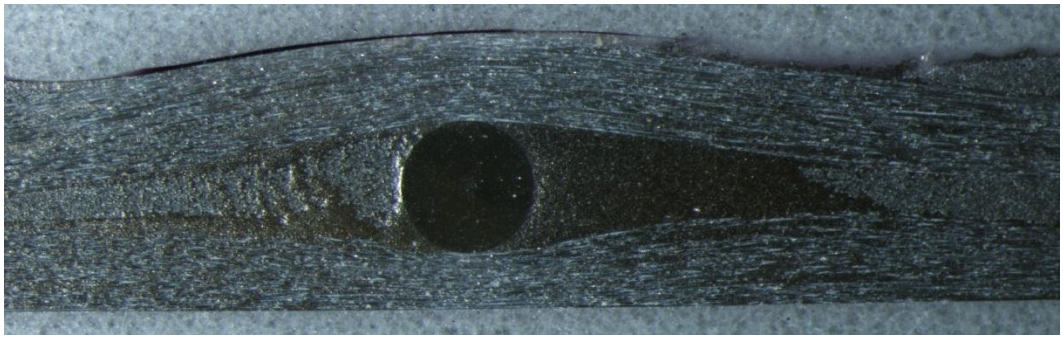

Figure A.26 Cross section of sample 2 with embedded POF

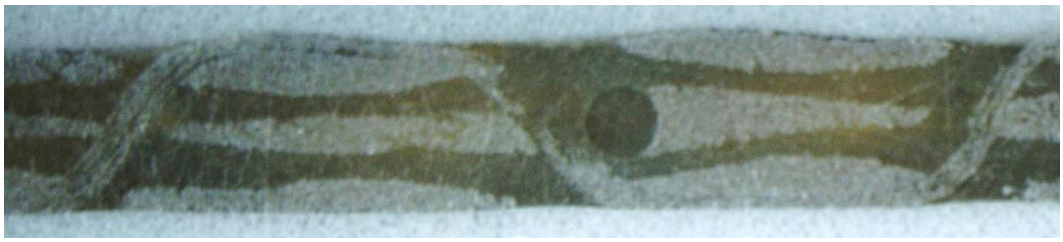

Figure A.27 Cross section of sample 4 with embedded POF

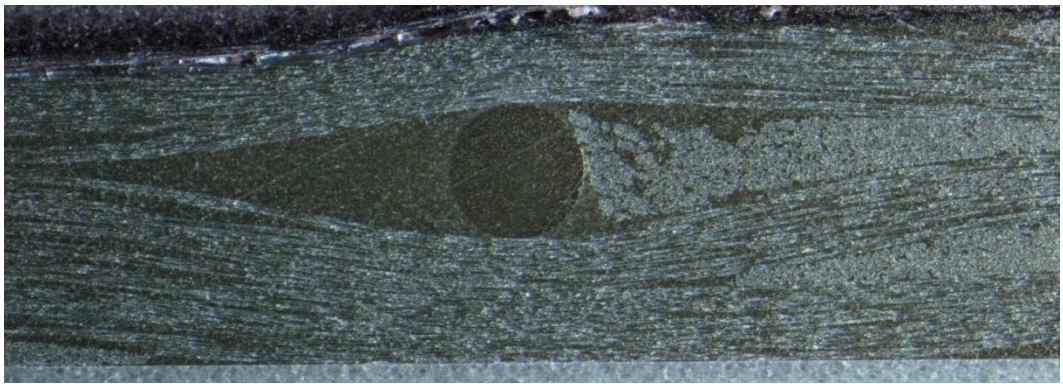

Figure A.28 Cross section of sample 6 with embedded POF

Figure A.29 Cross section of sample 8 with embedded POF

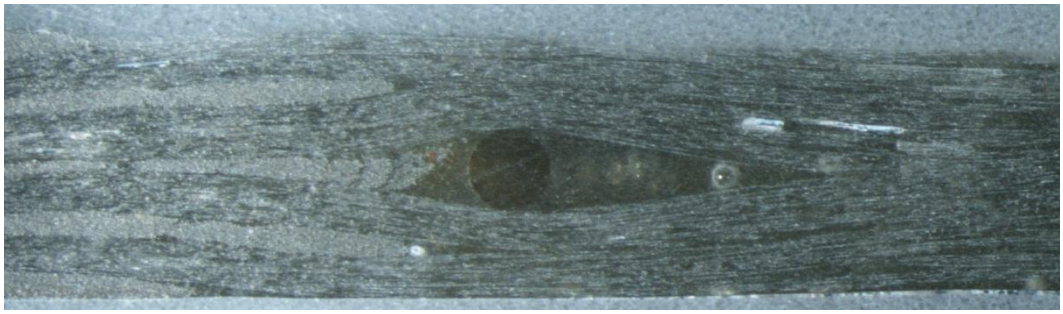

Figure A.30 Cross section of sample 10 with embedded POF

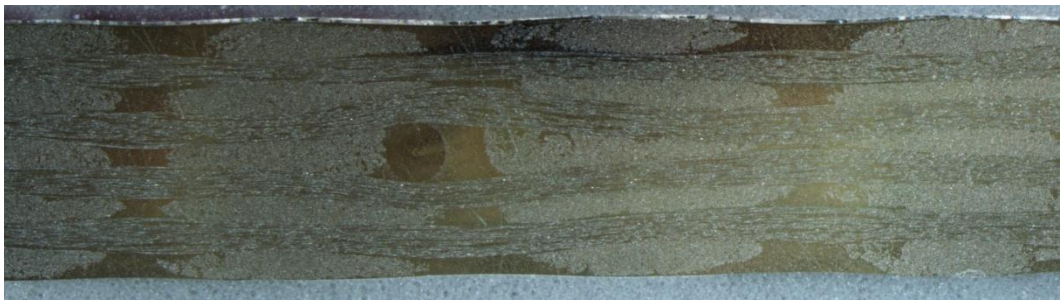

Figure A.31 Cross section of sample 12 with embedded POF (y-yarn level)

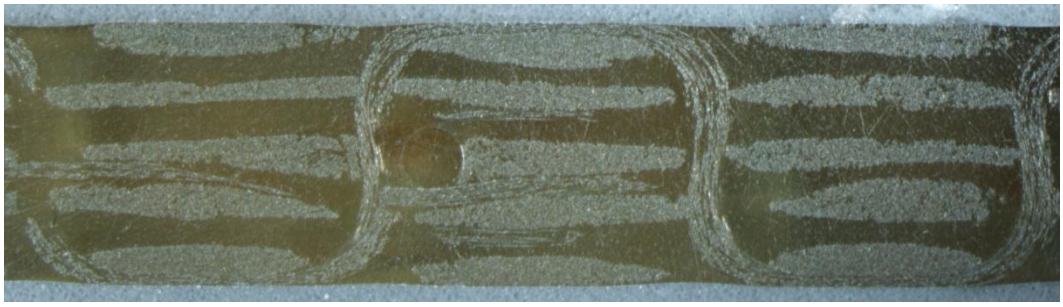

Figure A.32 Cross section of sample 12 with embedded POF (z-yarn level)

B. Signal loss under mechanical tests (3-point bending) of tested samples (chapter 7)

3D orthogonal woven composite fabrication process

Vacuum resin infusion technique was used to fabricate the 3D composites. In this process a vacuum pressure is used to remove air from the sample and pull resin into the preforms. The process increases the compaction of the structure and produces composite with low resin content. Vacuum bump supplied by vacmobile.com limited. Plexiglass top was cleaned to ensure no dust or contamination that may affect the prepared composite performance, layer of release film was laid on the plexiglass to prevent the produced composite from sticking to the plexiglass. Prepared 3D preform was laid on the release film (Figure B.1).

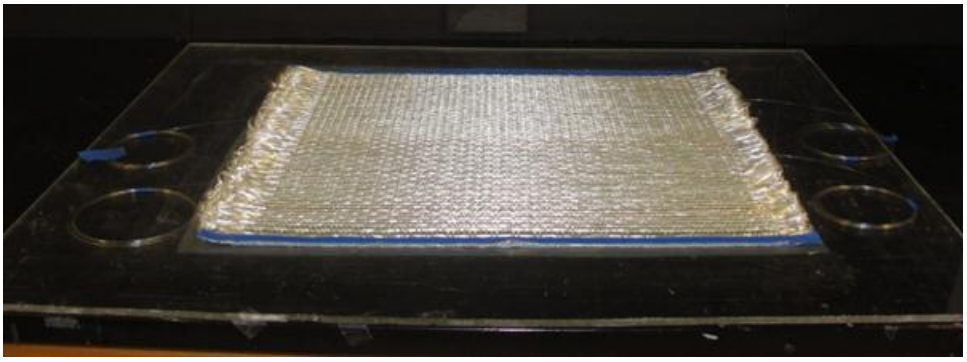

Figure B.1 3D preform laying on top of the release film on top of a clean plexiglass surface

Sealant sticky tape was used and placed around the preform to provide a good sealing to the vacuum bag when it placed. Then, Protruded POF threaded into 2 mm furcation tube to provide protection to POF during the fabrication process. furcation tubes was placed carefully on top of the sticky tape and additional small piece of sticky tape was placed on top of the furcation tube to ensure that no air gap that may cause air leak during the vacuum process (Figure B.2).

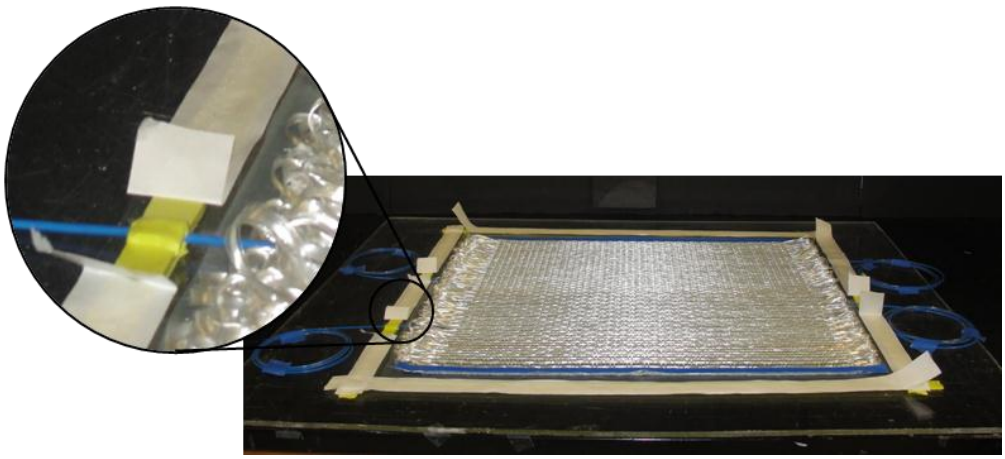

Figure B.2. Sticky tape placed around 3D preform

Nylon woven peel ply layer was placed on top of the 3D preform to ensure good and even resin distribution during the infusion process. Then, Resin flow media was placed on top of the peel play layer to allow a quick flow for resin and to travel fast across the preform during the infusion. For resin inlet and outlet, 1.5 cm diameter spiral tube was placed on both edges of the preform. Both inlet and outlet spiral tubes were connected to 1.5 cm diameter flexible polyethylene tube, inlet tube will be connected to resin supply and outlet tube will be connected to the vacuum bump. Spiral tube along the 3D preform edges were used to ensure good resin distribution along the preform. Sticky tape was used to hold both inlet and outlet on place. Nylon bagging film was used to cover the preform by sealant tape. Nylon bagging film was high temperature resistance, puncture resistance, and stretchable, which is very important to withstand the applied vacuum and prevent any air leak during the infusion. Also good attachment between the sealant tape and bagging film is critical to ensure the sealing process and prevent any air leak (**Figure B.3**).

Figure B.3. 3D preform after placing the resin inlet, outlet, and vacuum bagging

Vacuum bump was connected to resin outlet tube and resin inlet was connected to absolute pressure gage. 100 kPa negative pressure was applied to the prepared preform, ultrasonic air detector was used to find any air leaks or holes that may cause air leak. **Figure B.4** shows the 3D preform after applying vacuum, vacuum bump was switched off for 1 hour with observation to the vacuum gage to ensure that there is no air leak and the prepared sample is keeping the vacuum pressure. Then the pressure gage was disconnected and resin inlet was clamped until the resin was prepared.

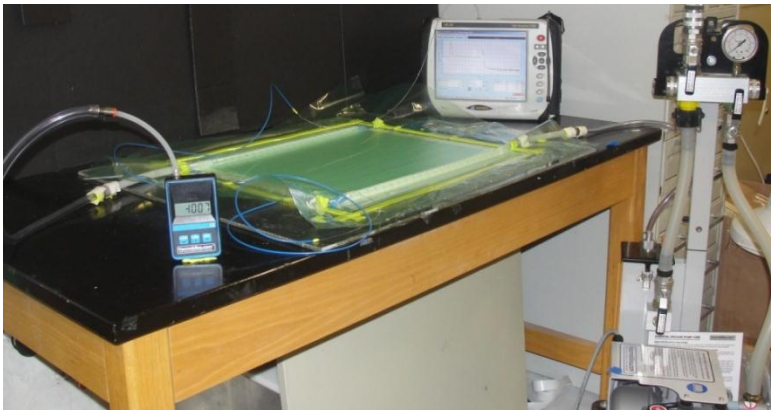

Figure B.4. Prepared preform for resin infusion under 100 kPa negative pressure

Then, 521.5 grams of resin was prepared by mixing 400 grams of Epoxy resin with 121.5 grams of hardener (mixing ratio 100:27 by weight). Prepared resin mixture had a pot life of 2 hours and curing time of 12 hours at room temperature (21º C). Prepared resin mixture was

then placed in a vacuum desiccator for degasing to removes all air bubbles that was created during stirring the mixture. Removing air bubbles from the resin mixture before the infusion will decrease the amount of void in the prepared composite and improve the performance of the produced composite. After 30 minutes, resin mixture was removed from the vacuum desiccator and carried to infusion table. Resin inlet tube was placed on the resin mixture bucket, then, vacuum pump was switched on and resin inlet was unclamped and resin start to flow from the resin bucket to spiral tube and then to the preform. When resin reached the outlet spiral tube and preform was fully impregnated with resin, resin inlet was clamped and vacuum pump was kept running for 15 minutes to take all excess resin and air (bleeding). Then vacuum bump was turned off and sample was kept for 12 hours for curing. **Figure B.5** shows the fabricated 3D woven composite with embedded POF.

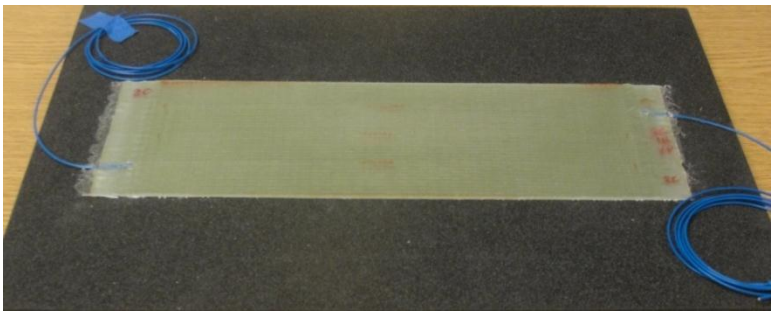

Figure B.5. Final 3D woven composite after resin infusion

B.1. Flexural stress-strain curves under incremental lad

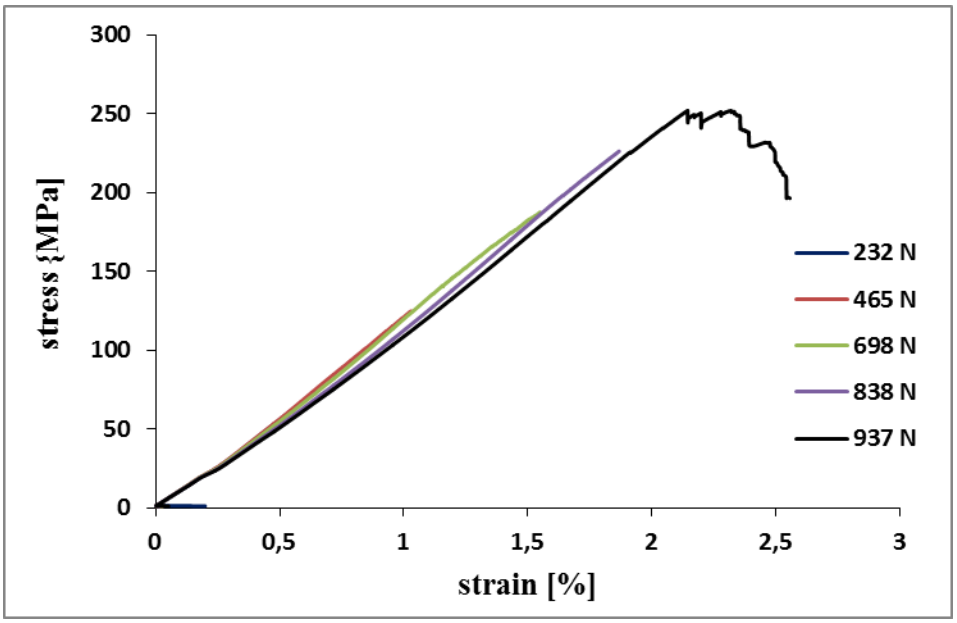

Figure B.6 Flexural stress-strain curves of sample I

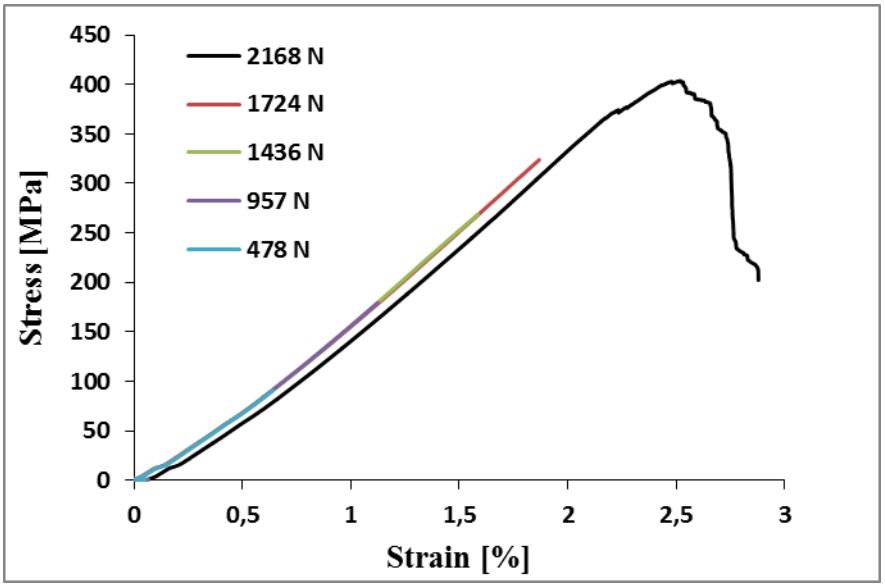

Figure B.7 Flexural stress-strain curves of sample II

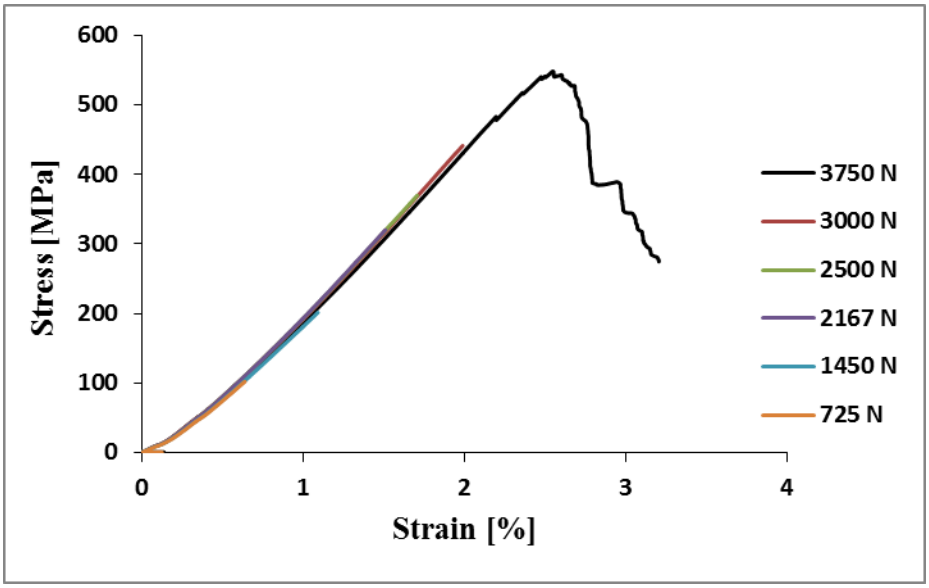

Figure B.8 Flexural stress-strain curves of sample III

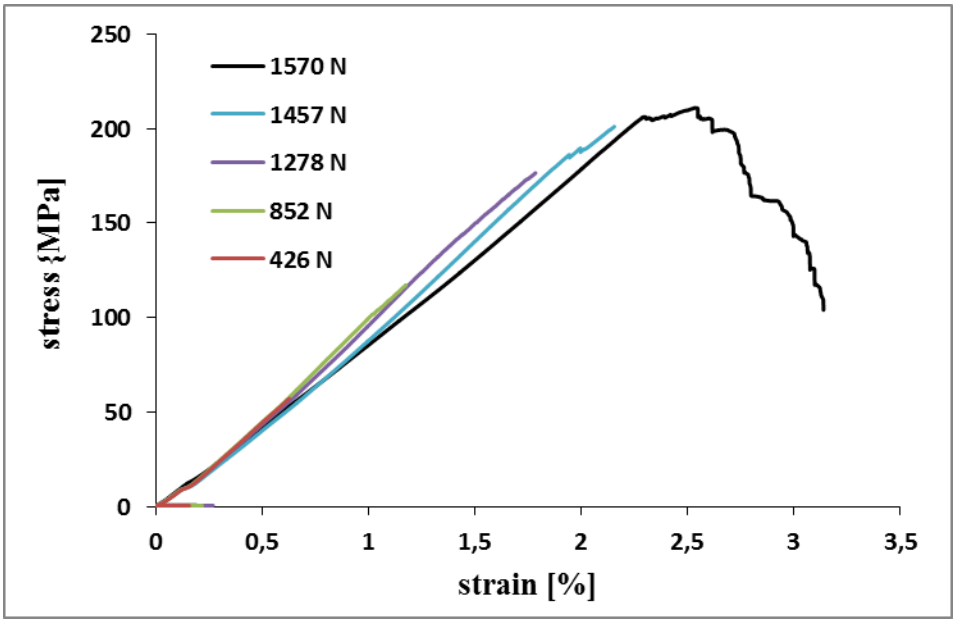

Figure B.9 Flexural stress-strain curves of sample IV

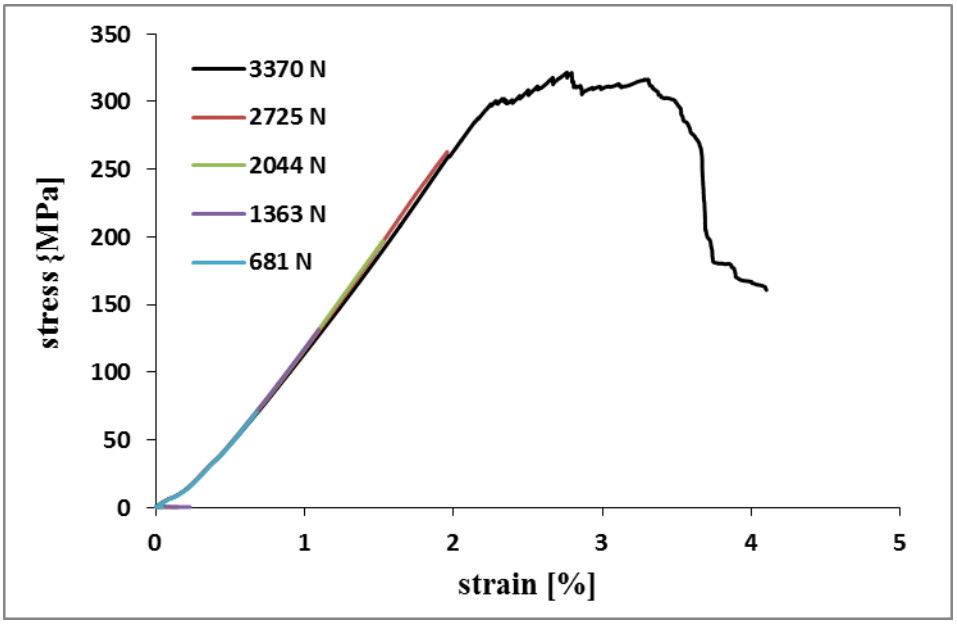

Figure B.10 Flexural stress-strain curves of sample V

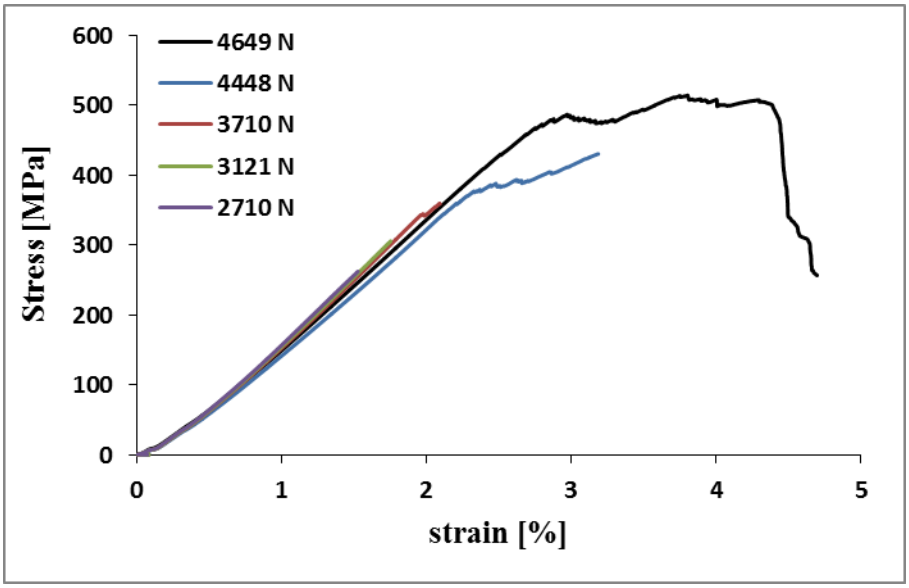

Figure B.11 Flexural stress-strain curves of sample VI

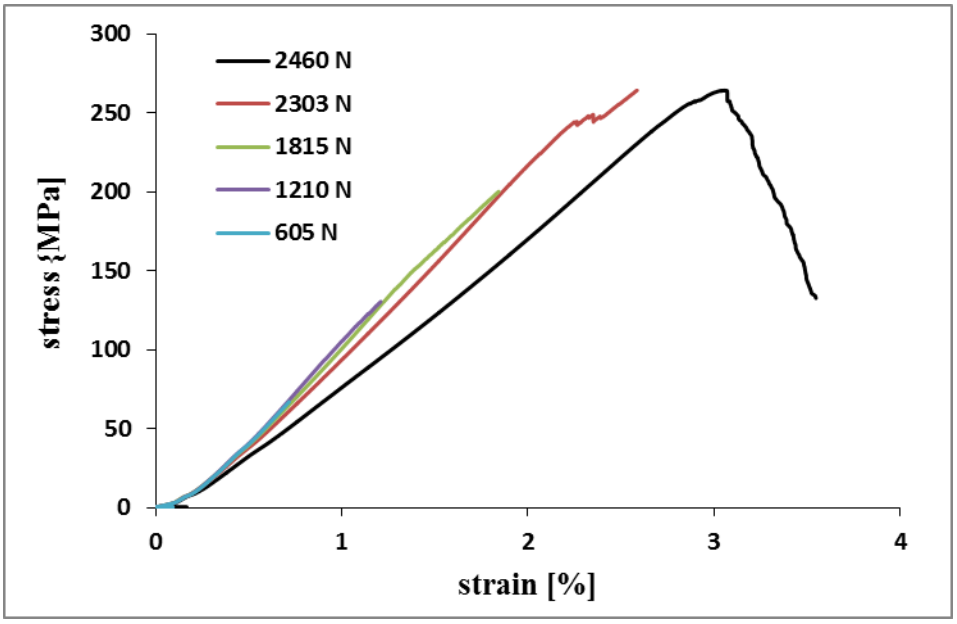

Figure B.12 Flexural stress-strain curves of sample VII

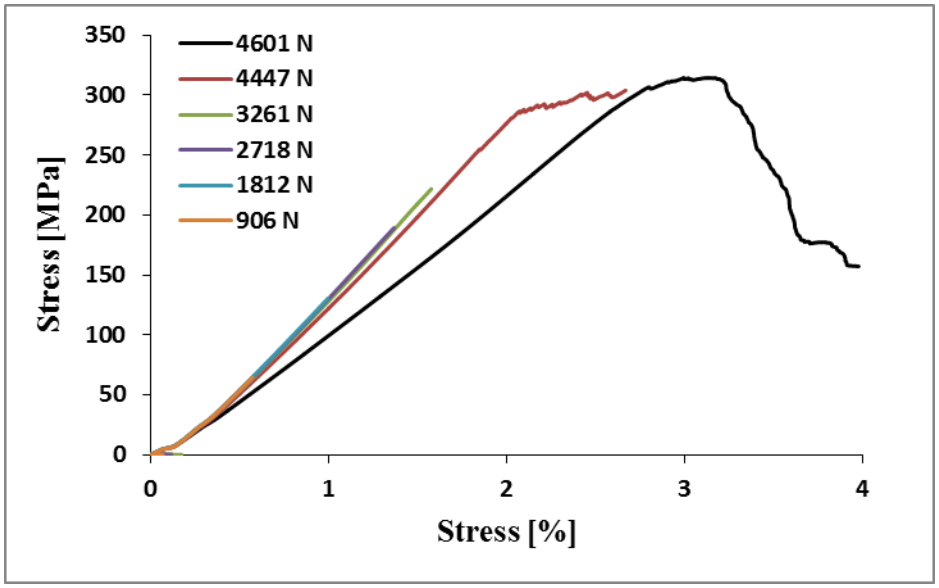

Figure B.13 Flexural stress-strain curves of sample VIII

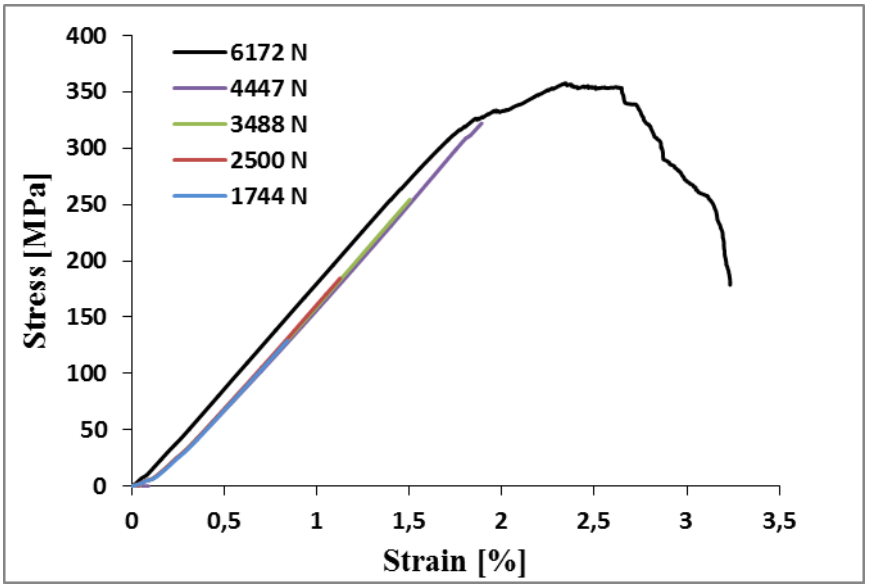

Figure B.14 Flexural stress-strain curves of sample IX

B.2 Backscattering levels under incremental load and after releasing load

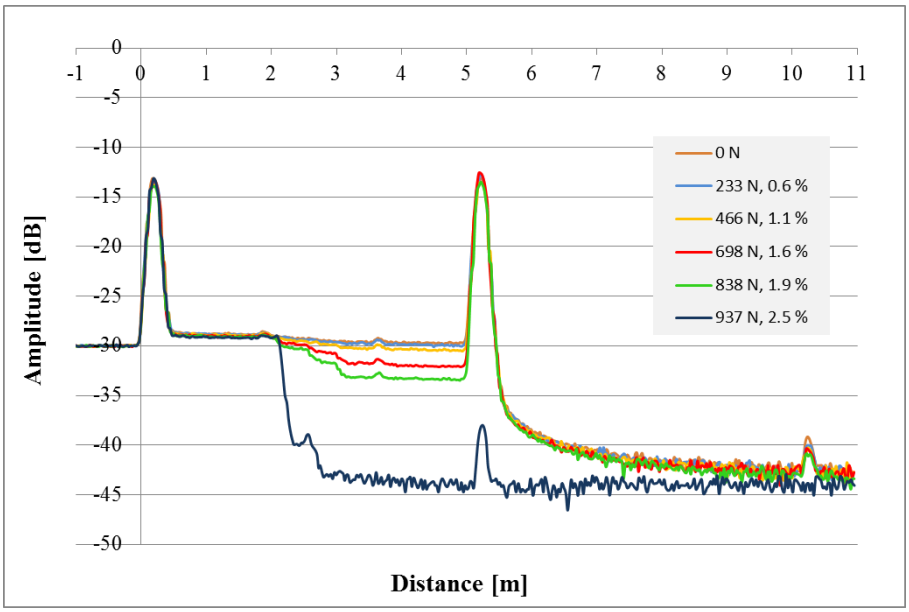

Figure B.15 Backscattering levels of sample I under bending load

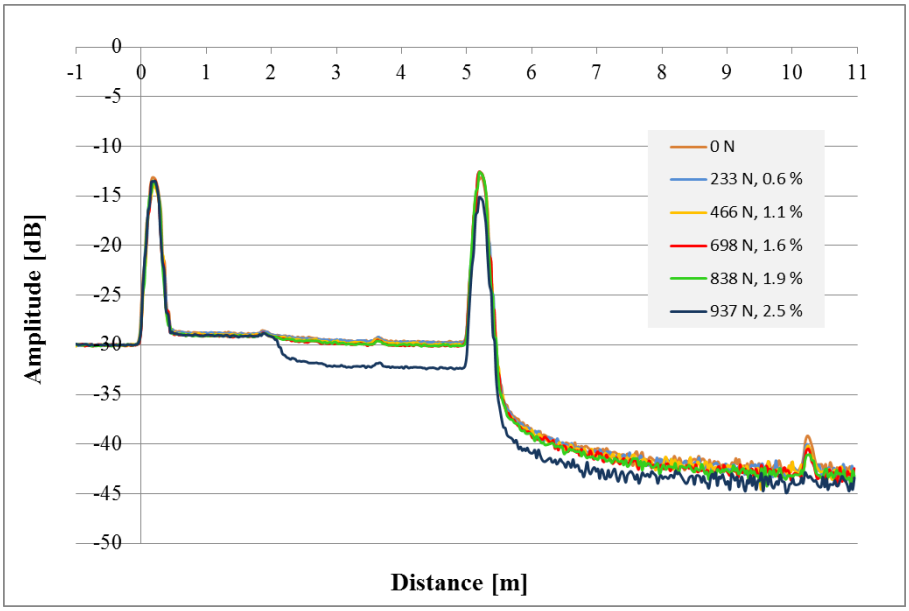

Figure B.16 Backscattering levels of sample I after releasing bending load

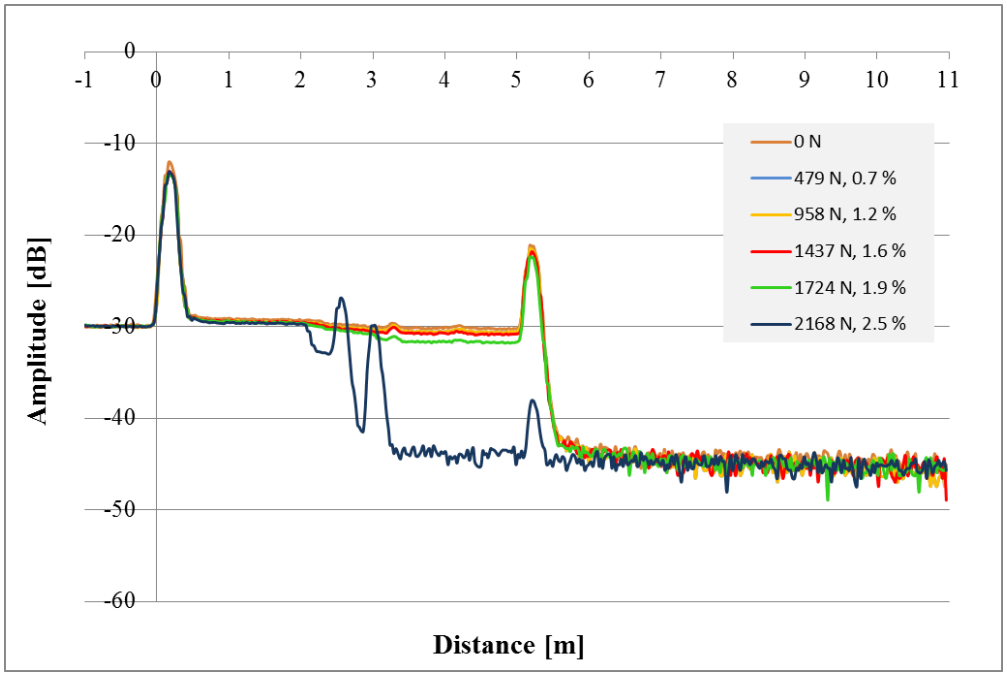

Figure B.17 Backscattering levels of sample II under bending load

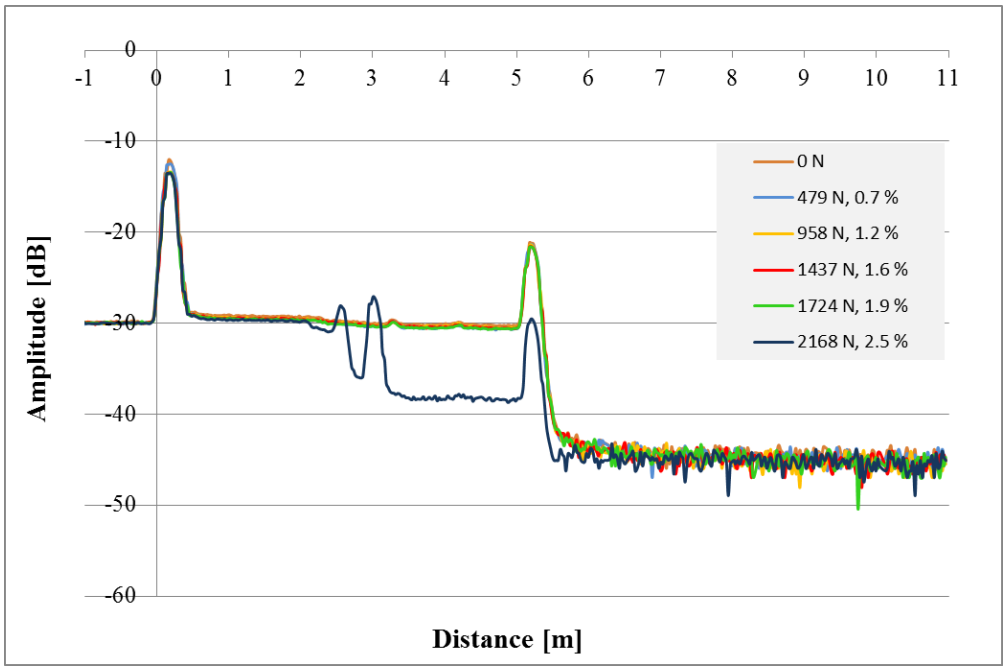

Figure B.18 Backscattering levels of sample II after releasing bending load

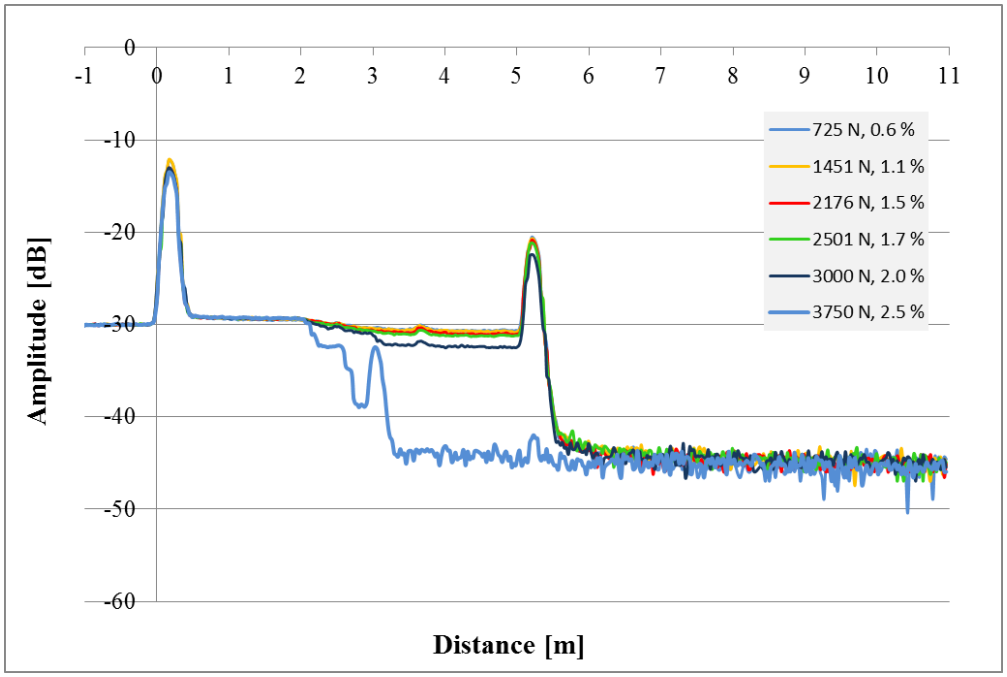

Figure B.19 Backscattering levels of sample III under bending load

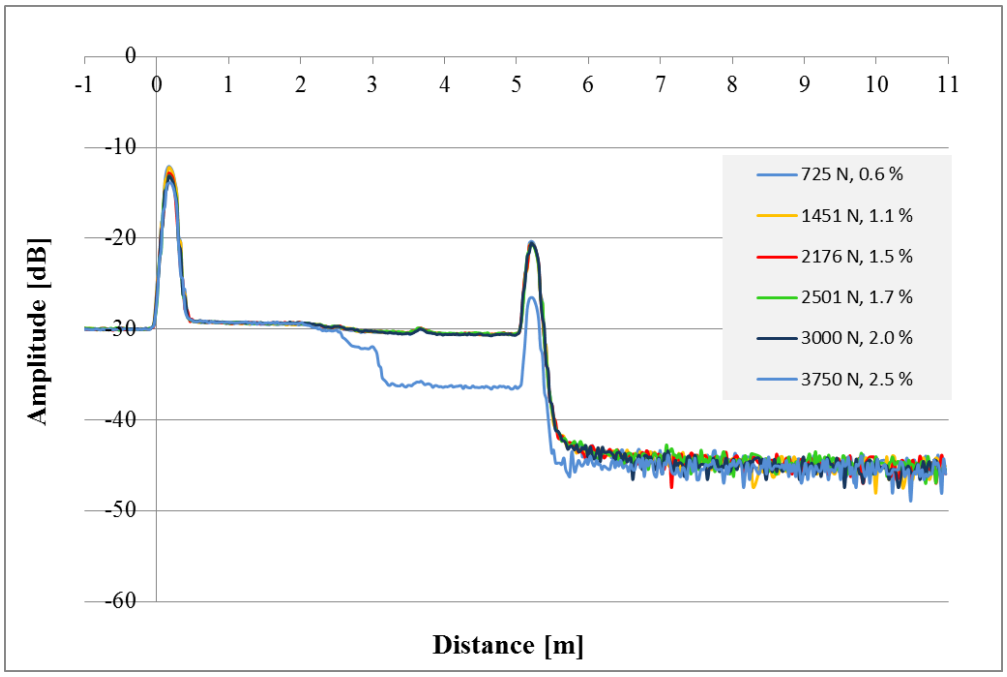

Figure B.20 Backscattering levels of sample III after releasing bending load

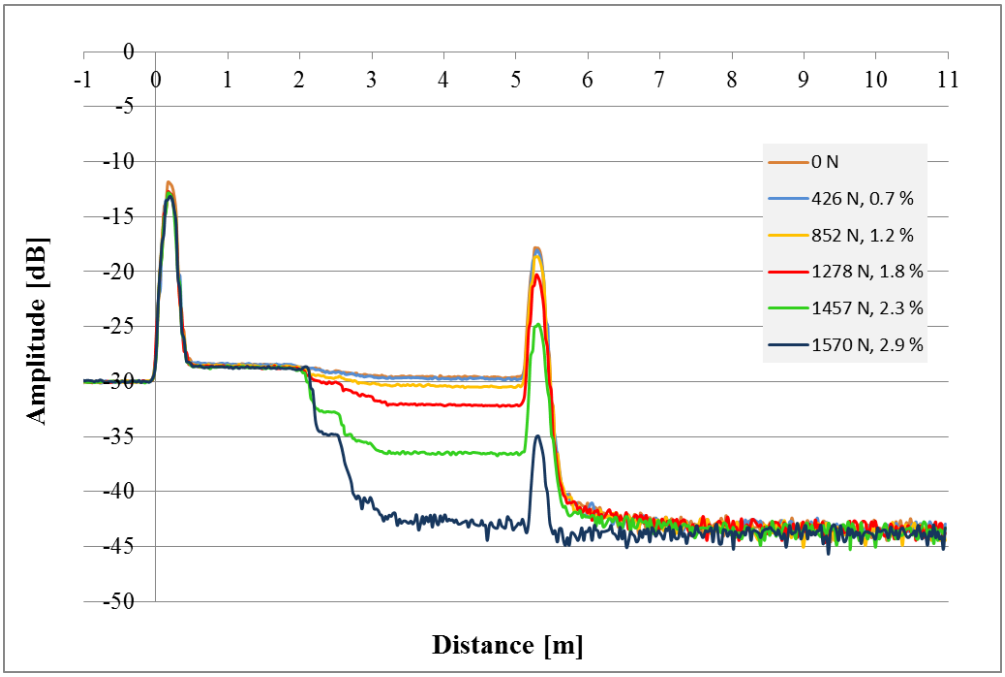

Figure B.21 Backscattering levels of sample IV under bending load

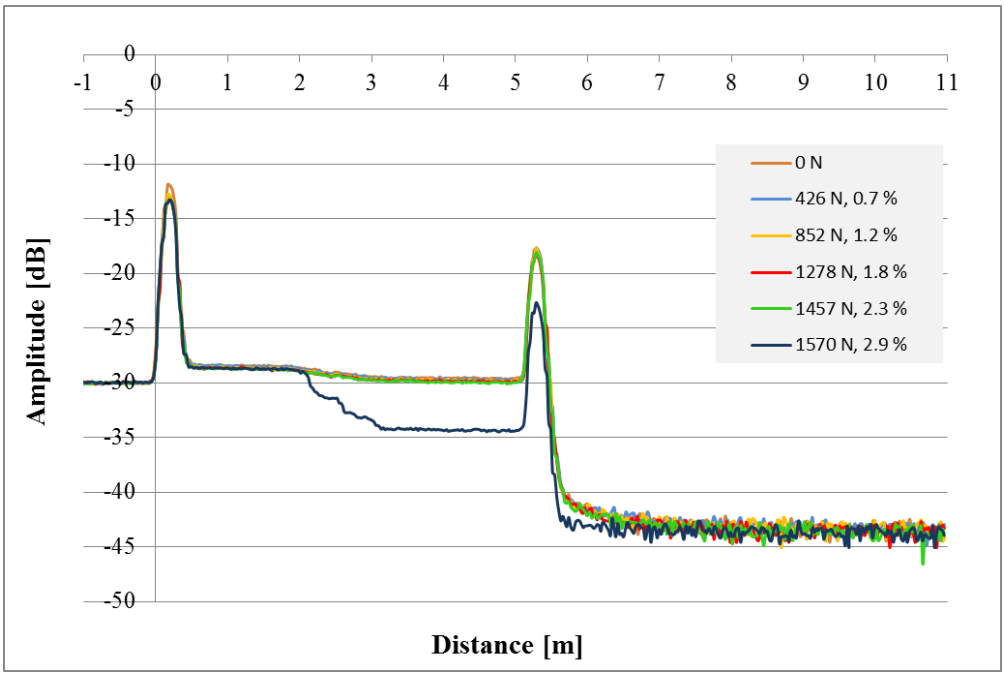

Figure B.22 Backscattering levels of sample IV after releasing bending load

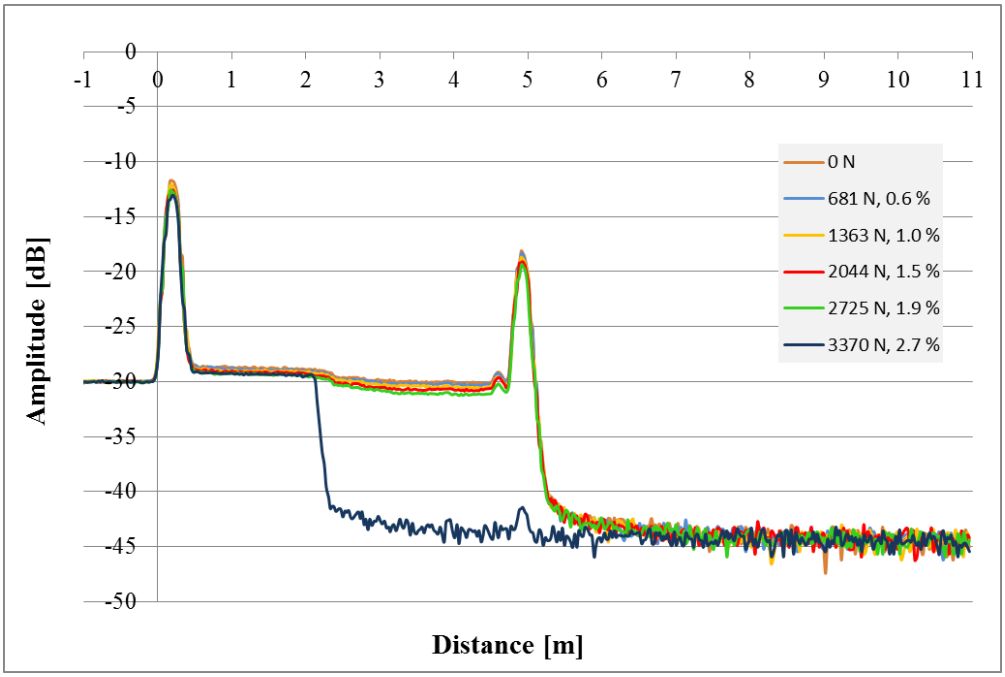

Figure B.23 Backscattering levels of sample V under bending load

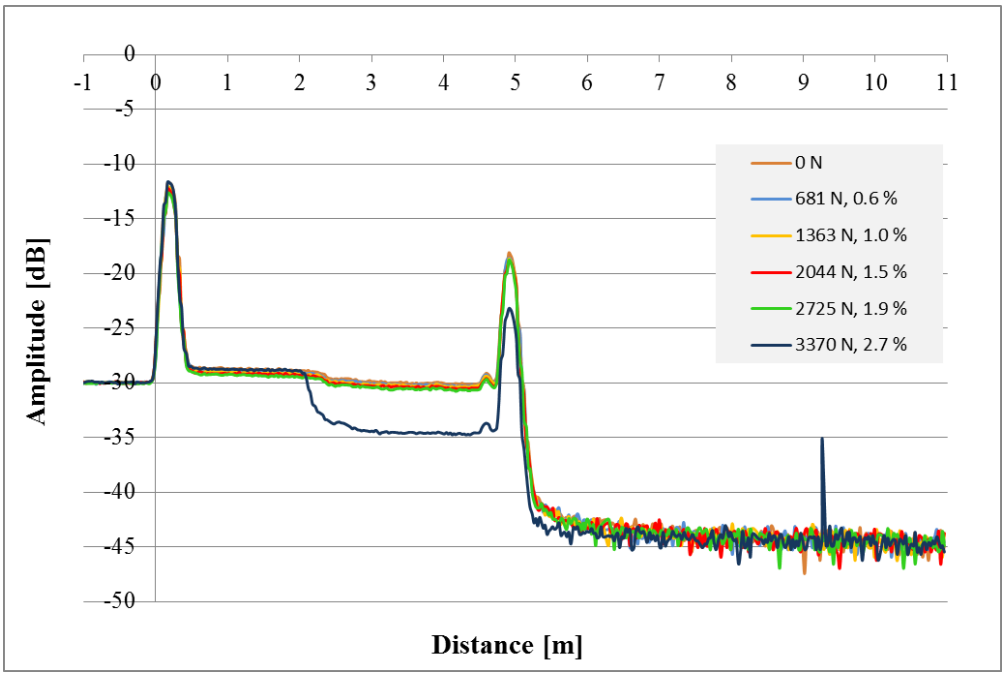

Figure B.24 Backscattering levels of sample V after releasing bending load

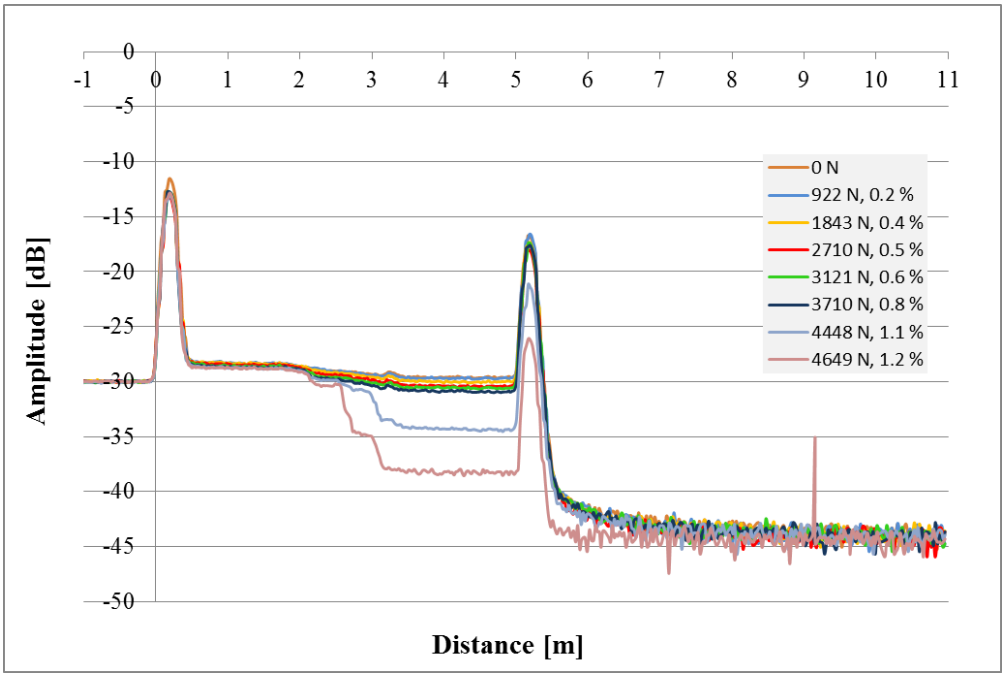

Figure B.25 Backscattering levels of sample VI under bending load

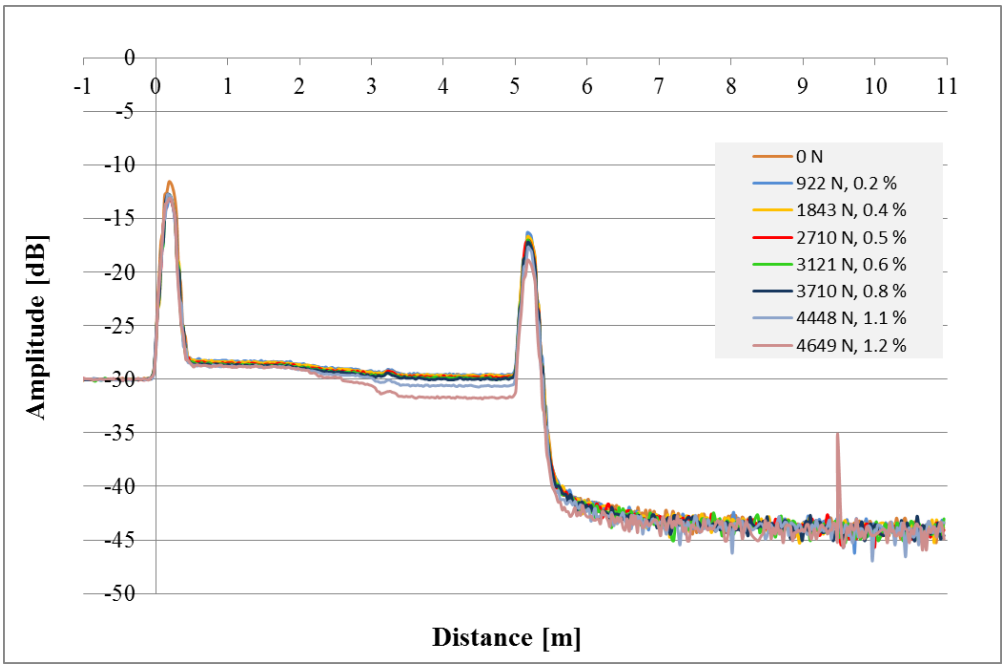

Figure B.26 Backscattering levels of sample VI after releasing bending load

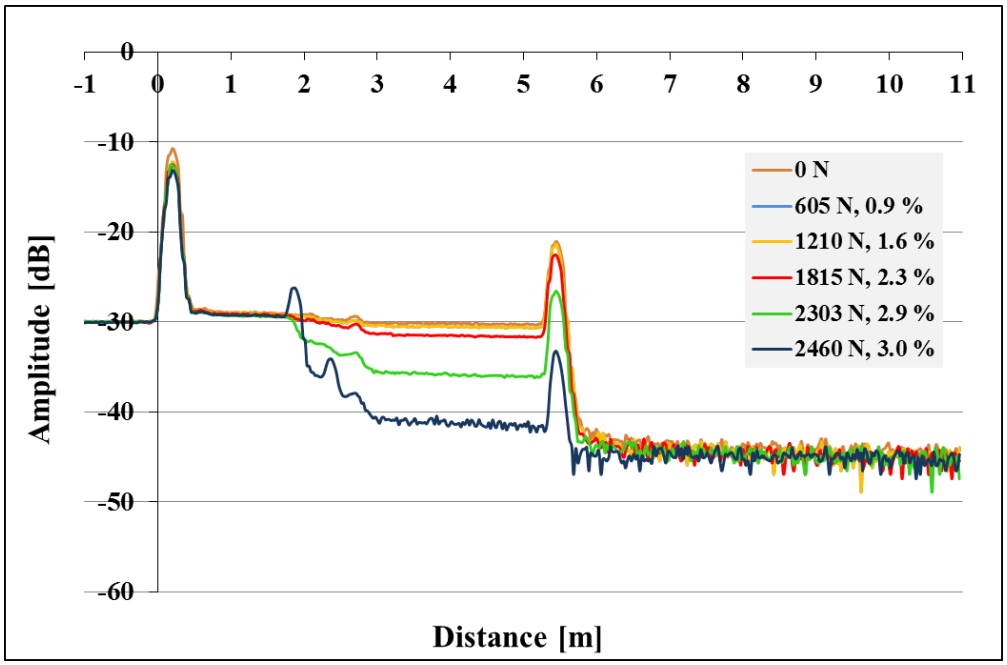

Figure B.27 Backscattering levels of sample VI under bending load

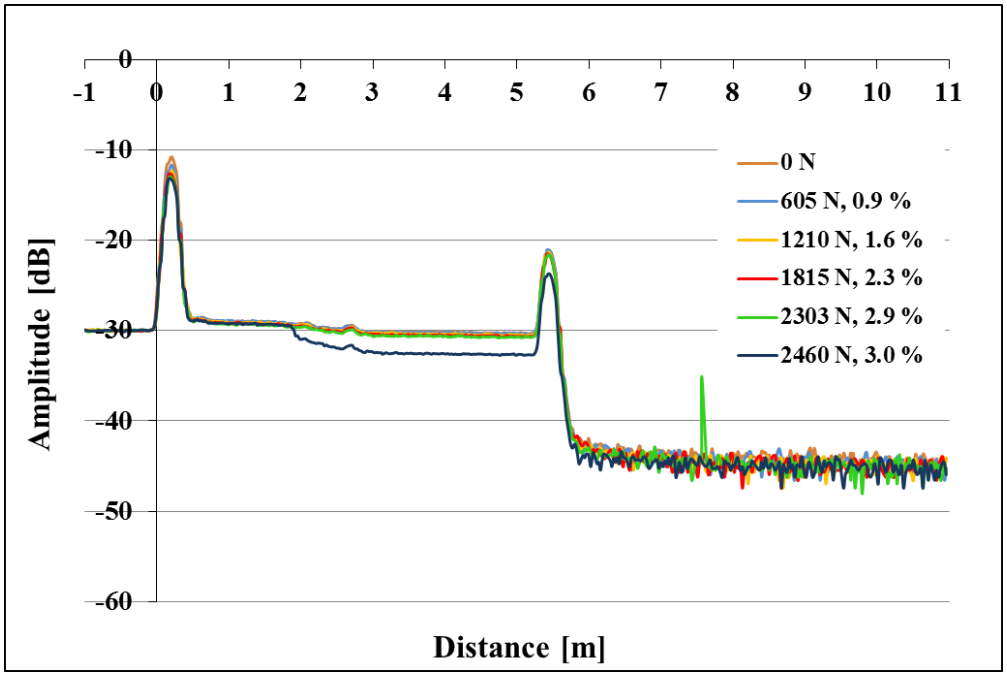

Figure B.28 Backscattering levels of sample VI after releasing bending load

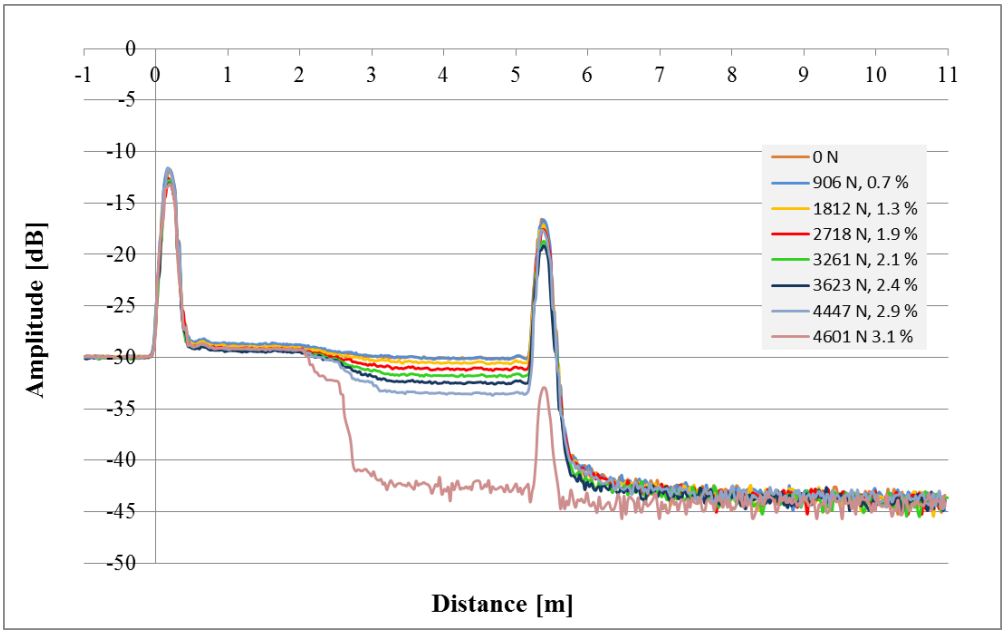

Figure B.29 Backscattering levels of sample VIII under bending load

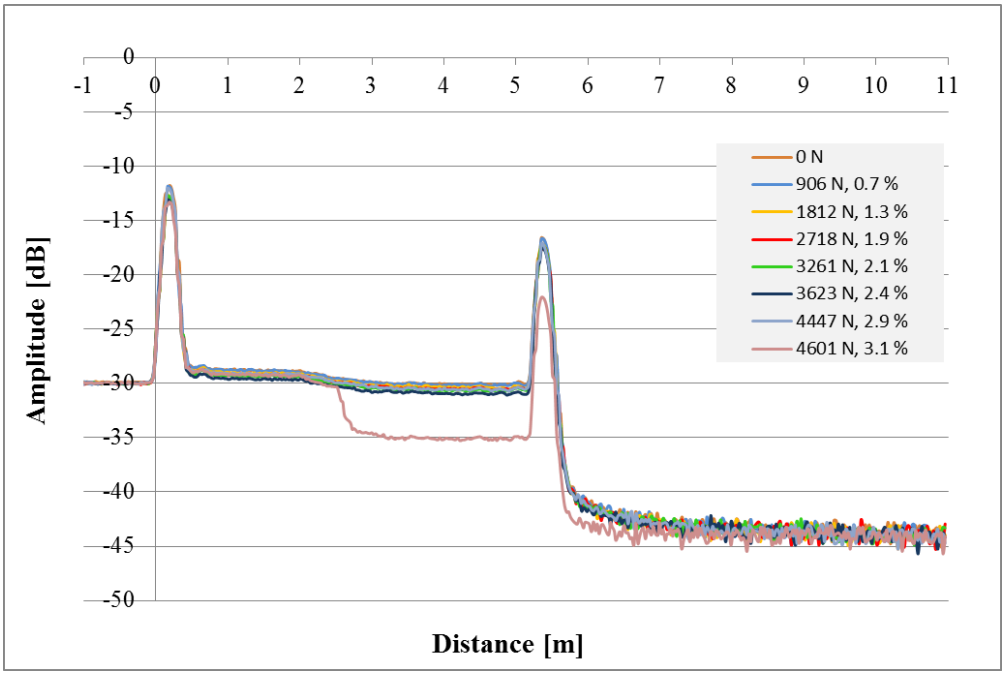

Figure B.30 Backscattering levels of sample VIII after releasing bending load

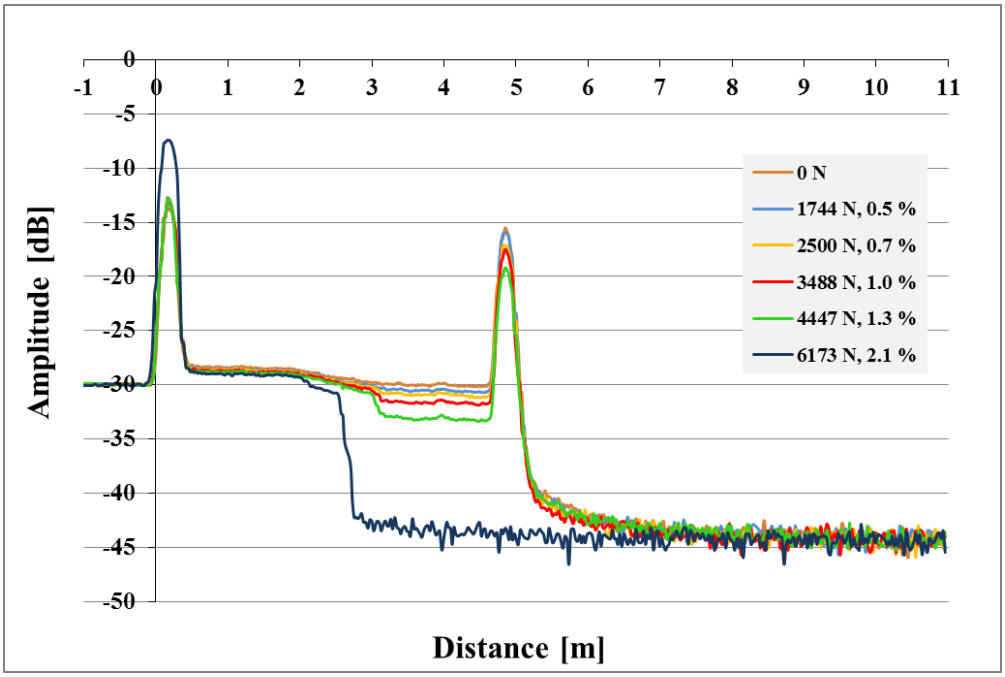

Figure B.31 Backscattering levels of sample IX under bending load

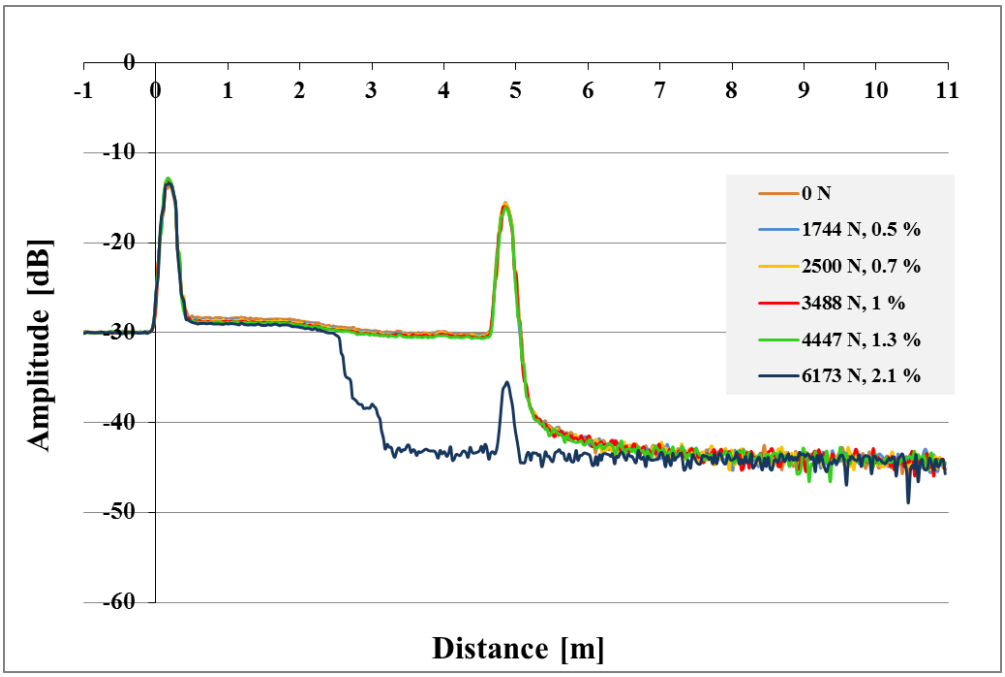

Figure B.32 Backscattering levels of sample IX after releasing bending load

B.3 Backscattering levels for all samples (chapter 7) under repeated impact of 9 J

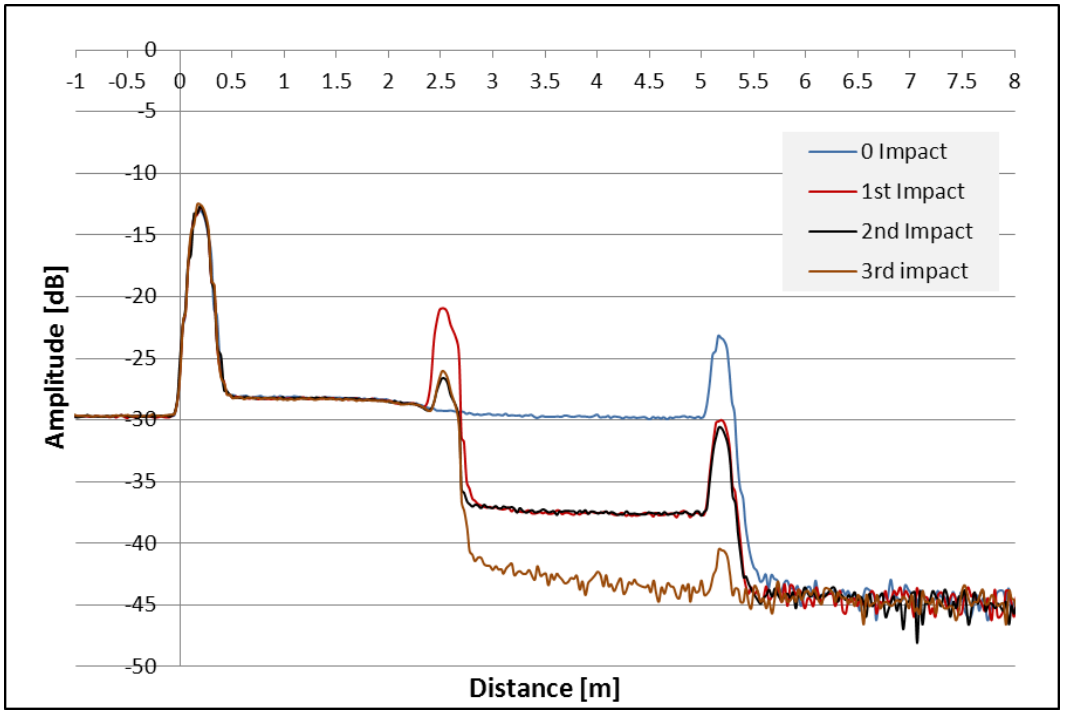

Figure B.33 Backscattering levels of sample I (2 y-yarn layers and x-yarn density of 1.57) under repeated impact

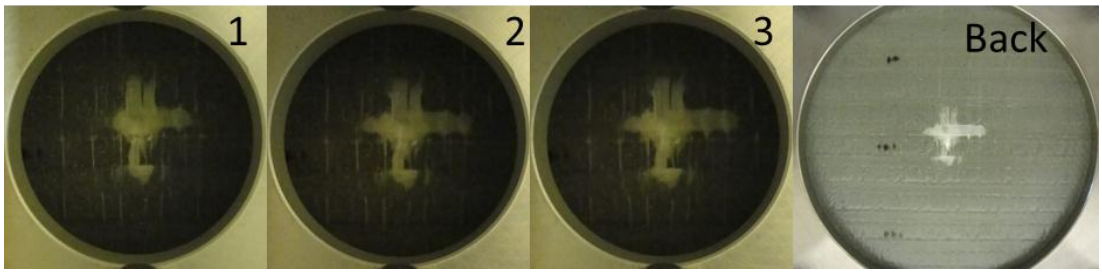

Figure B.34 Repeated impact images of sample I (2 y-yarn layers and x-yarn density of 1.57) under repeated impact

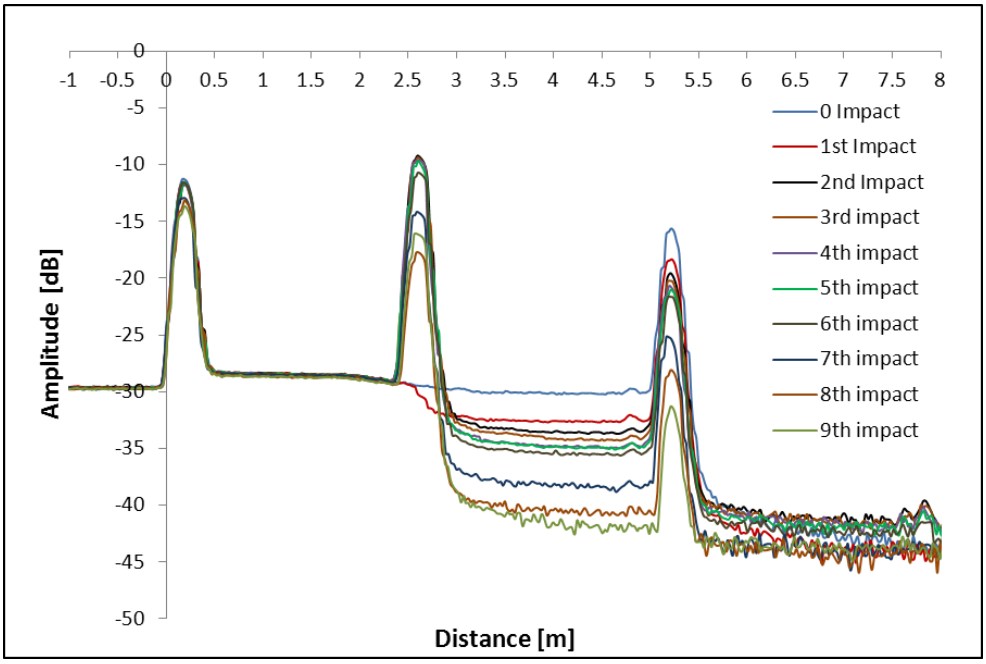

Figure B.35 Backscattering levels of sample III (2 y-yarn layers and x-yarn density of 4.72) under repeated impact

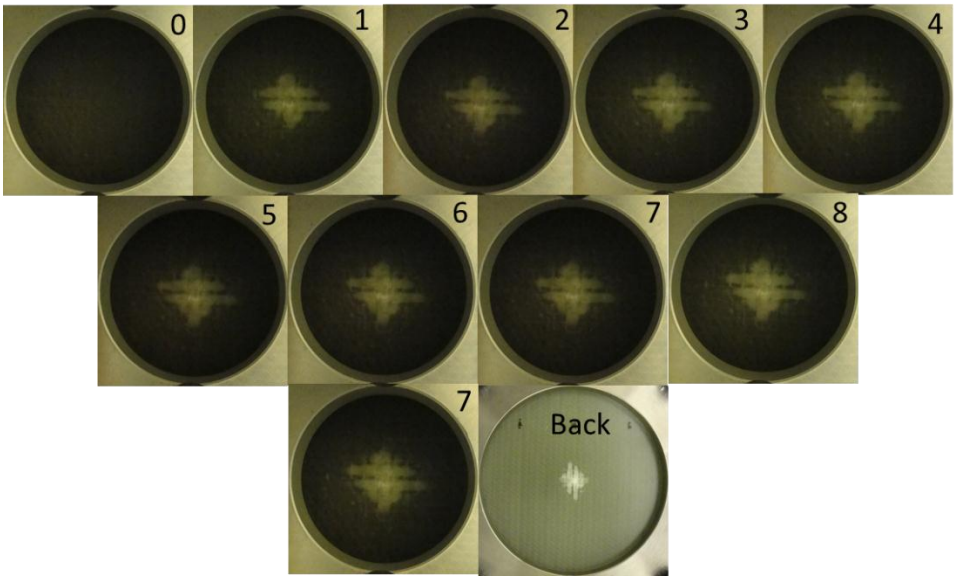

Figure B.36 Repeated impact images of sample III (2 y-yarn layers and x-yarn density of 4.72) under repeated impact

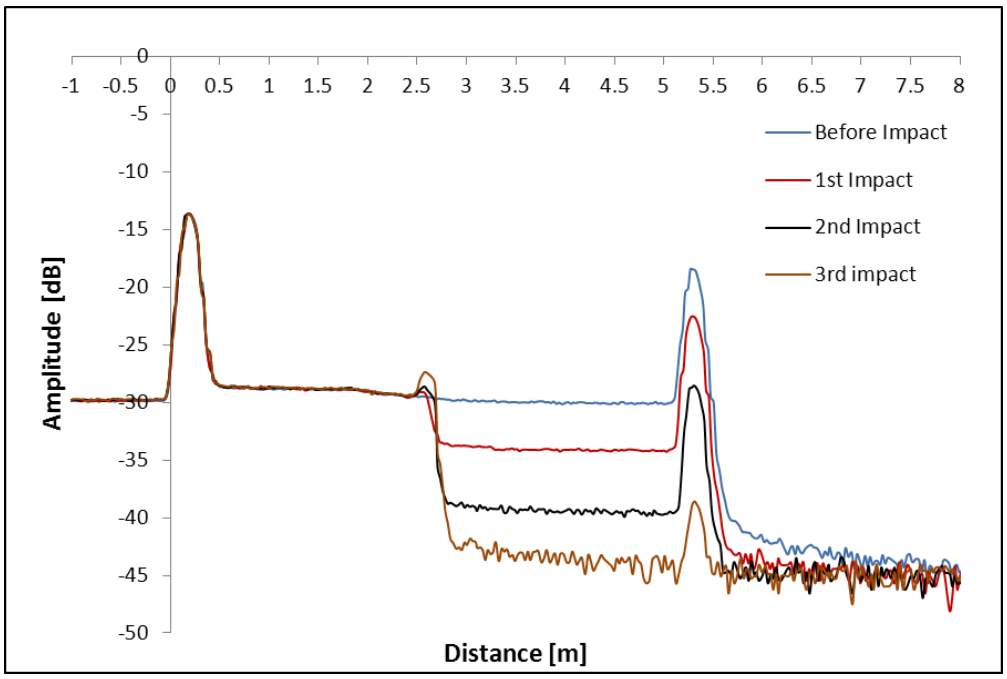

Figure B.37 Backscattering levels of sample IV of (3 y-yarn layers and x-yarn density of 4.72) under repeated impact

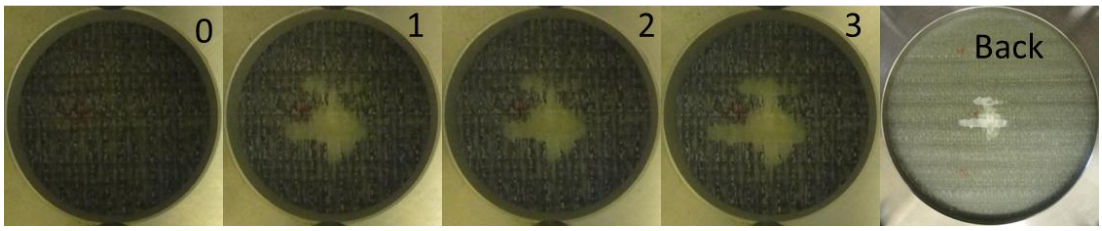

Figure B.38 Repeated impact images of sample IV (3 y-yarn layers and x-yarn density of 4.72) under repeated impact

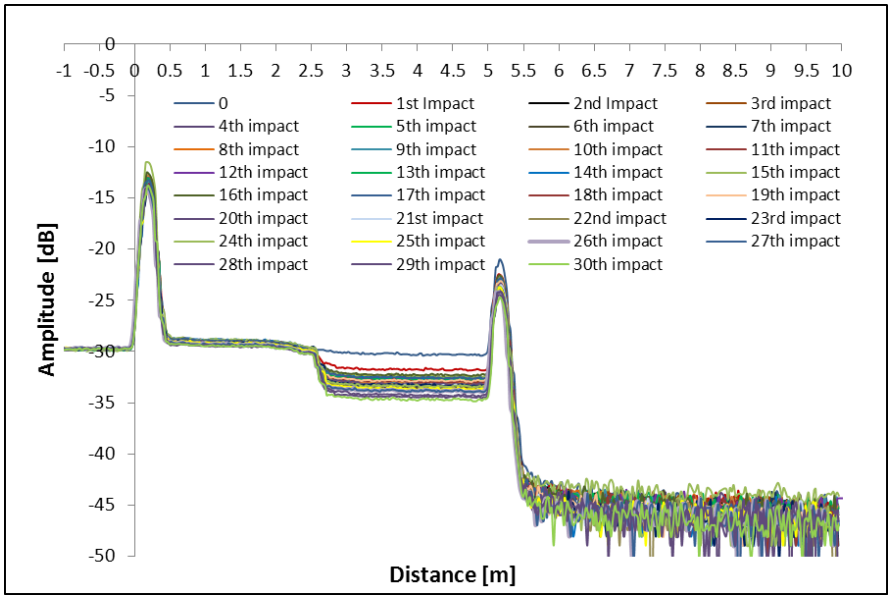

Figure B.39 Backscattering levels of sample VI (3 y-yarn layers and x-yarn density of 4.72) under repeated impact

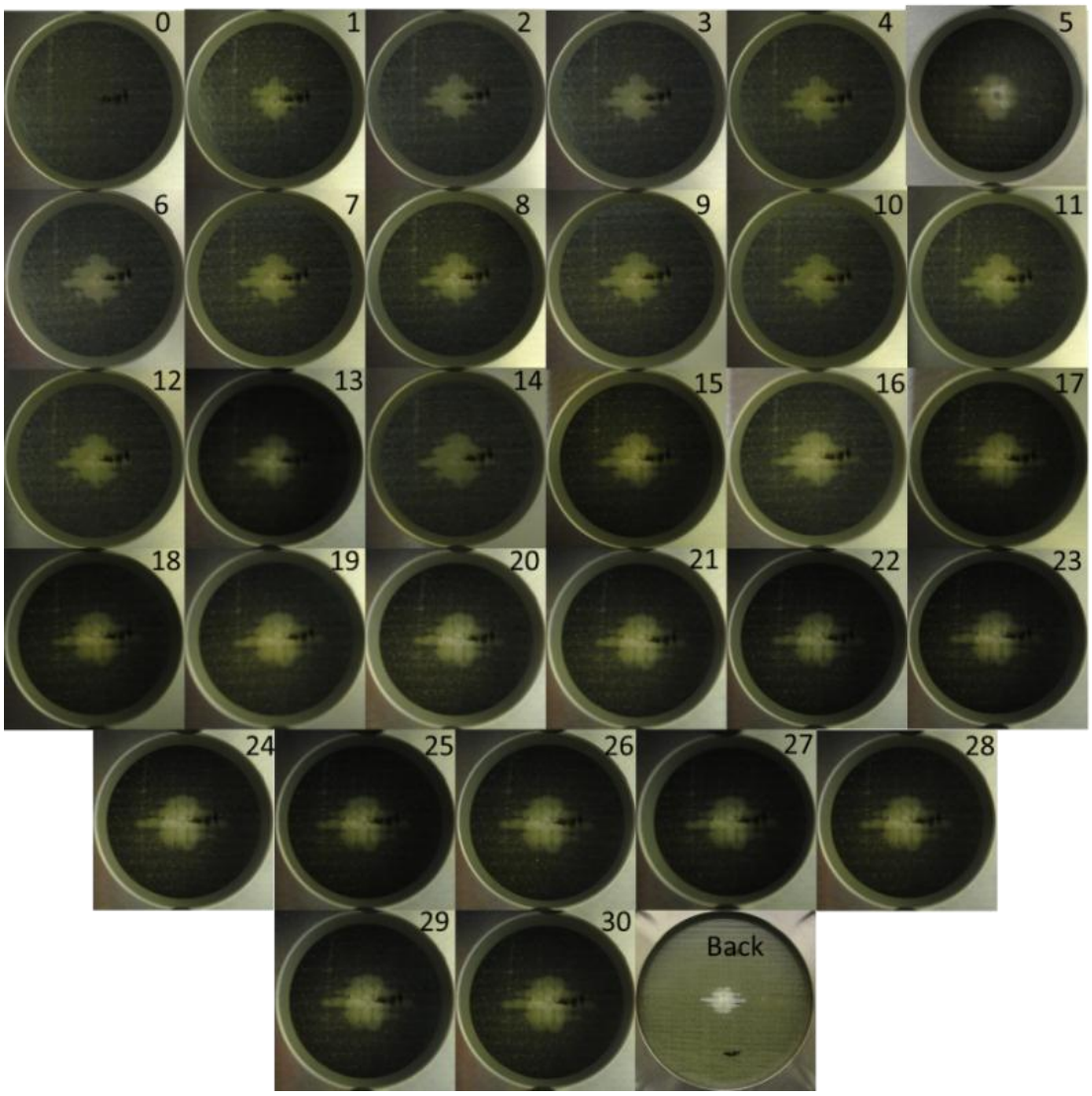

Figure B.40 Repeated impact images of sample VI (3 y-yarn layers and x-yarn density of 4.72) under repeated impact

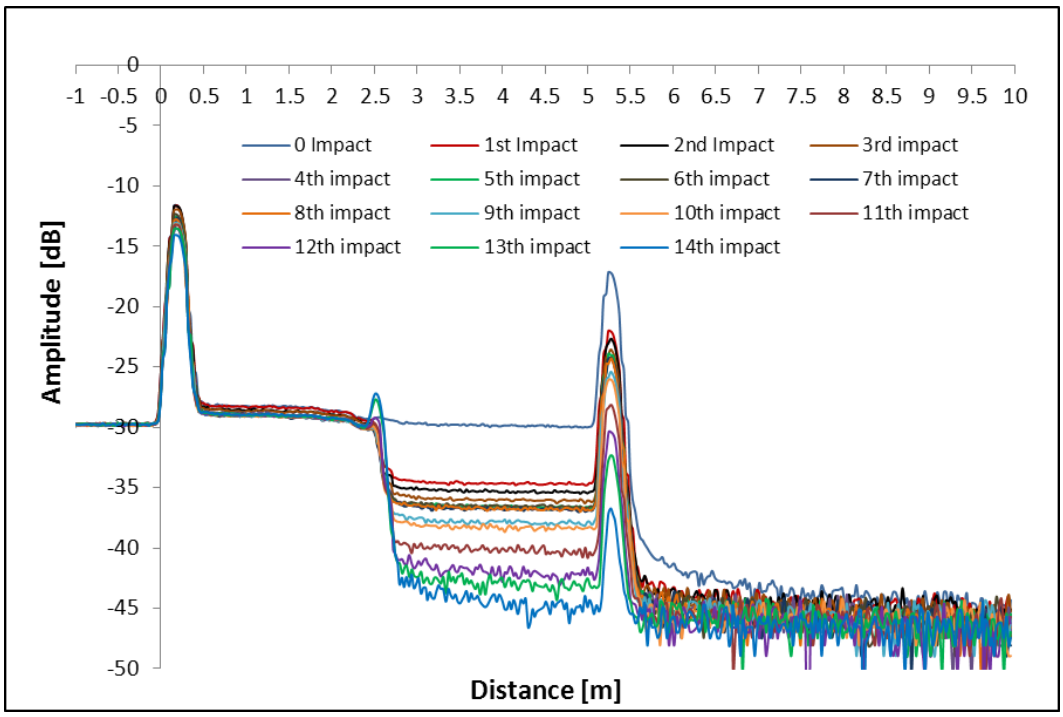

Figure B.41 Backscattering levels of sample VII (3 y-yarn layers and x-yarn density of 1.57) under repeated impact

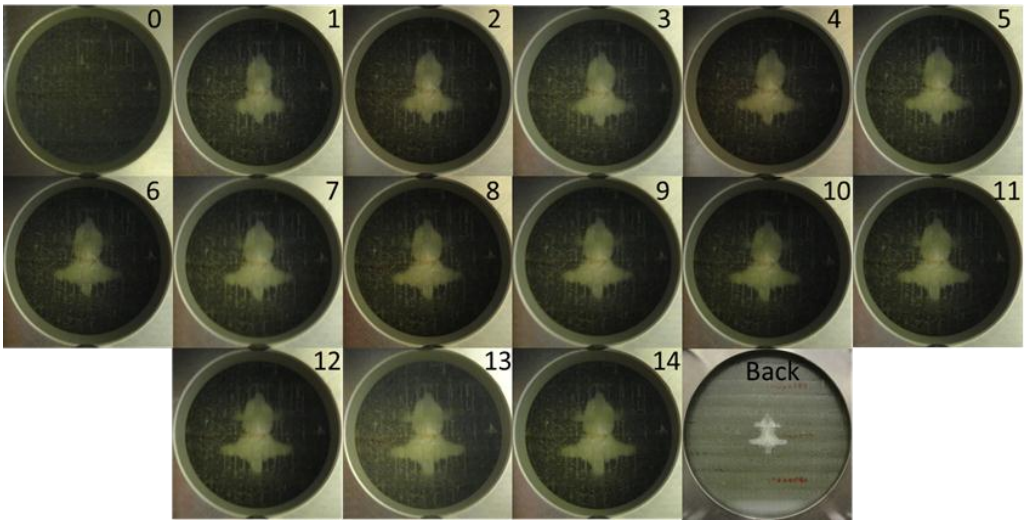

Figure B.42 Repeated impact images of sample VII (4 y-yarn layers and x-yarn density of 1.57) under repeated impact

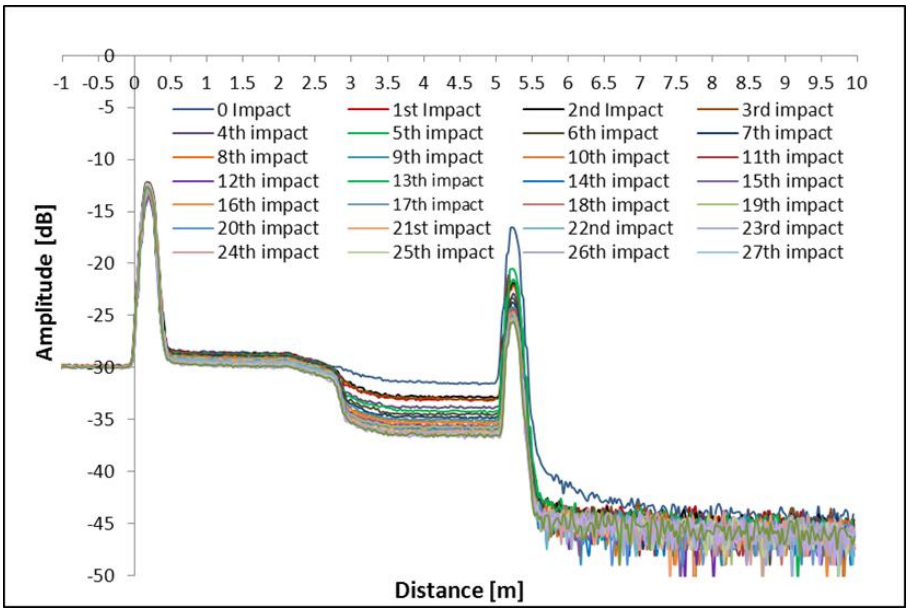

Figure B.43 Backscattering levels of sample IX (4 y-yarn layers and x-yarn density of 4.72) under repeated impact

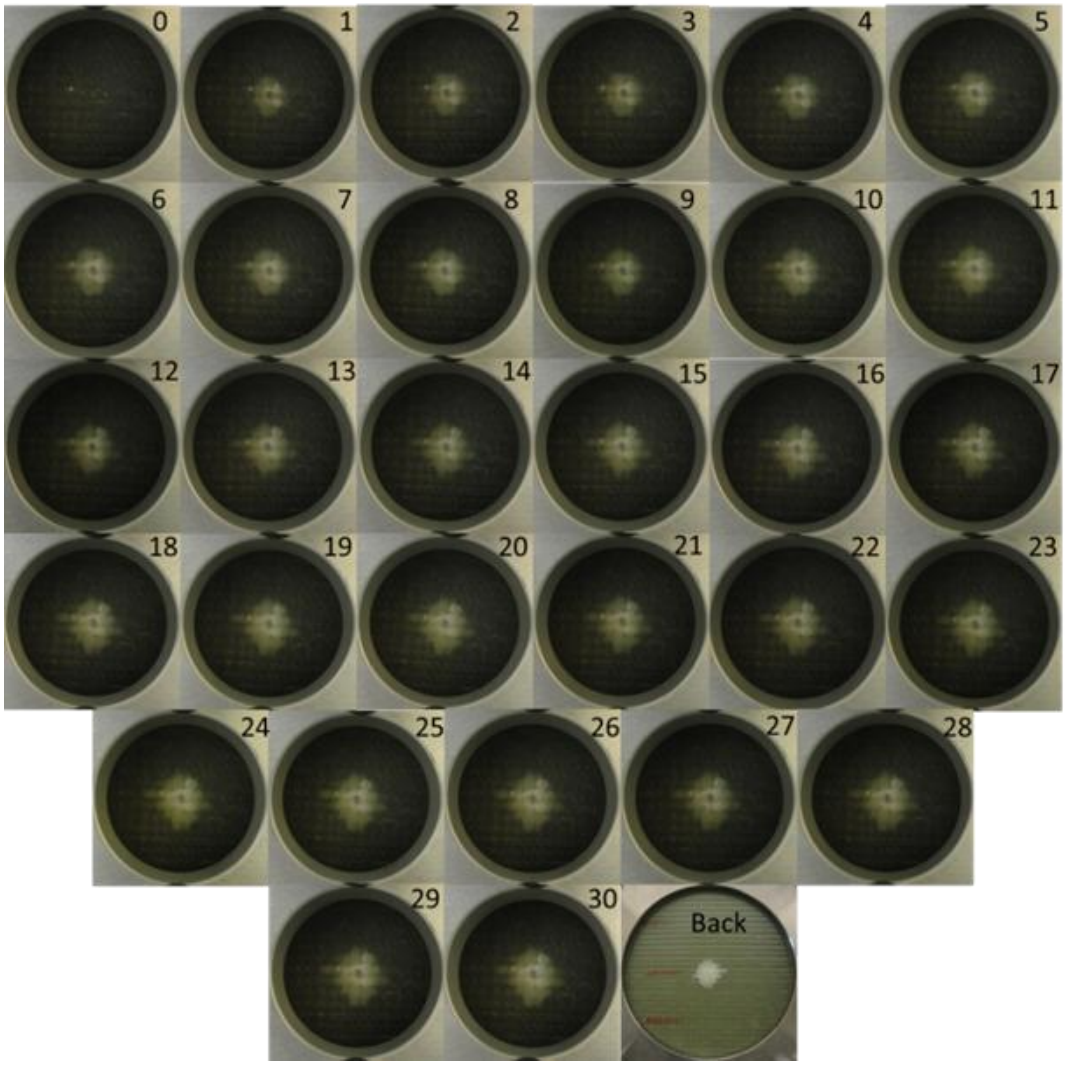

Figure B.44 Repeated impact images of sample IX (4 y-yarn layers and x-yarn density of 4.72) under repeated impact

C. Abbreviation

SHM	Fiber Reinforced Composite
3D	Three-dimensional
OTDR	Optical Time Domain Reflectometer
Gbps	Giga bits Per Second
dB	Decibel
FP	Fabry-Perot
FBG	Fiber Bragg Grating
NA	Numerical aperture
POF	Polymeric Optical Fiber
GOF	Glass Optical Fiber
PMMA	Polymethylmethacrylate
PS	Polystyrene
PC	Polycarbonate
SI	Step Index Profile
MMM	Methylmethacrylate
PMMA-d8	Deuterated PMMA
GI	Graded Refractive Index Profile
F	Fluorine
PF	Perfluorinated polymer
GE	Germanium
PF-GI-POF	Fluorinated-Graded Index-Polymer Optical Fiber
MC-SI-POF	Multi Core Step Index POF
ML-SI-POF	Multilayer step index POF
ORL	Optical Return Loss
WDM	Wavelength-Division Multiplexer
SNR	Signal-to-Noise Ratio
E-glass	Electrical glass
R-glass	Reinforcement glass
PMCs	Polymeric Matrices Composites
MMCs	Metal Matrix Composites
CMCs	Ceramic Matrix Composites
RTM	Resin Transfer Molding
PZT	**P**iezoelectric Transducer
AE	Acoustic Emission Sensors
GR/EP	Graphite/Epoxy
EFPI	Extrinsic Fabry-Perot Interferometer
CFRP	Carbon Fiber Reinforced Plastics
GFRP	Glass Fiber Reinforced Plastics
SOF	Silica Optical Fiber
LED	Luminescent
LDR	Light-Dependent Resistor

D. Definitions Related to Optic Fibers and Optic Signal Measurements

Reflection: when the light incidents surface like a mirror with specific angle it will reflect with same angle

Refraction: When light ray travels from medium to another the change of light direction will occur, this change in direction due to the change in light speed from one medium to another

Critical angle: is the smallest angle of the incident light that gives the total internal reflection

Total Internal Reflection: Light transmit in the fiber optics with incident angle greater than the critical angle then the light ray will reflect in a series of total internal reflection between two medium core and cladding having two different reflective indices

Refraction index: is a measure of how the light speed reduced inside this medium

Step index profile: refractive index for the core is constant along the cross section of the core diameter

Graded index profile: the core made of radius-dependent refractive index and the cladding made of a constant refractive index

Numerical aperture: is the sin of the half angle of the full acceptance cone

Core: is the center cylinder (glass of plastic) of the optics fiber that runs along the optics fiber length

Cladding: is a cylinder that surrounds the core material along the optics fiber length and has a higher index of refraction

Fluorinated Polymers: polymer that the hydrogen in C-H bond is replaced with fluorine in order to decrease the vibration absorption

Doping: is the process in which small molecules is added between the long chain of core material in order to increase the refractive index

OTDR Waveform: is the output signal response of the OTDR, and it shows the backscattering level as a function of distance

Dynamic range: is the maximum input optical power to a minimum output optical power

Event Dead Zone: is the minimum length of the fiber between two events that OTDR can detect separately

Attenuation Dead Zone: is the minimum distance from the beginning of the reflective event until the fiber backscattered return to 0.5 dB of its backscattered level

Rayleigh backscattering: when light hit fiber particles the light will scatter and redirected in different directions, which causes signal attenuation and backscattering

Fresnel Reflection: occurs when suddenly change happened to fiber refractive index (change from fiber material to air) and causes the light to reflect back on the fiber. This Fresnel reflection appears as a spike on OTDR waveform

E. OTDR Specifications

- Wavelengths : 650 nm, 850 nm
- Fixed optical pulses length : 1 ns
- Maximum length of network: variable between 1.25 km and 160 km
- Width of measurement window: variable, user-selectable
- Minimum spatial resolution (minimum distance between measurement points): approx. 2.5 cm (0.25 ns)
- Event dead zone: 10 cm
- Attenuation dead zone: 40 cm (Optical Return Loss = 45 dB)
- Dynamic range : > 20 dB
- Number of measurement points: variable according to resolution
- Measurement time: approx. 0.1 sec for each measurement point